NEW INSIGHTS INTO MECHANOTRANSDUCTION BY IMMUNE CELLS IN PHYSIOLOGICAL AND PATHOLOGICAL CONDITIONS

EDITED BY: Shaik O. Rahaman, David Krizaj, Nicholas Veldhuis and Shizuya Saika

PUBLISHED IN: Frontiers in Immunology

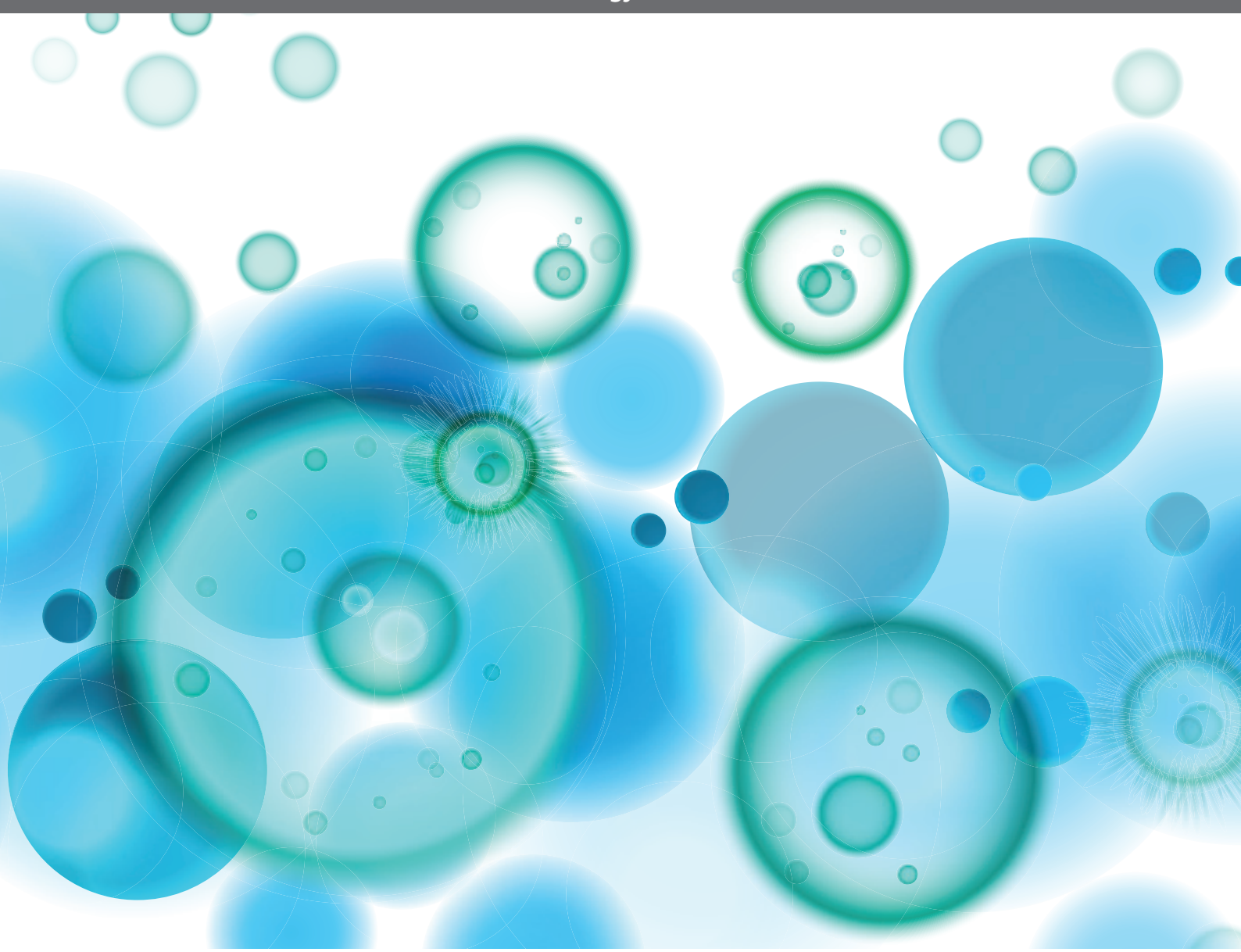

frontiers Research Topics

frontiers

ISSN 1664-8714
ISBN 978-2-88976-339-9
DOI 10.3389/978-2-88976-339-9

About Frontiers

Frontiers is more than just an open-access publisher of scholarly articles: it is a pioneering approach to the world of academia, radically improving the way scholarly research is managed. The grand vision of Frontiers is a world where all people have an equal opportunity to seek, share and generate knowledge. Frontiers provides immediate and permanent online open access to all its publications, but this alone is not enough to realize our grand goals.

Frontiers Journal Series

The Frontiers Journal Series is a multi-tier and interdisciplinary set of open-access, online journals, promising a paradigm shift from the current review, selection and dissemination processes in academic publishing. All Frontiers journals are driven by researchers for researchers; therefore, they constitute a service to the scholarly community. At the same time, the Frontiers Journal Series operates on a revolutionary invention, the tiered publishing system, initially addressing specific communities of scholars, and gradually climbing up to broader public understanding, thus serving the interests of the lay society, too.

Dedication to Quality

Each Frontiers article is a landmark of the highest quality, thanks to genuinely collaborative interactions between authors and review editors, who include some of the world's best academicians. Research must be certified by peers before entering a stream of knowledge that may eventually reach the public - and shape society; therefore, Frontiers only applies the most rigorous and unbiased reviews.
Frontiers revolutionizes research publishing by freely delivering the most outstanding research, evaluated with no bias from both the academic and social point of view. By applying the most advanced information technologies, Frontiers is catapulting scholarly publishing into a new generation.

What are Frontiers Research Topics?

Frontiers Research Topics are very popular trademarks of the Frontiers Journals Series: they are collections of at least ten articles, all centered on a particular subject. With their unique mix of varied contributions from Original Research to Review Articles, Frontiers Research Topics unify the most influential researchers, the latest key findings and historical advances in a hot research area! Find out more on how to host your own Frontiers Research Topic or contribute to one as an author by contacting the Frontiers Editorial Office: frontiersin.org/about/contact

NEW INSIGHTS INTO MECHANOTRANSDUCTION BY IMMUNE CELLS IN PHYSIOLOGICAL AND PATHOLOGICAL CONDITIONS

Topic Editors:
Shaik O. Rahaman, University of Maryland, College Park, United States
David Krizaj, The University of Utah, United States
Nicholas Veldhuis, Monash University, Australia
Shizuya Saika, Wakayama Medical University Hospital, Japan

Citation: Rahaman, S. O., Krizaj, D., Veldhuis, N., Saika, S., eds. (2022). New Insights Into Mechanotransduction by Immune Cells in Physiological and Pathological Conditions. Lausanne: Frontiers Media SA.
doi: 10.3389/978-2-88976-339-9

Table of Contents

frontiers | Frontiers in Immunology

EDITORIAL
published: 20 May 2022
doi: 10.3389/fimmu.2022.930362

Editorial: New Insights into Mechanotransduction by Immune Cells in Physiological and Pathological Conditions

Shizuya Saika[1], *Nicholas Veldhuis*[2], *David Križaj*[3] *and Shaik O. Rahaman*[4*]

[1] Department of Ophthalmology, Wakayama Medical University, Wakayama, Japan, [2] Drug Discovery Biology Theme, Monash Institute of Pharmaceutical Sciences, Monash University, Parkville, VIC, Australia, [3] Department of Ophthalmology, University of Utah School of Medicine, Salt Lake City, UT, United States, [4] Department of Nutrition and Food Science, University of Maryland, College Park, MD, United States

Keywords: mechanotransduction, inflammation, immunity, TRP channels, Piezo channels

Editorial on the Research Topic

New Insights into Mechanotransduction by Immune Cells in Physiological and Pathological Conditions

Mechanotransduction is the process in which mechanical and physical forces sensed by membrane receptors and/or channels ('mechanosensors') are converted into intracellular biochemical signals. This process plays fundamental functions in the regulation of development, immunity, inflammation, neurodegeneration, wound healing, fibrogenesis, pain transmission, and oncogenesis (1–6). Changes in matrix tension, stiffness (or rigidity), compression, and shear as well as cellular contact with neighboring cells and foreign bodies produce intracellular signals by acting on mechanosensors to affect a wide range of physiological or pathological outcomes (7–14, Gunasinghe et al.). Emerging data support a role for substrate tension, compression, and stiffness of the extracellular and intracellular matrix, in numerous cellular processes including gene expression, cell migration, cell proliferation, and differentiation (1–14, Gunasinghe et al.). Despite substantial progress in mechanotransduction field, the molecular pathways whereby mechanical and biochemical signals are integrated to elicit a specific cellular outcome are still poorly understood. The aim of this special Research Topic, which incorporates 6 original articles and 4 reviews - is to highlight the role of mechanotransduction by immune cells under physiological and pathological conditions.

All immune cells including T-cells, B-cells, Natural killer (NK) cells, macrophages/monocytes, neutrophils, and glial cells of peripheral and central nervous systems are subjected to biochemical and mechanical cues when in systemic circulation and in tissues. NK cells contribute to host immune protection against viruses and tumors by mediating target cell killing and secreting various cytokines. Santoni et al., reports findings on the involvement of mechanosensation and mechanotransduction that is mainly mediated by actin cytoskeleton, in the regulation of NK cell adhesion, migration, tissue infiltration and functions. Precise understanding of mechanotransduction in regulation of NK cell function may facilitate the development of nanomaterials tailored for NK cells, which would be important to develop new immunotherapeutic approaches.

Macrophages and neutrophils are mechanosensitive cells that perform diverse functions by sensing and responding to alteration of both physical and biochemical (soluble) cues in their tissue microenvironment.

OPEN ACCESS

Edited and reviewed by:
Francesca Granucci,
University of Milano-Bicocca, Italy

***Correspondence:**
Shaik O. Rahaman
srahaman@umd.edu

Specialty section:
This article was submitted to Molecular Innate Immunity, a section of the journal Frontiers in Immunology

Received: *27 April 2022*
Accepted: *29 April 2022*
Published: *20 May 2022*

Citation:
Saika S, Veldhuis N, Križaj D and Rahaman SO (2022) Editorial: New Insights into Mechanotransduction by Immune Cells in Physiological and Pathological Conditions. Front. Immunol. 13:930362. doi: 10.3389/fimmu.2022.930362

In contrast to the intense focus on soluble cues including cytokines, chemokines, as regulators of immune cell function, the physical microenvironment has traditionally received considerably less attention. Utilizing static and cyclic uniaxial stretch, Atcha et al. reports that the physical forces synergize with soluble signals to modulate macrophage morphology and function, and suggests a role for CD11b and Piezo1 crosstalk in mechanotransduction in macrophages. In this regard, Orsini et al. summarizes a systematic review to discuss the role of mechanosensitive ion channels, including Piezo1 and transient receptor potential vanilloid 4 (TRPV4), and cell adhesion molecules, including integrins, selectins, and cadherins in immune cells under various physiological and pathological conditions. They have highlighted that mechanical cues *via* activation of mechanosensitive ion channels and receptors activate intracellular signaling pathways, including MAPKs, YAP/TAZ, EDN1, NF-kB, and HIF-1α, to make a change in cellular responses. The precise understanding of the mechanisms by which immune cells transduce mechanosensitive cues presents novel targets to treat human diseases. The review by Nguyen et al. discusses recent understanding of cellular processes whereby macrophage TRPV4 plays a role in pathological conditions and inflammation, and the importance of applying unbiased methods including high-throughput and omics methods in future, for a broader understanding of the functional outcomes of TRPV4 activation.

Toft-Bertelsen and MacAulay, summarizes the current knowledge on cell volume regulation to discuss various mechanisms underlying the molecular coupling from cell swelling to TRPV4 channel activation and present the evidence of direct *versus* indirect swelling-activation of TRPV4. We believe the current knowledge discussed in this review will stimulate further research efforts in this area to precisely reveal TRPV4's role in numerous physiological and pathological conditions.

Matsuyama et al., summarizes the current knowledge on gateway reflex, a process that explains how autoreactive $CD4^+$ T cells cause inflammation in tissues harboring blood-barriers, such as the brain and retina, with a special interest on TRPV1 and mechanotransduction.

The role of TRP channels on inflammation during bacterial infections has been well recognized. Kono et al., reports a previously unsuspected role for TRPV1 and TRPV4 in *Streptococcus pneumoniae* nasal colonization and consequent development of pneumococcal disease in a mouse model. This results show that modulating host immune responses by TRPV1/TRPV4 could be a unique strategy against pathogenic bacteria generating local and/or systemic inflammation.

Trabecular meshwork (TM) cells are mechanosensitive cells with phagocytic and immune properties that actively regulate intraocular pressure (IOP). An increase in IOP stimulates actin polymerization *via* stretch-activated TRPV4 channels, which increases tissue resistance to outflow of aqueous humor to further elevate IOP. Yarishkin et al. report that sustained TRPV4 activation induces pacemaking calcium activity by stimulating TRPM4 (Transient Receptor Potential Melastatin 4), a calcium-activated sodium channel. By imbuing mechanotransduction with intrinsic time-dependence downstream from the tensile and compressive impact of IOP, TRPV4-TRPM4 interactions might provide immune regulation and outflow resistance in the anterior eye with an additional layer of signaling complexity.

Pathni et al., reports that activation of Cytotoxic T lymphocytes (CTLs) in the presence of interleukin (IL)-12 leads to differential modulation of the actomyosin and microtubule dynamics at the immune synapse leading to increased mechanical force exertion by CTLs to their targets. This result indicates a potential mechanotransduction *via* which IL-12 can augment the CTL response.

Initial studies probing mechanosensing role of T cells focused on planar hydrogel and elastomer surfaces. However, these approaches have several drawbacks including difficulties in separating mechanical stiffness from alterations in substrate chemistry required to regulate stiffness. Sachar and Kam, reports here the use of magnetically-actuated microscale elastomer pillars to change the stiffness of elastomer pillars, independent of substrate chemistry.

To precisely understand immune signaling and inflammation it is critical to define the mechanisms by which specific mechanotransduction processes occur, and how functional mechanosensing responses are influenced by the local, systemic and time-dependent biochemical factors. We would like to thank all the authors and reviewers who contributed to this special edition, for their time and expertise.

AUTHOR CONTRIBUTIONS

All authors listed have made a substantial, direct, and intellectual contribution to the work and approved it for publication.

FUNDING

This work was supported by an R01EB024556 grant to SR, the ARC Centre of Excellence in Convergent Bio-Nano Science and Technology to NV, R01EY027920, R01EY031817, P30EY014800 to DK, and unrestricted support from Research to Prevent Blindness to the Moran Eye Institute at the University of Utah.

REFERENCES

1. Tschumperlin DJ. Fibroblasts and the Ground They Walk on. *Physiol (Bethesda)* (2013) 28(6):380–90. doi: 10.1152/physiol.00024.2013
2. Trepat X, Chen Z, Jacobson K. Cell Migration. *Compr Physiol* (2012) 2 (4):2369–92. doi: 10.1002/cphy.c110012
3. Webster KD, Ng WP, Fletcher DA. Tensional Homeostasis in Single Fibroblasts. *Biophys J* (2014) 107(1):146–55. doi: 10.1016/j.bpj.2014.04.051
4. Plotnikov SV, Waterman CM. Guiding Cell Migration by Tugging. *Curr Opin Cell Biol* (2013) 25(5):619–26. doi: 10.1016/j.ceb.2013.06.003
5. Kumar S. Cellular Mechanotransduction: Stiffness Does Matter. *Nat Mater* (2014) 13(10):918–20. doi: 10.1038/nmat4094

6. Wells RG, Discher DE. Matrix Elasticity, Cytoskeletal Tension, and TGF-Beta: The Insoluble and Soluble Meet. *Sci Signal* (2008) 1(10):pe13. doi: 10.1126/stke.110pe13
7. Wong VW, Rustad KC, Akaishi S, Sorkin M, Glotzbach JP, Januszyk M, et al. Focal Adhesion Kinase Links Mechanical Force to Skin Fibrosis *via* Inflammatory Signaling. *Nat Med* (2011) 18(1):148–52. doi: 10.1038/nm.2574
8. Zhang H, Labouesse M. Signalling Through Mechanical Inputs: A Coordinated Process. *J Cell Sci* (2012) 125(Pt 13):3039–49. doi: 10.1242/jcs.093666
9. Wong SW, Lenzini S, Giovanni R, Knowles K, Shin JW. Matrix Biophysical Cues Direct Mesenchymal Stromal Cell Functions in Immunity. *Acta Biomater* (2021) 133:126–38. doi: 10.1016/j.actbio.2021.07.075
10. Farge E. Mechanotransduction in Development. *Curr Top Dev Biol* (2011) 95:243–65. doi: 10.1016/B978-0-12-385065-2.00008-6
11. Zhang X, Kim TH, Thauland TJ, Li H, Majedi FS, Ly C, et al. Unraveling the Mechanobiology of Immune Cells. *Curr Opin Biotechnol* (2020) 66:236–45. doi: 10.1016/j.copbio.2020.09.004
12. Dutta B, Arya RK, Goswami R, Alharbi MO, Sharma S, Rahaman SO. Role of Macrophage TRPV4 in Inflammation. *Lab Invest* (2020) 100(2):178–85. doi: 10.1038/s41374-019-0334-6
13. Zhu C, Chen W, Lou J, Rittase W, Li K. Mechanosensing Through Immunoreceptors. *Nat Immunol* (2019) 20(10):1269–78. doi: 10.1038/s41590-019-0491-1
14. Meli VS, Veerasubramanian PK, Atcha H, Reitz Z, Downing TL, Liu WF. Biophysical Regulation of Macrophages in Health and Disease. *J Leukoc Biol* (2019) 106(2):283–99. doi: 10.1002/JLB.MR0318-126R

Conflict of Interest: The authors declare that the research was conducted in the absence of any commercial or financial relationships that could be construed as a potential conflict of interest.

Publisher's Note: All claims expressed in this article are solely those of the authors and do not necessarily represent those of their affiliated organizations, or those of the publisher, the editors and the reviewers. Any product that may be evaluated in this article, or claim that may be made by its manufacturer, is not guaranteed or endorsed by the publisher.

frontiers in Immunology

MINI REVIEW
published: 15 July 2021
doi: 10.3389/fimmu.2021.688918

Mechanosensation and Mechanotransduction in Natural Killer Cells

Giorgio Santoni[1*], *Consuelo Amantini*[2], *Matteo Santoni*[3], *Federica Maggi*[1,4], *Maria Beatrice Morelli*[1] *and Angela Santoni*[4,5]

[1] School of Pharmacy, Section of Experimental Medicine, University of Camerino, Camerino, Italy, [2] School of Biosciences and Veterinary Medicine, University of Camerino, Camerino, Italy, [3] Macerata Hospital, Oncology Unit, Macerata, Italy, [4] Department of Molecular Medicine, Sapienza University, Rome, Italy, [5] IRCCS Neuromed, Pozzilli, Italy

Natural killer (NK) cells are a main subset of innate lymphocytes that contribute to host immune protection against viruses and tumors by mediating target cell killing and secreting a wide array of cytokines. Their functions are finely regulated by a balance between activating and inhibitory receptors and involve also adhesive interactions. Mechanotransduction is the process in which physical forces sensed by mechanosensors are translated into chemical signaling. Herein, we report findings on the involvement of this mechanism that is mainly mediated by actin cytoskeleton, in the regulation of NK cell adhesion, migration, tissue infiltration and functions. Actin represents the structural basis for NK cell immunological synapse (NKIS) and polarization of secretory apparatus. NK-target cell interaction involves the formation of both uropods and membrane nanotubes that allow target cell interaction over long distances. Actin retrograde flow (ARF) regulates NK cell signaling and controls the equilibrium between activation *versus* inhibition. Activating NKIS is associated with rapid lamellipodial ARF, whereas lower centripetal actin flow is present during inhibitory NKIS where β actin can associate with the tyrosine phosphatase SHP-1. Overall, a better knowledge of mechanotransduction might represent a future challenge: Realization of nanomaterials tailored for NK cells, would be important to translate *in vitro* studies in *in vivo* new immunotherapeutic approaches.

Keywords: mechanosensation, mechanotransduction, natural killer (NK) cells, immunological synapse, cytotoxicity

OPEN ACCESS

Edited by:
Shaik O. Rahaman, University of Maryland, College Park, United States

Reviewed by:
Yuri Sykulev, Thomas Jefferson University, United States
Marit Inngjerdingen, University of Oslo, Norway

***Correspondence:**
Giorgio Santoni
giorgio.santoni@unicam.it

Specialty section:
This article was submitted to Molecular Innate Immunity, a section of the journal Frontiers in Immunology

Received: *31 March 2021*
Accepted: *28 June 2021*
Published: *15 July 2021*

Citation:
Santoni G, Amantini C, Santoni M, Maggi F, Morelli MB and Santoni A (2021) Mechanosensation and Mechanotransduction in Natural Killer Cells. Front. Immunol. 12:688918. doi: 10.3389/fimmu.2021.688918

NATURAL KILLER (NK) CELL TARGET RECOGNITION AND FUNCTIONS

Natural Killer (NK) cells represent the prototype of innate lymphoid cells that act as first line of defense against microbial infections, and tumor cell transformation, growth and metastatic spreading (1–3). NK cells prompt the response mainly on their ability to release lytic mediators, such as perforin and granzymes, or to express ligands triggering death receptors on target cells; moreover, they can secrete a wide array of cytokines and chemokines to recruit and educate other immune cell types (4, 5). NK cell activation depends on a delicate balance between activating and inhibitory signals, being the latter mainly transduced by killer-cell immunoglobulin-like receptors

(KIRs), cluster of differentiation 94 (CD94)/natural-killer group 2, member A (NKG2A) receptors for class I MHC. Recognition of abnormal self on tumor or viral infected cells triggers a number of non MHC I-restricted activating receptors such as NKG2D, the receptor for the human MHC I-related sequence A and B (MICA/B) and UL16 binding proteins (ULBPs), DNAX accessory molecule-1 (DNAM-1) that recognizes nectin-2 (Nec2, CD112) and nectin-15 (Necl5, PVR, CD155), and the natural citotoxicity receptors (NCR) receptors (1). In addition, NK cells express receptors belonging to the β1 and β2 integrin family with lymphocyte function-associated antigen 1 (LFA-1) playing a central role in priming NK cells for cytotoxicity. The dialog of the β1 and β2 integrins with a number of chemokine receptors is also crucial for the homing and migration of NK cells in lymphoid and non-lymphoid organs.

Moreover, it is becoming clear that although they act in cooperative manner, different activating receptors can independently trigger discrete steps of NK cytolytic process (i.e. target cell contact and adhesion, granule polarization, degranulation and target lysis) by initiating diverse signaling cascades (6). In this regard, signaling components controlling cytoskeleton rearrangement, are emerging as critical events for NK cell cytotoxicity and migration.

NK/target cell interaction is regulated by adhesion molecules such as β1 and β2 integrins that play either a receptor or co-receptor role (7). High-avidity/affinity of integrins occurs in response of different activating receptors and depends on the activation of different signaling pathways including tyrosine kinases (PTK) belonging to the proto-oncogene tyrosine-protein kinase (Src) family, phosphoinositide 3-kinase (PI3K), small G proteins, and cytoskeletal integrity (inside-outside signaling). β2 integrins have been also shown to be critical in the interaction between NK and target cells by controlling the formation of the immunological synapse, which is an assembly of membrane receptors and signal transduction molecules largely driven by actin cytoskeleton. Development of NK cell cytotoxic functions requires the activation of a complex cascade of signaling pathways, including the activation of spleen tyrosine kinase (Syk) family PTKs, phospholipase C gamma (PLC-γ) and D (PLD), PI3K, Vav/Rac pathway, ERK, p38 and MAPKs (6). Some of these events are shared by different activating receptors, but distinct signals are also transduced depending on the type of receptor or the sensitive target triggering the cytotoxicity. In this regard, it has been reported that the activation of focal adhesion PTK Pyk2, that has been shown to be activated by β1 and β2 integrins, is a discriminating event between natural and antibody-mediated cytotoxicity. Moreover, ligation of integrins on human NK cells transduces intracellular signals leading to tyrosine phosphorylation of paxillin, intracellular calcium elevation (8), and co-stimulation of NK cell cytotoxic functions.

MECHANOSENSING IN THE NK CELL-MEDIATED IMMUNE RESPONSES

Mechanotransduction is the process in which physical forces sensed by mechanosensors are translated into chemical signaling pathways. This mechanism mediated by the cytoskeleton that serves as a global mechanosensor apparatus, permits cells to sense their extracellular environment and rapidly respond to different stimuli. NK cell mechanosensors include a large range of activating receptors as well as β1 and β2 integrins and CD62L selectin (9, 10).The actomyosin network plays an important role in mechanotransduction, in that actin polymerization generates a "pushing" force, whereas the myosin produces a "pulling" force, and together are translated into several signaling cascades (11, 12). Thus, the actin cytoskeleton provides the mechanical forces necessary for adhesion, migration and tissue infiltration of NK cells as well as for their cytotoxic function. The actin interactome represents the structural basis for the formation of a stable NKIS, integration of molecular complexes and signaling components, and the secretion of cytolytic granules and mediators (e.g., perforin) leading to target cell killing. The mature activating NKIS contains a central and peripheral supramolecular activation cluster (SMAC). The β2 integrins, namely $\alpha_L\beta2$ (LFA-1) and $\alpha_M\beta2$ (Mac-1) and F-actin accumulate in the peripheral SMAC (pSMAC), whereas perforin is present in the central SMAC. The accumulation of F-actin and β2 integrins is rapid, it depends on Wiskott–Aldrich syndrome protein (WASp)-driven actin polymerization, and is not affected by microtubule depolymerization. Conversely, the polarization of perforin is slower and requires intact actin, WASp protein, and microtubule function (13–15).

UROPODS AND NANOTUBES MEDIATE MECHANOTAXIS IN NK CELLS

Cell guiding is involved in a number of biological processes, but however, its mechanisms remain still partially elucidated. Immune cells are able to migrate directionally thanks to chemical guiding or chemotaxis in response to chemo-attractants, to haptotaxis in response to surface-bound chemicals, and to mechanical guiding or mechanotaxis in response to mechanical stimuli such as substrate stiffness, cell deformation or osmotic stress (16).

A large body of evidences mainly regard chemotaxis, whereas mechanotaxis has been considered only recently. Although a role in the activation of leukocytes has been reported (17), the basic remain largely elusive. Immune cell trafficking is not only supported by chemical signals, but also involves mechanical signals like hydrodynamic shear stress (18–21). The external forces are perceived by leukocytes mainly through the integrin receptors, which undergo conformational changes by inside-out (22) and outside-in (23) signaling, and initiate an intracellular signaling cascade in response to mechanical forces. Thus, integrins are key players both in the tissue recruitment of leukocytes from blood flow, and in leukocyte mechanotaxis under flow.

Two types of orientation mechanisms by flow have been suggested to mediate leukocyte integrin-mediated adhesion. Shear stress involves integrin-mediated outside-in signaling at anchoring sites (24–26). Such mechanisms are considered "active", in that a specific intracellular signaling pathway is

initiated in response to flow, and relies on mechanotransduction. Alternatively, a "passive" model that does not require signaling by the external cue, has been also proposed for upstream crawling lymphocytes (27). In this model, flow direction is detected by the passive orientation uropod, which is not adherent and freely rotates. Reorientation of the whole cell against flow, follows tail orientation *via* the cell realignment by front-rear polarization. At molecular level, the cross-talk between LFA-1 and integrin very late antigen-4 (VLA-4, α4β1) and the opposite polarization of LFA-1 and VLA-4 integrins sustain a differential adhesion of leukocytes either by their leading or trailing edge.

NK cells circulate in the blood against fluid flow, as shown by the orientation of the non-adherent cell rear, the uropod. Uropods sense and transmit flow directions into cell steering through the polarity maintenance (27). In addition, NK cell migration involves the convergence of signaling events triggered by engagement of both β2 and β1 integrins, and a number of chemokine receptors including C–X–C motif chemokine receptor (CXCR) 4, C–C chemokine receptor type (CCR) 2, CCR5 and CXCR3 (28, 29).

Cell polarization is also a crucial event for the formation of NK/target cell conjugates. NK cells contact target cells exploiting the region with high concentration of CCR2 and CCR5, whereas the ligands of β2 integrin intercellular adhesion molecule (ICAM)-1 and ICAM-3, are concentrated at the distal pole in the uropods. Blocking cell polarization and adhesion receptor redistribution, inhibits NK cell cytotoxic activity as result of impaired effector–target cell conjugate formation. Thus, cell polarization regulates different steps of NK cell functions: the leading edge where the CCR are concentrated, is involved in the adhesion to target cells, polarization of the secretory apparatus and release of lytic granules during the NK cell killing (30, 31); remarkably, different types of lytic granules undergo polarized secretion to the site of membrane contact between NK and target cells (32). The uropods by accumulating ICAM molecules, are involved in the recruitment of NK cells.

Cell polarization and cytotoxic activity, can be blocked by adenosine diphosphate (ADP) ribosylation of the guanosine-5'-triphosphate (GTP) binding protein Ras homolog family member A (RhoA), indicating the important role of this signaling pathway triggered by LFA-1 as well as by CCR in these events (33, 34).

Notably, formation of NK/target cell conjugates also stimulates chemokine release, which can further promote NK cell binding to target cells by inducing integrin inside-outside signaling and support NK cell migration.

Beside the involvement of uropods in the regulation of the intimate NK cell contact with target cells, NK cells can also generate membrane nanotubes that allow these cells to functionally interact with targets over long distances. Target cells that relocate along the nanotube path, are polarized with their uropods facing the direction of movement, are then lysed. Removing the nanotubes by a micromanipulator reduces target cell lysis (35). The frequency of nanotube formation depends on the number of interactions between activating receptor and the respective ligand(s), and increases upon the NK cell activation. Imaging studies have demonstrated that proteins, such as the signaling adaptor that associates with NKG2D, DAP10, the G protein exchange factor Vav-1, and the NKG2D ligand MICA accumulate at nanotube synapses in a such high concentration to stimulate cell activation (35).

NK IMMUNOLOGICAL SYNAPSE (NKIS): ROLE OF THE ACTIN CYTOSKELETON AND RETROGRADE FLOW IN CONTROLLING NK CELL RESPONSES

As above mentioned, NK cell cytotoxicity is a tightly regulated multistep process. It moves through the initial contact between NK cells with target cells which is mediated by tethering receptors such as CD2 and the selectin CD62L, adhesive integrin receptors (LFA1 and Mac1) that interact with ICAM1, and activating receptors such as NCRs, NKG2D and DNAM1 (36). Both activating and integrin signaling initiate the formation of NKIS. In particular, engagement of β2 integrins, but not of CD-16 activating receptor on CD16.NK-92 cells, was found to affect the size and the dynamics of signaling microclusters in a Pyk2-dependent manner (37).

Signaling is required for cytoskeleton remodeling, formation of activating microclusters and adhesion ring junction, polarization of effector cells and cytolytic granule releases (34). Accumulation of F-actin at the NKIS is the pre-requisite for the clustering of activating receptors which stimulate the polarization of cytolytic granules to the immunological synapse (IS). Lytic granules navigate to actin meshwork at the IS and reach the plasma membrane through gaps sized to accommodate lytic granule movements. The movement of lytic granules is dependent to myosin IIa that generates force and movements along actin filaments. In NK cells, myosin IIa mediates the interaction between lytic granules and F-actin UNC45-dependent manner at the NKIS, and facilitates the movement of lytic cargo along actin filaments (38). The movement of lytic granules toward the IS, initially depends on dynein that mediates the movement of secretory vesicles to the MTOC (39), and then on the granule-associated small GTPase Rab27a that recruits the Slp3–kinesin-1 complex, thus enabling the polarized cytotoxic granules to reach the membrane and release their contents at the IS (9, 40, 41). Activating receptor-triggered secretion of lytic granules requires binding of Rab27a to Munc13-4, with formation of a complex that co-localizes with lytic granules (42). Lytic granules docked and tethered to NKIS, are primed through interaction between Munc 13-4 and STX11 to form a trans-soluble NSF attachment protein receptor (SNARE) complex comprising the syntaxin STX11 and synaptosomal SNAP23 protein together with the SNARE proteins vesicle associated membrane protein (VAMP) 4 and VAMP7, likely mediated by syntaxin-binding protein 2 (STXBP2) (43). After the fusion of lytic granules at the synaptic cleft, the lytic granule membrane proteins are endocytosed to replenish lytic granules for further killing.

F-actin is a major driver of the IS formation between NK and target cells, and the polarization of the secretory apparatus (44–46). Actin retrograde flow (ARF) regulates NK cell signaling and controls the equilibrium between NK cell activation *versus* inhibition. The actomyosin dynamics is responsible for the "mechanotransduction" (11, 12, 47). The F-actin turnover and myosin IIa force at the NKIS are the most important forces involved in the guide of the F-actin centripetal flow, with actin polymerization pushing at the external part of the spreading cell, and the contractile myosin force pulling the F-actin away from the cell membrane (48). It has been well accepted that the actin flow plays a pivotal role in the centralization of receptors and signaling proteins. Activating NKIS is associated with a rapid lamellipodial ARF, whereas a lower centripetal actin flow is present during inhibitory NKIS (49). It has been recently demonstrated that tyrosine protein phosphatase (SHP)-1 and β-actin specifically associate at the inhibitory NKIS where ARF is slower. In addition, SHP-1 is maintained in a closed status and catalytically inactive form, if actin flow is inhibited by using jasplakinolide or cytochalasin D pharmacological inhibitors, or by growing cells on rigid surfaces. Thus, SHP-1 inhibition is the result of actin flow reduction that leads to increased Vav-1 and PLCγ-1/2 tyrosine phosphorylation and to NK cell activation. SHP-1 does not interact with the actin machinery when ARF velocity is rapid and activating NK cell interactions occur; in this case it has a closed catalytically inactive conformation, allowing Vav-1 and PLC-γ1/2 tyrosine phosphorylation (**Figure 1**) (47, 50). Thus, stimulation of NK cell activating receptors induces a fast actin flow that inhibits the binding of SHP-1 with the actin network. This NK activating status favors SHP-1 closed inactive conformation promoting target cell killing. Engagement of KIR inhibitory receptors results in slow actin flow, enabling the formation of the SHP-1/β-actin complex. SHP-1 inhibits NK cell activation by dephosphorylating important signaling molecules. Given that the actin flow dynamics rapidly change, it may enable a rapid switching from an inhibitory to activating NK cell response (47).

NK cell inhibition is also mediated by SHP-2 recruitment to KIR receptors (51, 52), and in non-immune cells SHP-2 is associated with the actin cytoskeleton (53). Given that SHP-1 and SHP-2 display a high level of structural homology, it can be suggested that a similar regulation of SHP-2 occurs also in NK cells *via* dynamic actin movement.

Overall, these data indicate that actin mechanotransduction is essential to increase the NK cell capability to rapidly respond to local environmental changes. While NKIS formation requires minutes/hours and is a slow process, alterations of the actin flow dynamics and the following SHP-1 status are fast events (seconds/minutes) that permit a rapid on/off control of inhibitory signaling (47). Thus, ARF, by controlling actin dynamics, represents a novel mechanism to regulate the functional outcome of NK cells.

MECHANICAL PROPERTIES OF SURROUNDING MATRIX AND TARGETS DRIVE NK CELL RESPONSIVENESS

During their lifetime, NK cells infiltrate a variety of normal, inflamed, or neoplastic tissues with different mechanical properties, exposing the NK cells to big fluctuations in matrix stiffness with potential impact on their responsiveness (54). Moreover, during the development, bone-marrow NK cells are

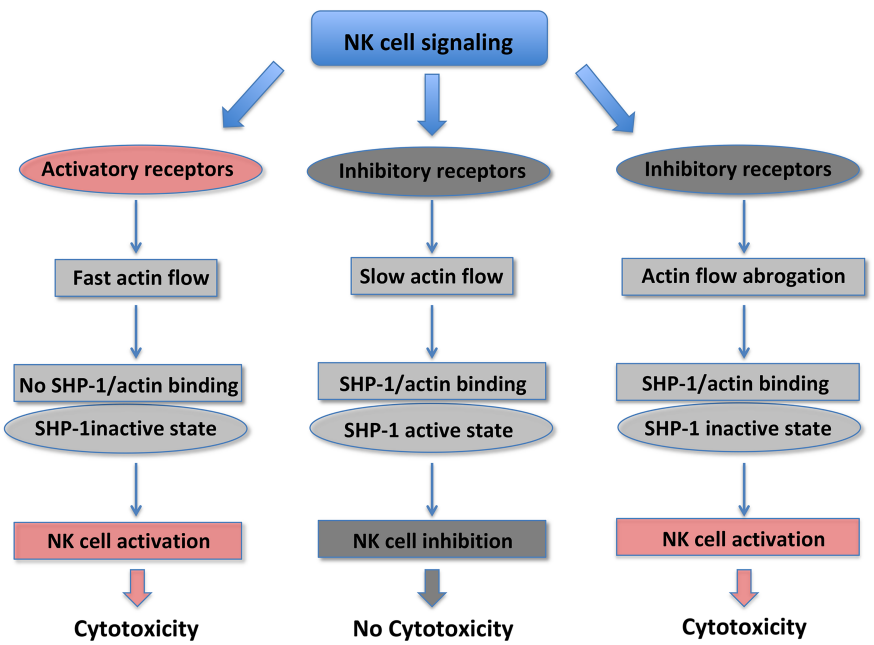

FIGURE 1 | NK cell cytotoxicity is regulated by changes in SHP-1 conformational state.

exposed to substrate stiffness ranging from 25 to 100 kPa (55). Both NK cell degranulation and cytokine production are modified by the rigidity of the target substrate. In the study by Malaton and colleagues, the effect of substrate stiffness on efficiency of NK cell degranulation was evaluated by using a cell-sized beads coated with sodium alginate at defined soft (9 kPa), medium (34 kPa) or stiff (254 kPa) alone, or in the presence of antibodies directed against LFA-1 or the NCR receptor NKp30. Increased substrate stiffness stimulated NK cell degranulation, that was further enhanced by NKp30 and LFA1 triggering. The lower degranulating capacity of NK cells contacting soft targets was suggested to depend on an impaired recruitment of phosphorylated zinc-finger antiviral protein (Zap) 70 PTK to the NKIS (47). Similarly, a recent report demonstrated that target rigidity impacts on perforin granule polarization and degranulation, being secretion of granzymes A and B, granulysin and FAS ligand improved with increased substrate stiffness (56). Soft target stiffness was found to reduce F-actin accumulation and talin polarization and recruitment at the NKIS, leading to the formation of an instable asymmetrical synapse and decreased proportion of NK cells in the conjugates with targets. In addition, interaction with softer targets resulted in impaired microtubule organizing center (MTOC) and lytic granule polarization (**Figure 2**) (56).

Stiffness of the activating substrates not only impacts on NK cell cytotoxic function, but secretion of cytokines, namely interferon-gamma (IFN-γ), is also modulated, with increased release observed upon NK cell interaction with the stiffer substrates.

The stiffness properties of a cell undergoes changes during the neoplastic process, with primary tumor cells being stiffer than healthy cells, and conversely metastatic cells showing profound reduction in stiffness (58); in addition, also viral infection increases stiffness by inducing cortical actin rearrangement (59). Thus, we would like to envisage that stiffening or softening would be able to profoundly affect the responsiveness of NK cells infiltrating neoplastic or infected tissues. Because no evidences are presently addressing this issue, we would like to suggest that investigation of mechanotransduction mechanisms in tissue resident NK cells would represent a research area of increasing interest.

NANOMATERIALS IN THE REGULATION OF NK CELL FUNCTIONS

The use of nanowires or nanodots functionalized or not with ligands, permits now to explore more in depth the mechanosensitivity of NK cells, and in particular the mechanical features of NKIS. Shaping NK cell activity by nanomaterials to functionally upregulate their activating receptors, may represent an emerging strategy for NK-cell based adaptive immunotherapy. Enhanced NK cell activation on antigen-functionalized and mechanically stimulating nanowires and nanodots, and the isolation of activated NK cell subpopulations, foreruns novel nanoengineered platforms for cell expansion toward therapeutic purposes, with improved efficiency and control of cytotoxic activity (60).

Finally, in the recent years with the development of chimeric antigen receptor (CARs) of T and NK lineages, researchers are closer to achieving high specificity and low off-side effects, with clinical trials achieving remission rates. In this regard, a role of mechanosensing in the antigen/target discrimination is a key to engineered high specific CARs. Further work would be required to completely address the mechanosensing properties of NK cells *in vivo*. These studies can provide important fundamental insights on cytotoxic functions of NK cells and allow rational design of future immunotherapies.

CONCLUDING REMARKS

Cells sense their environment by transducing mechanical stimuli into biochemical signals. Conventional tools for study cell mechanosensing provide limited spatial and force resolution. Recent advances in biomaterials and device engineering have

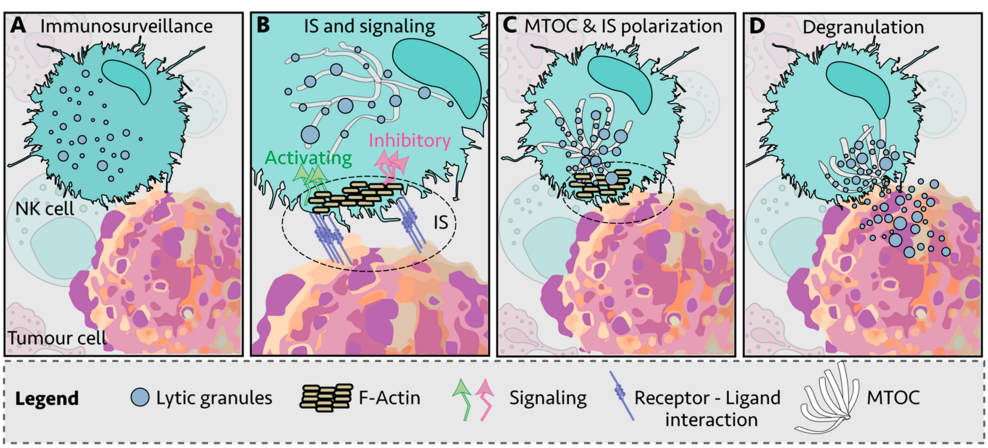

FIGURE 2 | Immunological synapse (IS) of Natural Killer (NK) cell and target cell. **(A)** NK cells engage other cells to create an immunological synapse (IS); **(B)** First, filamentous actin (F-actin) is recruited to the IS; **(C)** NK lytic granules move along microtubules by dynein–dynactin motor proteins toward the microtubule-organizing center (MTOC); **(D)** the polarized lytic granules and MTOC dock at the IS, and degranulate (57).

facilitated the generation of numerous artificial cellular microenvironments, which produce synthetic signals mimicking those delivered by the physiological environment. Several advanced materials and devices have been recently produced for the study of mechanical activity in NK cells. NK cells exposed to nanowires functionalized with MICA ligands exhibit higher expression of CD107 degranulation marker, suggesting that the combination of a physical stimulus with the chemical stimulus of MICA, enhances NK cell activation (60, 61). This model may mimic the *in vivo* NK cell/dendritic cell interaction, where the branched projections of DC are similar in size and shape to nanowires (62).

AUTHOR CONTRIBUTIONS

GS and AS drafted the manuscript. GS conceived and designed the study. MM, CA, FM, and MS critically revised the manuscript. All authors contributed to the article and approved the submitted version.

FUNDING

PRIN-2017 Italian Ministry of Education Ministry of University and Research.

REFERENCES

1. Trinchieri G. Biology of Natural Killer Cells. *Adv Immunol* (1989) 47:187–376. doi: 10.1016/s0065-2776(08)60664-1
2. Lanier LL. NK Cell Recognition. *Annu Rev Immunol* (2005) 23:225–74. doi: 10.1146/annurev.immunol.23.021704.115526
3. Spits H, Di Santo JP. The Expanding Family of Innate Lymphoid Cells: Regulators and Effectors of Immunity and Tissue Remodeling. *Nat Immunol* (2011) 12:21–7. doi: 10.1038/ni.1962
4. Moretta L, Bottino C, Pende D, Castriconi R, Mingari MC, Moretta A. Surface NK Receptors and Their Ligands on Tumor Cells. *Semin Immunol* (2006) 18:151–8. doi: 10.1016/j.smim.2006.03.002
5. Moretta L, Ferlazzo G, Bottino C, Vitale M, Pende D, Mingari MC, et al. Effector and Regulatory Events During Natural Killer-Dendritic Cell Interactions. *Immunol Rev* (2006) 214:219–28. doi: 10.1111/j.1600-065X.2006.00450.x
6. Bryceson YT, March ME, Ljunggren H-G, Long EO. Activation, Coactivation, and Costimulation of Resting Human Natural Killer Cells. *Immunol Rev* (2006) 214:73–91. doi: 10.1111/j.1600-065X.2006.00457.x
7. Helander TS, Timonen T. Adhesion in NK Cell Function. *Curr Top Microbiol Immunol* (1998) 230:89–99. doi: 10.1007/978-3-642-46859-9_7
8. Long EO, Kim HS, Liu D, Peterson ME, Rajagopalan S. Controlling Natural Killer Cell Responses: Integration of Signals for Activation and Inhibition. *Annu Rev Immunol* (2013) 31:227–58. doi: 10.1146/annurev-immunol-020711-075005
9. Phatarpekar PV, Billadeau DD. Molecular Regulation of the Plasma Membrane-Proximal Cellular Steps Involved in NK Cell Cytolytic Function. *J Cell Sci* (2020) 133(5):jcs240424. doi: 10.1242/jcs.240424
10. Zhang X, Kim T-H, Thauland TJ, Li H, Majedi FS, Ly C, et al. Unraveling the Mechanobiology of Immune Cells. *Curr Opin Biotechnol* (2020) 66:236–45. doi: 10.1016/j.copbio.2020.09.004
11. Vogel V, Sheetz M. Local Force and Geometry Sensing Regulate Cell Functions. *Nat Rev Mol Cell Biol* (2006) 7:265–75. doi: 10.1038/nrm1890
12. Jaalouk DE, Lammerding J. Mechanotransduction Gone Awry. *Nat Rev Mol Cell Biol* (2009) 10:63–73. doi: 10.1038/nrm2597
13. Orange JS, Harris KE, Andzelm MM, Valter MM, Geha RS, Strominger JL. The Mature Activating Natural Killer Cell Immunologic Synapse Is Formed in Distinct Stages. *Proc Natl Acad Sci USA* (2003) 100:14151–6. doi: 10.1073/pnas.1835830100
14. Roda-Navarro P. Assembly and Function of the Natural Killer Cell Immune Synapse. *Front Biosci (Landmark Ed)* (2009) 14:621–33. doi: 10.2741/3268
15. Stabile H, Carlino C, Mazza C, Giliani S, Morrone S, Notarangelo LD, et al. Impaired NK-Cell Migration in WAS/XLT Patients: Role of Cdc42/WASp Pathway in the Control of Chemokine-Induced β2 Integrin High-Affinity State. *Blood* (2010) 115:2818–26. doi: 10.1182/blood-2009-07-235804
16. Swaney KF, Huang C-H, Devreotes PN. Eukaryotic Chemotaxis: A Network of Signaling Pathways Controls Motility, Directional Sensing, and Polarity. *Annu Rev Biophys* (2010) 39:265–89. doi: 10.1146/annurev.biophys.093008.131228
17. Feng Y, Brazin KN, Kobayashi E, Mallis RJ, Reinherz EL, Lang MJ. Mechanosensing Drives Acuity of αβ T-Cell Recognition. *Proc Natl Acad Sci* (2017) 114:E8204–13. doi: 10.1073/pnas.1703559114
18. Smith LA, Aranda-Espinoza H, Haun JB, Hammer DA. Interplay Between Shear Stress and Adhesion on Neutrophil Locomotion. *Biophys J* (2007) 92:632–40. doi: 10.1529/biophysj.105.079418
19. Dominguez GA, Anderson NR, Hammer DA. The Direction of Migration of T-lymphocytes Under Flow Depends Upon Which Adhesion Receptors are Engaged. *Integr Biol (Camb)* (2015) 7:345–55. doi: 10.1039/c4ib00201f
20. Sumagin R, Prizant H, Lomakina E, Waugh RE, Sarelius IH. LFA-1 and Mac-1 Define Characteristically Different Intralumenal Crawling and Emigration Patterns for Monocytes and Neutrophils In Situ. *J Immunol* (2010) 185:7057–66. doi: 10.4049/jimmunol.1001638
21. Valignat M-P, Theodoly O, Gucciardi A, Hogg N, Lellouch AC. T Lymphocytes Orient Against the Direction of Fluid Flow During LFA-1-Mediated Migration. *Biophys J* (2013) 104:322–31. doi: 10.1016/j.bpj.2012.12.007
22. Grönholm M, Jahan F, Bryushkova EA, Madhavan S, Aglialoro F, Soto Hinojosa L, et al. LFA-1 Integrin Antibodies Inhibit Leukocyte α4β1-Mediated Adhesion by Intracellular Signaling. *Blood* (2016) 128:1270–81. doi: 10.1182/blood-2016-03-705160
23. Schürpf T, Springer TA. Regulation of Integrin Affinity on Cell Surfaces. *EMBO J* (2011) 30:4712–27. doi: 10.1038/emboj.2011.333
24. Hoffman BD, Grashoff C, Schwartz MA. Dynamic Molecular Processes Mediate Cellular Mechanotransduction. *Nature* (2011) 475:316–23. doi: 10.1038/nature10316
25. del Rio A, Perez-Jimenez R, Liu R, Roca-Cusachs P, Fernandez JM, Sheetz MP. Stretching Single Talin Rod Molecules Activates Vinculin Binding. *Science* (2009) 323:638–41. doi: 10.1126/science.1162912
26. Sawada Y, Tamada M, Dubin-Thaler BJ, Cherniavskaya O, Sakai R, Tanaka S, et al. Force Sensing by Mechanical Extension of the Src Family Kinase Substrate p130Cas. *Cell* (2006) 127:1015–26. doi: 10.1016/j.cell.2006.09.044
27. Valignat M-P, Nègre P, Cadra S, Lellouch AC, Gallet F, Hénon S, et al. Lymphocytes Can Self-Steer Passively With Wind Vane Uropods. *Nat Commun* (2014) 5:5213. doi: 10.1038/ncomms6213
28. Robertson MJ. Role of Chemokines in the Biology of Natural Killer Cells. *J Leukoc Biol* (2002) 71:173–83.
29. Bernardini G, Antonangeli F, Bonanni V, Santoni A. Dysregulation of Chemokine/Chemokine Receptor Axes and NK Cell Tissue Localization During Diseases. *Front Immunol* (2016) 7:402. doi: 10.3389/fimmu.2016.00402
30. Lang P, Guizani L, Vitté-Mony I, Stancou R, Dorseuil O, Gacon G, et al. ADP-Ribosylation of the Ras-Related, GTP-Binding Protein RhoA Inhibits Lymphocyte-Mediated Cytotoxicity. *J Biol Chem* (1992) 267:11677–80. doi: 10.1016/S0021-9258(19)49747-0
31. Billadeau DD, Brumbaugh KM, Dick CJ, Schoon RA, Bustelo XR, Leibson PJ. The Vav–Rac1 Pathway in Cytotoxic Lymphocytes Regulates the Generation of Cell-mediated Killing. *J Exp Med* (1998) 188:549–59. doi: 10.1084/jem.188.3.549
32. Griffiths GM, Argon Y. Structure and Biogenesis of Lytic Granules. *Curr Top Microbiol Immunol* (1995) 198:39–58. doi: 10.1007/978-3-642-79414-8_3

33. Lang P, Gesbert F, Delespine-Carmagnat M, Stancou R, Pouchelet M, Bertoglio J. Protein Kinase A Phosphorylation of RhoA Mediates the Morphological and Functional Effects of Cyclic AMP in Cytotoxic Lymphocytes. *EMBO J* (1996) 15:510–9. doi: 10.1002/j.1460-2075.1996.tb00383.x
34. Ben-Shmuel A, Sabag B, Biber G, Barda-Saad M. The Role of the Cytoskeleton in Regulating the Natural Killer Cell Immune Response in Health and Disease: From Signaling Dynamics to Function. *Front Cell Dev Biol* (2021) 9:609532. doi: 10.3389/fcell.2021.609532
35. Chauveau A, Aucher A, Eissmann P, Vivier E, Davis DM. Membrane Nanotubes Facilitate Long-Distance Interactions Between Natural Killer Cells and Target Cells. *Proc Natl Acad Sci* (2010) 107:5545–50. doi: 10.1073/pnas.0910074107
36. Orange JS. Formation and Function of the Lytic NK-cell Immunological Synapse. *Nat Rev Immunol* (2008) 8:713–25. doi: 10.1038/nri2381
37. Steblyanko M, Anikeeva N, Campbell KS, Keen JH, Sykulev Y. Integrins Influence the Size and Dynamics of Signaling Microclusters in a Pyk2-Dependent Manner. *J Biol Chem* (2015) 290:11833–42. doi: 10.1074/jbc.M114.614719
38. Iizuka Y, Cichocki F, Sieben A, Sforza F, Karim R, Coughlin K, et al. Unc-45a Is a Nonmuscle Myosin IIA Chaperone Required for NK Cell Cytotoxicity Via Control of Lytic Granule Secretion. *J Immunol* (2015) 195:4760–70. doi: 10.4049/jimmunol.1500979
39. Mentlik AN, Sanborn KB, Holzbaur EL, Orange JS. Rapid Lytic Granule Convergence to the MTOC in Natural Killer Cells Is Dependent on Dynein But Not Cytolytic Commitment. *Mol Biol Cell* (2010) 21:2241–56. doi: 10.1091/mbc.e09-11-0930
40. Wood SM, Meeths M, Chiang SCC, Bechensteen AG, Boelens JJ, Heilmann C, et al. Different NK Cell–Activating Receptors Preferentially Recruit Rab27a or Munc13-4 to Perforin-Containing Granules for Cytotoxicity. *Blood* (2009) 114:4117–27. doi: 10.1182/blood-2009-06-225359
41. Kurowska M, Goudin N, Nehme NT, Court M, Garin J, Fischer A, et al. Terminal Transport of Lytic Granules to the Immune Synapse Is Mediated by the kinesin-1/Slp3/Rab27a Complex. *Blood* (2012) 119:3879–89. doi: 10.1182/blood-2011-09-382556
42. Elstak ED, Neeft M, Nehme NT, Voortman J, Cheung M, Goodarzifard M, et al. The munc13-4-rab27 Complex Is Specifically Required for Tethering Secretory Lysosomes at the Plasma Membrane. *Blood* (2011) 118:1570–8. doi: 10.1182/blood-2011-02-339523
43. Capuano C, Paolini R, Molfetta R, Frati L, Santoni A, Galandrini R. PIP2-Dependent Regulation of Munc13-4 Endocytic Recycling: Impact on the Cytolytic Secretory Pathway. *Blood* (2012) 119:2252–62. doi: 10.1182/blood-2010-12-324160
44. Fassett MS, Davis DM, Valter MM, Cohen GB, Strominger JL. Signaling at the Inhibitory Natural Killer Cell Immune Synapse Regulates Lipid Raft Polarization But Not Class I MHC Clustering. *Proc Natl Acad Sci USA* (2001) 98:14547–52. doi: 10.1073/pnas.211563598
45. Poggi A, Panzeri MC, Moretta L, Zocchi MR. CD31-Triggered Rearrangement of the Actin Cytoskeleton in Human Natural Killer Cells. *Eur J Immunol* (1996) 26:817–24. doi: 10.1002/eji.1830260414
46. Radošsević K, van Leeuwen AMT, Segers-Nolten IMJ, Figdor CG, de Grooth BG, Greve J. Changes in Actin Organization During the Cytotoxic Process. *Cytometry* (1994) 15:320–6. doi: 10.1002/cyto.990150407
47. Matalon O, Ben-Shmuel A, Kivelevitz J, Sabag B, Fried S, Joseph N, et al. Actin Retrograde Flow Controls Natural Killer Cell Response by Regulating the Conformation State of SHP-1. *EMBO J* (2018) 37(5):e96264. doi: 10.15252/embj.201696264
48. Hammer JA, Burkhardt JK. Controversy and Consensus Regarding Myosin II Function at the Immunological Synapse. *Curr Opin Immunol* (2013) 25:300–6. doi: 10.1016/j.coi.2013.03.010
49. Jankowska KI, Williamson EK, Roy NH, Blumenthal D, Chandra V, Baumgart T, et al. Integrins Modulate T Cell Receptor Signaling by Constraining Actin Flow at the Immunological Synapse. *Front Immunol* (2018) 9:25. doi: 10.3389/fimmu.2018.00025
50. Davis DM. Mechanisms and Functions for the Duration of Intercellular Contacts Made by Lymphocytes. *Nat Rev Immunol* (2009) 9:543–55. doi: 10.1038/nri2602
51. Yusa S, Campbell KS. Src Homology Region 2-Containing Protein Tyrosine Phosphatase-2 (Shp-2) Can Play a Direct Role in the Inhibitory Function of Killer Cell Ig-Like Receptors in Human Nk Cells. *J Immunol* (2003) 170:4539–47. doi: 10.4049/jimmunol.170.9.4539
52. Purdy AK, Campbell KS. Natural Killer Cells and Cancer: Regulation by the Killer Cell Ig-like Receptors (KIR). *Cancer Biol Ther* (2009) 8:2209–18. doi: 10.4161/cbt.8.23.10455
53. Xu F, Zhao R, Peng Y, Guerrah A, Zhao ZJ. Association of Tyrosine Phosphatase SHP-2 With F-Actin at Low Cell Densities. *J Biol Chem* (2001) 276:29479–84. doi: 10.1074/jbc.M104428200
54. Mace EM, Orange JS. Multiple Distinct NK-Cell Synapses. *Blood* (2011) 118:6475–6. doi: 10.1182/blood-2011-10-381392
55. Wells RG. Tissue Mechanics and Fibrosis. *Biochim Biophys Acta - Mol Basis Dis* (2013) 1832:884–90. doi: 10.1016/j.bbadis.2013.02.007
56. Friedman D, Simmonds P, Hale A, Bere L, Hodson NW, White MRH, et al. Natural Killer Cell Immune Synapse Formation and Cytotoxicity Are Controlled by Tension of the Target Interface. *J Cell Sci* (2021) 134:jcs.258570. doi: 10.1242/jcs.258570
57. Meza Guzman LG, Keating N, Nicholson SE. Natural Killer Cells: Tumor Surveillance and Signaling.. *Cancers (Basel)* (2020) 12(4):952. doi: 10.3390/cancers12040952
58. Zoeller RT, Vandenberg LN. Assessing Dose-Response Relationships for Endocrine Disrupting Chemicals (Edcs): A Focus on Non-Monotonicity. *Environ Health* (2015) 14:42. doi: 10.1186/s12940-015-0029-4
59. Kräter M, Sapudom J, Bilz N, Pompe T, Guck J, Claus C. Alterations in Cell Mechanics by Actin Cytoskeletal Changes Correlate With Strain-Specific Rubella Virus Phenotypes for Cell Migration and Induction of Apoptosis. *Cells* (2018) 7:136. doi: 10.3390/cells7090136
60. Le Saux G, Schvartzman M. Advanced Materials and Devices for the Regulation and Study of NK Cells. *Int J Mol Sci* (2019) 20:646. doi: 10.3390/ijms20030646
61. Le Saux G, Bar-Hanin N, Edri A, Hadad U, Porgador A, Schvartzman M. Nanoscale Mechanosensing of Natural Killer Cells is Revealed by Antigen-Functionalized Nanowires. *Adv Mater* (2019) 31:1805954. doi: 10.1002/adma.201805954
62. Verdijk P, van Veelen PA, de Ru AH, Hensbergen PJ, Mizuno K, Koerten HK, et al. Morphological Changes During Dendritic Cell Maturation Correlate With Cofilin Activation and Translocation to the Cell Membrane. *Eur J Immunol* (2004) 34:156–64. doi: 10.1002/eji.200324241

Conflict of Interest: The authors declare that the research was conducted in the absence of any commercial or financial relationships that could be construed as a potential conflict of interest.

frontiers in Immunology

ORIGINAL RESEARCH
published: 09 August 2021
doi: 10.3389/fimmu.2021.704693

Probing T Cell 3D Mechanosensing With Magnetically-Actuated Structures

Chirag Sachar and Lance C. Kam *

Department of Biomedical Engineering, Columbia University, New York, NY, United States

The ability of cells to recognize and respond to the mechanical properties of their environment is of increasing importance in T cell physiology. However, initial studies in this direction focused on planar hydrogel and elastomer surfaces, presenting several challenges in interpretation including difficulties in separating mechanical stiffness from changes in chemistry needed to modulate this property. We introduce here the use of magnetic fields to change the structural rigidity of microscale elastomer pillars loaded with superparamagnetic nanoparticles, independent of substrate chemistry. This magnetic modulation of rigidity, embodied as the pillar spring constant, changed the interaction of mouse naïve $CD4^+$ T cells from a contractile morphology to one involving deep embedding into the array. Furthermore, increasing spring constant was associated with higher IL-2 secretion, showing a functional impact on mechanosensing. The system introduced here thus separates local substrate stiffness and long-range structural rigidity, revealing new facets of T cell interaction with their environment.

Keywords: mechanobiology, $CD4^+$ T cell, magnetic, micropillar, activation

OPEN ACCESS

Edited by:
Nicholas Veldhuis, Monash University, Australia

Reviewed by:
Kate Poole, University of New South Wales, Australia
Paris Von Lockette, The Pennsylvania State University (PSU), United States

***Correspondence:**
Lance C. Kam
lance.kam@columbia.edu

Specialty section:
This article was submitted to Molecular Innate Immunity, a section of the journal Frontiers in Immunology

Received: *03 May 2021*
Accepted: *23 August 2021*
Published: *09 August 2021*

Citation:
Sachar C and Kam LC (2021) Probing T Cell 3D Mechanosensing With Magnetically-Actuated Structures. Front. Immunol. 12:704693. doi: 10.3389/fimmu.2021.704693

1 INTRODUCTION

T cells are key agents of the adaptive immune response, coordinating precise and robust protection against pathogens, but in other settings also contributing to a range of diseases. These cells can also be leveraged to treat disease, and there is growing interest in the design of materials that direct ex vivo production of these living drugs in the context of cellular immunotherapy. In particular, tuning the mechanical properties of a biomaterial used to activate T cells can enhance subsequent function including cytokine secretion, proliferation, and population expansion (1–4). The early studies investigating T cell mechanosensing were carried out with flat, planar surfaces presenting ligands to the T Cell Receptor (TCR) and CD28, which provide activating and costimulatory signaling, respectively (3, 5). However, interactions between T cells and antigen presenting cells (APCs) are topographically complex, involving cellular protrusions, extensions, and other features that are defined over a range of spatial scales (6, 7). Subsequent studies using microstructured surfaces (8–11) showed that T cells can interact intimately with these topographies in model systems, altering a range of outputs associated with cell activation and function. Notably, T cells appear to respond to the structural rigidity of microscale elastomer pillars organized into long-range arrays, a system originally developed for measuring forces exerted by cells onto an underlying substrate (12). T cells respond to changes in pillar rigidity, expressed as that structure's spring constant (the ratio of force

applied tangentially at the tip to the tip deflection), by modulating microtubule organizing center (MTOC) transport and cytokine secretion (10). These experiments were carried out by altering the geometry (height and cross section) of each pillar, as previously described for other types of cells (13–15). This approach addressed a frequently-voiced critique of mechanobiology studies using planar substrates such as hydrogels in that stiffness was controlled through material chemistry; changing cross-linker density could affect local, nanoscale interactions with cells rather than substrate modulus alone (16). Microscale structuring allowed control over the larger-range mechanical response of a substrate while using the same material formulation, but introduced other issues. Changing parameters such as pillar width and depth also alters features such as local substrate curvature, area avaiable for cell adhesion, and/or nutrient availability which may alter cell response independently of system rigidity. This report introduces the use of magnetic fields to change the rigidity of micropillar arrays while keeping the structure dimensions constant, addressing such concerns.

The approach introduced here (**Figure 1A**) is a variation of a magnetic actuation micropillar system introduced by Sniakecki et al. (17). In that system, magnetic wires are embedded inside individual pillars. Application of a magnetic field tangential to the arrays (along the direction of multiple pillars and thus perpendicular to an individual pillar) imparts a torque to the wire. Since the wire is anchored to the substrate through the pillar, this torque is transmitted to adherent cells as a lateral force. In the present study, the magnetic field is applied perpendicular to the arrays rather than tangential, in the direction represented by B_{mod} in **Figure 1A**. The pillars are loaded with superparamagnetic nanoparticles (NPs). A magnetic field applied in this configuration induces a moment along the pillar axis which will tend to align with the field. Deflection of the pillar away from this alignment, for example by a cell producing F_{cell} in **Figure 1A**, will produce a restoring torque, τ, that seeks to realign the magnetic moment and field. The magnitude of this torque and resultant force applied to the cell are approximately linear to pillar tip deflection for small displacements. In short, application of a magnetic field in this configuration increases the

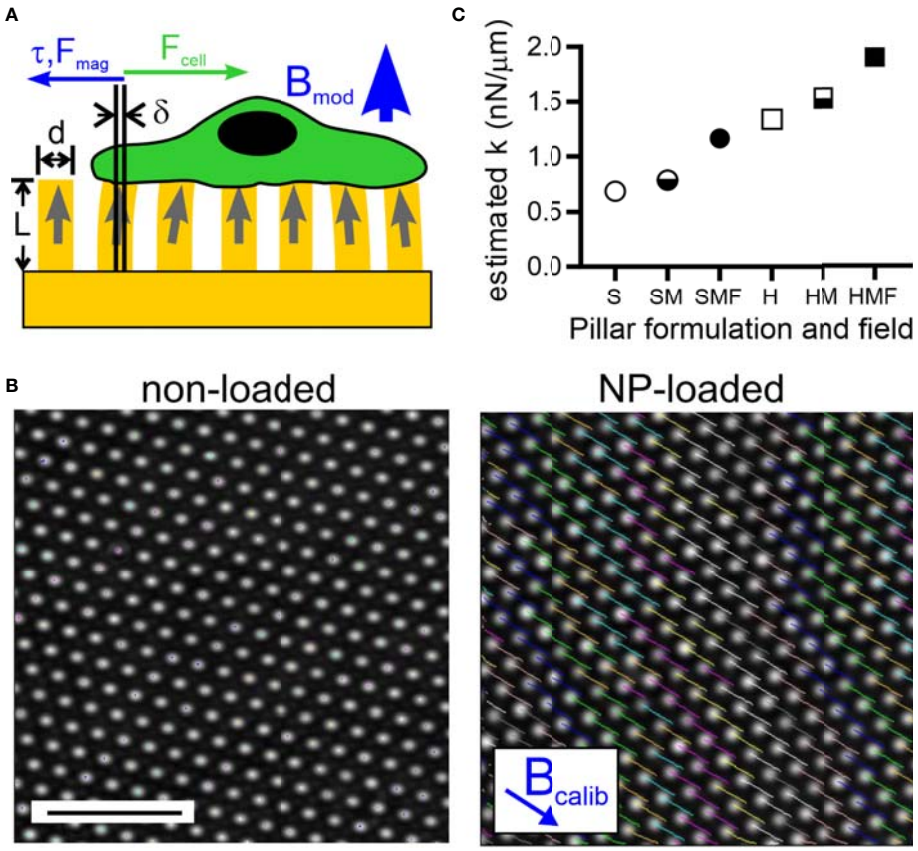

FIGURE 1 | Magnetic modulation of pillar rigidity. **(A)** A magnetic field applied perpendicularly to an array of pillars (thus along the axis of individual pillars, as indicated by B_{mod}) loaded with magnetic nanoparticles (NPs) produces a torque and associated force (τ, F_{mag}) that counter deflections, such as those induced by an adherent cell (F_{cell}). **(B)** Application of a magnetic field tangentially to the array (thus perpendicular to the axis of individual pillars, as indicated by B_{calib}) causes deflection of pillars that are loaded with NP's (right panel). Pillars without NPs do not respond to the applied field (left panel). Scale bar = 10 μm. **(C)** Estimation of the spring constant presented by individual pillars, modulated by controlling the bulk Young's modulus of elastomer used to fabricate these arrays (Soft, S, or Hard, H), loading of pillars with NPs (M), and application of a magnetic field (F).

apparent spring constant of NP-loaded pillars. This approach promises the ability to change the structural rigidity of a substrate independent of geometry or material formulation. This approach also avoids the need to introduce chemical or biomolecular agents into the system. Here, we use this magnetic actuation platform to investigate the interaction of T cells with topographically complex surfaces.

2 MATERIALS AND METHODS

2.1 Cell Culture

Mouse CD4+ T cells were isolated from the spleens of C57BL/6 mice, age 6-10 weeks. After filtering through a 40 μm mesh, naive CD4+ cells were enriched *via* negative selection using the Miltenyi $CD4^+$ T cell isolation system. Complete culture media consisted of RPMI 1640 supplemented with 10% fetal bovine serum, 10 mM HEPES, 2 mM L-glutamine, 50 μM β-mercaptoethanol (Sigma), 50 U/mL penicillin, and 50 μg/mL streptomyosin, and 50 U/mL rhIL-2 (Peprotech), all reagents from Thermo unless otherwise noted. Cells were used immediately in experiments as described below. Incubations were carried out under standard cell culture conditions (37°C, 5% CO_2/95% air). For live-cell experiments, this environment was maintained using a Tokai Hit stage top incubation system. For inhibition experiments, cells were pretreated with inhibitor in complete culture media for 15 minutes, and then seeded onto experimental surfaces. Inhibitors included Y-27632 (ROCK inhibitor, 20 μM; Sigma-Aldrich) and CK-666 (Arp2/3 inhibitor, 100 μM; Sigma-Aldrich).

2.2 Elastomer Pillar Fabrication

Arrays of elastic micropillars were fabricated following a double-casting approach described by Tan et al. (12). Briefly, masters of the microscale pillar arrays were generated by nanolithography as previously described (10, 11, 18). Each array is made up of roughly 1000 by 1000 pillars. Individual pillars are of 6 μm height and 1 μm diameter of 1 μm, spaced 2 μm center-to-center in hexagonal arrays. Negative molds, containing pits that are the negative of the pillars, were prepared by pouring polydimethylsiloxane (PDMS, Sylgard 184, Dow Corning, mixed at the manufacturer-specified elastomer base: cross-linker ratio of 10:1) onto the silicon masters then curing for 8 hours at 65°C. These negative molds were then silanized over night with (tridecafluoro-1,1,2,2,-tetrahydrooctyl)-1-trichlorosilane (United Chemical Technologies). The negative molds were used to cast PDMS pillar arrays (curing at 65°C for 8 hours) directly onto glass coverslips (thickness #0 Fisherbrand) (**Figure 3**). To release the pillars, the molds were inverted, peeled off in 100% ethanol to prevent pillar collapse, and the remaining upright pillars were washed in 3X phosphate-buffered saline (PBS).

The PDMS used to create the arrays consisted of either Sylgard 184 alone or Sylgard 527 mixed with Sylgard 184 at a ratio of 1:3 (v/v), each prepared following the manufacturers specifications (Dow Corning). The stiffness of each elastomer was estimated by indentation, using a flat cylindrical head of 8-mm diameter (D). Young's modulus (E) was calculated from the deflection of the surface (h) in response to an applied weight of specified mass (m), using the Hertizan contact model, with Poisson ratio (v) = 0.5 and gravitational field (g) = 9.81 m/sec^2,

$$E = (1 - \nu^2)m(\frac{g}{Dh})$$

The samples used for these measurements were approximately 1 cm thick, and surface deflection was less than 10% of that depth.

2.3 Magnetic Pillar Fabrication

To fabricate magnetic pillars, the negative pillar molds were loaded with superparamagnetic nanoparticles (NP, 10-nm magnetite, EMG 1200) prior to casting of PDMS. The NP solution was prepared by dissolving 0.06 g of dry powder in 3mL Toluene in a 15mL round flask using a vortexer. Then, 5mL of Hexane and 5 mL of Hexadecane were added into the solution, and the solution was poured into a Teflon beaker. A drill mixer was used to dissolve the particles into the organic solvent for 5 minutes. Then, the mixture was sonicated with a wand sonicator (Branson SFX150 Sonifier) for 5 minutes. Finally, the mixture was sonicated in a bath (Branson B1510-MT) for 20 minutes. In preparation for loading, negative molds were placed on top of a neodymium permanent magnet (DXO8B, 1" D X 1/2" H cylindrical, N52, K&J magnetics). NPs were introduced into the negative molds using multiple loading cycles. For each cycle, 15 uL of the NP solution was placed directly onto the mold tops and allowed to sit for 15 minutes. The molds were then placed in a centrifuge dish, and 10 more microliters of the NP solution added to the system. Molds were then centrifuged for 8 minutes at 3100 rcf. After completion of all loading cycles, PDMS was poured onto the molds and cured as described for the elastomer-only pillars, incorporating the NPs into the resultant structure. Preliminary experiments showed that after 8 loading cycles, NPs overflowed the cylindrical holes of the pillar molds. Targeting pillars in which the upper half is loaded with NPs, four cycles of loading were used to prepare the arrays throughout this report.

2.4 Magnetic Field Application

To calibrate the NP-loaded pillars, a magnetic field was applied tangential to the array (horizontal in **Figure 1A** and perpendicular to individual pillars) by placing a spherical permanent earth magnet (SXO, 1" D spherical, N42, K&J magnetics) approximately 8 mm from the edge of the magnet to the edge of the pillar array. This allowed for an application of a 0.4 T field onto the pillars. To modulate the apparent spring constant of the pillars, a magnetic field was applied perpendicular to the array (vertical in **Figure 1A** and along the axis of individual pillars) using a cylindrical permanent magnet (DXO8B, N52, K&J magnetics) was mounted 7 mm above the pillar array, producing a field of 0.3 T at the pillar array surface. Magnetic field strength at the array position was confirmed using a gaussmeter (PCE-MFM 3500, PCE Instruments).

This report makes the simplifying assumption that magnetic field are uniform across the area of cell culture. To approximate a uniform magnetic field, the arrays were placed in line with the

axis of the cylindrical magnet; it is recognized that the field produced by an individual, simple magnet is not completely uniform. However, the forces associated with such fields are small compared to those exerted by cells. In particular, the magnetic field along the axis of the DXO8B magnet was estimated to produce a gradient of approximately 300 Gauss/mm. For a coaxially oriented pillar with magnetic moment as described in the following section, this corresponds to a force of 1 pN, several orders of magnitude lower than those associated with cell traction forces.

2.5 Estimation of Pillar Mechanics

PDMS micropillars (not loaded with NPs) were modeled using Euler-Bernoulli beam theory (12) applied to a cylindrical beam of specified diameter (d), length (L), and material Young's modulus (E); the spring constant (k) of this structure under a bending force (F) applied to the pillar tip and producing a resultant displacement (δ) can be estimated for small deflections as

$$k_{PDMS} = \frac{F}{\delta} = \frac{3\pi E d^4}{64 L^3}$$

It is noted that the actual pillars exhibit a slight tapering, being narrower at the tip that interacts with the cells and wider at the base (**Figure 2A**). This tapering was incorporated into the fabrication process to allow better release of pillars from the molds. From images of fluorescently-labeled pillars (such as **Figure 2A**), pillars measured 1 μm diameter at a height of 2 μm from their base. It is noted that the same molds were used for all pillar formulations, so an adjustment to the spring constant calculation that would result from this slight tapering would affect all conditions equally. For this reason, all calculations were based on the design parameters of uniform, 1-μm diameter cross section, 6-μm height pillars.

Magnetic pillars were modeled as containing NPs in the upper half of each pillar, as suggested by the position of arrows indicating induced moments in **Figure 1A**. As an extreme approximation, it was considered that the NP-loaded material of each pillar is much stiffer than the non-loaded counterpart, $E_{PDMS+NP} >> E_{PDMS}$. The spring constant of these structures in the absence of magnetic field was estimated using Castigliano's method (19),

$$k_{PDMS+NP} = \frac{3\pi E d^4}{64\left(L^3 - \left(\frac{L}{2}\right)^3\right)} = \frac{3\pi E d^4}{56 L^3}$$

The impact of an applied magnetic field on NP-loaded pillars was estimated by assuming a uniform magnetic field (B) that is along the axis of an individual pillar (B_{mod} in **Figure 1A**, perpendicular to the array). In this configuration, the induced magnetic field is aligned with the applied field, producing no torque (and under the assumption of a uniform, non-diverging field, no force). An applied force (F_{cell} in **Figure 1A**) will induce a misalignment between the pillar and field, resulting in a torque, $\tau = \mu \times B$ where μ is the pillar magnetic moment. In terms of magnitude, $|\tau| = |\mu|*|B|*\sin(\theta)$ where θ is the angle between the μ and B vectors. For small displacements, $\theta \sim \delta/L$ and the resultant τ would be associated with a restoring force $F_{mag} = \tau/L$. Consequently, misalignment between μ and B results in a force F_{mag} that is proportional to the displacement δ, or

$$k_{mag} = \frac{F}{\delta} = \frac{\mu B}{L^2}$$

The total apparent spring constant of a magnetically actuated pillar is thus the sum of $k_{PDMS+NP}$ and k_{mag}.

Finally, the induced moment of NP-loaded PDMS pillars in the presence of an applied magnetic field was estimated using the framework presented by Sniadecki et al. (19). In this case, a magnetic field (B, corresponding to B_{calib} in **Figure 1B**) is applied tangential to the array (perpendicular to an individual pillar) as specified for the configuration of Sniadecki et al. This configuration induces a deflection of a magnetically loaded pillar,

$$\delta = \frac{28 L^2 \tau}{E\pi d^4} \sim \frac{28 L^2 \mu B}{E\pi d^4},$$

with the last approximation arising since in this configuration, $\sin(\theta) \sim 1$.

2.6 Substrate Preparation

Pillars were coated with fluorescently labeled streptavidin (AlexaFluor 568, Thermo Fisher) at a concentration of 20 ug/mL, and then coated with biotinylated molecules anti-CD3 and anti-CD28 antibodies (eBioscience, clones 145-2C11 and 37.51) at a concentration of 20 ug/mL each, as described in previously (5). For experiments with diluted antibodies, anti-CD3 and anti-C28 were diluted with biotinylated rat anti-human IgG Antibody (BioLegend, 410718). Each step was performed for 1 hour at room temperature followed by 3X wash with PBS. The coated pillars were then immersed in complete media before cell seeding and imaging.

2.7 Immunostaining

Immunostaining was carried out using standard techniques. To label cell membranes, cells were stained with antibodies targeting CD45.2 (AlexaFluor 488, Biolegend, clone 104) before seeding onto substrates. For fixed-cell experiments, cells were fixed at the specified time points with 4% paraformaldehyde for 15 minutes, then washed 2X with PBS. To assay TCR activation, cells were stained with a primary antibody against phosphorylated Zap70 Tyr-319 (Biolegend B282374). The pZap70 signal was measured by fluorescence microscopy on cell-by-cell basis. All samples to be compared were included in each experiment, and all were stained, imaged, and processed in the same session. For experiments where a magnetic field was applied, the magnetic field was applied throughout the total incubation period upon cell seeding.

2.8 Cytokine Assays

Assays of IL-2 secretion were carried out using a surface-capture method as previously described (20, 21). Briefly, cells were incubated with an IL-2 capture reagent from a secretion assay kit (Miltenyi Biotec) before seeding. One hour after seeding, samples were rinsed with warm (37° C) RPMI-1640 media. After

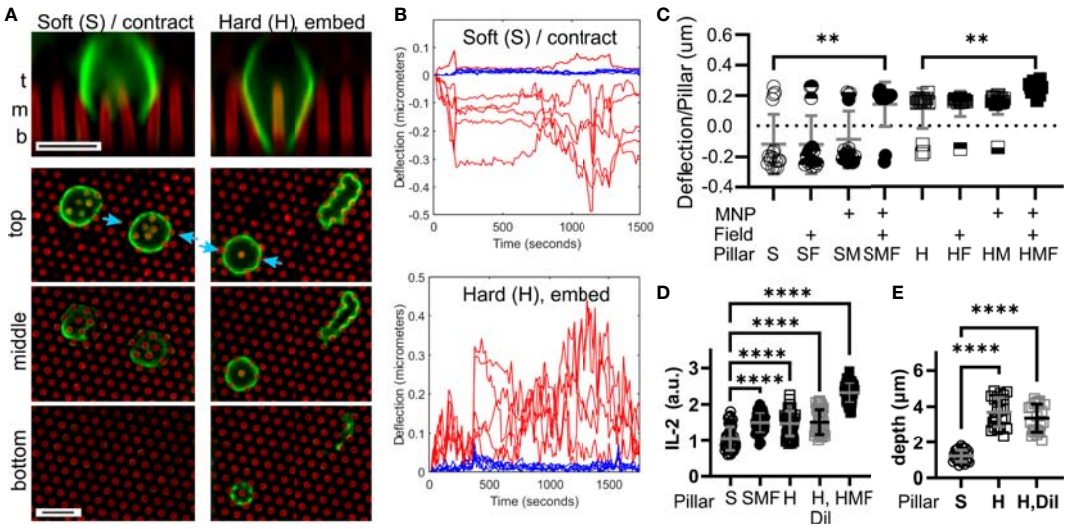

FIGURE 2 | T cells respond to the microscale rigidity of micropillar arrays. **(A)** Comparison of mouse naïve CD4$^+$ T cell interaction with arrays made of Soft (S) or Hard (H) PDMS. Focal planes representing the top, middle, and bottom of the arrays are shown, along with vertical projections collected at sites indicated by blue arrows. Cells were fixed 25 minutes after seeding, and were labeled with an anti-CD45 antibody (green). Pillars are shown in red. Scale bars = 5 μm. **(B)** Example trajectories illustrating deflections associated with a single cell on either Soft (S) or Hard (H) arrays. Red traces report deflections of individual pillars being manipulated by the cell, while blue traces illustrate movement of background pillars. These traces were derived from **Movies S1**, **S2**. Deflections towards the edge of the cell were assigned a positive sign, while those towards the cell center were negative. **(C)** Comparison of pillar deflections as a function of array formulation and magnetic field manipulation. Each data point reports the average deflection of all pillars underlying one cell. Data were compared using Kruskal-Wallis test, and only comparisons within a PDMS formulation are indicated; additional comparisons are discussed in the main text. Bars represent mean ± s.d., representing at least 15 cells per condition from 4 independent experiments. **(D)** Comparison of IL-2 secretion. Each data point represents one cell. Bars are mean ± s.d., representing at least 35 cells per condition from 3 independent experiments. **(E)** Cell penetration depth into the pillar arrays, measured by microscopy of cell morphology. Each data point represent one cell. Bars are mean ± s.d., representing at least 22 cells per condition from 3 independent experiments. Data were analyzed by ANOVA. For all analyses, **P < 0.01, ****P < 0.0001.

6 hours of incubation (37°C), cells were rinsed and incubated on ice with a fluorescently labeled antibody to IL-2. The fluorescence intensity associated with APC-labeled IL-2 was measured by fluorescence microscopy on cell-by-cell basis. All samples to be compared were included in each experiment, and all were stained, imaged, background-subtracted, and processed in the same session to allow comparison among samples. For experiments where a magnetic field was applied, the magnetic field was applied throughout the total incubation period upon cell seeding.

2.9 Data Acquisition

Images were collected using an Olympus IX-81 fluorescence microscope with an Andor iXon3 EM-CCD and equipped with a 100X/1.45 NA Plan Apochromat objective (Olympus). Illumination channels 488, 568, and 647 nm were used for visualization of lymphocytes, pillars, cytokine markers, and fluorescent proteins. MetaMorph for Olympus was used to collect images. Image processing was performed with ImageJ/Fiji. Cell activity on pillars was carried out by seeding 1 x 10^5 T cells in a 100 μl volume onto prepared pillars. Cell physical activity was recorded by live-cell microscopy in the half hour after seeding using a stage top incubator (Tokai). Images were collected at 15 second intervals over the 30-minute observation period. For experiments with magnetic field application, the custom magnetic rig was placed within the stage top incubator upon cell seeding.

Image processing was carried out using Fiji (22). Pillar displacements were tracked using the Particle Tracker plug-in (Mosaic ETH). Traces were then imported into MATLAB where background pillars were identified and cellular deflection measurements of pillars of interest were calculated. To determine the sign of a pillar deflection, pillars under the cell periphery were used to identify the cell centroid, which was denoted the center. Then, the sign of each pillar deflection was determined by calculating the dot product between the pillar displacement and vector from cell center to the specific pillar. Pillars that deflected away from the cell center were thus assigned a positive sign, while those deflected towards the cell center were given a negative sign. The average directionality was taken across the pillars under a single cell. Deconvolution of image stacks was carried out using the Deconvolution Lab plugin (23).

2.10 Statistical Analysis

Quantitative comparisons conducted using t-tests (for two conditions) and one way ANOVA (three or more conditions) for parametric data. Multiple comparisons, when justified by ANOVA, were carried out using Tukey's range test methods. Kruskal-Wallis with Dunn's multiple correction tests and Mann-Whitney tests were used for non-parametric data, as indicated

for each analysis. Statistical tests were carried out using a significance level $\alpha = 0.05$. All data is representative of at least two independent experimental runs, each of which contained multiple independent surfaces and discrete cell cultures.

2.11 Ethics Approval

The animal study was reviewed and approved by Columbia University's Institutional Animal Care and Use Committee (IACUC).

3 RESULTS

3.1 Fabrication and Characterization of Magnetic Pillar Arrays

The multi-micrometer-scale pillars often used for traction force microscopy are not suitable for use with T cells, given their comparatively small size (5 – 10 μm). As such, we adopt a standard geometry of 6-μm tall, 1-μm diameter pillars spaced in hexagonal arrays at 2 μm center-to-center spacing for this study. The small diameter of these pillars made high-occupancy loading of pillars using the nanowire approach (19) or others for fabricating larger, magnetically actuated cilia (24, 25) impractical. Instead, micro-scale magnetic structures were created by loading what will be the upper half of each elastomer with 10-nm superparamagnetic iron oxide nanoparticles (as detailed in *2.3 Magnetic Pillar Fabrication*); coupling between NPs in the presence of an applied field recapitulates the behavior of the nanowires, leading to torque generation (26). The ability of these nanoparticle-loaded pillars to respond to magnetic fields was measured using approaches developed by Sniadecki et al. (19). Specifically, a 0.4 T field placed tangential to the array (in the direction of B_{calib}, **Figure 1B**) caused the tips of NP-loaded pillars cast of the standard Sylgard 184 elastomer (Young's modulus, E, of 1.96 ± .09 MPa, mean ± s.d., n = 5, see *2.2 Elastomer Pillar Fabrication*) to deflect 1.98 ± 0.38 μm (mean ± s.d., n > 500 pillars); by comparison pillars that were not loaded with NPs showed negligible deflections. From this calibration, it was estimated (*2.5 Estimation of Pillar Mechanics*) that the application of a 0.3 T magnetic field perpendicular to the array (B_{mod} in **Figure 1A**) would impart a spring constant, k_{mag}, of 0.38 nN/μm.

Combining this approach with modulation of PDMS formulation produced a series of pillars presenting a range of estimated spring constants shown in **Figure 1C**. When cast from the standard Sylgard 184 elastomer, denoted "Hard" PDMS, the spring constant of each pillar is estimated to be 1.34 nN/μm (H in **Figure 1C**). Loading the upper half of each pillar with NPs is estimated to increase its spring constant to 1.53 nN/μm (HM, section *2.5 Estimation of Pillar Mechanics*). This calculation is based on $E_{PDMS+NP} >> E_{PDMS}$, but even with this extreme approximation, the pillar spring constant increased by only 14%. Application of the magnetic field B_{mod} (HMF in **Figure 1C**) is estimated to increase the pillar total spring constant to 1.91 nN/μm, an increase of 43% compared to the PDMS pillar. Pillars were also cast from a comparatively soft Sylgard 527 elastomer mixed 1: 3 (v/v) with Sylgard 184. This mixture, denoted "Soft", exhibited a Young's modulus of 1.01 ± .06 MPa (mean ± s.d., n = 5) yielding the pillars designated as S in **Figure 1C** along with the NP-loaded condition SM and magnetically actuated SMF. Notably, the estimated spring constant for SMF is similar to that of H, allowing comparison between pillars made of the different PDMS formulations.

3.2 T Cells Respond to Pillar Spring Constant

The ability T cells to recognize differences in macroscopic rigidity was tested using the micropillar array series defined in **Figure 1C**. Comparing the interaction of mouse naïve $CD4^+$ T cells with micropillar arrays cast from the Sylgard 184 ("Hard") and Sylgard 527 + Sylgard 184 mix ("Soft") PDMS formulations revealed two distinct types of interaction. Within minutes of contact with S arrays, T cells exhibited a contractile morphology, deflecting groups of pillar towards the center of the cell – substrate interface (**Figures 2A, B** and **Movie S1**). Cells extended processes partly into the arrays, but did not reach the bottom of the pillars. In contrast, cells on the H arrays embedded deeply between pillars, extending processes to the bottom of the arrays and pushing pillars towards the edge of the cell (**Figures 2A, B** and **Movie S2**). A lone pillar embedded inside these cells was frequently observed (vertical projection in **Figure 2A** and indicated by blue arrows), which would often be manipulated at later timepoints in the 30 minute observation period. Towards a cell-level representation of these behaviors, deflections of pillars towards the cell edge were assigned a positive sign, while those towards the cell center were negative in magnitude. These signed deflections were averaged over all pillars under a cell and used as a single measure of cell state, with positive average deflections suggesting an embedding interaction and negative reflecting a contractile state. The propensity of cells to exhibit contraction and embedding on S and H pillar arrays respectively is seen in **Figure 2C** ($P < 0.005$, Mann Whitney test). Notably, the contractile and embedding cell morphologies were stable on each substrate up to 6 hours, the longest that was examined in this report.

Comparisons of cell response across the entire pillar series addressed whether the change in cell interaction between the S and H pillars was associated with spring constant (structural rigidity) or elastomer formulation (local stiffness). For the Soft series, application of the magnetic field switched T cells from contractile to embedding interaction (S vs. SMF, **Figure 2C**). This effect was not observed for pillars either loaded with NPs (SM) or subjected to a magnetic field (SF), indicating that neither modification alone provided this effect. Notably, cell response on the SMF arrays was similar to that on the H arrays ($P > 0.99$), indicating that pillar spring constant, rather than difference in formulation between Hard and Soft PDMS was associated with promoting an embedded rather than contractile morphology. Finally, application of a magnetic field to NP-loaded Hard arrays further increased average deflection (**Figure 2C**) indicating that this effect extended to higher spring constants.

To determine if pillar spring constant had a functional impact on T cell response, we next compared secretion of the cytokine

IL-2. This was measured using a cell-surface capture assay over six hours, providing a cell-by-cell picture of activation. As shown in **Figure 2D**, the H pillars promoted a stronger IL-2 response than the S counterparts. In addition, SMF pillars exhibited IL-2 secretion that was higher than the S arrays, and similar to H, indicating that a higher spring constant induced stronger IL-2 secretion. IL-2 secretion was highest on HMF arrays ($P < 0.001$ comparison with H but not indicated on **Figure 2D**), supporting the observation that increasing spring constant produced higher activation. However, it is noted that the H arrays also promoted more interaction between cells and pillars than S (**Figure 2E**), and it is possible that simply being exposed to additional activating antibody on the pillar walls led to enhanced IL-2 secretion. To address this possibility, 46% of the activating antibodies in the coating solution was replaced with an inert counterpart, reflecting the difference in process extension depth between S and H surfaces (**Figure 2E**). This dilution had no effect on IL-2 secretion or process extension length (**Figures 2D, E**), indicating that simply access to activating antibody does not explain the observed differences.

Towards molecular insights into T cell sensing of pillar rigidity, Zap70 activation was compared 15 minutes after seeding onto the substrates. On the soft S arrays, phospho-Zap70 (pZap70, Tyr319) was localized in small clusters along the cell membrane (**Figure 3A**). On H arrays, membrane localization was more uniform, conforming with the cell shape

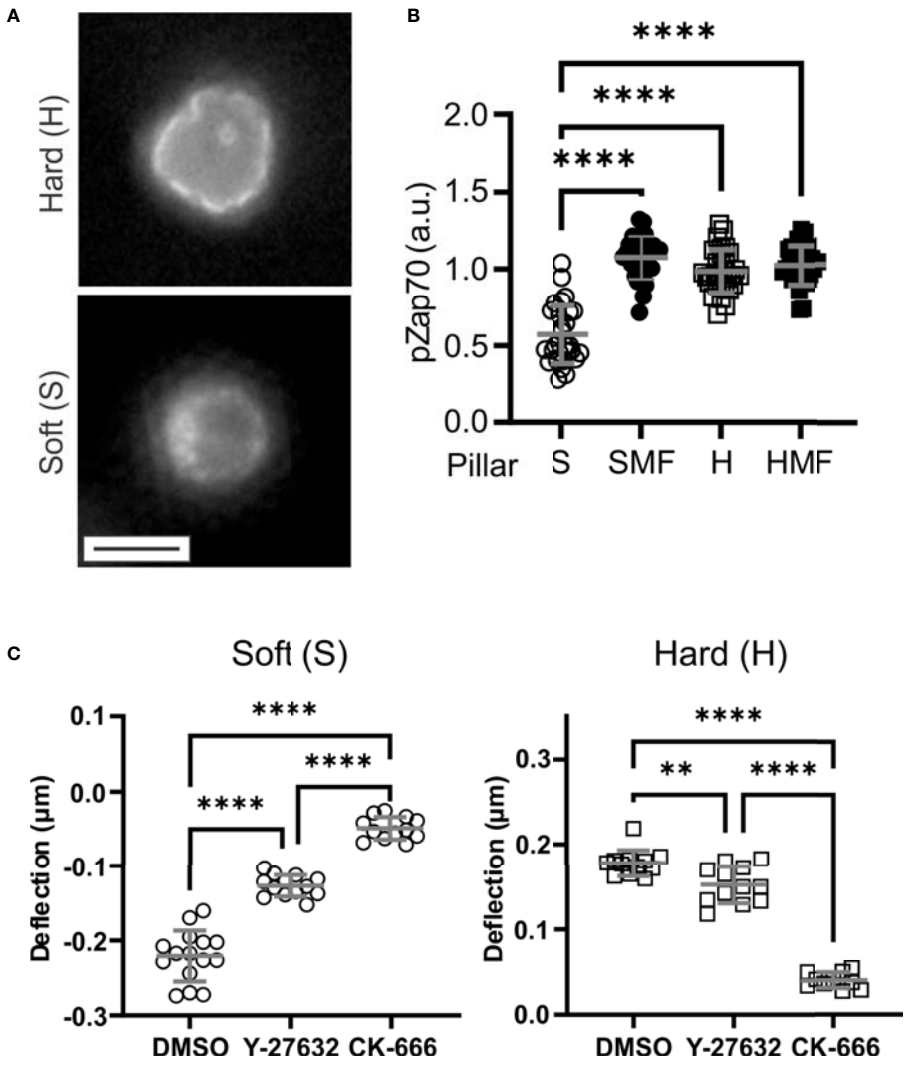

FIGURE 3 | Molecular mechanisms of T cell mechanosensing. **(A)** Distribution of phsopho-Zap70 (Tyr 319). Cells were fixed 15 minutes after seeding. These images illustrate a plane through cells at the pillar tips. Scale bar = 5 µm. **(B)** Quantitative comparison of pZap70. Each data point represents an individual cell, and bars report mean ± s.d., from at least 30 cells per condition from 3 independent experiments. Only significant comparisons with the Soft (S) condition are indicated; additional comparison are reported in the main text. **(C)** Effect of inhibitors of cytoskeletal dynamics on pillar deflection. Each data point represents an individual cell, and bars report mean ± s.d., from at least 15 cells per condition from 3 independent experiments. DMSO = vehicle control for both inhibitors. For all panels, data were analyzed by one way ANOVA; **$P < 0.01$, ****$P < 0.0001$.

and even around pillars that protruded into the cells. Total pZap70 staining, measured on a cell-by-cell basis, was higher on more rigid SMF, H, and HMF conditions (**Figure 3B**), mirroring the wider localization suggests by microscopy. This result suggests that increased spring constant is associated with stronger TCR activation. However, no difference was detected between the HMF and SMF or H formulations. This was unexpected since HMF promoted higher IL-2 secretion than the other two systems, and suggests that additional aspects of cell signaling, such as duration of Zap70 phosphorylation or recruitment of alternative pathways, are involved in T cell mechanosensing sensing.

3.3 Actin Polymerization Contributes to T Cell Embedding

This final section explores the systems of cytoskeletal dynamics that are involved with the ability of T cells to conform to and manipulate the pillar arrays. This was carried out by pretreating T cells with inhibitors of actin dynamics before seeding on arrays. Inhibition of Apr2/3-mediated actin polymerization with CK-666 largely abrogated pillar deflection on both S and H surfaces (**Figure 3C**). The effect was more pronounced on the H surfaces, for which cells did not embed into the micropillar arrays; cells on the S surfaces remained on the pillar tops. Pretreatment with the Rho/ROCK inhibitor Y-27632 had a smaller effect on cells, reducing pillar deflections but not to the same extent as CK-666. In addition, cells on the H surfaces in the presence of Y-27632 were able to reach the bottom of the arrays. These results indicate a major role of actin polymerization in both contractile and embedding morphologies. We note that these results do not consider all pathways modulating actomyosin contractility in T cells, and indeed blebbistatin is often included as an inhibitor for studies of mechanosensing (5). However, the hydrophobic characteristic of blebbistatin makes its use in the presence of PDMS substrates, which absorb hydrophobic molecules, problematic; for this reason, inhibition of contractility through this mechanism was not explored in the present study.

4 DISCUSSION

Forces play increasingly recognized roles in T cell activation at many levels of organization. At the molecular level, mechanical loading of the TCR – Major Histocompatibility Complex (MHC) alters bond lifetime revealing a catch-bond behavior for specific subsets of interactions (27–29). Complementary studies using substrate-immobilized anti-CD3 and anti-CD28 revealed a cell-wide role of forces, in which forces applied to CD3 leads to TCR activation and the ability of T cells to sense the mechanical stiffness of an underlying substrate (3, 5, 30–33); the TCR-pMHC catch binds is an additional layer of complexity over this CD3 mechanical response. However, studies of T cell mechanosensing, like those for other cell types (34, 35), rely predominantly on hydrogels (such as polyacrylamide (PA) or alginate) or PDMS elastomer. These two systems provide different capabilities and benefits for mechanosensing studies, but neither is without complications (16). Many of these considerations center around the concept that changing mechanical stiffness involves altering the concentration of components (such as crosslinkers) if not the formulation itself. The use of photoactive crosslinkers, bivalent ions, and nucleic acid chains to alter stiffness provide evidence that mechanosensing is independent of chemical formulation, but do not completely address this question. The use of an applied magnetic field to alter rigidity avoids the use of chemical and exposure to light, and promises reversible, rapid modulation. Our system is a first demonstration of this approach, seen most directly in the difference in response between SM and SMF arrays (**Figure 2C**). This approach also avoids considerations that changing the pillar dimensions many have on cell response (10, 13, 15); we anticipate that the system presented here can be used for other cell types, including fibroblasts, epithelial cells, and stem cells.

Magnetic manipulation of pillar spring constant along with changing PDMS formulation also demonstrated that T cells are sensitive to structural rigidity; while nanoscale, molecular effects such as catch bonds influence signaling, the mechanical resistance of a system at the scale of micrometers can be recognized by these cells. The S configuration represents low material stiffness and structural rigidity, promoting a contractile response from cells. Cytoskeletal inhibition assays suggest that branching actin polymerization contributes to this morphology, potentially by promoting centripetal flow of material from the cell edge towards the center. Inhibition of actomyosin contractility (through the Rho/ROCK inhibitor Y-27632) also reduced inward pillar deflection, supporting the concept that these systems interact in defining the cytoskeletal state of T cells. Increasing pillar spring constant by either magnetic manipulation (SMF) or using a stiffer PDMS (H) increased cell activation as evidenced by increased IL-2 secretion. This was accompanied by a switch to the embedding morphology, which resembles amoeboid migration of T cells which is dependent on robust polymerization of actin through Arp2/3. Such polymerization would underlie the observed extension of processes between pillars and deflection of pillars away from the cell center as supported by experiments of CK-666 inhibition on the H arrays. It is recognized that T cell activation is a complex process, and full understanding of how nanoscale, molecular mechanosensing and microscale structural rigidity influence each other remains incomplete. Further studies using the tools introduced here could shed new light into signaling withing the complex T cell – APC interface, as well as provide new strategies for designing biomaterials that modulate adaptive immunity.

DATA AVAILABILITY STATEMENT

The raw data supporting the conclusions of this article will be made available by the authors, without undue reservation.

ETHICS STATEMENT

The animal study was reviewed and approved by Institutional Animal Care and Use Committee, Columbia University.

AUTHOR CONTRIBUTIONS

CS and LK designed the study and also carried out data collection and analysis. CS conducted the experiments. All authors contributed to the article and approved the submitted version.

FUNDING

This work was supported in part by the National Institutes of Health (R21AI119953 and R01AI110593 to LK).

ACKNOWLEDGMENTS

The authors thank Dr. Charles T. Black (Brookhaven National Laboratory) for assistance in fabrication of the master substrates.

This research used resources of the Center for Functional Nanomaterials, a U.S. DOE Office of Science Facility at Brookhaven National Laboratory operated under Contract No. DE-SC0012704.

SUPPLEMENTARY MATERIAL

The Supplementary Material for this article can be found online at: https://www.frontiersin.org/articles/10.3389/fimmu.2021.704693/full#supplementary-material

Supplementary Movie S1 | Manipulation of pillars by a cell exhibiting a contractile interaction. This video shows motion of pillar tops being manipulated by a cell on a Soft (S) array. Timestamp is in MM : SS, and scale bar = 5 μm.

Supplementary Movie S2 | Manipulation of pillars by a cell exhibiting an embeddinginteraction. This video shows motion of pillar tops being manipulated by a cell on a Hard (H) array. Timestamp is in MM : SS, and scale bar = 5 μm.

REFERENCES

1. Dang AP, De Leo S, Bogdanowicz DR, Yuan DJ, Fernandes SM, Brown JR, et al. Enhanced Activation and Expansion of T Cells Using Mechanically Soft Elastomer Fibers. *Adv Biosyst* (2018) 2:1700167. doi: 10.1002/adbi.201700167
2. Lambert LH, Goebrecht GK, De Leo SE, O'Connor RS, Nunez-Cruz S, Li TD, et al. Improving T Cell Expansion With a Soft Touch. *Nano Lett* (2017) 17:821–6. doi: 10.1021/acs.nanolett.6b04071
3. O'Connor RS, Hao X, Shen K, Bashour K, Akimova T, Hancock WW, et al. Substrate Rigidity Regulates Human T Cell Activation and Proliferation. *J Immunol* (2012) 189:1330–9. doi: 10.4049/jimmunol.1102757
4. Wahl A, Dinet C, Dillard P, Nassereddine A, Puech PH, Limozin L, et al. Biphasic Mechanosensitivity of T Cell Receptor-Mediated Spreading of Lymphocytes. *Proc Natl Acad Sci USA* (2019) 116:5908–13. doi: 10.1073/pnas.1811516116
5. Judokusumo E, Tabdanov E, Kumari S, Dustin ML, Kam LC. Mechanosensing in T Lymphocyte Activation. *Biophys J* (2012) 102:L5–7. doi: 10.1016/j.bpj.2011.12.011
6. Sage PT, Varghese LM, Martinelli R, Sciuto TE, Kamei M, Dvorak AM, et al. Antigen Recognition is Facilitated by Invadosome-Like Protrusions Formed by Memory/Effector T Cells. *J Immunol* (2012) 188:3686–99. doi: 10.4049/jimmunol.1102594
7. Ueda H, Morphew MK, McIntosh JR, Davis MM. CD4+ T-Cell Synapses Involve Multiple Distinct Stages. *Proc Natl Acad Sci* (2011) 108:17099–104. doi: 10.1073/pnas.1113703108
8. Basu R, Whitlock BM, Husson J, Le Floc'h A, Jin W, Oyler-Yaniv A, et al. Cytotoxic T Cells Use Mechanical Force to Potentiate Target Cell Killing. *Cell* (2016) 165:100–10. doi: 10.1016/j.cell.2016.01.021
9. Chaudhuri PK, Wang MS, Black CT, Huse M, Kam LC. Modulating T Cell Activation Using Depth Sensing Topographic Cues. *Adv Biosyst* (2020) 4:e2000143. doi: 10.1002/adbi.202000143
10. Jin W, Tamzalit F, Chaudhuri PK, Black CT, Huse M, Kam LC. T Cell Activation and Immune Synapse Organization Respond to the Microscale Mechanics of Structured Surfaces. *Proc Natl Acad Sci USA* (2019) 116:19835–40. doi: 10.1073/pnas.1906986116
11. Tamzalit F, Wang MS, Jin W, Tello-Lafoz M, Boyko V, Heddleston JM, et al. Interfacial Actin Protrusions Mechanically Enhance Killing by Cytotoxic T Cells. *Sci Immunol* (2019) 4:eaav5445. doi: 10.1126/sciimmunol.aav5445
12. Tan JL, Tien J, Pirone DM, Gray DS, Bhadriraju K, Chen CS. Cells Lying on a Bed of Microneedles: An Approach to Isolate Mechanical Force. *Proc Natl Acad Sci USA* (2003) 100:1484–9. doi: 10.1073/pnas.0235407100
13. Fu J, Wang YK, Yang MT, Desai RA, Yu X, Liu Z, et al. Mechanical Regulation of Cell Function With Geometrically Modulated Elastomeric Substrates. *Nat Methods* (2010) 7:733–6. doi: 10.1038/nmeth.1487
14. Saez A, Buguin A, Silberzan P, Ladoux B. Is the Mechanical Activity of Epithelial Cells Controlled by Deformations or Forces? *Biophys J* (2005) 89:L52–4. doi: 10.1529/biophysj.105.071217
15. Saez A, Ghibaudo M, Buguin A, Silberzan P, Ladoux BT. Rigidity-Driven Growth and Migration of Epithelial Cells on Microstructured Anisotropic Substrates. *Proc Natl Acad Sci* (2007) 104:8281–6. doi: 10.1073/pnas.0702259104
16. Trappmann B, Gautrot JE, Connelly JT, Strange DG, Li Y, Oyen ML, et al. Extracellular-Matrix Tethering Regulates Stem-Cell Fate. *Nat Mater* (2012) 11:642–9. doi: 10.1038/nmat3339
17. Sniadecki NJ, Anguelouch A, Yang MT, Lamb CM, Liu Z, Kirschner SB, et al. Magnetic Microposts as an Approach to Apply Forces to Living Cells. *Proc Natl Acad Sci* (2007) 104:14553–8. doi: 10.1073/pnas.0611613104
18. Bashour KT, Gondarenko A, Chen H, Shen K, Liu X, Huse M, et al. CD28 and CD3 Have Complementary Roles in T-Cell Traction Forces. *Proc Natl Acad Sci USA* (2014) 111:2241–6. doi: 10.1073/pnas.1315606111
19. Sniadecki NJ, Lamb CM, Liu Y, Chen CS, Reich DH. Magnetic Microposts for Mechanical Stimulation of Biological Cells: Fabrication, Characterization, and Analysis. *Rev Sci Instruments* (2008) 79:044302. doi: 10.1063/1.2906228
20. Shen K, Thomas VK, Dustin ML, Kam LC. Micropatterning of Costimulatory Ligands Enhances CD4+ T Cell Function. *Proc Natl Acad Sci* (2008) 105:7791–6. doi: 10.1073/pnas.0710295105
21. Sims TN, Soos TJ, Xenias HS, Dubin-Thaler B, Hofman JM, Waite JC, et al. Opposing Effects of PKCθ and WASp on Symmetry Breaking and Relocation of the Immunological Synapse. *Cell* (2007) 129:773–85. doi: 10.1016/j.cell.2007.03.037
22. Schindelin J, Arganda-Carreras I, Frise E, Kaynig V, Longair M, Pietzsch T, et al. Fiji: An Open-Source Platform for Biological-Image Analysis. *Nat Methods* (2012) 9:676–82. doi: 10.1038/nmeth.2019
23. Sage D, Donati L, Soulez F, Fortun D, Schmit G, Seitz A, et al. DeconvolutionLab2: An Open-Source Software for Deconvolution Microscopy. *Methods* (2017) 115:28–41. doi: 10.1016/j.ymeth.2016.12.015
24. le Digabel J, Biais N, Fresnais J, Berret JF, Hersen P, Ladoux B. Magnetic Micropillars as a Tool to Govern Substrate Deformations. *Lab chip* (2011) 11:2630–6. doi: 10.1039/c1lc20263d
25. Wang Y, Gao Y, Wyss H, Anderson P, den Toonder J. Out of the Cleanroom, Self-Assembled Magnetic Artificial Cilia. *Lab Chip* (2013) 13:3360–6. doi: 10.1039/c3lc50458a
26. Lockette PV, Lofland SE, Biggs J, Roche J, Mineroff J, Babcock M. Investigating New Symmetry Classes in Magnetorheological Elastomers: Cantilever Bending Behavior. *Smart Mater Structures* (2011) 20:105022. doi: 10.1088/0964-1726/20/10/105022
27. Hong J, Ge C, Jothikumar P, Yuan Z, Liu B, Bai K, et al. A TCR Mechanotransduction Signaling Loop Induces Negative Selection in the Thymus. *Nat Immunol* (2018) 19:1379–90. doi: 10.1038/s41590-018-0259-z

28. Hong J, Persaud SP, Horvath S, Allen PM, Evavold BD, Zhu C. Force-Regulated In Situ TCR-Peptide-Bound MHC Class II Kinetics Determine Functions of CD4+ T Cells. *J Immunol* (2015) 195:3557–64. doi: 10.4049/jimmunol.1501407
29. Liu B, Chen W, Evavold BD, Zhu C. Accumulation of Dynamic Catch Bonds Between TCR and Agonist Peptide-MHC Triggers T Cell Signaling. *Cell* (2014) 157:357–68. doi: 10.1016/j.cell.2014.02.053
30. Hu KH, Butte MJ. T Cell Activation Requires Force Generation. *J Cell Biol* (2016) 213:535–42. doi: 10.1083/jcb.201511053
31. Kim ST, Takeuchi K, Sun ZY, Touma M, Castro CE, Fahmy A, et al. The Alphabeta T Cell Receptor is an Anisotropic Mechanosensor. *J Biol Chem* (2009) 284:31028–37. doi: 10.1074/jbc.M109.052712
32. Li YC, Chen BM, Wu PC, Cheng TL, Kao LS, Tao MH, et al. Cutting Edge: Mechanical Forces Acting on T Cells Immobilized via the TCR Complex can Trigger TCR Signaling. *J Immunol* (2010) 184:5959–63. doi: 10.4049/jimmunol.0900775
33. Liu Y, Blanchfield L, Ma VP, Andargachew R, Galior K, Liu Z, et al. DNA-Based Nanoparticle Tension Sensors Reveal That T-Cell Receptors Transmit Defined pN Forces to Their Antigens for Enhanced Fidelity. *Proc Natl Acad Sci USA* (2016) 113:5610–5. doi: 10.1073/pnas.1600163113
34. Engler AJ, Sen S, Sweeney HL, Discher DE. Matrix Elasticity Directs Stem Cell Lineage Specification. *Cell* (2006) 126:677–89. doi: 10.1016/j.cell.2006.06.044
35. Pelham RJJr., Wang Y-L. Cell Locomotion and Focal Adhesions are Regulated by Substrate Flexibility. *Proc Natl Acad Sci* (1997) 94:13661–5. doi: 10.1073/pnas.94.25.13661

Conflict of Interest: The authors declare that the research was conducted in the absence of any commercial or financial relationships that could be construed as a potential conflict of interest.

frontiers in Immunology

REVIEW
published: 20 September 2021
doi: 10.3389/fimmu.2021.730982

TRPing on Cell Swelling - TRPV4 Senses It

Trine L. Toft-Bertelsen * *and Nanna MacAulay*

Department of Neuroscience, University of Copenhagen, Copenhagen, Denmark

The transient receptor potential vanilloid 4 channel (TRPV4) is a non-selective cation channel that is widely expressed and activated by a range of stimuli. Amongst these stimuli, changes in cell volume feature as a prominent regulator of TRPV4 activity with cell swelling leading to channel activation. In experimental settings based on abrupt introduction of large osmotic gradients, TRPV4 activation requires co-expression of an aquaporin (AQP) to facilitate such cell swelling. However, TRPV4 readily responds to cell volume increase irrespectively of the molecular mechanism underlying the cell swelling and can, as such, be considered a sensor of increased cell volume. In this review, we will discuss the proposed events underlying the molecular coupling from cell swelling to channel activation and present the evidence of direct *versus* indirect swelling-activation of TRPV4. With this summary of the current knowledge of TRPV4 and its ability to sense cell volume changes, we hope to stimulate further experimental efforts in this area of research to clarify TRPV4's role in physiology and pathophysiology.

Keywords: TRPV4 (transient receptor potential vanilloid 4), volume-sensitive channels, volume regulation, osmo-sensing, aquaporins (AQPs)

OPEN ACCESS

Edited by:
Shizuya Saika, Wakayama Medical University Hospital, Japan

Reviewed by:
Kenjiro Matsumoto, Kyoto Pharmaceutical University, Japan
Feng Qin, University at Buffalo, United States
Sailaja Paruchuri, University of Toledo Medical Center, United States

***Correspondence:**
Trine L. Toft-Bertelsen
trineto@sund.ku.dk

Specialty section:
This article was submitted to Molecular Innate Immunity, a section of the journal Frontiers in Immunology

Received: *25 June 2021*
Accepted: *30 August 2021*
Published: *20 September 2021*

Citation:
Toft-Bertelsen TL and MacAulay N (2021) TRPing on Cell Swelling - TRPV4 Senses It. Front. Immunol. 12:730982. doi: 10.3389/fimmu.2021.730982

CELLULAR DETECTION OF VOLUME CHANGES

Accurate and rapid sensing of the surrounding environment is key to survival for cells and organisms. Upon exposure to challenges that alter the cell volume, cellular regulatory mechanisms required for an appropriate physiological reaction to the condition causing cell swelling or shrinkage are set in motion.

The Discovery of TRPV4

Detection of cell volume changes is perceived through sensory mechanisms, one of which was characterized in the invertebrates *Drosophila melanogaster* and *Caenorhabditis elegans* (1). Organisms with mutations in *osm-9* or *ocr-2*, which are genes encoding ion channels belonging to the transient receptor potential (TRP) channel superfamily, the vanilloid subfamily (TRPV) (2–4), were unable to produce cellular responses to stimuli leading to cell volume changes (1, 5). Such genes had at that point not been identified in vertebrate cells, and the search for mammalian homologues of *osm-9* was on.

In the year 2000, an ion channel was described that related to *osm-9* and VRL-1 (vanilloid receptor-like 1 protein, or TRPV2, a member of the vanilloid subfamily) and was gated by osmotic challenges (6). This ion channel, now known as TRPV4, was, using a combination of *in silico* analysis of expressed sequence tag databases and conventional molecular cloning, isolated as a novel

vanilloid-like receptor from the human kidney (7). At the time, the channel was named VRL-2 due to its resemblance to VRL-1 (or TRPV2), a homologue of the capsaicin receptor, a heat-activated ion channel in the pain pathway (8) with a high threshold for noxious heat, and later known as VR-OAC (*v*anilloid *r*eceptor *r*elated *o*smotically *a*ctivated *c*hannel) (6). VRL-2 was subsequently identified in mouse, chicken and rat (6, 7, 9, 10).

The TRP Family and Biophysical Properties

The TRP superfamily is grouped into six major subfamilies based on nucleotide sequence homology: TRPA (ankyrin); TRPC (canonical); TRPM (melastin); TRPML (mucolipin); TRPP (polycystin) and TRPV (vanilloid), the latter of which can further be subdivided into six isoforms (TRPV1-6). TRPV4 has 871 amino acid residues and topological features of the channel are six transmembrane spanning segments (S1-S6), a re-entrant pore forming loop between S5-S6, intracellular N- and C-termini, and ankyrin domains in the cytosolic N-terminus (11). The channel preferentially forms homomers (12), although heteromers may occur with other members of the TRP superfamily (13–15). Biophysically, TRPV4 is characterized as a non-selective cation channel with a moderately high Ca^{2+} permeability ratio of PCa/PNa = 6-10 (16–18) with two aspartate residues (Asp^{672} and Asp^{682}) dictating the Ca^{2+} selectivity of the TRPV4 pore (16). Cryo-EM studies demonstrated that the narrowest part of the TRPV4 selectivity filter had a wider diameter than the pore of the open TRPV1 channel (19). In addition, TRPV4 appears to lack an extracellular gate (19), which, taken together, allows for a broader variety of permeant ions (20). It remains unresolved whether the reported physiological TRPV4 activators work through the selectivity filter of TRPV4 to activate the channel (20).

TRPV4 as an Osmo-Sensor

TRPV4 was defined as a nonspecific cation channel gated by osmotic stimuli (2–4) and characterized as such as such from a study done in TRPV4-transfected CHO cells (21). The cells were exposed to osmotic challenges of ± 110 mOsm, and a robust Ca^{2+} transient was observed within seconds of a cell volume increase. Such hyposmotically-induced gating was proposed to take place *via* subtle changes in membrane tension (22, 23). Swelling-induced activation of TRPV4-mediated Ca^{2+} influx was shortly thereafter confirmed in HEK293 cells expressing 'OTRPC4' (*osm9*-like *t*ransient *r*eceptor *p*otential *c*hannel, member *4*, another name for TRPV4) (9). Hence, TRPV4 was set forward as an osmo-sensor activated by hyposmolar stress. The physiological impact of TRPV4-mediated osmosensing was demonstrated by the impaired regulation of systemic tonicity in mice genetically devoid of TRPV4 (24, 25). The dysregulation of the systemic fluid homeostasis in the $TRPV4^{-/-}$ mice arose, at least in part, from impaired osmosensing in the circumventricular organ of the lamina terminalis and associated modification of antidiuretic hormone (ADH) secretion into the blood (24, 25). The $TRPV4^{-/-}$ mice thus displayed lesser water intake (24, 25) and, in addition, presented with enlarged bladder capacity as a consequence of impaired stretch and pressure sensing in the bladder wall (25, 26). TRPV4 has, in addition, been implicated in pulmonary edema formation, partly *via* the observed down regulation of the co-localized AQP5 in the pulmonary epithelium obtained from $TRPV4^{-/-}$ mice (27). Tissue obtained from meningioma patients demonstrated AQP4/TRPV4 co-expression in both edematous and non-edematous meningiomas, although in the surrounding peri-meningioma tissue, only AQP4 was upregulated (28). TRPV4 thus appears to be involved in physiological and pathophysiological processes involving fluid dynamics, in addition to its roles in skeletal dysplasias [for review of TRPV4 in pathology, see (29)]. However, the coupling between cell volume regulation and TRPV4 activity remains elusive.

TRPV4 Is a Genuine Sensor of Cell Volume Dynamics

Since the initial findings, swelling-induced activation of TRPV4 has been further documented upon heterologous expression of TRPV4 in yeast (30, 31) and in *Xenopus laevis* oocytes (30, 32, 33). In its native setting in retinal cells, TRPV4 responded to cell swelling with slow-onset, but sustained, activity in Müller glia, whereas in retinal ganglion neurons, TRPV4 responded with fast, but brief, bursts of activity (33, 34). Astrocytes respond to hyposmotically-induced cell swelling with TRPV4-mediated Ca^{2+} dynamics, which were proposed to be implicated in the subsequent regulatory volume decrease (35). However, during a more physiologically relevant astrocytic volume transient, as that observed during neuronal activity (in the absence of an experimentally-inflicted osmotic challenge) (36), the regulatory volume decrease was unaffected by TRPV4 inhibition, **Figure 1** (37). The molecular coupling between the altered osmolarity of the extracellular fluid and activation of TRPV4 was proposed to require the presence of an aquaporin, possibly even of a certain isoform: In renal cells; AQP2 (38), in salivary glands; AQP5 (39), and in astrocytes; AQP4 (35, 40, 41). However, these conclusions arose from experimental approaches based on abrupt exposure of the TRPV4-expressing cells to excessively large osmotic gradients of 100-250 mOsm. Such osmotic gradients will rarely, if ever, be observed outside the kidney in physiology or even pathophysiology – and not as an abruptly arising challenge. Still, the introduction of such non-physiological osmotic challenges is a common manner of experimental induction of cell volume changes for reasons of technical ease. Under such experimental conditions, *the rate* with which the cells swell upon an introduced osmotic challenge will depend on expression of an AQP of any isoform. Experiments employing such osmotic gradients will thus favor a concept of TRPV4 requiring the presence of an AQP to respond to a volume change (21, 32, 35, 39), see (37) for discussion of technical challenges with such experimental approaches. Notably, with smaller osmotic challenges (of the order of 20-40 mOsm) that promote cell swelling of a more physiological caliber, TRPV4-mediated Ca^{2+} dynamics vanished from retinal ganglion cells, but persisted in the Muller glia (33).

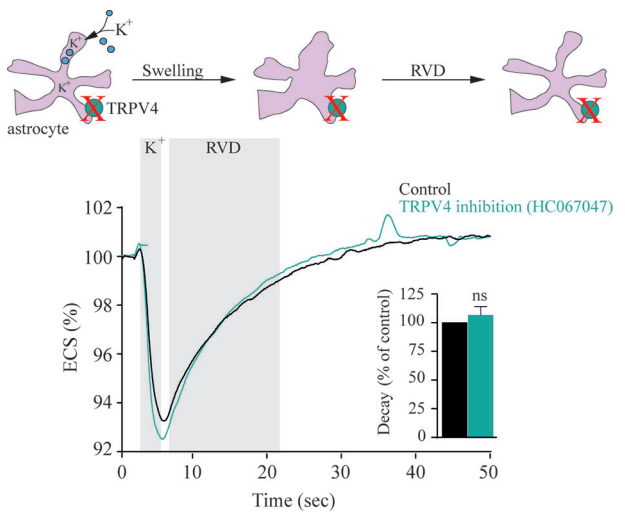

FIGURE 1 | TRPV4 does not modulate astrocytic regulatory volume decrease following activity evoked astrocyte volume dynamics. Electrical stimulation of acute hippocampal slices from rats results in neuronal activity associated with a $[K^+]_o$ transient that leads to a brief change in cell volume of nearby astrocytic structures without application of an osmotic gradient to the test solution. Graphs illustrate a representative recording and summarized volume decay rates of the activity-evoked extracellular space dynamics in the absence or presence of a TRPV4 inhibitor [1 μM HC067047, same results obtained with the less specific TRPV4 inhibitor ruthenium red (1 μM)]. ns, not significant. Modified from (37) with permission.

To resolve the ability of TRPV4 to sense altered osmolarity *versus* simply the resulting cell changes, TRPV4 was heterologously expressed in *Xenopus laevis* oocytes with notoriously low intrinsic water permeability, either alone or co-expressed with an AQP (32). Introduction of a hyposmotic challenge led to abrupt cell swelling in the TRPV4-AQP-expressing oocytes and a resulting TRPV4-mediated membrane current, irrespective of the AQP isoform (32). None of these observations were detected in oocytes expressing TRPV4 alone (in the absence of an AQP), demonstrating that TRPV4 responded to the cell volume increase rather than the introduced osmotic challenge itself, **Figure 2** (32). These data are consistent with other reports in cortical and retinal glia, concluding that membrane expression of an AQP permitted a rapid cell swelling upon experimentally-inflicted osmotic challenges and thus allowed TRPV4 to respond to the resulting abrupt cell swelling (41, 42). This notion was cemented by a demonstration that swelling of TRPV4-expressing oocytes achieved without introduction of an osmotic challenge and in the absence of AQP co-expression sufficed to activate TRPV4, **Figure 3** (32). Such oocyte cell swelling was achieved by co-expression of a water-translocating cotransporter, the Na^+, K^+, $2Cl^-$ cotransporter (NKCC1), which upon activation leads to cell swelling by inward transport of its substrates along with a fixed number of water molecules (43, 44). TRPV4 is thereby established as a genuine volume-sensor, rather than an osmo-sensor (32), possibly induced by the membrane stretch achieved as a consequence of cell swelling (6, 24, 45). At the time, the molecular mechanisms coupling cell swelling to TRPV4 channel opening remained obscure.

FROM CELL SWELLING TO TRPV4 ACTIVATION

TRPV4 represents a sensor of cell swelling. The underlying molecular link between cell swelling and channel opening has proven elusive, but can occur either directly or *via* an indirect pathway of cellular modulators.

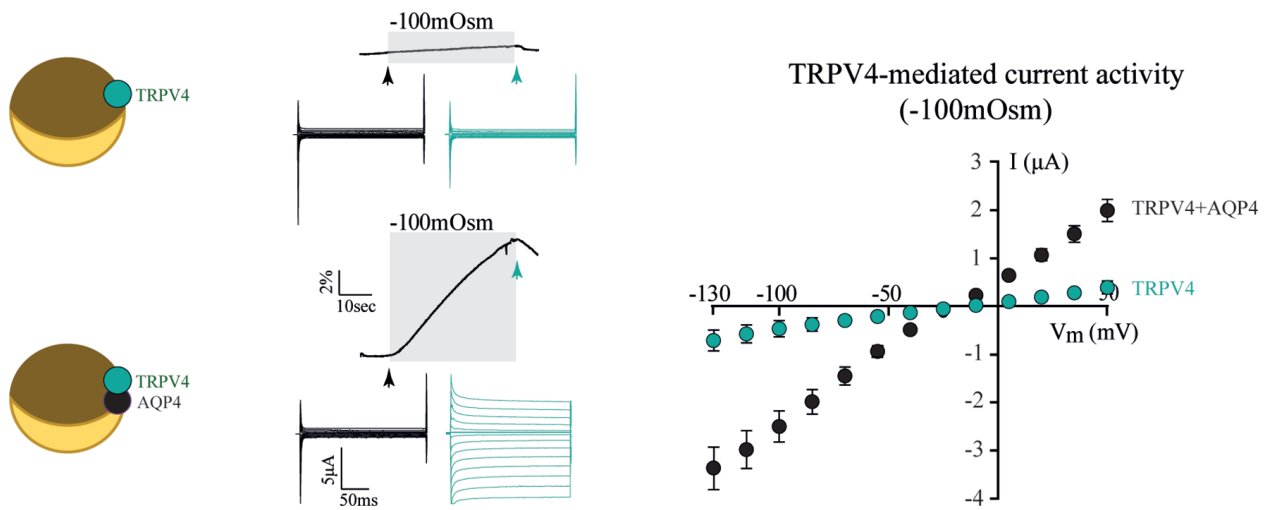

FIGURE 2 | TRPV4 is activated by increased cell volume. Oocytes expressing TRPV4 alone (top traces) did not swell when exposed to a hyposmotic gradient (-100 mOsm) and did not respond with TRPV4-mediated currents during this challenge. Oocytes co-expressing TRPV4 and AQP4 (bottom traces) responded to the osmotic challenge with an abrupt volume increase and a resultant large membrane current (summarized in right panel). Modified from (32) with permission.

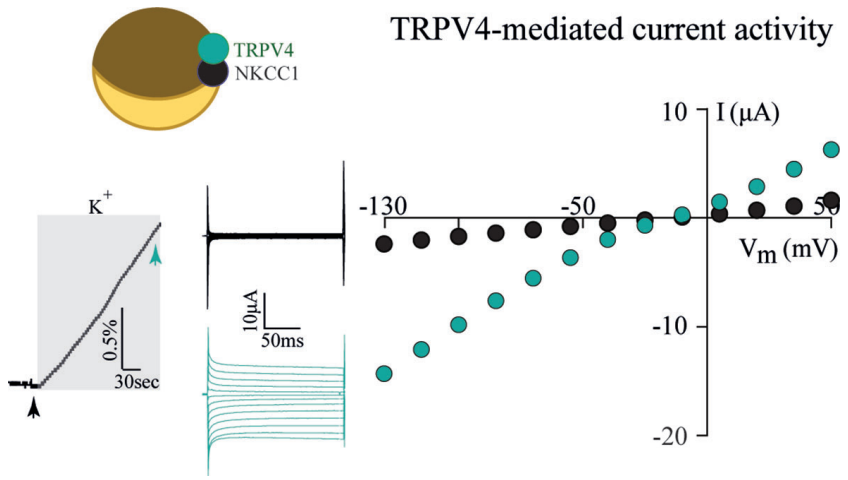

FIGURE 3 | TRPV4 is activated by cell swelling, independently of AQPs and osmotic gradients. The water-transporting cotransporter NKCC1, co-expressed with TRPV4 in *Xenopus* oocytes, was activated by exposure to K^+ (15 mM, equimolar replacement of Na^+). This transporter activation led to a rapid volume increase (left panel) in the absence of an external introduction of an osmotic gradient. This cell volume increase promoted TRPV4 activation in the form of TRPV4-mediated currents (middle and right panels). Modified from (32) with permission.

Direct Coupling of Cell Volume Changes to TRPV4 Activation

TRPV4 Gating *via* Mechanical Probing *Versus* Cell Volume Increase

Cell swelling may modulate TRPV4 gating in a more or less direct manner, or the resulting membrane stretch may serve as a mechanical disturbance that could be distinguished from the cellular volume dynamics. Various experimental strategies have been employed to distinguish the two, i.e. stretching of the cell membrane in the absence of a volume change (46–48) which has been employed to demonstrate (49–51) or not to demonstrate (9, 52, 53) direct activation of TRPV4 by mechanical probing. It therefore remains unresolved to what extent TRPV4 activation occurs by direct mechanical probing, rather than as a consequence of the cell volume changes.

TRPV4 Gating *via* Coupling to Cytoskeletal Components

A direct coupling of cell swelling to channel activation could be obtained by a tethering of intracellular components of TRPV4 to the cytoskeleton. Such coupling could provide the swelling-induced mechanical impact on the channel required to promote channel opening. TRPV4 has been demonstrated to co-localize with cytoskeletal components such as actin, microtubules, and microfilaments (54–56), with a specific binding site for F-actin in the TRPV4 N-terminus (55). Modulation of actin, *via* manipulation of the β1-integrins that couple the extracellular matrix and actin filaments, promoted TRPV4 activity (57). Inhibition of cytoskeletal rearrangements disrupted actin-TRPV4 co-localization (58) and reduced TRPV4 activity (54, 55) in a manner that did not affect cell swelling-induced TRPV4-activation (33). Cytoskeletal tethering of TRPV4 thus affects TRPV4 activity and therefore most likely also its volume regulation, although dynamic rearrangements within the cytoskeleton are not required for the swelling-induced channel activation (33).

TRPV4 Gating *via* Its N-Terminal Volume Sensor

TRPV4 contains an extensive cytoplasmic N-terminus that contains ankyrin repeats (59, 60). These protein domains can be potential binding hubs for cytoskeletal components (55, 56) and various proteins and small ligands (61). In addition to the ankyrin repeats, the proline-rich region of the N-terminus interacts with the SH3 domain of PACSINs, proteins involved in vesicular membrane trafficking and endocytosis (62, 63). The TRPV4 N-terminus could thus serve as an essential structural element coupling cell volume changes to TRPV4 channel gating. Full deletion of the TRPV4 N-terminus rendered the channel non-functional (33). However, replacing the N-terminus with that of the shrinkage-sensitive variant of the related TRPV1 (the splice variant VR.5'sv) (64) converted the chimeric TRPV4 channel into a sensor of cell shrinkage rather than a sensor of cell swelling, **Figure 4** (33). The N-terminus of these TRP channels thus dictates the volume-sensitivity of the individual channels, with the distal proline-rich domain serving as a key structural element in the process (33).

Phosphorylation of TRPV4 Is Not Required for Volume-Sensitivity

The TRPV4 N and C termini contain an abundance of consensus sites for protein kinases, **Figure 5** (65, 66) and, in addition, serve as anchors for regulatory kinase complexes (54). Some of these kinases may modulate basal TRPV4 activity, rather than directly activate the channel, by altering channel sensitization (66). Such increased channel sensitivity was observed with cell swelling-induced activation of TRPV4 following PKC and Src kinase activity

(66, 67). Nevertheless, cell volume-dependent activation of TPV4 occurred readily in the absence of protein kinase activity (PKA, PKC, or PKG), and this cell swelling-induced channel activation regime therefore does not require phosphorylation events (33).

Indirect Coupling of Cell Volume Changes to TRPV4 Activation

Phospholipase A2 and Epoxyeicosatrienoic Acid Metabolites

The molecular coupling from cell swelling to TRPV4 activation may require intermediate steps involving swelling-mediated enzyme activation. Phospholipase A2 (PLA_2) is activated by large cell volume increases occurring following experimental exposure of the cells to substantial osmotic challenges of up to 200 mOsm (68–71). Swelling-induced PLA_2 activation promotes occurrence of anandamide and its metabolite arachidonic acid. Subsequent cytochrome P450 epoxygenase-dependent formation of epoxyeicosatrienoic acids may lead to TRPV4 channel opening (72–74), possibly *via* their direct interaction with a binding pocket on TRPV4 (75). Such PLA_2 activity appeared essential for cell swelling-induced TRPV4 activation in Müller glia and TRPV4-expressing HEK293 cells (18, 33, 34, 72–74). However, in other cell types, i.e. retinal ganglion neurons, sensory neurons, TRPV4-expressing *Xenopus laevis* oocytes or yeast, cell swelling-mediated TRPV4 activation occurred readily in the absence of PLA_2 activity (30, 31, 33, 41, 76), suggesting that TRPV4 can be directly activated by cell swelling irrespective of PLA_2 enzymatic products. Curiously, experimental application of downstream products of PLA_2 enzyme activation, such as 5',6'-epoxyeicosatrienoic acids, directly activate TRPV4 (in the absence of cell swelling) both in its native setting of Müller glia and upon heterologous expression in HEK293 cells (18, 34). In other cell types, i.e. retinal ganglion neurons and TRPV4-expressing oocytes, these downstream metabolites of the PLA_2 signaling pathway (e.g. oleic acid, anandamide, 5',6'-epoxyeicosatrienoic acids) fail to activate TRPV4 (31, 33, 34). PLA_2 activity thus modulates TRPV4 channel opening differentially in distinct cell types and appears to be a requirement for cell swelling-induced activation of TRPV4 in cell types that permit direct activation of TRPV4 by the PLA_2 products and metabolites thereof.

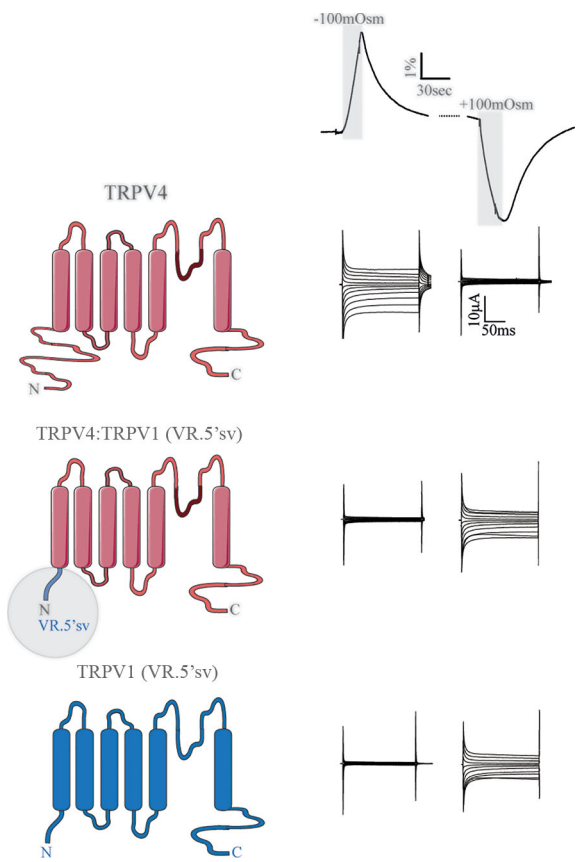

FIGURE 4 | The N-terminus of TRPV4 dictates the directionality of the volume sensing. Channel structures of TRPV4 (top), TRPV4:TRPV1 (VR.5'sv) chimera (with the TRPV4 N terminus replaced by that of VR.5'sv, middle) and VR.5'sv (bottom). The constructs were co-expressed with AQP4 in *Xenopus laevis* oocytes, which were exposed to a hyposmotic or hyperosmotic gradient (Δ100 mOsm) leading to robust cell swelling or cell shrinkage (volume trace, top). TRPV4 responded with augmented membrane currents to a cell volume increase unless its N-terminus was replaced by that of the shrinkage-sensitive VR.5'sv variant of TRPV1 (middle and right panels). Modified from (33).

TRPV4 MODULATION BY INFLAMMATORY MEDIATORS AND OTHER STIMULI

TRPV4 has been proposed a key role in the response mechanism to pathological events, with excessive TRPV4-mediated Ca^{2+} influx possibly driving reactive gliosis and glial cytokine release (34, 77), and predisposing cells to activation of Ca^{2+}-dependent pro-apoptotic signaling cascades (34). Inflammatory mediators are released during activation of inflammatory signaling pathways. A selection of such proinflammatory mediators (TNF-α, IL-1β, TGF-β1) was demonstrated to diminished TRPV4 function after prolonged (24h), but not acute, exposure (78). Inflammatory markers thus join the growing list of TRPV4 modulators, which includes plant extracts such as bisandrographolide and citric acid, apigenin (4'5,7-trihydroxyflavone), a flavone found in many plants (79), RN-1747 (80), dimethylallyl pyrophosphate, an intermediate in the cholesterol synthesis pathway (81), phorbol esters (17, 74, 79), but see (82), and the synthetic lipid GSK1016790A (32, 33). GSK1016790A promotes an open channel conformation similar to that obtained following cell volume-dependent TPV4 activation, suggesting that GSK1016790A stimulates TRPV4 opening in a manner similar to that of swelling-induced channel activation (32). In addition to the cell swelling-mediated activation of TRPV4 and the above-mentioned molecular TRPV4 mediators, TRPV4 senses temperature changes, mechanical stimuli, and flow-related sheer-stress [for review, see (29)], underscoring the polymodality of TRPV4 activation (**Figure 6**).

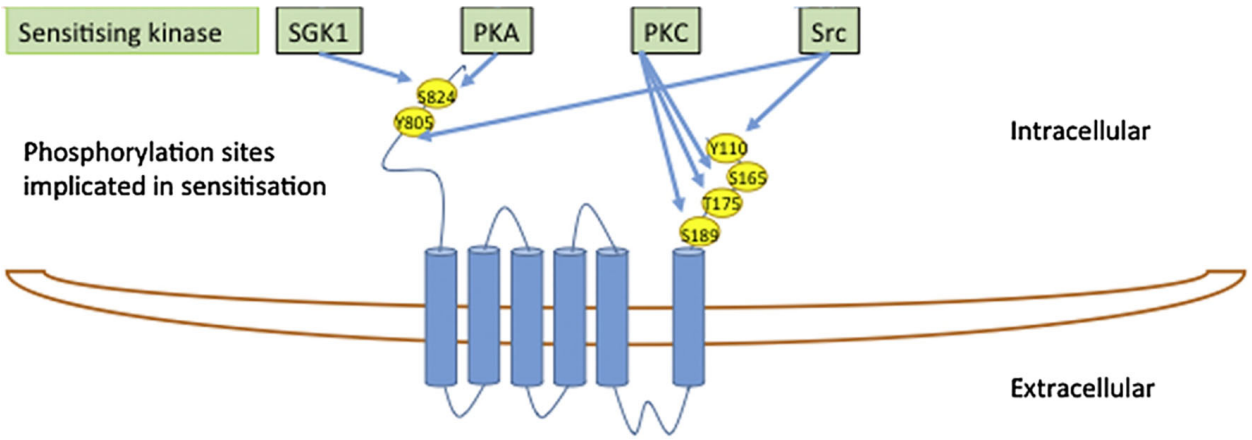

FIGURE 5 | The TRPV4 N- and C-termini contain an abundance of consensus sites for protein kinases. Modified from (65) with permission.

CONCLUSION

In summary, TRPV4 is a genuine sensor of volume changes rather than an osmo-sensor, and is activated by increased cell volume irrespective of the molecular mechanism underlying swelling. The molecular mechanisms that couple altered cell volume to gating of TRPV4 remain obscure, although its distal N-terminus appears to be involved in dictating the volume response (**Figure 6**). Some of the experimental discrepancies over the years regarding TRPV4 activation may originate in cell-specific requirements of volume-dependent activation of TRPV4. Future experimental efforts may reveal how this cell type-specific response is orchestrated.

PERSPECTIVE

The polymodality of the TRPV4 remains a topic of continued fascination in the scientific field. The lists of TRPV4-activating stimuli and protein-protein interaction partners rapidly grow. We believe that the field needs to identify which of these are physiologically relevant (perhaps even additive) and which are curious biophysical phenomena, which may never occur in physiology or pathophysiology. The latter may arise due to technical issues in the experimental design i.e. large osmotic gradients, excessively high concentrations of stimulants (which may even be

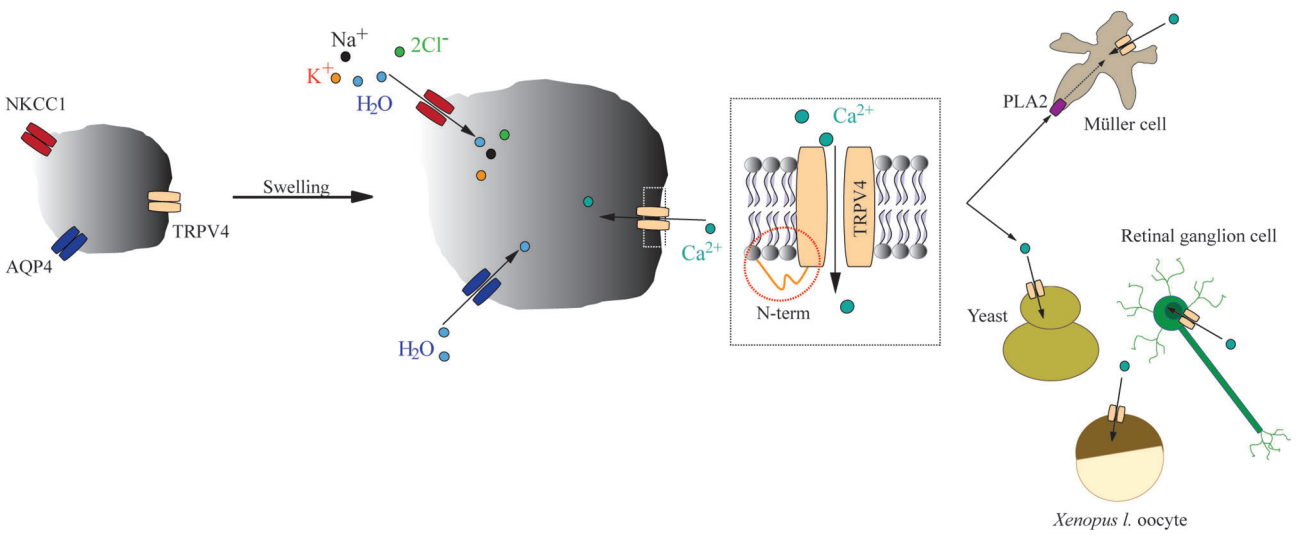

FIGURE 6 | A schematic depicting the mechanisms underlying swelling-induced TRPV4 activation. Increased cell volume activates TRPV4 irrespective of the molecular mechanism underlying the cell swelling. The TRPV4-mediated response to cell volume changes is dictated by its distal-most part of the N terminus, with cell-specific requirement for PLA_2 activity as permissive for swelling-induced activation of TRPV4.

synthetic), extensive mechanical insults, etc. If TRPV4, in the end, is cemented as a true volume sensor in physiological settings, it will be highly relevant to determine the molecular link between volume changes and channel activation. It follows that a revelation of the cellular implications of swelling-activated TRPV4 activation must be resolved; does TRPV4 activation aid the return to the original cell volume or does it in fact worsen the outcome of the cell swelling by promoting a Ca^{2+} overload? We anticipate future exploration of these outstanding research questions alongside the clear definition of TRPV4's role in diverse human diseases.

AUTHOR CONTRIBUTIONS

TLTB drafted the manuscript. TLTB and NM edited and revised the manuscript. All authors contributed to the article and approved the submitted version.

FUNDING

The research conducted by the authors was funded (to TLTB) by the Lundbeck Foundation (R208-2015-2859).

REFERENCES

1. Goodman MB, Schwarz EM. Transducing Touch in Caenorhabditis Elegans. *Annu Rev Physiol* (2003) 65:429–52. doi: 10.1146/annurev.physiol.65.092101.142659
2. Montell C, Birnbaumer L, Flockerzi V, Bindels RJ, Bruford EA, Caterina MJ, et al. A Unified Nomenclature for the Superfamily of TRP Cation Channels. *Mol Cell* (2002) 9:229–31. doi: 10.1016/S1097-2765(02)00448-3
3. Clapham DE, Runnels LW, Strübing C. The TRP Ion Channel Family. *Nat Rev Neurosci* (2001) 2:387–96. doi: 10.1038/35077544
4. Harteneck C, Plant TD, Schultz G. From Worm to Man: Three Subfamilies of TRP Channels. *Trends Neurosci* (2000) 23:159–66. doi: 10.1016/S0166-2236(99)01532-5
5. Duggan A, García-Añoveros J, Corey DP. Insect Mechanoreception: What a Long, Strange TRP It's Been. *Curr Biol* (2000) 10:R384–7. doi: 10.1016/S0960-9822(00)00478-4
6. Liedtke W, Choe Y, Martí-Renom MA, Bell AM, Denis CS, Sali A, et al. Vanilloid Receptor-Related Osmotically Activated Channel (VR-OAC), a Candidate Vertebrate Osmoreceptor. *Cell* (2000) 103:525–35. doi: 10.1016/S0092-8674(00)00143-4
7. Delany NS, Hurle M, Facer P, Alnadaf T, Plumpton C, Kinghorn I, et al. Identification and Characterization of a Novel Human Vanilloid Receptor-Like Protein, VRL-2. *Physiol Genomics* (2001) 4:165–74. doi: 10.1152/physiolgenomics.2001.4.3.165
8. Caterina MJ, Schumacher MA, Tominaga M, Rosen TA, Levine JD, Julius D. The Capsaicin Receptor: A Heat-Activated Ion Channel in the Pain Pathway. *Nature* (1997) 389:816–24. doi: 10.1038/39807
9. Strotmann R, Harteneck C, Nunnenmacher K, Schultz G, Plant TD. OTRPC4, a Nonselective Cation Channel That Confers Sensitivity to Extracellular Osmolarity. *Nat Cell Biol* (2000) 2:695–702. doi: 10.1038/35036318
10. Wissenbach U, Bödding M, Freichel M, Flockerzi V. Trp12, a Novel Trp Related Protein From Kidney. *FEBS Lett* (2000) 485:127–34. doi: 10.1016/S0014-5793(00)02212-2
11. Nilius B, Voets T. The Puzzle of TRPV4 Channelopathies. *EMBO Rep* (2013) 14:152–63. doi: 10.1038/embor.2012.219
12. Hellwig N, Albrecht N, Harteneck C, Schultz G, Schaefer M. Homo- and Heteromeric Assembly of TRPV Channel Subunits. *J Cell Sci* (2005) 118:917–28. doi: 10.1242/jcs.01675
13. Ma X, Cheng KT, Wong CO, O'Neil RG, Birnbaumer L, Ambudkar IS, et al. Heteromeric TRPV4-C1 Channels Contribute to Store-Operated Ca2+ Entry in Vascular Endothelial Cells. *Cell Calcium* (2011) 50:502–9. doi: 10.1016/j.ceca.2011.08.006
14. Sewart AP, Smith GD, Sandford RN, Edwardson JM. Atomic Force Microscopy Reveals the Alternating Subunit Arrangement of the TRPP2-TRPV4 Heterotetramer. *Biophys J* (2010) 99:790–7. doi: 10.1016/j.bpj.2010.05.012
15. Du J, Ma X, Shen B, Huang Y, Birnbaumer L, Yao X. TRPV4, TRPC1, and TRPP2 Assemble to Form a Flow-Sensitive Heteromeric Channel. *FASEB J* (2014) 28:4677–85. doi: 10.1096/fj.14-251652
16. Voets T, Prenen J, Vriens J, Watanabe H, Janssens A, Wissenbach U, et al. Molecular Determinants of Permeation Through the Cation Channel TRPV4. *J Biol Chem* (2002) 277:33704–10. doi: 10.1074/jbc.M204828200
17. Watanabe H, Davis JB, Smart D, Jerman JC, Smith GD, Hayes P, et al. Activation of TRPV4 Channels (hVRL-2/Mtrp12) by Phorbol Derivatives. *J Biol Chem* (2002) 277:13569–77. doi: 10.1074/jbc.M200062200
18. Watanabe H, Vriens J, Janssens A, Wondergem R, Droogmans G, Nilius B. Modulation of TRPV4 Gating by Intra- and Extracellular Ca2+. *Cell Calcium* (2003) 33:489–95. doi: 10.1016/S0143-4160(03)00064-2
19. Deng Z, Paknejad N, Maksaev G, Sala-Rabanal M, Nichols CG, Hite RK, et al. Cryo-EM and X-Ray Structures of TRPV4 Reveal Insight Into Ion Permeation and Gating Mechanisms. *Nat Struct Mol Biol* (2018) 25:252–260. doi: 10.1038/s41594-018-0037-5
20. Harper AGS, Sage SO. TRP-Na+/Ca2+exchanger Coupling. *Adv Exp Med Biol* (2016) 898:67–85. doi: 10.1007/978-3-319-26974-0_4
21. Ye L, Kleiner S, Wu J, Sah R, Gupta RK, Banks AS, et al. TRPV4 Is a Regulator of Adipose Oxidative Metabolism, Inflammation, and Energy Homeostasis. *Cell* (2012) 151:96–110. doi: 10.1016/j.cell.2012.08.034
22. Kernan M, Zuker C. Genetic Approaches to Mechanosensory Transduction. *Curr Opin Neurobiol* (1995) 5:443–8. doi: 10.1016/0959-4388(95)80003-4
23. Sackin H. Mechanosensitive Channels. *Annu Rev Physiol* (1995) 57:333–53. doi: 10.1146/annurev.ph.57.030195.002001
24. Liedtke W, Tobin DM, Bargmann CI, Friedman JM. Mammalian TRPV4 (VR-OAC) Directs Behavioral Responses to Osmotic and Mechanical Stimuli in Caenorhabditis Elegans. *Proc Natl Acad Sci USA* (2003) 100(Suppl):14531–6. doi: 10.1073/pnas.2235619100
25. Suzuki M, Mizuno A, Kodaira K, Imai M. Impaired Pressure Sensation in Mice Lacking TRPV4. *J Biol Chem* (2003) 278:22664–8. doi: 10.1074/jbc.M302561200
26. Gevaert T, Vriens J, Segal A, Everaerts W, Roskams T, Talavera K, et al. Deletion of the Transient Receptor Potential Cation Channel TRPV4 Impairs Murine Bladder Voiding. *J Clin Invest* (2007) 117:3453–62. doi: 10.1172/JCI31766
27. Weber J, Rajan S, Schremmer C, Chao YK, Krasteva-Christ G, Kannler M, et al. TRPV4 Channels Are Essential for Alveolar Epithelial Barrier Function as Protection From Lung Edema. *JCI Insight* (2020) 5:e134464. doi: 10.1172/jci.insight.134464
28. Faropoulos K, Polia A, Tsakona C, Pitaraki E, Moutafidi A, Gatzounis G, et al. Evaluation of AQP4/TRPV4 Channel Co-Expression, Microvessel Density, and Its Association With Peritumoral Brain Edema in Intracranial Meningiomas. *J Mol Neurosci* (2021). doi: 10.1007/s12031-021-01801-1
29. Toft-Bertelsen TL, MacAulay N. TRPing to the Point of Clarity: Understanding the Function of the Complex TRPV4 Ion Channel. *Cells* (2021) 10:165. doi: 10.3390/cells10010165
30. Teng J, Loukin S, Zhou X, Kung C. Yeast Luminometric and Xenopus Oocyte Electrophysiological Examinations of the Molecular Mechanosensitivity of TRPV4. *J Visualized Experiments : JoVE* (2013) 82:50816. doi: 10.3791/50816
31. Loukin SH, Su Z, Kung C. Hypotonic Shocks Activate Rat TRPV4 in Yeast in the Absence of Polyunsaturated Fatty Acids. *FEBS Lett* (2009) 583:754–8. doi: 10.1016/j.febslet.2009.01.027
32. Toft-Bertelsen TL, Križaj D, MacAulay N. When Size Matters: Transient Receptor Potential Vanilloid 4 Channel as a Volume-Sensor Rather Than an Osmo-Sensor. *J Physiol* (2017) 595:3287–302. doi: 10.1113/JP274135
33. Toft-Bertelsen TL, Yarishkin O, Redmon S, Phuong TTT, Križaj D, MacAulay N. Volume Sensing in the Transient Receptor Potential Vanilloid 4 Ion

Channel Is Cell Type-Specific and Mediated by an N-Terminal Volume-Sensing Domain. *J Biol Chem* (2019) 294:18421–34. doi: 10.1074/jbc.RA119.011187
34. Ryskamp DA, Jo AO, Frye AM, Vazquez-Chona F, MacAulay N, Thoreson WB, et al. Swelling and Eicosanoid Metabolites Differentially Gate TRPV4 Channels in Retinal Neurons and Glia. *J Neuroscience: Off J Soc Neurosci* (2014) 34:15689–700. doi: 10.1523/JNEUROSCI.2540-14.2014
35. Benfenati V, Caprini M, Dovizio M, Mylonakou MN, Ferroni S, Ottersen OP, et al. An Aquaporin-4/Transient Receptor Potential Vanilloid 4 (AQP4/TRPV4) Complex Is Essential for Cell-Volume Control in Astrocytes. *Proc Natl Acad Sci USA* (2011) 108:2563–8. doi: 10.1073/pnas.1012867108
36. Larsen BR, Assentoft M, Cotrina ML, Hua SZ, Nedergaard M, Kaila K, et al. Contributions of the Na+/K+-ATPase, NKCC1, and Kir4.1 to Hippocampal K+ Clearance and Volume Responses. *GLIA* (2014) 62:608–22. doi: 10.1002/glia.22629
37. Toft-Bertelsen TL, Larsen BR, MacAulay N. Sensing and Regulation of Cell Volume – We Know So Much and Yet Understand So Little: TRPV4 as a Sensor of Volume Changes But Possibly Without a Volume-Regulatory Role? *Channels* (2018) 12:100–8. doi: 10.1080/19336950.2018.1438009
38. Galizia L, Pizzoni A, Fernandez J, Rivarola V, Capurro C, Ford P. Functional Interaction Between AQP2 and TRPV4 in Renal Cells. *J Cell Biochem* (2012) 113:580–9. doi: 10.1002/jcb.23382
39. Liu X, Bandyopadhyay BC, Bandyopadhyay B, Nakamoto T, Singh B, Liedtke W, et al. A Role for AQP5 in Activation of TRPV4 by Hypotonicity: Concerted Involvement of AQP5 and TRPV4 in Regulation of Cell Volume Recovery. *J Biol Chem* (2006) 281:15485–95. doi: 10.1074/jbc.M600549200
40. Iuso A. Križaj D. TRPV4-AQP4 Interactions 'Turbocharge' Astroglial Sensitivity to Small Osmotic Gradients. *Channels* (2016) 10:172–4. doi: 10.1080/19336950.2016.1140956
41. Jo AO, Ryskamp DA, Phuong TTT, Verkman AS, Yarishkin O, MacAulay N. Križaj D. TRPV4 and AQP4 Channels Synergistically Regulate Cell Volume and Calcium Homeostasis in Retinal Müller Glia. *J Neuroscience: Off J Soc Neurosci* (2015) 35:13525–37. doi: 10.1523/JNEUROSCI.1987-15.2015
42. Mola MG, Sparaneo A, Gargano CD, Spray DC, Svelto M, Frigeri A, et al. The Speed of Swelling Kinetics Modulates Cell Volume Regulation and Calcium Signaling in Astrocytes: A Different Point of View on the Role of Aquaporins. *Glia* (2016) 64:139–54. doi: 10.1002/glia.22921
43. Zeuthen T, Macaulay N. Cotransport of Water by Na^+-K^+-$2Cl^-$ Cotransporters Expressed in Xenopus Oocytes: NKCC1 *Versus* NKCC2. *J Physiol* (2012) 590:1139–54. doi: 10.1113/jphysiol.2011.226316
44. Zeuthen T, MacAulay N. Transport of Water Against Its Concentration Gradient: Fact or Fiction? *Wiley Interdiscip Reviews: Membrane Transport Signaling* (2012) 1:373–81. doi: 10.1002/wmts.54
45. Liedtke W. TRPV4 Plays an Evolutionary Conserved Role in the Transduction of Osmotic and Mechanical Stimuli in Live Animals. *J Physiol* (2005) 567:53–8. doi: 10.1113/jphysiol.2005.088963
46. Coste B, Mathur J, Schmidt M, Earley TJ, Ranade S, Petrus MJ, et al. Piezo1 and Piezo2 Are Essential Components of Distinct Mechanically Activated Cation Channels. *Science* (2010) 330:55–60. doi: 10.1126/science.1193270
47. Lee W, Leddy HA, Chen Y, Lee SH, Zelenski NA, McNulty AL, et al. Synergy Between Piezo1 and Piezo2 Channels Confers High-Strain Mechanosensitivity to Articular Cartilage. *Proc Natl Acad Sci USA* (2014) 111:E5114–22. doi: 10.1073/pnas.1414298111
48. Poole K, Herget R, Lapatsina L, Ngo HD, Lewin GR. Tuning Piezo Ion Channels to Detect Molecular-Scale Movements Relevant for Fine Touch. *Nat Commun* (2014) 5:3520. doi: 10.1038/ncomms4520
49. Loukin S, Su Z, Zhou X, Kung C. Forward Genetic Analysis Reveals Multiple Gating Mechanisms of TRPV4. *J Biol Chem* (2010) 285:19884–90. doi: 10.1074/jbc.M110.113936
50. Nikolaev YA, Cox CD, Ridone P, Rohde PR, Cordero-Morales JF, Vásquez V, et al. Mammalian TRP Ion Channels Are Insensitive to Membrane Stretch. *J Cell Sci* (2019) 132:jcs238360. doi: 10.1242/jcs.238360
51. Servin-Vences MR, Moroni M, Lewin GR, Poole K. Direct Measurement of TRPV4 and PIEZO1 Activity Reveals Multiple Mechanotransduction Pathways in Chondrocytes. *eLife* (2017) 6:e21074. doi: 10.7554/eLife.21074
52. Sianati S, Schroeter L, Richardson J, Tay A, Lamandé SR, Poole K. Modulating the Mechanical Activation of TRPV4 at the Cell-Substrate Interface. *Front Bioengineering Biotechnol* (2021) 8:608951. doi: 10.3389/fbioe.2020.608951
53. Tay A, Sohrabi A, Poole K, Seidlits S, di Carlo D. A 3d Magnetic Hyaluronic Acid Hydrogel for Magnetomechanical Neuromodulation of Primary Dorsal Root Ganglion Neurons. *Adv Mat* (2018) 30:e1800927. doi: 10.1002/adma.201800927
54. Goswami C, Kuhn J, Heppenstall PA, Hucho T. Importance of Non-Selective Cation Channel TRPV4 Interaction With Cytoskeleton and Their Reciprocal Regulations in Cultured Cells. *PloS One* (2010) 5:e11654. doi: 10.1371/journal.pone.0011654
55. Becker D, Bereiter-Hahn J, Jendrach M. Functional Interaction of the Cation Channel Transient Receptor Potential Vanilloid 4 (TRPV4) and Actin in Volume Regulation. *Eur J Cell Biol* (2009) 88:141–52. doi: 10.1016/j.ejcb.2008.10.002
56. Ramadass R, Becker D, Jendrach M, Bereiter-Hahn J. Spectrally and Spatially Resolved Fluorescence Lifetime Imaging in Living Cells: TRPV4-Microfilament Interactions. *Arch Biochem biophysics* (2007) 463:27–36. doi: 10.1016/j.abb.2007.01.036
57. Matthews BD, Thodeti CK, Tytell JD, Mammoto A, Overby DR, Ingber DE. Ultra-Rapid Activation of TRPV4 Ion Channels by Mechanical Forces Applied to Cell Surface β1 Integrins. *Integr Biol* (2010) 2:435–42. doi: 10.1039/c0ib00034e
58. Herman B, Langevin MA, Albertini DF. The Effects of Taxol on the Organization of the Cytoskeleton in Cultured Ovarian Granulosa Cells. *Eur J Cell Biol* (1983) 31. doi: 10.1002/cm.970060505
59. Arniges M, Fernández-Fernández JM, Albrecht N, Schaefer M, Valverde MA. Human TRPV4 Channel Splice Variants Revealed a Key Role of Ankyrin Domains in Multimerization and Trafficking. *J Biol Chem* (2006) 281:1580–6. doi: 10.1074/jbc.M511456200
60. Gaudet R. A Primer on Ankyrin Repeat Function in TRP Channels and Beyond. *Mol Biosyst* (2008) 4:327–9. doi: 10.1039/b801481g
61. Garcia-Elias A, Mrkonjic S, Pardo-Pastor C, Inada H, Hellmich UA, Rubio-Moscardó F, et al. Phosphatidylinositol-4,5-Biphosphate-Dependent Rearrangement of TRPV4 Cytosolic Tails Enables Channel Activation by Physiological Stimuli. *Proc Natl Acad Sci USA* (2013) 110:9553–8. doi: 10.1073/pnas.1220231110
62. Goretzki B, Glogowski NA, Diehl E, Duchardt-Ferner E, Hacker C, Gaudet R, et al. Structural Basis of TRPV4 N Terminus Interaction With Syndapin/PACSIN1-3 and PIP 2. *Structure* (2018) 26:1583–93.e5. doi: 10.1016/j.str.2018.08.002
63. D'Hoedt D, Owsianik G, Prenen J, Cuajungco MP, Grimm C, Heller S, et al. Stimulus-Specific Modulation of the Cation Channel TRPV4 by PACSIN 3. *J Biol Chem* (2008) 283:6272–80. doi: 10.1074/jbc.M706386200
64. Schumacher MA, Eilers H. TRPV1 Splice Variants: Structure and Function. *Front Biosci* (2010) 15:872–82. doi: 10.2741/3651
65. Darby WG, Grace MS, Baratchi S, McIntyre P. Modulation of TRPV4 by Diverse Mechanisms. *Int J Biochem Cell Biol* (2016) 78:217–28. doi: 10.1016/j.biocel.2016.07.012
66. Wegierski T, Lewandrowski U, Müller B, Sickmann A, Walz G. Tyrosine Phosphorylation Modulates the Activity of TRPV4 in Response to Defined Stimuli. *J Biol Chem* (2009) 284:2923–33. doi: 10.1074/jbc.M805357200
67. Fan HC, Zhang X, McNaughton PA. Activation of the TRPV4 Ion Channel Is Enhanced by Phosphorylation. *J Biol Chem* (2009) 284:27884–91. doi: 10.1074/jbc.M109.028803
68. Basavappa S, Pedersen SF, Jørgensen NK, Ellory JC, Hoffmann EK. Swelling-Induced Arachidonic Acid Release *via* the 85-KDa Cplaa2 in Human Neuroblastoma Cells. *J Neurophysiol* (1998) 79:1441–9. doi: 10.1152/jn.1998.79.3.1441
69. Pedersen S, Lambert IH, Thoroed SM, Hoffmann EK. Hypotonic Cell Swelling Induces Translocation of the α Isoform of Cytosolic Phospholipase A2 But Not the γ Isoform in Ehrlich Ascites Tumor Cells. *Eur J Biochem* (2000) 267:5531–9. doi: 10.1046/j.1432-1327.2000.01615.x
70. Ryskamp DA, Frye AM, Phuong TTT, Yarishkin O, Jo AO, Xu Y, et al. TRPV4 Regulates Calcium Homeostasis, Cytoskeletal Remodeling, Conventional Outflow and Intraocular Pressure in the Mammalian Eye. *Sci Rep* (2016) 6:30583. doi: 10.1038/srep30583
71. Jo AO, Lakk M, Frye AM, Phuong TTT, Redmon SN, Roberts R, et al. Križaj D. Differential Volume Regulation and Calcium Signaling in Two Ciliary Body Cell Types Is Subserved by TRPV4 Channels. *Proc Natl Acad Sci USA* (2016) 113:3885–90. doi: 10.1073/pnas.1515895113

72. Watanabe H, Vriens J, Prenen J, Droogmans G, Voets T, Nilius B. Anandamide and Arachidonic Acid Use Epoxyeicosatrienoic Acids to Activate TRPV4 Channels. *Nature* (2003) 424:434–8. doi: 10.1038/nature01807
73. Nilius B, Vriens J, Prenen J, Droogmans G, Voets T. TRPV4 Calcium Entry Channel: A Paradigm for Gating Diversity. *Am J Physiol Cell Physiol* (2004) 286:C195–205. doi: 10.1152/ajpcell.00365.2003
74. Vriens J, Watanabe H, Janssens A, Droogmans G, Voets T, Nilius B. Cell Swelling, Heat, and Chemical Agonists Use Distinct Pathways for the Activation of the Cation Channel TRPV4. *Proc Natl Acad Sci USA* (2004) 101:396–401. doi: 10.1073/pnas.0303329101
75. Berna-Erro A, Izquierdo-Serra M, Sepúlveda RV, Rubio-Moscardo F, Doñate-Macián P, Serra SA, et al. Structural Determinants of 5′,6′-Epoxyeicosatrienoic Acid Binding to and Activation of TRPV4 Channel. *Sci Rep* (2017) 7:10522. doi: 10.1038/s41598-017-11274-1
76. Lechner SG, Markworth S, Poole K, Smith ESJ, Lapatsina L, Frahm S, et al. The Molecular and Cellular Identity of Peripheral Osmoreceptors. *Neuron* (2011) 69:332–44. doi: 10.1016/j.neuron.2010.12.028
77. Matsumoto H, Sugio S, Seghers F, Krizaj D, Akiyama H, Ishizaki Y, et al. Retinal Detachment-Induced Müller Glial Cell Swelling Activates TRPV4 Ion Channels and Triggers Photoreceptor Death at Body Temperature. *J Neurosci* (2018) 38:8745–58. doi: 10.1523/JNEUROSCI.0897-18.2018
78. Simpson S, Preston D, Schwerk C, Schroten H, Blazer-Yost B. Cytokine and Inflammatory Mediator Effects on TRPV4 Function in Choroid Plexus Epithelial Cells. *Am J Physiol - Cell Physiol* (2019) 317:C881–93. doi: 10.1152/ajpcell.00205.2019
79. Vriens J, Owsianik G, Janssens A, Voets T, Nilius B. Determinants of 4α-Phorbol Sensitivity in Transmembrane Domains 3 and 4 of the Cation Channel TRPV4. *J Biol Chem* (2007) 282:12796–803. doi: 10.1074/jbc.M610485200
80. Vincent F, Acevedo A, Nguyen MT, Dourado M, DeFalco J, Gustafson A, et al. Identification and Characterization of Novel TRPV4 Modulators. *Biochem Biophys Res Commun* (2009) 389:490–4. doi: 10.1016/j.bbrc.2009.09.007
81. Bang S, Yoo S, Yang TJ, Cho H, Hwang SW. Nociceptive and Pro-Inflammatory Effects of Dimethylallyl Pyrophosphate *via* TRPV4 Activation. *Br J Pharmacol* (2012) 166:1433–43. doi: 10.1111/j.1476-5381.2012.01884.x
82. Alexander R, Kerby A, Aubdool AA, Power AR, Grover S, Gentry C, et al. 4α-Phorbol 12,13-Didecanoate Activates Cultured Mouse Dorsal Root Ganglia Neurons Independently of TRPV4. *Br J Pharmacol* (2013) 168. doi: 10.1111/j.1476-5381.2012.02186.x

Conflict of Interest: The authors declare that the research was conducted in the absence of any commercial or financial relationships that could be construed as a potential conflict of interest.

frontiers in Immunology

ORIGINAL RESEARCH
published: 22 September 2021
doi: 10.3389/fimmu.2021.689397

Crosstalk Between CD11b and Piezo1 Mediates Macrophage Responses to Mechanical Cues

Hamza Atcha[1,2], *Vijaykumar S. Meli*[1,2], *Chase T. Davis*[1,2], *Kyle T. Brumm*[1,2], *Sara Anis*[1,2], *Jessica Chin*[1,2], *Kevin Jiang*[1,2], *Medha M. Pathak*[1,3,4] *and Wendy F. Liu*[1,2,5,6*]

[1] *Department of Biomedical Engineering, University of California, Irvine, Irvine, CA, United States,* [2] *The Edwards Lifesciences Center for Advanced Cardiovascular Technology, University of California, Irvine, Irvine, CA, United States,* [3] *Sue and Bill Gross Stem Cell Research Center, University of California, Irvine, Irvine, CA, United States,* [4] *Department of Physiology and Biophysics, University of California, Irvine, Irvine, CA, United States,* [5] *Department of Chemical Engineering and Materials Science, University of California, Irvine, Irvine, CA, United States,* [6] *Department of Molecular Biology and Biochemistry, University of California, Irvine, Irvine, CA, United States*

OPEN ACCESS

Edited by:
Nicholas Veldhuis, Monash University, Australia

Reviewed by:
Hye Young Kim, Seoul National University, South Korea
Peter Monk, The University of Sheffield, United Kingdom

***Correspondence:**
Wendy F. Liu
wendy.liu@uci.edu

Specialty section:
This article was submitted to Molecular Innate Immunity, a section of the journal Frontiers in Immunology

Received: *31 March 2021*
Accepted: *12 August 2021*
Published: *22 September 2021*

Citation:
Atcha H, Meli VS, Davis CT, Brumm KT, Anis S, Chin J, Jiang K, Pathak MM and Liu WF (2021) Crosstalk Between CD11b and Piezo1 Mediates Macrophage Responses to Mechanical Cues. Front. Immunol. 12:689397. doi: 10.3389/fimmu.2021.689397

Macrophages are versatile cells of the innate immune system that perform diverse functions by responding to dynamic changes in their microenvironment. While the effects of soluble cues, including cytokines and chemokines, have been widely studied, the effects of physical cues, including mechanical stimuli, in regulating macrophage form and function are less well understood. In this study, we examined the effects of static and cyclic uniaxial stretch on macrophage inflammatory and healing activation. We found that cyclic stretch altered macrophage morphology and responses to IFNγ/LPS and IL4/IL13. Interestingly, we found that both static and cyclic stretch suppressed IFNγ/LPS induced inflammation. In contrast, IL4/IL13 mediated healing responses were suppressed with cyclic but enhanced with static stretch conditions. Mechanistically, both static and cyclic stretch increased expression of the integrin CD11b (α_M integrin), decreased expression of the mechanosensitive ion channel Piezo1, and knock down of either CD11b or Piezo1 through siRNA abrogated stretch-mediated changes in inflammatory responses. Moreover, we found that knock down of CD11b enhanced the expression of Piezo1, and conversely knock down of Piezo1 enhanced CD11b expression, suggesting the potential for crosstalk between integrins and ion channels. Finally, stretch-mediated differences in macrophage activation were also dependent on actin, since pharmacological inhibition of actin polymerization abrogated the changes in activation with stretch. Together, this study demonstrates that the physical environment synergizes with biochemical cues to regulate macrophage morphology and function, and suggests a role for CD11b and Piezo1 crosstalk in mechanotransduction in macrophages.

Keywords: macrophage, stretch, integrin, piezo1, inflammation

INTRODUCTION

Mechanical cues are present in tissues throughout the body, and studies over the last several decades have shown that these signals play a major role in influencing cellular form and function (1, 2). Active mechanical forces including stretch, shear stress, compression, and tension are now widely appreciated to be essential for the function of cells within tissues that regularly endure stress and strain, such as cardiovascular or musculoskeletal tissues (3–7). In contrast, much less is known about how these forces influence immune cells, despite the fact that immune cells exist, function, and migrate throughout the body, including within mechanically active tissues (8). Macrophages are innate immune cells that naturally reside within tissues, or are recruited from blood monocytes to tissues during injury or infection. These cells play a critical role in pathogen or damage surveillance and promoting inflammation and wound healing. This diversity in macrophage function stems from their ability to respond dynamically to cues in their microenvironment (9–11). While the effects of soluble or biochemical stimuli, including pathogens- or damage-associated molecular patterns, cytokines, and chemokines on macrophage function are well- characterized, the role of physical stimuli in regulating macrophage function is not as well understood.

Several recent studies have found that physical cues indeed influence macrophage function. For example, macrophages respond to physical features of biomaterials such as surface grooves or micropatterned adhesive lines and elongate, aligning in the direction of grooves or lines, and polarize towards an alternatively activated phenotype (12, 13). In addition, increasing the stiffness of substrates upon which macrophages are cultured enhances their response to inflammatory or wound healing stimuli, suggesting that mechanical cues have the ability to tune the macrophage response to soluble agonists (14, 15). In response to varying degrees of mechanical stretch, macrophages have been reported to change their morphology, enzymatic activity, proliferation, and activation states (16–19). For example, cyclic stretch was observed to suppress the expression of the inflammatory cytokine IL1β (18). However, the molecular mediators responsible for macrophage mechanotransduction remain elusive.

Mechanoreceptors on the cell surface including integrins and stretch-activated ion channels are major transducers of external physical cues, leading to changes in biochemical signals within the cell (20, 21). Integrins, or adhesion receptors that bind to the extracellular matrix (ECM), cluster in response to force, directly transmit mechanical signals through their connection with the cytoskeleton, and contribute to the activation of intracellular signal transduction pathways (22). In macrophages, integrins are essential in the modulation of various cell functions, such as motility, phagocytosis, and activation, and are also thought to play a role in mechanosensation (23–26). Stretch-activated ion channels, such as Piezo1, respond to changes in membrane tension and transduce external physical stimuli into electrochemical activity, also influencing signaling and cell behavior (20, 21, 27). Moreover, Piezo1 activity is thought to enhance integrin activation and regulate actin polymerization (28–32). A few recent studies including our own work have identified a role for Piezo1 in mechanosensation of hydrostatic pressure, fluid shear stress, and environmental stiffness in myeloid cells (28, 33, 34). Piezo1 activity was also found to promote inflammation (28, 33, 35). However, the role of integrins, Piezo1, and the interplay between these molecules in macrophages, specifically in the context of stretch mechanotransduction is yet to be studied.

In this study, we investigated the effects of cyclic uniaxial stretch on macrophage behavior. We subjected murine bone marrow derived macrophages (BMDMs) to IFNγ/LPS (pro-inflammatory, referred to as M1) or IL4/IL13 (pro-healing, referred to as M2) stimuli along with a 5%, 10%, or 20% cyclic or static uniaxial strain. We observed that uniaxial cyclic stretch led to elongation and alignment of macrophages in the direction of stretch, with a small percentage of cells aligning perpendicularly. While cyclic stretch alone had no influence on macrophage activation, stretch in conjunction with soluble stimuli altered the expression of inflammatory or healing responses. Mechanistically, we found that CD11b (integrin α_M) expression was enhanced and Piezo1 expression diminished with stretch, and siRNA-mediated knockdown of either receptor led to abrogation of stretch-mediated effects. Moreover, we also observed the potential for crosstalk between CD11b and the mechanically activated ion channel Piezo1. We found that suppressing the expression of one molecule (CD11b/Piezo1) resulted in increased expression of the other molecule. Functionally, reduction in CD11b was observed to enhance Piezo1 expression and resulted in increased inflammatory activation regardless of the presence of stretch. Reduced Piezo1 expression, on the other hand, enhanced CD11b expression and suppressed inflammation independent of stretch. Finally, we found that actin is involved in the transduction of mechanical stretch as pharmacological inhibition of actin polymerization prevented stretch-mediated changes in macrophage activation. Together, these findings suggest that soluble and physical stimuli synergize to alter macrophage function and point to a pivotal role of CD11b and Piezo1 in macrophage sensing of mechanical stretch.

MATERIALS AND METHODS

Cell Isolation and Culture

BMDMs were obtained from the femurs of 6-12 week old female C57BL/6J mice (Jackson Labs). Cells were collected by flushing the bone marrow of the femur with DMEM supplemented with 10% heat-inactivated FBS, 2mM L-glutamine, 1% penicillin/streptomyocin (all from Thermo Fisher), and a 10% conditioned media produced from CMG 14-12 cells expressing recombinant murine macrophage colony stimulating factor (MCSF), which induces differentiation of bone marrow cells to macrophages. To remove red blood cells, the collected bone marrow cells were treated with a red cell lysis buffer, and then centrifuged before being resuspended in the previously mentioned media. After 7 days, the cells were harvested using an enzyme-free dissociation buffer (Fisher Scientific) and seeded onto stretchable silicone-based experimental substrates coated with fibronectin using a 10μg/mL solution. BMDMs were seeded

onto the experimental substrates at a density of 2 x 10^5 cells per substrate (~3.9 x 10^4 cells/cm^2). All experiments involving murine macrophages were performed in compliance with the University of California, Irvine's Institutional Animal Care and Use Committee.

Application of Static and Cyclic Stretch

The fabrication and validation of the uniaxial cell stretching device used in this study have been previously described (36). Once seeded on the experimental substrates, the cells were incubated for 24 hours at 37°C prior to treatment with soluble stimuli and application of stretch. Following incubation, soluble agonists were added to the wells resulting in either unstimulated, 0.3ng/mL IFNγ (R&D Biosystems) and LPS (Sigma), or 0.1ng/mL IL4 and IL13 (both from BioLegend) containing media. Once the media was replenished static and cyclic uniaxial stretch at a 5%, 10%, or 20% stretch amplitude was initiated for a period of 18 hours. For experiments involving the modulation of adhesion, BMDMs were allowed to adhere for 4 hours prior to stimulation and the application of stretch. In addition, for experiments involving the reduction of CD11b or Piezo1 expression, unstimulated macrophages were exposed to non-target, CD11b, or Piezo1 siRNA (all Dharmacon) in a Nucleofector® solution obtained from a primary cell 4D-Nucleofector® kit (Lonza). The cell suspension was loaded into Nucleocuvettes® and transfection was accomplished through the use of a 4D-Nucleofector® system (Lonza). Following transfection, the cells were supplemented with warm media before being seeded onto experimental substrates. The transfected cells were allowed to adhere for 24-72 hours prior to stimulation and stretch for an additional 18 hours.

Western Blotting

Following the application of stretch, the cells were rinsed with PBS before being exposed to a lysis buffer, a combination of RIPA lysis buffer and 1% protease inhibitor (both from Fisher Scientific). The substrates were scraped to release the adhered cells and the lysate was collected. The lysate was spun at 14000rpm for 15 minutes and the supernatant was obtained. The proteins were denatured through the use of a Laemmli buffer supplemented with 5% 2-mercaptoethanol at 95°C for 10 minutes before each sample was loaded into a well of a 4-15% mini-PROTEAN™ precast gel (all from Biorad). Gel electrophoresis resulted in the separation of proteins before being transferred onto nitrocellulose membranes through the use of the iBlot dry blotting system (Thermo Fisher Scientific). Following electroblotting, the membranes were blocked using 5% nonfat milk in TBST overnight at 4°C. After 30 minutes of washing in TBST, the membranes were probed with one of the following primary antibodies for 1 hour at room temperature: rabbit anti-iNOS (Abcam), goat anti-arginase-1 (Abcam), rabbit anti-CD11b (Abcam), or mouse anti-GAPDH (BioLegend), used as a loading control. An additional 30 minutes of washing in TBST followed before the membranes were probed with secondary antibodies at room temperature for 1 hour. The membrane was then washed in TBST and immersed into a chemiluminescent HRP substrate solution (Thermo Scientific) and imaged using a ChemiDoc XRS System (Biorad).

Analysis of Cell Viability

Following cyclic stretch, cells were collected and frozen at -80°C, and analysis of cell viability was conducted using the Cyquant cell proliferation assay kit (Fisher Scientific). The assay was conducted following the manufacturer's instructions.

ELISA

Following cyclic stretch, the supernatants were collected and analyzed for the presence of TNF-α, IL-6, and MCP-1 using ELISA kits (BioLegend). The assays were conducted following the manufacturer's instructions.

Immunofluorescence

BMDMs isolated from WT mice were used for actin and CD11b staining, and BMDMs isolated from *Piezo1*$^{P1\text{-}tdT}$ mice, which express a Piezo1-tdTomato fusion protein that is used to label endogenous Piezo1 channels, were used for visualizing Piezo1 (34, 37). For actin staining, BMDMs were fixed in 4% paraformaldehyde following the application of stretch or siRNA knockdown. The fixed cells were washed in PBS prior to permeabilization in 0.1% Triton-X. Following additional PBS washes the cells were incubated with Alexa Fluor 488 phalloidin (Fisher Scientific), diluted 1:100 in PBS, and Hoechst (Invitrogen), diluted 1:2000 in PBS, for 30 minutes at room temperature. The cells were further rinsed in PBS prior to being mounted onto glass slide. For CD11b or Piezo1 staining, the cells were blocked in 2% BSA following fixation prior to being incubated with rat anti-CD11b (BioLegend) and rabbit anti-RFP (Rockland) primary antibodies, diluted 1:50 for CD11b and 1:400 for RFP antibodies in 2% BSA for 1 hour at room temperature. The cells were then repeatedly washed with 2% BSA and incubated with donkey anti-rat (Jackson Immunoresearch Laboratories Inc) or goat anti-rabbit (Thermo Fisher Scientific) secondary antibodies, diluted 1:200 or 1:800 in 2% BSA, for 1 hour at room temperature, respectively. After repeated washing with 2% BSA, the cells were incubated with Alexa Fluor 488 phalloidin (Fisher Scientific), diluted 1:100 in PBS, and Hoechst (Invitrogen), diluted 1:2000 in PBS, for 30 minutes at room temperature. The cells were thoroughly washed with PBS, before being mounted onto a glass slide and imaged using a Zeiss LSM780 confocal microscope.

RNA Isolation and Quantitative Real-Time PCR

Cells were lysed using TRI Reagent (Sigma-Aldrich) and RNA was isolated using manufacturer's protocols. cDNA was generated using a High-Capacity cDNA Reverse Transcription Kit (Applied Biosystems) and qRT-PCR was performed using PerfeCTa® SYBR® Green SuperMix (QuantaBio). All assays were performed using manufacturer's protocols. The primers used in this study include: *Arg1* (forward, CTCTGTCTTTTAGGGTTACGG and reverse, CTCGAGGCTGTCCTTTTGAG), *Mrc1* (forward,

TGTTTTGGTTGGGACTGACC and reverse, TGCAGTAA CTGGTGGATTGTC), *Retnla* (forward, GCCAATCCA GCTAACTATCCC and reverse, AGTCAACGAGTAA GCACAGG), *Chi3l3* (forward, AGTGCTGATCTCAAT GTGGATTC and reverse, TAGGGGCACCAATTCCAGTC), *Itgam* (forward, ATGGACGCTGATGGCAATACC and reverse, TCCCCATTCACGTCTCCCA), *Itgb1* (forward, ATGCC AAATCTTGCGGAGAAT and reverse, TTTGCTGCGAT TGGTGACATT), *Itgb2* (forward, TCACCTTCCAGGT AAAGGTCAT and reverse, AGTTTTTCCCAATGTAGC CAGA), *Itgb3* (forward, CCCCGATGTAACCTGAAGGAG and reverse, GAAGGGCAATCCTCTGAGGG), and *Piezo1* (forward, GTTACCCCCTGGGAACATCT and reverse, TTCAG GAGAGAGGTGGCTGT).

Image Analysis

Phase contrast images were captured following 18 hours of cyclic mechanical stretch using the EVOS cell imaging system (Thermo Fisher Scientific). At least 150 cells from each condition, per experiment, were manually outlined and analyzed using ImageJ, which fits an ellipse to each outlined cell. The ratio of the major and minor axis of the fitted ellipse were used to determine the aspect ratio. The software was also used to compute the angle of the major axis relative to the direction of stretch and the area of each cell. Cells aligned in the direction of the stretch will, therefore, have an angle of 0°. To quantify the percent of aligned cells, alignment parallel to the uniaxial strain was defined as having an angle between -30° to 30° and alignment perpendicular to the strain was defined as an angle between -60° to -90° and 60° to 90°. Percentages were then obtained by taking the ratio of aligned cells to the total number of cells circled. Quantification of mean fluorescence intensity was performed similarly. Approximately 50 cells in each condition were outlined per experiment and the mean intensity was computed for each cell using ImageJ.

Flow Cytometry

Unstimulated macrophages were gently scraped from the surface of the experimental substrates and fixed with 4% paraformaldehyde. After repeated washing with PBS, the cells were resuspended in 1% BSA and incubated at 4°C overnight before being blocked with anti CD16/32 antibodies (Tonba) for 45 minutes at room temperature. The cells were then incubated for an additional 45 minutes at room temperature with PE anti-mouse/human CD11b antibodies (clone: M1/70) or PE rat IgG2b antibodies (clone: RTK4530), used as an isotype control (both from BioLegend). Following repeated washes, flow cytometry was performed using BD LSRII (BD Bioscience) and quantification of the median fluorescent intensity of the obtained data was performed using FlowJo software (FlowJo, LLC).

Statistical Analysis

Data are presented as the mean ± standard deviation of the mean across at least three independent experiments, unless otherwise noted. Comparisons were performed using a two-tailed Student's t-test or paired t-test and $p < 0.05$ was considered significant.

RESULTS

Biochemical Stimuli and Mechanical Stretch Synergize to Regulate Macrophage Morphology and Function

To explore the effects of cyclic mechanical strain and soluble stimuli in regulating macrophage form and function, a uniaxial cell stretcher was used to mechanically stretch unstimulated (Unstim.), IFNγ/LPS, or IL4/IL13 stimulated BMDMs. Cells were cultured on stretchable substrates overnight prior to stimulation and exposure to a 1 Hz, 20% uniaxial strain for 18 hrs, similar stretch amplitude to what has previously been used to replicate mechanical stretch experienced within the heart (38). Given our own work identifying the importance of cell shape in regulating macrophage function (12), we first analyzed the role of cyclic forces in modulating macrophage cell morphology when compared to static controls (**Figure 1A**). Unstimulated macrophages exhibited a range of aspect ratios and had no distinct orientation. Macrophages stimulated with IFNγ/LPS, adopted a flat and round cell shape, whereas macrophages stimulated with IL4/IL13, were elongated, as we have previously observed in macrophages cultured on other material surfaces (14). When exposed to cyclic uniaxial strain, macrophages in all soluble stimulation conditions display alignment parallel to the uniaxial stretch (**Figure 1A**). Interestingly, stretch also caused perpendicular alignment of a small fraction of cells, although to a lesser extent for the unstimulated and IL4/IL13 stimulated macrophages when compared to an unstretched control (**Figure S1A**). This could be attributed to over-extending of the stretchable membranes resulting in the generation of perpendicular strains, as has previously been reported (36). Increases in elongation, or the ratio of the length of the major axis to the length of the minor axis, were observed only in the IFNγ/LPS stimulated macrophages exposed to cyclic strain (**Figure S1B**), suggesting that stretch causes classically activated macrophages to deviate from their typical round morphology and instead adopt a more elongated morphology. Cell area across all stimulation and stretch conditions were unchanged (**Figure S1C**). Together, these results show that cyclic uniaxial stretch leads to changes in macrophage elongation, particularly in the IFNγ/LPS-stimulated condition, and alignment along the direction of stretch.

Given that we have previously found that cell elongation is associated with enhanced wound healing and diminished inflammatory responses (12, 39), we next investigated the role of cyclic mechanical stretch in influencing macrophage function. Following stretch, we observed no changes in the expression of the inflammatory marker iNOS or the healing marker arginase-1 (ARG1) in stretched unstimulated macrophages compared to unstretched controls (**Figure 1B**). This finding suggests that stretch, and its resulting effects on cell morphology, alone are unable to regulate macrophage activation, in contrast to what we have previously found with elongation induced healing activation in BMDMs cultured on micropatterned line or grooves (12, 13). However, the addition of IFNγ/LPS enhanced expression of iNOS,

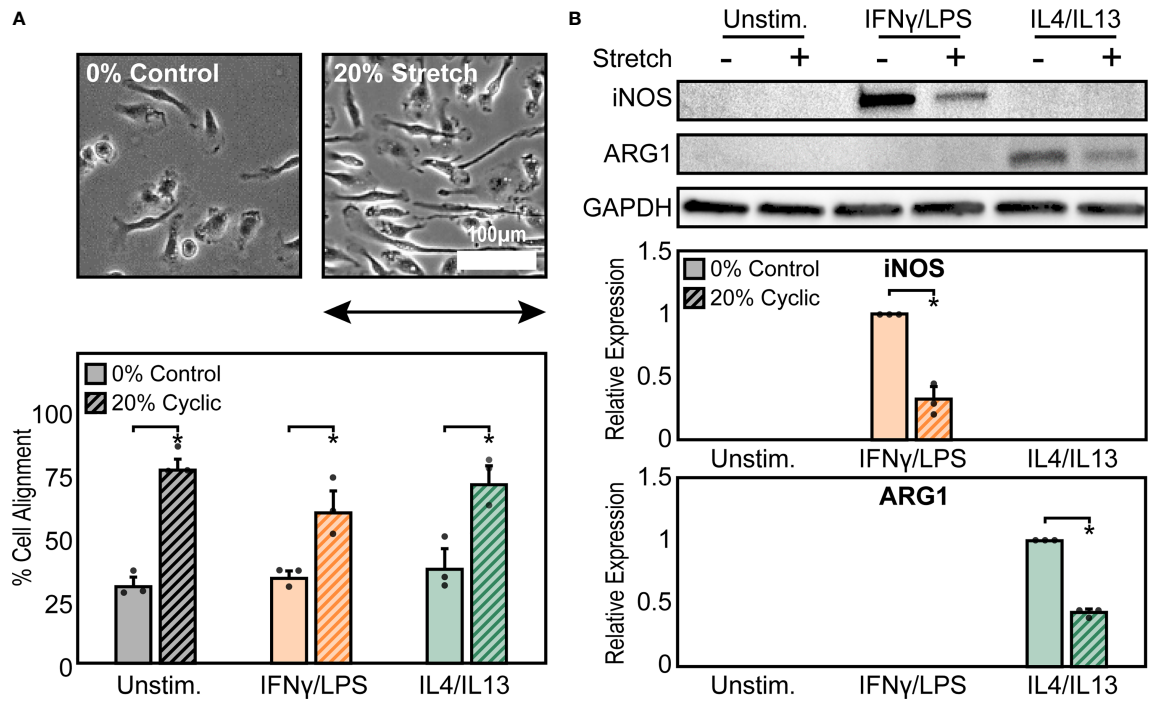

FIGURE 1 | Mechanical stretch alters macrophage morphology and activation. **(A)** Phase contrast images (top) and quantification of percent cell alignment (bottom) of unstimulated macrophages exposed to 0% and 20% cyclic uniaxial stretch. Uniaxial strain was applied in the horizontal direction as indicated by the arrow. **(B)** Representative western blots (top) and corresponding quantification for iNOS (middle) and ARG1 (bottom) for unstimulated, IFNγ/LPS, and IL4/IL13 stimulated macrophages. Values were normalized to GAPDH and made relative to IFNγ/LPS or IL4/IL13 stimulated and 0% stretch conditions, respectively. Error bars indicate standard deviation of the mean for three separate experiments and $^*p < 0.05$ when compared to the indicated condition as determined by Student's t-test **(A)** or paired t-test **(B)**.

as expected, and expression significantly decreased upon application of stretch. Similarly, ARG1 expression in IL4/IL13 stimulated macrophages decreased with stretch (**Figure 1B**). Moreover, no significant differences in macrophage viability were observed with stretch, thus confirming that stretch was able to influence IFNγ/LPS or IL4/IL13 induced inflammatory and healing responses, respectively (**Figure S2**).

We next sought to further characterize functional differences in macrophage responses to mechanical strain through exposing BMDMs to both cyclic and static stretch at 5%, 10%, and 20% amplitudes. Similar to our previous results, unstimulated macrophages displayed no significant differences in inflammatory marker secretion with stretch alone, but in the presence of IFNγ/LPS stimulation cells exhibited a significant decrease in the secretion of inflammatory markers TNFα, IL6, and MCP1 in response to static and cyclic stretch regardless of strain amplitude, when compared to the unstretched and IFNγ/LPS stimulated control conditions (**Figure 2A**). In contrast, IL4/IL13 stimulated BMDMs displayed differential expression of healing markers with stretch. More specifically, static stretch increased the expression of ARG1 regardless of stretch amplitude, whereas increasing amplitudes of cyclic stretch resulted in lower ARG1 expression, with significant decreases observed at both 10% and 20% amplitudes (**Figure 2B**). Stretch had similar effects on additional healing markers, with increases in expression resulting from 20% static stretch and decreases observed with a 20% cyclic stretch, as measured by qRT-PCR (**Figure 2C**). These data suggest that soluble stimuli and stretch act synergistically to modulate the function of macrophages, and that inflammatory activation is inhibited consistently by different stretch regimes, whereas wound healing responses are more varied depending on the stretch profile.

Increased CD11b Expression Dampens Stretch-Mediated Changes in Inflammatory Activation

Macrophage interactions with matrix-coated surfaces and the subsequent remodeling of the cytoskeleton are facilitated by adhesion molecules including integrins, which are thought to be critical transducers of physical stimuli including stretch (21). Among the many integrin subtypes, CD11b, or α_M integrin, is the most abundant integrin in macrophages and its expression is often used as a marker of macrophage differentiation (40). We measured the expression of CD11b under the different conditions described above and found that 20% static or 20% cyclic stretch alone led to no differences in CD11b expression in unstimulated macrophages (**Figure 3A**). However, IFNγ/LPS stimulation caused significant increases in CD11b expression,

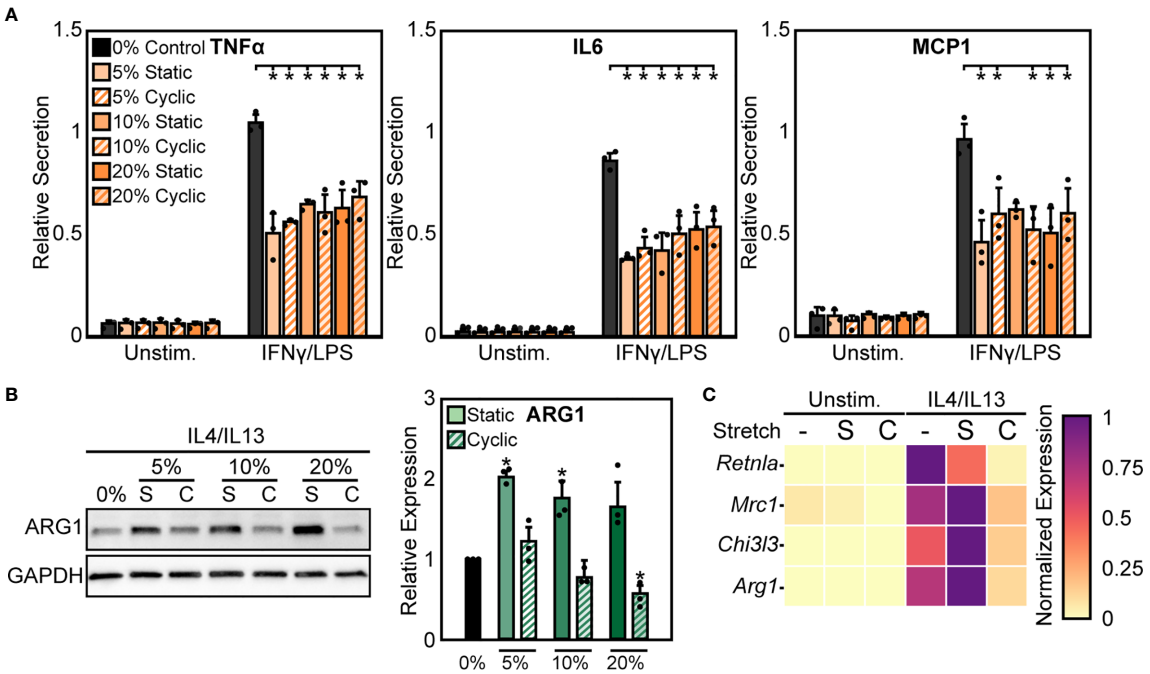

FIGURE 2 | Static and cyclic stretch differentially regulate macrophage inflammatory and healing activation. **(A)** Secretion of TNFα, IL6, and MCP1 for unstimulated and IFNγ/LPS stimulated macrophages exposed to 0%, 10%, and 20% static and cyclic strains. Values are normalized to a 0% stretch and IFNγ/LPS stimulated internal control within each biological replicate. **(B)** Representative western blots (left) and quantification (right) of ARG1 expression for three independent experiments in IL4/IL13 stimulated macrophages exposed to 0%, 10%, and 20% static and cyclic stretch conditions for 18 hrs. Values normalized and statistical comparisons made to IL4/IL13 stimulated condition. **(C)** Gene expression of *Arg1*, *Chi3l3*, *Mrc1*, and *Retnla* for unstimulated and IL4/IL13 stimulated macrophages exposed to 0% (-), 20% static (S), and 20% cyclic (C) strains. Data represents three independent experiments and made relative to the highest expressing condition within each gene. Error bars indicate standard deviation of the mean for three separate experiments and $^*p < 0.05$ when compared to the indicated condition as determined by Student's t-test **(A)** or paired t-test with Bonferroni correction used for multiple comparisons **(B)**.

consistent with our earlier work (24), and further increases were observed following static or cyclic stretch (**Figure 3A**). IL4/IL13 stimulation also increased CD11b expression. Stretch, on the other hand, decreased IL4/IL13-induced CD11b expression with significant decreases observed following 20% cyclic stretch (**Figure 3A**).

CD11b has previously been shown to play an important role in regulating macrophage inflammatory responses. Macrophages from CD11b deficient mice exhibit enhanced inflammation in response to LPS, suggesting that CD11b negatively regulates macrophage inflammatory activation (26). However, the role of this integrin in transducing mechanical stretch in macrophages has not been explored. To better understand the role of CD11b in stretch mechanotransduction, we first investigated changes in macrophage activation following exposure to CD11b siRNA (siCD11b). We found that siCD11b treated cells had reduced integrin expression when compared to non-target (siControl) treated controls, confirming knock down of CD11b (**Figure 3B**). In addition, siCD11b treated cells had enhanced secretion of inflammatory cytokines, particularly TNFα and IL6, when compared to siControl treated cells, consistent with previous work using CD11b knockout macrophages (26). Furthermore, knock down of CD11b abrogated stretch-induced inhibition of inflammation, which was observed in siControl treated macrophages (**Figure 3C**). Instead, the inflammatory response to IFNγ/LPS and stretch was moderately enhanced. In contrast, IL4/IL13 and siCD11b treatment reduced the expression of *Arg1* and prevented any stretch induced changes, suggesting that CD11b also plays an important role in the effects of stretch on healing responses (**Figure 3D**).

As a second method to modulate CD11b expression, we altered the time of adhesion to the substrate prior to stretch. We found that expression of CD11b was dependent on time of adhesion to the substrate, with significantly higher CD11b expressed at longer adhesion times (**Figure 4A**). After 4 hrs of adhesion, macrophage cell spreading was heterogeneous, with some cells clearly adhered and spread whereas others just adhering and beginning to spread. In contrast, after 24 hrs of adhesion, cells appeared to be more homogenous and well-spread (**Figure 4B**). Interestingly, similar changes in cell alignment and morphology were observed following stretch in cells adhered for 4 hrs as was previously noted for cells adhered for 24 hrs (**Figure S3**). However, while morphology was similar, the stretch mediated inflammatory responses differed as reduced adhesion times prevented strain induced negative regulation of inflammation, and in fact caused higher levels of TNFα

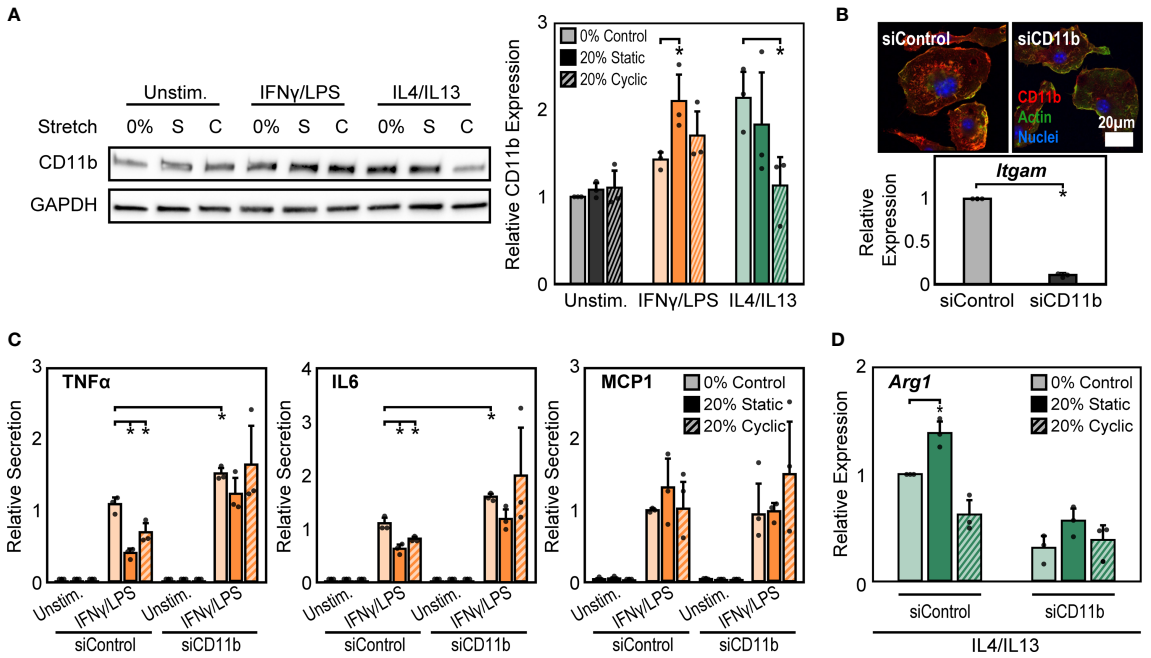

FIGURE 3 | CD11b is required for stretch-mediated changes in macrophage activation. **(A)** Representative Western blot of CD11b and GAPDH for unstimulated, IFNγ/LPS, and IL4/IL13 stimulated macrophages exposed to 0% and 20% static and cyclic stretch (left). Quantification of average across three independent experiments for CD11b expression (right). Values were normalized to GAPDH and made relative to 0% stretch and unstimulated condition. **(B)** Representative immunofluorescence images (top) and quantification of relative *Itgam* gene expression in unstimulated macrophages treated with non-target (siControl) or CD11b (siCD11b) siRNA. Data relative to siControl condition. **(C)** Secretion of TNFα, IL6, and MCP1 for unstimulated and IFNγ/LPS stimulated macrophages treated with siControl or siCD11b and exposed to either 0% control, 20% static, or 20% cyclic stretch. Data normalized to a siControl and IFNγ/LPS treated internal control exposed to 0% stretch within each biological replicate. **(D)** Relative *Arg1* gene expression in IL4/IL13 stimulated and siControl or siCD11b treated BMDMs exposed to 0% control, 20% static, or 20% cyclic stretch. Data relative to 0% siControl condition. Error bars indicate standard deviation of the mean for three separate experiments and $^*p < 0.05$ when compared to the corresponding 0% stretch condition as determined by Student's t-test **(A, C)** or paired t-test **(B, D)**.

compared to unstretched controls (**Figure 4C**). No such changes were observed with respect to healing responses, as both 4 hrs (**Figure 4D**) and 24 hrs of adhesion (**Figure 1B**) resulted in suppressed ARG1 expression. Together, these data suggest that IFNγ/LPS and stretch treatment enhances CD11b expression, which reduces the inflammatory response, while IL4/IL13 and cyclic stretch treatment suppresses CD11b expression resulting in a decreased healing response.

Integrin and Ion Channel Crosstalk Could Regulate Macrophage Response to Stretch

In addition to integrins, mechanically activated ion channels are also present on the cell surface and are involved in transducing mechanical stimuli and modulating cell function. Influx of Ca^{2+} through ion channels has been shown to play important roles in regulating macrophage activation and adhesion (28, 41, 42). Of these channels, Piezo1 has recently been shown to be highly expressed in macrophages and is known to sense and transduce cyclic hydrostatic pressure, shear stresses, and stiffness, while also regulating macrophage inflammatory activation (28, 33–35). To evaluate the role of Piezo1 in regulating stretch-mediated macrophage inflammatory responses we examined Piezo1 expression, and modulated Piezo1 activity or expression using pharmacologic and genetic approaches. We first evaluated changes in Piezo1 expression following stretch using cells from a mouse expressing tdTomato fused to endogenously expressed Piezo1. We visualized tdTomato signal after stretch using fluorescence microscopy, and found that IFNγ/LPS treatment resulted in enhanced Piezo1 channel expression, as has previously been observed (34). In addition, both static and cyclic stretch suppressed IFNγ/LPS mediated channel expression (**Figure 5A**). No such differences were observed in the Unstim. or IL4/IL13 conditions. To determine the significance of reduced Piezo1 expression in sensing stretch, we next treated BMDMs with Piezo1 siRNA (siPiezo1) prior to IFNγ/LPS stimulation and stretch. We found that siPiezo1 treated BMDMs had reduced inflammatory responses regardless of stretch when compared to the siControl condition (**Figure 5B**). Furthermore, we also evaluated changes in stretch-induced macrophage inflammation following Piezo1 activation. We treated BMDMs with 5 μM Yoda1, a Piezo1 specific agonist (43), prior to stimulation with IFNγ/LPS and stretch, and found that Yoda1 treatment enhanced TNFα secretion in both control and stretch conditions and prevented stretch-mediated decreases in cytokine production as was observed in DMSO controls

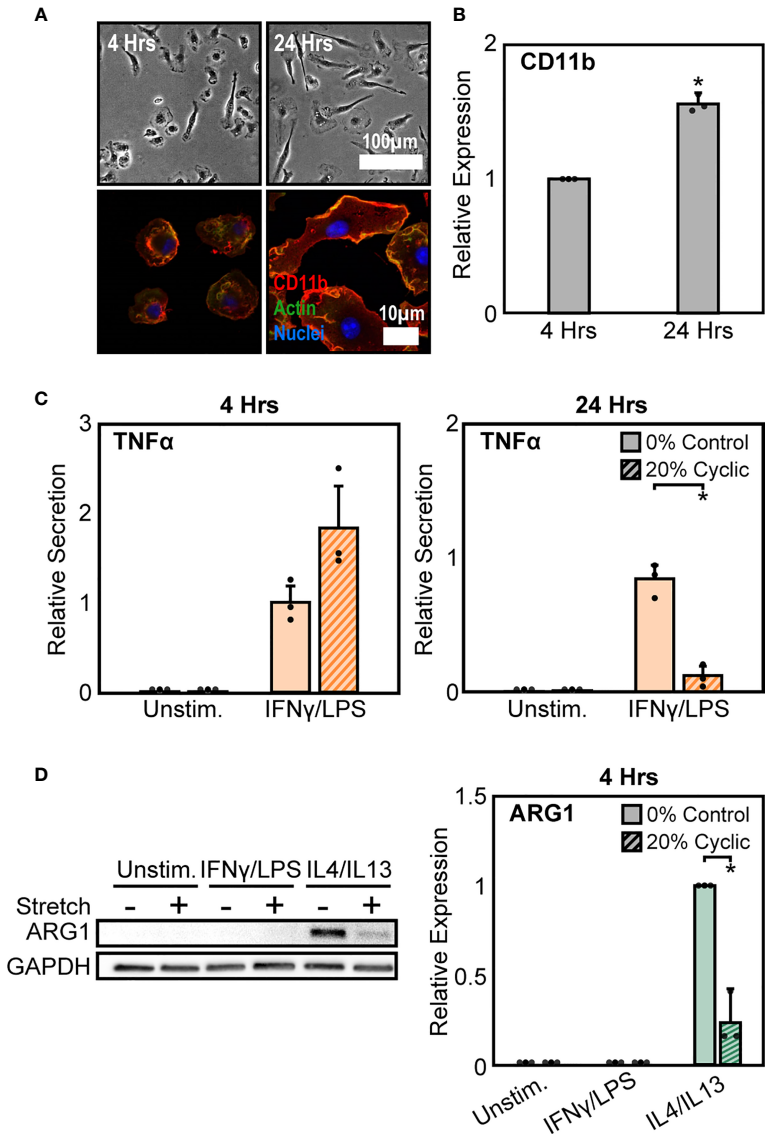

FIGURE 4 | Modulation of CD11b by adhesion time regulates stretch-mediated macrophage inflammatory responses. **(A)** Phase contrast images (top) of macrophages following 4 hrs (left) and 24 hrs (right) of adhesion prior to stimulation and stretch. Fluorescence images (bottom) of macrophages labelled for CD11b (red), actin (green), and nuclei (blue) following 4 hrs (left) and 24 hrs (right) of culture. **(B)** Averaged relative median fluorescence intensity across three independent experiments of CD11b as measured by flow cytometry. Values normalized to 4 hrs adhesion condition. **(C)** Secretion of TNFα for unstimulated and IFNγ/LPS stimulated macrophages exposed to 0% and 20% cyclic stretch after 4 hrs (left) and 24 hrs (right) of adhesion. Values are normalized to a 0% stretch IFNγ/LPS internal control within each biological replicate. **(D)** Representative Western blots (left) and corresponding quantification for ARG1 (right) for unstimulated, IFNγ/LPS, and IL4/IL13 stimulated macrophages allowed to adhere for 4 hrs prior to stimulation and stretch. Values were normalized to GAPDH and made relative to IL4/IL13 stimulated and 0% stretch conditions, respectively. Error bars indicate standard deviation of the mean for three separate experiments and * $p < 0.05$ when compared to the corresponding 0% stretch condition as determined by Student's t-test **(C)** or paired t-test **(B, D)**.

(**Figure 5C**). These data suggest that mechanical stretch downregulates Piezo1 expression, thus suppressing IFNγ/LPS mediated inflammation, and the addition of Yoda1 rescues Piezo1 activity which, in turn, enhances inflammation.

Our findings show that stretch increases CD11b expression while concomitantly decreasing Piezo1 expression, each of which lead to decreases in inflammation in response to IFNγ/LPS. Piezo1 has been shown to enhance the activation of integrins in different cell types (28–30), so we next explored a potential connection between CD11b and Piezo1 in our system. Interestingly, we found that cells treated with siCD11b had increased Piezo1 expression compared to siControl treated cells (**Figure 5D**). In contrast, cells treated with siPiezo1 had increased expression of *Itgam, Itgb1, Itgb2, and Itgb3* (integrin α_M, β_1, β_2, β_3, respectively) (**Figure 5E**). These data suggest a potential interplay between integrins and ion channels, where the

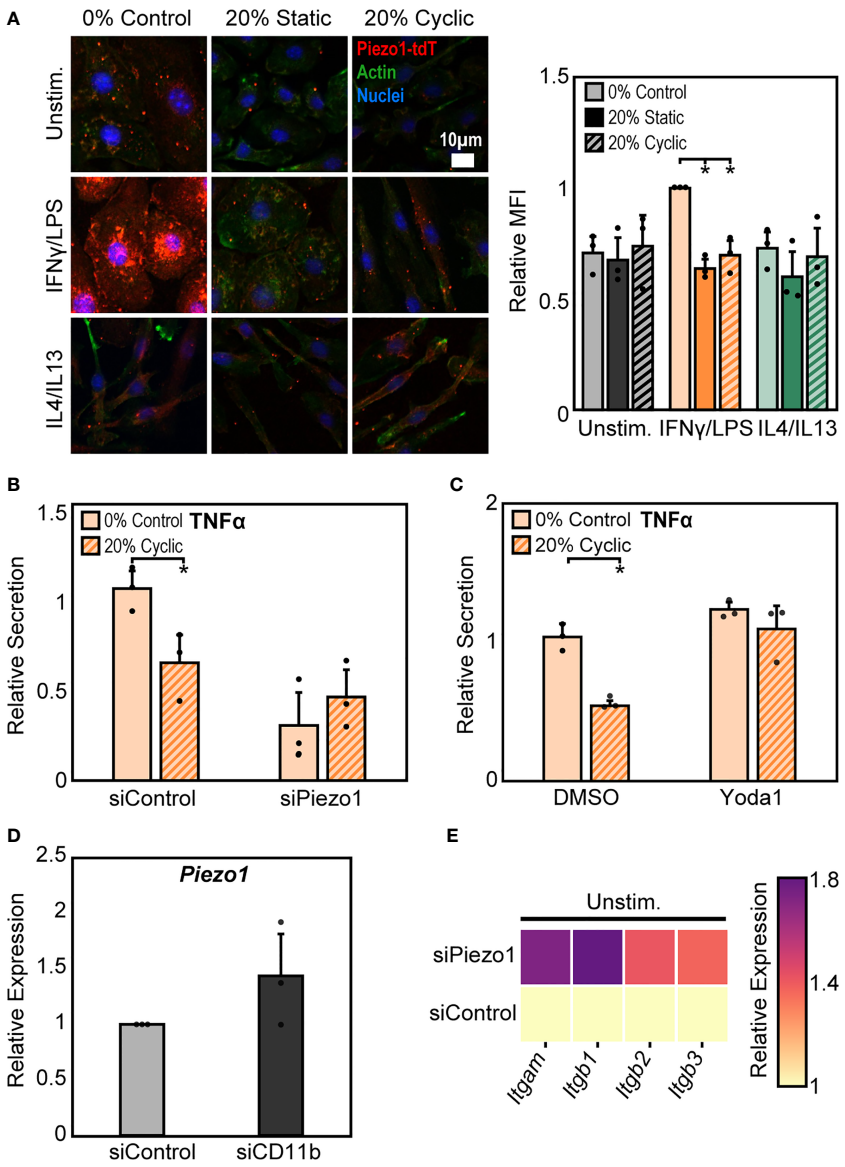

FIGURE 5 | Crosstalk between Piezo1 and CD11b mediates macrophage response to stretch. **(A)** Representative immunofluorescence images (left) and quantification of mean Piezo1-tdT intensity in unstimulated, IFNγ/LPS, and IL4/IL13 treated macrophages exposed to 0% control, 20% static, or 20% cyclic stretch. Data normalized to the 0% control condition. **(B)** Secretion of TNFα in IFNγ/LPS stimulated macrophages treated with siControl or siPiezo1 and exposed to either 0% or 20% cyclic stretch. Data normalized to a siControl treated internal control exposed to 0% stretch within each biological replicate. **(C)** Secretion of TNFα in IFNγ/LPS stimulated macrophages treated with DMSO or Yoda1 and exposed to either 0% or 20% cyclic stretch. Data normalized to a DMSO treated internal control exposed to 0% stretch within each biological replicate. **(D)** Relative *Piezo1* gene expression in unstimulated macrophages treated with non-target (siControl) or CD11b (siCD11b) siRNA. Gene expression is normalized to the siControl treated condition. **(E)** Relative *Itgam, Itgb1, Itgb2*, and *Itgb3* gene expression in unstimulated and siControl or siPiezo1 treated macrophages. Gene expression is normalized to the siControl treated condition. Error bars indicate standard deviation of the mean for three separate experiments and $*p < 0.05$ when compared to the corresponding 0% stretch condition as determined by Student's t-test.

expression of one leads to the downregulation of the other. In addition, high CD11b and low Piezo1 are associated with a reduced inflammatory response to IFNγ/LPS and low CD11b and high Piezo1 are associated with higher inflammation. Finally, stretch-induced changes in expression of these surface proteins may be responsible for the changes in inflammation associated with stretched conditions.

Stretch-Mediated Modulation of Actin Regulates Macrophage Activation

To probe potential intracellular mediators of stretch, we next investigated the role of actin, a cytoskeletal protein connected to integrins. The cytoskeleton is pivotal to the transduction of various mechanical stimuli, and numerous studies in macrophages and other cell types have shown that inhibition

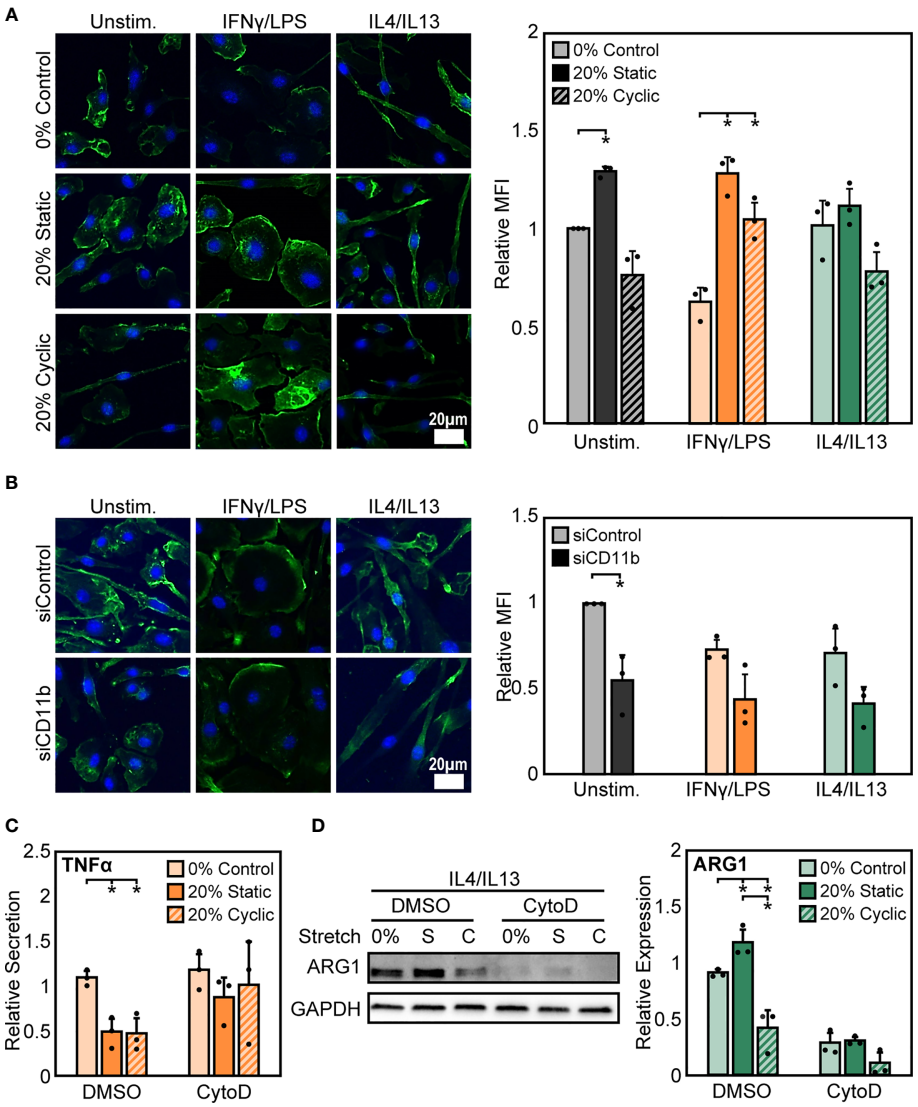

FIGURE 6 | Stretch-induced changes in macrophage activation require modulation of actin. **(A)** Representative images of F-actin in unstimulated, IFNγ/LPS, and IL4/IL13 stimulated macrophages exposed to 0%, 20% static, and 20% cyclic stretch. Quantification of mean F-actin fluorescence intensity across three independent experiments (right). Data normalized to the unstimulated and 0% stretch control. **(B)** Representative images of F-actin in unstimulated, IFNγ/LPS, and IL4/IL13 stimulated macrophages exposed to siControl or CD11b siRNA. Quantification of mean F-actin fluorescence intensity across three independent experiments (right). Values normalized to unstimulated and siControl condition. **(C)** Secretion of TNFα in IFNγ/LPS stimulated macrophages treated with DMSO or CytoD and exposed to 0% and 20% static or cyclic strains. Values are normalized to a DMSO, 0% stretch, and IFNγ/LPS stimulated internal control within each biological replicate. **(D)** Representative Western blot (left) and quantification of ARG1 expression in IL4/IL13 stimulated macrophages treated with DMSO or CytoD and exposed to 0% and 20% static or cyclic strains. Expression is relative to GAPDH. Error bars indicate standard deviation of the mean for three separate experiments and $^*p < 0.05$ when compared to the corresponding 0% stretch condition as determined by paired t-test **(A, B)** and Student's t-test **(C, D)**.

of the cytoskeleton prevents mechanically-mediated changes in cell function (44, 45). To investigate the potential role of actin, we quantified mean fluorescence intensity of phalloidin stained F-actin after stretch and stimulation with IFNγ/LPS or IL4/IL13. We observed that, stimulation alone alters F-actin composition in macrophages, with IFNγ/LPS stimulation resulting in reduced F-actin intensity when compared to unstimulated or IL4/IL13 stimulated macrophages. Following both static and cyclic stretch, we found enhanced F-actin in unstimulated and IFNγ/LPS stimulated cells. In contrast, we observed a modest stretch-induced increase in actin in IL4/IL13 stimulated macrophages (**Figure 6A**). This differential regulation of F-actin composition in IFNγ/LPS stimulated macrophages mirrors the changes observed in stretch-mediated macrophage function, with decreases in actin correlating with decreased levels of inflammation.

To determine the role of CD11b in influencing actin, we measured F-actin intensity in siCD11b and siControl

macrophages. We found that siCD11b treatment reduced F-actin intensity when compared to siControl treated cells (**Figure 6B**). Changes in actin due to loss of CD11b could potentially indicate a role for this integrin in establishing cytoskeletal integrity. To further elucidate the role of actin in transducing stretch, we evaluated changes in stretch-induced macrophage activation following exposure to cytochalasin D (CytoD), an actin polymerization inhibitor. We found that CytoD resulted in enhanced IFNγ/LPS induced TNFα secretion with no stretch-mediated reduction in inflammation observed when compared to DMSO controls (**Figure 6C**). In contrast, CytoD treatment suppressed IL4/IL13 induced ARG1 expression in all conditions (**Figure 6D**). Together, our results indicate that the actin cytoskeleton lies downstream of CD11b, and is critical for transducing mechanical stretch.

DISCUSSION

In this study, we demonstrate that mechanical stretch modulates macrophage morphology and functional response to soluble signals in their microenvironment. In response to cyclic uniaxial stretch, macrophages elongated and aligned in the direction of stretch. The degree of alignment and elongation was dependent on macrophage activation state, where unstimulated and IL4/IL13 stimulated cells displayed significant alignment in the direction of stretch, and IFNγ/LPS stimulated cells displayed significant elongation when stretched, in comparison to a static control. Moreover, a small number of cells were also found to align perpendicularly to the direction of applied stretch, which may be due to perpendicular compressive strains resulting from extension of the silicone substrate. The morphological response of macrophages to strain was consistent with what has been shown previously in other macrophage cell lines (16, 46). Cyclic mechanical stretch not only caused differences in cell morphology, but also resulted in functional changes of macrophages in response to soluble signals. Interestingly, although macrophage elongation has previously been observed to increase healing or alternative activation (ARG1 expression) when cells were cultured on micropatterned lines or grooves (12, 13), elongation caused by cyclic stretch itself did not appear to alter macrophage function. Stretch alone had no significant impact on macrophage inflammatory or healing functions, suggesting that soluble cues are needed in addition to stretch, to synergistically alter macrophage function, as has been observed by others (47). Further characterization of stretch responses showed that static strain promotes IL4/IL13 induced healing activation, whereas high amplitude cyclic stretch suppresses healing activation. Our results are consistent with previous work which shows that static strains enhance healing activation in murine skin (19). In contrast to healing activation, IFNγ/LPS stimulated macrophages were observed to have similar and reduced inflammatory responses when exposed to varying amplitudes of both cyclic and static stretch. While this observation is consistent with some reports, others provide contradictory conclusions as stretch provides no effect or may even enhance inflammatory activation in macrophages (18, 48–52). This, however, could be attributed to the numerous differences in experimental setup (stretch amplitudes, duration, and frequency as well as macrophage source and addition of stimulation relative to onset of stretch), as our studies have shown that differences in the stretch profile and the time of adhesion prior to stretch can have dramatic effects. Nonetheless, our findings indicate that mechanical stimulation modulates macrophage activation in response to soluble stimuli (**Table 1**).

To better understand the molecules responsible for stretch-induced changes in macrophage activation, we analyzed the role of integrins. CD11b is the most highly expressed integrin in macrophages and its expression has been shown to modulate the effects of inflammatory signaling by LPS-induced TLR4 mediated signaling in several myeloid cell types. Using peritoneal macrophages, Han et al. showed CD11b negatively regulates TLR4 since CD11b deficient cells exhibited a higher inflammatory response to LPS when compared to wild type cells (26). We show that stretch-mediated CD11b expression could potentially be responsible for downregulation of LPS-induced TLR4 signaling, since stretch led to higher levels of CD11b and decreases in inflammation with IFNγ/LPS. Cells expressing lower levels of CD11b as induced by siRNA or reduced adhesion time, did not exhibit this response. Moreover, we also show that cyclic stretch mediated reduction in CD11b expression dampens IL4/IL13 induced healing responses. These results suggest that stretch modulates CD11b expression, which impacts the functional response of macrophages to soluble stimuli (**Table 1**). However, future studies will need to further elucidate the effects of stretch on inflammatory and healing signaling pathways.

TABLE 1 | Summary of stretch mediated changes in macrophage function.

Stimulation	Effects of Stretch	Stretch mediated changes in expression		
		CD11b	Piezo1	Actin
Unstim.	No effect	No effect	No effect	Static: enhance
IFNγ/LPS	Stretch: suppress inflammation	Stretch: enhance	Stretch: suppress	Stretch: enhance
IL4/IL13	Static: enhance healing Cyclic: suppress healing	Cyclic: suppress	No effect	No effect

Changes in stretch mediated effects in macrophage inflammatory/healing responses as well as differences in CD11b, Piezo1, and F-actin expression are summarized. Stretch denotes similar observations between both cyclic and static stretch conditions.

Mechanically activated ion channels are also present on the cell surface and play a critical role in transducing mechanical stimuli (28, 30, 41, 42). In macrophages, Piezo1 has been shown to play a role in sensing pressure, shear stresses, and stiffness, while also regulating inflammation and healing responses as well as phagocytosis (28, 33, 35, 53). Our data suggest that prolonged exposure to mechanical stretch suppresses Piezo1 expression. We also show that reduction of Piezo1 with siRNA resulted in similarly reduced IFNγ/LPS-mediated inflammatory responses in both control and stretch conditions. In contrast, Yoda1 enhanced inflammatory responses in both control and stretch conditions. Several studies have reported interactions among Piezo1, integrins, and the actin cytoskeleton (28, 30–32). We found that Piezo1 and CD11b are coregulated, with increased expression in CD11b suppressing Piezo1, and vice versa. Furthermore, our data suggest that prolonged mechanical stretch reduces Piezo1-induced inflammation and enhances CD11b-mediated suppression of inflammatory responses. Recent studies have also identified a role for Piezo1 in promoting hypoxia inducible factor alpha (HIF1α) or nuclear factor kappa-light-chain-enhancer of activated B cells (NFκB) activation resulting in enhanced inflammation (33, 34). Given our observations whereby mechanical stretch decreases Piezo1 expression, it is possible that suppressed HIF1α or NFκB could result in dampened inflammation in response to stretch. In contrast to inflammation, our previous work has shown that transient siRNA mediated reduction in Piezo1 expression has no effect in regulating IL4/IL13 mediated healing responses (34). We also found that stretch leads to changes in the actin cytoskeleton (**Table 1**), which is known to influence several macrophage functions including phagocytosis and activation (39, 54, 55). Moreover, inhibition of actin polymerization prevented stretch-mediated changes in macrophage inflammatory and healing responses. Our results indicate a potential role for integrin and ion channel crosstalk to modulate the transduction of stretch through the actin cytoskeleton.

Macrophages *in vivo* reside within tissues, and are also recruited from circulation to tissues throughout the body. Some resident macrophages are continuously exposed to mechanical stresses, whereas recruited macrophages experience dynamic changes in adhesion as they extravasate from the blood vessel into tissue and are exposed to physical stimuli. Inflammatory signals induce immune cell recruitment through upregulation of many adhesion molecules including CD11b (56) or activation of ion channels (28, 33, 35), which likely also affects their perception of mechanical stimuli. However, prolonged exposure to mechanical stress, such as those experienced by lung alveolar macrophages, may desensitize the cells and therefore exhibit limited effects of Piezo1 (33). Our results support this idea since prolonged stretch caused a decrease in Piezo1 expression. Future work examining Piezo1 expression levels and activity of other resident macrophage populations that reside within different mechanical environments will be of significant interest. Our results also show that CD11b and Piezo1 expression levels influence the macrophage inflammatory response during mechanical stretch, and may suggest that stretch differentially impacts macrophages as they progressively adhere within tissues. Differential regulation of macrophages over time may be important for the progression of healing processes.

Our study describes how different mechanical stretch profiles regulate macrophage function, and also provide new insight into the potential role of CD11b, Piezo1, and the actin cytoskeleton in transducing mechanical stimuli. While the current study is limited to the effects of stretch in cells cultured on a two-dimensional substrate, future work will consider macrophages in three-dimensional tissues and subjected to a multitude of mechanical forces, including stretch and fluid shear or interstitial stresses (57). Further studies will be needed to explore the mechanisms by which combinations of mechanical cues affect macrophages in a three-dimensional microenvironment that represent physiological tissues. This work may further our understanding of how mechanical forces contribute to macrophage behavior during homeostasis, wound healing, as well as the progression of inflammatory diseases.

DATA AVAILABILITY STATEMENT

The raw data supporting the conclusions of this article will be made available by the authors, without undue reservation.

ETHICS STATEMENT

The animal study was reviewed and approved by University of California Institutional Animal Care and Use Committee.

AUTHOR CONTRIBUTIONS

HA, VM, CD, MP, and WL designed research. HA, VM, KB, SA, JC, and KJ performed research. HA and WL analyzed data. HA, MP, and WL wrote the paper. All authors contributed to the article and approved the submitted version.

FUNDING

This work was supported by the National Institutes of Health (NIH) National institute of Dental and Craniofacial Research (NIDCR) and Office of Director's Grant DP2DE023319, National Institutes of Allergy and Infectious Diseases (NIAID) R21AI128519 and R01AI151301 (to WL), National Institute for Neurological Disorders and Stroke (NINDS) R01NS109810 (to MP), and the University of California Irvine Undergraduate Research Opportunities Program (UROP). HA was supported by NIH National Institute T32 Training Grant in Cardiovascular Applied Research and Entrepreneurship (5T32 HL116270-3) and American Heart Association Pre-Doctoral Fellowship (20PRE35200220). This study was made possible, in part, through access to the Optical Biology Core Facility of the Developmental Biology Center, a shared resource supported by

the Cancer Center Support Grant (CA-62203) and Center for Complex Biological Systems Support Grant (GM-076516) at the University of California, Irvine.

ACKNOWLEDGMENTS

We thank L. McCarthy for technical assistance in the laboratory, V. Scarfone for assistance with flow cytometry, A. Syed for assistance with confocal microscopy, and the Lodoen laboratory for guidance with cell isolation and culture.

SUPPLEMENTARY MATERIAL

The Supplementary Material for this article can be found online at: https://www.frontiersin.org/articles/10.3389/fimmu.2021.689397/full#supplementary-material

REFERENCES

1. Barthes J, Özçelik H, Hindié M, Elik H, Ndreu-Halili A, Hasan A, et al. Cell Microenvironment Engineering and Monitoring for Tissue Engineering and Regenerative Medicine: The Recent Advances. *BioMed Res Int* (2014) 2014: e921905. doi: 10.1155/2014/921905
2. Davies PF. Flow-Mediated Endothelial Mechanotransduction. *Physiol Rev* (1995) 75:519–60. doi: 10.1152/physrev.1995.75.3.519
3. Haga JH, Li Y-SJ, Chien S. Molecular Basis of the Effects of Mechanical Stretch on Vascular Smooth Muscle Cells. *J Biomechanics* (2007) 40:947–60. doi: 10.1016/j.jbiomech.2006.04.011
4. Shyy YJ, Hsieh HJ, Usami S, Chien S. Fluid Shear Stress Induces a Biphasic Response of Human Monocyte Chemotactic Protein 1 Gene Expression in Vascular Endothelium. *PNAS* (1994) 91:4678–82. doi: 10.1073/pnas.91.11.4678
5. Walpola PL, Gotlieb AI, Cybulsky MI, Langille BL. Expression of ICAM-1 and VCAM-1 and Monocyte Adherence in Arteries Exposed to Altered Shear Stress. *Arteriosclerosis Thrombosis Vasc Biol* (1995) 15:2–10. doi: 10.1161/01.ATV.15.1.2
6. Rosa N, Simoes R, Magalhães FD, Marques AT. From Mechanical Stimulus to Bone Formation: A Review. *Med Eng Phys* (2015) 37:719–28. doi: 10.1016/j.medengphy.2015.05.015
7. Wang J, Fan B, Wei Y, Suo X, Ding Y. A Simple Multi-Well Stretching Device to Induce Inflammatory Responses of Vascular Endothelial Cells. *Lab Chip* (2016) 16:360–7. doi: 10.1039/C5LC01416F
8. McWhorter FY, Davis CT, Liu WF. Physical and Mechanical Regulation of Macrophage Phenotype and Function. *Cell Mol Life Sci* (2015) 72:1303–16. doi: 10.1007/s00018-014-1796-8
9. Biswas SK, Mantovani A. Macrophage Plasticity and Interaction With Lymphocyte Subsets: Cancer as a Paradigm. *Nat Immunol* (2010) 11:889–96. doi: 10.1038/ni.1937
10. Mosser DM, Edwards JP. Exploring the Full Spectrum of Macrophage Activation. *Nat Rev Immunol* (2008) 8:958. doi: 10.1038/nri2448
11. Sica A, Mantovani A. Macrophage Plasticity and Polarization: *in Vivo* Veritas. *J Clin Invest* (2012) 122:787–95. doi: 10.1172/JCI59643
12. McWhorter FY, Wang T, Nguyen P, Chung T, Liu WF. Modulation of Macrophage Phenotype by Cell Shape. *PNAS* (2013) 110:17253–8. doi: 10.1073/pnas.1308887110
13. Wang T, Luu TU, Chen A, Khine M, Liu WF. Topographical Modulation of Macrophage Phenotype by Shrink-Film Multi-Scale Wrinkles. *Biomater Sci* (2016) 4:948–52. doi: 10.1039/C6BM00224B
14. Blakney AK, Swartzlander MD, Bryant SJ. The Effects of Substrate Stiffness on the *in Vitro* Activation of Macrophages and *in Vivo* Host Response to Poly (Ethylene Glycol)-Based Hydrogels. *J BioMed Mater Res A* (2012) 100:1375–86. doi: 10.1002/jbm.a.34104
15. Previtera ML, Sengupta A. Substrate Stiffness Regulates Proinflammatory Mediator Production Through TLR4 Activity in Macrophages. *PloS One* (2015) 10:e0145813. doi: 10.1371/journal.pone.0145813
16. Matheson LA, Jack Fairbank N, Maksym GN, Paul Santerre J, Labow RS. Characterization of the Flexcell™ Uniflex™ Cyclic Strain Culture System With U937 Macrophage-Like Cells. *Biomaterials* (2006) 27:226–33. doi: 10.1016/j.biomaterials.2005.05.070
17. Sager HB, Hulsmans M, Lavine KJ, Moreira MBB, Heidt T, Courties G, et al. Proliferation and Recruitment Contribute to Myocardial Macrophage Expansion in Chronic Heart Failure. *Circ Res* (2016) 119:853–64. doi: 10.1161/CIRCRESAHA.116.309001
18. Maruyama K, Sakisaka Y, Suto M, Tada H, Nakamura T, Yamada S, et al. Cyclic Stretch Negatively Regulates IL-1β Secretion Through the Inhibition of NLRP3 Inflammasome Activation by Attenuating the AMP Kinase Pathway. *Front Physiol* (2018) 9:802. doi: 10.3389/fphys.2018.00802
19. Chu S-Y, Chou C-H, Huang H-D, Yen M-H, Hong H-C, Chao P-H, et al. Mechanical Stretch Induces Hair Regeneration Through the Alternative Activation of Macrophages. *Nat Commun* (2019) 10:1524. doi: 10.1038/s41467-019-09402-8
20. Mobasheri A, Carter SD, Martín-Vasallo P, Shakibaei M. Integrins and Stretch Activated Ion Channels; Putative Components of Functional Cell Surface Mechanoreceptors in Articular Chondrocytes. *Cell Biol Int* (2002) 26:1–18. doi: 10.1006/cbir.2001.0826
21. Wang JH-C, Thampatty BP. An Introductory Review of Cell Mechanobiology. *Biomech Model Mechanobiol* (2006) 5:1–16. doi: 10.1007/s10237-005-0012-z
22. Wang N, Butler JP, Ingber DE. Mechanotransduction Across the Cell Surface and Through the Cytoskeleton. *Science* (1993) 260:1124–7. doi: 10.1126/science.7684161
23. Li R, Serrano JC, Xing H, Lee TA, Azizgolshani H, Zaman M, et al. Interstitial Flow Promotes Macrophage Polarization Toward an M2 Phenotype. *Mol Biol Cell* (2018) 29:1927–40. doi: 10.1091/mbc.E18-03-0164
24. Hsieh JY, Keating MT, Smith TD, Meli VS, Botvinick EL, Liu WF. Matrix Crosslinking Enhances Macrophage Adhesion, Migration, and Inflammatory Activation. *APL Bioengineering* (2019) 3:016103. doi: 10.1063/1.5067301
25. Jaumouillé V, Cartagena-Rivera AX, Waterman CM. Coupling of β 2 Integrins to Actin by a Mechanosensitive Molecular Clutch Drives Complement Receptor-Mediated Phagocytosis. *Nat Cell Biol* (2019) 21:1357–69. doi: 10.1038/s41556-019-0414-2
26. Han C, Jin J, Xu S, Liu H, Li N, Cao X. Integrin CD11b Negatively Regulates TLR-Triggered Inflammatory Responses by Activating Syk and Promoting Degradation of Myd88 and TRIF *via* Cbl-b. *Nat Immunol* (2010) 11:734–42. doi: 10.1038/ni.1908
27. Kefauver JM, Ward AB, Patapoutian A. Discoveries in Structure and Physiology of Mechanically Activated Ion Channels. *Nature* (2020) 587:567–76. doi: 10.1038/s41586-020-2933-1
28. Baratchi S, Zaldivia MTK, Wallert M, Loseff-Silver J, Al-Aryahi S, Zamani J, et al. Transcatheter Aortic Valve Implantation Represents an Anti-Inflammatory Therapy via Reduction of Shear Stress–Induced, Piezo-1–Mediated Monocyte Activation. *Circulation* (2020) 142:1092–105. doi: 10.1161/CIRCULATIONAHA.120.045536
29. McHugh BJ, Murdoch A, Haslett C, Sethi T. Loss of the Integrin-Activating Transmembrane Protein Fam38A (Piezo1) Promotes a Switch to a Reduced Integrin-Dependent Mode of Cell Migration. *PloS One* (2012) 7:e40346. doi: 10.1371/journal.pone.0040346
30. McHugh BJ, Buttery R, Lad Y, Banks S, Haslett C, Sethi T. Integrin Activation by Fam38A Uses a Novel Mechanism of R-Ras Targeting to the Endoplasmic Reticulum. *J Cell Sci* (2010) 123:51–61. doi: 10.1242/jcs.056424
31. Nonomura K, Lukacs V, Sweet DT, Goddard LM, Kanie A, Whitwam T, et al. Mechanically Activated Ion Channel PIEZO1 Is Required for Lymphatic Valve Formation. *PNAS* (2018) 115:12817–22. doi: 10.1073/pnas.1817070115
32. Nourse JL, Pathak MM. How Cells Channel Their Stress: Interplay Between Piezo1 and the Cytoskeleton. *Semin Cell Dev Biol* (2017) 71:3–12. doi: 10.1016/j.semcdb.2017.06.018

33. Solis AG, Bielecki P, Steach HR, Sharma L, Harman CCD, Yun S, et al. Mechanosensation of Cyclical Force by PIEZO1 Is Essential for Innate Immunity. *Nature* (2019) 573:69–74. doi: 10.1038/s41586-019-1485-8
34. Atcha H, Jairaman A, Holt JR, Meli VS, Nagalla RR, Veerasubramanian PK, et al. Mechanically Activated Ion Channel Piezo1 Modulates Macrophage Polarization and Stiffness Sensing. *Nat Commun* (2021) 12:3256. doi: 10.1038/s41467-021-23482-5
35. Aykut B, Chen R, Kim JI, Wu D, Shadaloey SAA, Abengozar R, et al. Targeting Piezo1 Unleashes Innate Immunity Against Cancer and Infectious Disease. *Sci Immunol* (2020) 5(50):eabb5168. doi: 10.1126/sciimmunol.abb5168
36. Atcha H, Davis CT, Sullivan NR, Smith TD, Anis S, Dahbour WZ, et al. A Low-Cost Mechanical Stretching Device for Uniaxial Strain of Cells: A Platform for Pedagogy in Mechanobiology. *J Biomech Eng* (2018) 140:081005-081005–9. doi: 10.1115/1.4039949
37. Ranade SS, Qiu Z, Woo S-H, Hur SS, Murthy SE, Cahalan SM, et al. Piezo1, a Mechanically Activated Ion Channel, Is Required for Vascular Development in Mice. *PNAS* (2014) 111:10347–52. doi: 10.1073/pnas.1409233111
38. Dandel M, Lehmkuhl H, Knosalla C, Suramelashvili N, Hetzer R. Strain and Strain Rate Imaging by Echocardiography – Basic Concepts and Clinical Applicability. *Curr Cardiol Rev* (2009) 5:133–48. doi: 10.2174/157340309788166642
39. Jain N, Vogel V. Spatial Confinement Downsizes the Inflammatory Response of Macrophages. *Nat Materials* (2018) 17:1134–44. doi: 10.1038/s41563-018-0190-6
40. Misharin AV, Morales-Nebreda L, Mutlu GM, Budinger GRS, Perlman H. Flow Cytometric Analysis of Macrophages and Dendritic Cell Subsets in the Mouse Lung. *Am J Respir Cell Mol Biol* (2013) 49:503–10. doi: 10.1165/rcmb.2013-0086MA
41. Chauhan A, Sun Y, Sukumaran P, Quenum Zangbede FO, Jondle CN, Sharma A, et al. M1 Macrophage Polarization Is Dependent on TRPC1-Mediated Calcium Entry. *iScience* (2018) 8:85–102. doi: 10.1016/j.isci.2018.09.014
42. Schappe MS, Szteyn K, Stremska ME, Mendu SK, Downs TK, Seegren PV, et al. Chanzyme TRPM7 Mediates the Ca2+ Influx Essential for Lipopolysaccharide-Induced Toll-Like Receptor 4 Endocytosis and Macrophage Activation. *Immunity* (2018) 48:59–74.e5. doi: 10.1016/j.immuni.2017.11.026
43. Syeda R, Xu J, Dubin AE, Coste B, Mathur J, Huynh T, et al. Chemical Activation of the Mechanotransduction Channel Piezo1. *Elife* (2015) 4. doi: 10.7554/eLife.07369
44. Patel NR, Bole M, Chen C, Hardin CC, Kho AT, Mih J, et al. Cell Elasticity Determines Macrophage Function. *PloS One* (2012) 7(9):e41024. doi: 10.1371/journal.pone.0041024
45. Walker M, Rizzuto P, Godin M, Pelling AE. Structural and Mechanical Remodeling of the Cytoskeleton Maintains Tensional Homeostasis in 3D Microtissues Under Acute Dynamic Stretch. *Sci Rep* (2020) 10:7696. doi: 10.1038/s41598-020-64725-7
46. Matsumoto T, Delafontaine P, Schnetzer KJ, Tong BC, Nerem RM. Effect of Uniaxial, Cyclic Stretch on the Morphology of Monocytes/Macrophages in Culture. *J Biomech Eng* (1996) 118:420–2. doi: 10.1115/1.2796026
47. Pugin J, Dunn I, Jolliet P, Tassaux D, Magnenat J-L, Nicod LP, et al. Activation of Human Macrophages by Mechanical Ventilation in Vitro. *Am J Physiol - Lung Cell Mol Physiol* (1998) 275:L1040–50. doi: 10.1152/ajplung.1998.275.6.L1040
48. Maruyama K, Nemoto E, Yamada S. Mechanical Regulation of Macrophage Function - Cyclic Tensile Force Inhibits NLRP3 Inflammasome-Dependent IL-1β Secretion in Murine Macrophages. *Inflammation Regeneration* (2019) 39:3. doi: 10.1186/s41232-019-0092-2
49. Dziki JL, Giglio RM, Sicari BM, Wang DS, Gandhi RM, Londono R, et al. The Effect of Mechanical Loading Upon Extracellular Matrix Bioscaffold-Mediated Skeletal Muscle Remodeling. *Tissue Eng Part A* (2017) 24:43–46. doi: 10.1089/ten.tea.2017.0011
50. Ballotta V, Driessen-Mol A, Bouten CVC, Baaijens FPT. Strain-Dependent Modulation of Macrophage Polarization Within Scaffolds. *Biomaterials* (2014) 35:4919–28. doi: 10.1016/j.biomaterials.2014.03.002
51. Wu J, Yan Z, Schwartz DE, Yu J, Malik AB, Hu G. Activation of NLRP3 Inflammasome in Alveolar Macrophages Contributes to Mechanical Stretch-Induced Lung Inflammation and Injury. *J Immunol* (2013) 190:3590–9. doi: 10.4049/jimmunol.1200860
52. Shan S, Fang B, Zhang Y, Wang C, Zhou J, Niu C, et al. Mechanical Stretch Promotes Tumoricidal M1 Polarization *via* the FAK/NF-κb Signaling Pathway. *FASEB J* (2019) 33:13254–66. doi: 10.1096/fj.201900799RR
53. Ma S, Cahalan S, LaMonte G, Grubaugh ND, Zeng W, Murthy SE, et al. Common PIEZO1 Allele in African Populations Causes RBC Dehydration and Attenuates Plasmodium Infection. *Cell* (2018) 173:443–55.12. doi: 10.1016/j.cell.2018.02.047
54. Davidson AJ, Wood W. Macrophages Use Distinct Actin Regulators to Switch Engulfment Strategies and Ensure Phagocytic Plasticity in Vivo. *Cell Rep* (2020) 31:107692. doi: 10.1016/j.celrep.2020.107692
55. Pergola C, Schubert K, Pace S, Ziereisen J, Nikels F, Scherer O, et al. Modulation of Actin Dynamics as Potential Macrophage Subtype-Targeting Anti-Tumour Strategy. *Sci Rep* (2017) 7:41434. doi: 10.1038/srep41434
56. Imhof BA, Aurrand-Lions M. Adhesion Mechanisms Regulating the Migration of Monocytes. *Nat Rev Immunol* (2004) 4:432. doi: 10.1038/nri1375
57. Lu D, Kassab GS. Role of Shear Stress and Stretch in Vascular Mechanobiology. *J R Soc Interface* (2011) 8:1379–85. doi: 10.1098/rsif.2011.0177

Conflict of Interest: The authors declare that the research was conducted in the absence of any commercial or financial relationships that could be construed as a potential conflict of interest.

Publisher's Note: All claims expressed in this article are solely those of the authors and do not necessarily represent those of their affiliated organizations, or those of the publisher, the editors and the reviewers. Any product that may be evaluated in this article, or claim that may be made by its manufacturer, is not guaranteed or endorsed by the publisher.

frontiers in Immunology

MINI REVIEW
published: 02 November 2021
doi: 10.3389/fimmu.2021.767319

Stretching the Function of Innate Immune Cells

*Erica M. Orsini[1], Apostolos Perelas[2], Brian D. Southern[1,3], Lisa M. Grove[3], Mitchell A. Olman[1,3] and Rachel G. Scheraga[1,3]**

[1] Respiratory Institute, Cleveland Clinic, Cleveland, OH, United States, [2] Department of Pulmonary and Critical Care, Virginia Commonwealth University, Richmond, VA, United States, [3] Department of Inflammation and Immunity, Lerner Research Institute, Cleveland Clinic, Cleveland, OH, United States

The importance of innate immune cells to sense and respond to their physical environment is becoming increasingly recognized. Innate immune cells (e.g. macrophages and neutrophils) are able to receive mechanical signals through several mechanisms. In this review, we discuss the role of mechanosensitive ion channels, such as Piezo1 and transient receptor potential vanilloid 4 (TRPV4), and cell adhesion molecules, such as integrins, selectins, and cadherins in biology and human disease. Furthermore, we explain that these mechanical stimuli activate intracellular signaling pathways, such as MAPK (p38, JNK), YAP/TAZ, EDN1, NF-kB, and HIF-1α, to induce protein conformation changes and modulate gene expression to drive cellular function. Understanding the mechanisms by which immune cells interpret mechanosensitive information presents potential targets to treat human disease. Important areas of future study in this area include autoimmune, allergic, infectious, and malignant conditions.

Keywords: innate immunity, mechanotranduction, macrophage, neutrophil, integrins, TRPV4, Piezo1

OPEN ACCESS

Edited by:
Shaik O. Rahaman, University of Maryland, College Park, United States

Reviewed by:
Ken Takahashi, Okayama University, Japan
Violetta Borelli, University of Trieste, Italy

***Correspondence:**
Rachel G. Scheraga
scherar@ccf.org

Specialty section:
This article was submitted to Molecular Innate Immunity, a section of the journal Frontiers in Immunology

Received: *30 August 2021*
Accepted: *11 October 2021*
Published: *02 November 2021*

Citation:
Orsini EM, Perelas A, Southern BD, Grove LM, Olman MA and Scheraga RG (2021) Stretching the Function of Innate Immune Cells. Front. Immunol. 12:767319. doi: 10.3389/fimmu.2021.767319

INTRODUCTION

The ability of innate immune cells to sense and respond to the physical environment is critical for their function. Through the study of mechano-immunology, it is now increasing understood that mechanical cues are just as important as biochemical cues for determining immune cell activation (1). Immune cells encounter a wide range of environmental conditions while performing immune functions. For example, different tissues have vastly different mechanical properties with bone (10-20x10^6 kPa) significantly stiffer than lung (1 kPa) (2, 3). Pathologic condition may cause the stiffness of tissue to change, for example, pulmonary inflammation/fibrosis causes the stiffness of the lung to increase 6-20-fold from 1 kPa to 6-20 kPa (3). During both physiological and pathological states, cells receive mechanical input from the biophysical properties of the extracellular environment, including matrix stiffness, stretch, shear force, elasticity, and shape (4).

Through mechanotransduction, cells translate force into cellular messages that induce protein conformation changes, activate intracellular signaling pathways, and modulate gene expression to drive cellular function (1, 5, 6). For example, depending on the stiffness of the *in vitro* environment, macrophages can develop into the different classically described macrophage phenotypes, pro-inflammatory ("M1-like") or pro-healing ("M2-like"), however direct extrapolation of the *in vitro* macrophage phenotypes to *in vivo* function is problematic (7, 8). Spatial confinement has also been shown to influence macrophage phenotype with macrophages confined by crowding having less

expression of pro-inflammatory cytokines (IL-6, IL-1β) in response to lipopolysaccharide (LPS) in a manner that correlates with impaired actin polymerization and reduced nuclear translocation of myocardin-related transcription factor A (MRTF-A) (9). Similarly in neutrophils, mechanical deformations generated through optical stretching have been shown to influence cytokine secretion (10). Mechanotransduction is critical in non-immune cells as well, where mechanosensitive mechanisms regulate many cell functions including regulation of blood pressure and myotube and bone formation (11–13).

Ion channels, such as Piezo1 and Transient receptor potential cation channel subfamily V member 4 (TRPV4), and cell adhesion molecules (CAMs), such as integrins, selectins, and cadherins, have been shown to play a role in mechanotransduction in innate immune cells (5, 14). In this review, we will explore what is known about the role of ion channels and adhesion molecules in controlling macrophage and neutrophil function. Given the brevity and focus of this review, we acknowledge that we could not include all published work in this area. For further inquiry on this topic, we direct you to comprehensive reviews in this area (1, 5, 15).

ION CHANNELS

Cation channels are membrane proteins containing a cation-permeable pore which allow for the passage of cations (including calcium Ca^{2+}, magnesium Mg^{2+}, potassium K^{+}, and sodium Na^{2+}) along their electrochemical gradients. Ca^{2+} plays a critical role in innate immune cell signaling. For example, in macrophages, Ca^{2+} has been shown to be an important second messenger in Tumor Necrosis Factor-α (TNF-α) secretion and phagocytosis (16, 17). In neutrophils, the influx of Ca^{2+} allows for degranulation, NADPH oxidase activation, and the generation of reactive oxygen species (18, 19). Ion channels, which control influx of Ca^{2+}, have a critical role in cellular mechanotransduction. Mechanosensitive ion channels are ubiquitously expressed in cells and tissues, and recently have been recognized for their important role in immune function. Mechanosensitive mechanisms were initially discovered in neurons, which has now led to exploration of their function in numerous cell types (20). The importance of ion channels in mechanobiology has been recently highlighted by the awarding of the Nobel Prize in Medicine to David Julius and Ardem Patapoutian for their work examining the role of TRP and Piezo channels in sensory function (21). This review will focus on 2 of the best studied mechanosensitive channels for their role in inflammation, Piezo1 and TRPV4.

PIEZO1

The Piezo channels, which include Piezo 1 and 2, are mechanically gated ion channels activated directly (e.g. mechanical stretch, chemical stimulus) or indirectly (e.g. through other channel or force generated downstream signals) (22). In addition to its role in immune function, Piezo1 has been shown to have a role in blood pressure regulation and myoblast fusion during skeletal muscle formation, while Piezo2 regulates sensation of light touch and proprioception (11, 12, 23, 24). Piezo1, Piezo2, and TRPV4 act as key force sensors during bone development and osteoblast differentiation (13, 25). Direct activation of Piezo1 occurs through mechanical stretch of the lipid bilayer which permits the flow of Ca^{2+} across the membrane (26). The mechanogating function of the Piezo1 channel is achieved through a lever-like mechanism which involves both the intracellular and transmembrane domains (27). In the absence of mechanical stimuli, Piezo1 can be activated by the small molecule, Yoda1 (28). During myotube formation, inward translocation of phosphatidylserine (PS) from the phospholipid bilayer of myoblasts is an important mechanism for Ca^{2+} influx *via* Piezo1, which leads to actomyosin assemby, although it is unknown if inward translocation of PS is an important mechanism of Piezo1 activation in myeloid cells (12). There is evidence of Piezo1 activation by force transduction *via* "inside-out" activation through interaction with intracellular cytoskeletal filaments (29). Traction force generated by the cytoskeletal contractile protein Myosin II by Myosin Light Chain Kinase (MLCK) mediates Ca^{2+} influx *via* Piezo1 (30).

Once Piezo1 is activated by mechanical stimuli (pressure or stretch), the Piezo1 signal integrates with that of chemical pro-inflammatory signals to regulate macrophage function. In response to cyclical hydrostatic pressure in murine bone marrow derived macrophages (BMDM), Piezo1 mediates Ca^{2+} influx leading to activator protein-1 (AP-1) activation, production of endothelin-1 (EDN1), and stabilization of hypoxia inducible factor 1α (HIF1α) to modulate important genes that lead to the production of pro-inflammatory mediators, such as IL-6, TNF-α, chemokine ligand 2 (CXCL2), and prostaglandin E2 (31). Stiffer substrates (~kPa-GPa, e.g. tissue culture plastic or glass) lead to increased macrophage bacterial clearance and production of "M1-like" pro-inflammatory cytokines, such as IL-6 and TNF-α, and suppression of "M2-like" pro-healing markers, such as arginase 1 (ARG1) (32). BMDM cultured on stiffer substrates also have increased expression of Piezo1 and enhanced Ca^{2+} influx, suggesting a possibility of a positive feedback loop of matrix stiffness on Piezo1-mediated macrophage function (32).

In addition to mechanical stimuli, Piezo1 has been shown to influence macrophage polarization in response to stimulation by IFN-γ/LPS. Toll-like receptor 4 (TLR4) has been shown to mediate Ca^{2+} influx *via* interaction with Piezo1 in response to LPS (33). Macrophages from mice with myeloid specific deletion of Piezo1 ($Piezo1\Delta^{LysM}$) have increased signal transducer and activator of transcription 6 (STAT6) activation, and decreased nuclear factor kappa-light-chain-enhancer of activated B cells (NF-kB) activation, leading to a pro-healing phenotype after stimulation with IFN-γ/LPS (32). It has been shown that $Piezo1\Delta^{LysM}$ mice have impaired clearance of *P. aeruginosa* in the lungs compared with wild-type mice, demonstrating that Piezo1 is required for bacterial clearance in a relevant *in vivo* model (31). However, the opposite was shown in a mouse model

of polymicrobial sepsis *via* cecal ligation and puncture (CLP). The CLP model, CD11b+ myeloid cells from Piezo1Δ^{LysM} mice had decreased pro-inflammatory cytokines, enhanced peritoneal bacterial clearance, and less sepsis-related death than their Piezo1$^{fl/fl}$ littermates (34). These conflicting data illustrate the need for further research to understand the precise role of Piezo1 in the innate immune system using multiple complementary model systems.

Studies support the existence of a positive feedback loop between mechanosensitive channels, such as Piezo1, and the cytoskeleton in macrophages (32). Inhibition of actin polymerization reduced Ca^{2+} influx *via* Piezo1 (32). Feedback loops between Piezo1 and the cytoskeleton have also been demonstrated in other cell types. For example, Piezo1 activation is necessary for orientation of vascular endothelial cells during embryonic development in mice. This process depends on the coordinated assembly and disassembly of the actin cytoskeleton which does not occur correctly in global Piezo1 KO mice (35).

TRPV4

The Transient Receptor Potential (TRP) family of ion channels has many diverse roles, with TRPV4 being the most studied mechanically-gated channel for its role in innate immune cell function (36). TRPV4 is a mechanosensitive, non-selective, Ca^{2+}-permeable cation channel that is ubiquitously expressed and responds to both chemical and mechanical signals (37, 38). TRPV4 channel is assembled into a symmetric tetramer with six transmembrane domains, which provide the gating mechanism surrounding a central ion-conducting pore (39). The TRPV4 channel, unlike other channels in the TRP family, lacks an upper gate in its selectivity mechanism, perhaps explaining the relatively nonselective permeability of TRPV4 (39). The exact mechanism of mechanical activation of TRPV4 is unknown, with both direct and indirect mechanisms proposed (38, 40). Similar to Piezo1 activation, mechanical stimuli, such as membrane stretch, may activate the TRPV4 channel, resulting in Ca^{2+} influx (41). Additionally, the TRPV4 channel is regulated by temperature and endogenous ligands, including arachidonic acid metabolites, such as epoxyeicosatrienoic acids (EETs) (42, 43). Conformational change to the cytosolic tail of TRPV4 may increase the likelihood of TRPV4 binding to stimuli-generated messengers (e.g., EET) versus stimulus-generated channel activation (e.g., hypotonicity, heat) (44). Indirect activation occurs through intracellular signaling cascades utilizing focal adhesions, integrins, adhesins, and various second messengers (38). In fact, applying force to β1 integrins resulted in rapid calcium influx through TRPV4 channels (45). These data suggest that TRPV4 is activated by deformation of the cytoskeletal backbone rather than direct membrane stretch (45). Activation of TRPV4, whether direct or indirect, results in Ca^{2+} influx, cytoskeletal rearrangement, intracellular signaling, and altered gene expression which influence cellular phenotype and function (46).

Increased cytosolic Ca^{2+} is necessary for proper phagosome maturation. *M. tuberculosis* can inhibit TRPV4 expression in macrophages, reducing intracellular Ca^{2+} resulting in dysfunctional delivery of mycobacteria to phago-lysosomal components and impaired acidification of phagosomes, which are necessary for effective infection control (47). TRPV4$^{-/-}$ mice had higher mycobacterial colony counts after aerosolization into the lung compared with wild-type mice, and hence impaired control of the initial *M. tuberculosis* infection (24-48 hours after aerosolization) (47). Interestingly, despite worse control of initial infection, TRPV4$^{-/-}$ mice had improved control of chronic infection at 150 days, as shown by reduced colony forming units compared to wild-type mice (47). Improved control of chronic infection was proposed to be secondary to decreased interferon-γ (INF-γ) and diminished neutrophil-driven inflammation in the TRPV4 KO mice (47). *M. tuberculosis* infection results in significant scaring which changes the mechanical properties of the lung. Although TRPV4-dependant control of *M. tuberculosis* in macrophages has not yet been shown to be tissue-stiffness initiated, macrophage function is influenced by a stiffness-dependent mechanism *via* TRPV4 (46). Furthermore, *M. tuberculosis* also induces TRPV4 protein expression in macrophages, suggesting a complex interaction between TRPV4, *M. tuberculosis*, and the mechanical properties of the lung matrix (47). This is a fruitful area for future investigation.

TRPV4 represents an important link between environmental cues and immune cell function (38). Our group has published that TRPV4 in macrophages mediates both LPS-stimulated phagocytosis and downregulation of pro-inflammatory cytokines in both *in vitro* and *in vivo* models (48). The mechanism of TRPV4 action in immune cells has yet to be fully elucidated, but we show that mitogen-activated protein kinases (MAPKs) play an important role (49). We go on to show that TRPV4 regulates phagocytosis and pro-inflammatory cytokine secretion through a molecular switch from JNK to predominately p38 MAPK (49). We further show that the master regulator of MAPK phosphorylation/de-phosphorylation, dual-specificity phosphatase 1 (DUSP1), controls the MAPK molecular switch (49). Overall, our work shows that TRPV4 modulates LPS-induced MAPK switching in stiffness-dependent manner, illustrating the interplay between mechanical force and soluble pro-inflammatory factors that drive innate immunity (49).

TRPV4 activation has also been shown to be instrumental for nuclear translocation of Yes-associated protein/transcriptional co-activator with PDZ-binding motif (YAP/TAZ) in some cell types (50). YAP is a transcriptional co-activator that regulates macrophage polarization towards a pro-inflammatory phenotype in response to substrate stiffness (8, 51). For example, YAP nuclear localization increased with substrate stiffness which correlated with an increase in TNF-α secretion in macrophages plated on substrates of varying stiffness (1, 20, and 280 kPa) (8). The macrophages plated on soft fibrin gel (~0.1 kPa) compared with polystyrene (~10^6 kPa) had lower total YAP protein, and increased YAP phosphorylation, which leads to its degradation in the cytoplasm (8). The polystyrene-plated macrophages had higher TNF-α secretion in response to LPS, while the fibrin-plated macrophages had increased anti-inflammatory cytokine (IL-10) secretion (8). Therefore, YAP/TAZ participates in the integration of LPS and matrix stiffness

signals to modulate macrophage activation. TRPV4 activation has been shown to result in nuclear translocation of YAP/TAZ in other cell types and YAP/TAZ has been shown to mediate macrophage immune function, but whether TRPV4 mediates YAP/TAZ translocation in macrophages in response to pro-inflammatory signals has yet to be shown (8, 51). In summary, TRPV4 signals integrate with canonical inflammatory signals to mediate unique cell type and context-specific responses in macrophages.

PIEZO1 AND TRPV4 CROSSTALK

The possibility of molecular cross-talk between the Piezo1 and TRPV4 channels and its role in cellular responses is an area of active investigation. Not only have Piezo1 and TRPV4 been shown to have individual effects on innate immune function, these channels have also been shown to work in conjunction. While work on TRPV4 and Piezo1 cross-talk has thus far focused on non-immune cells, this work provides insight into possible mechanisms of cooperation between Piezo1 and TRPV4 in immune cells. Based on data from our lab, TRPV4 activation in macrophages by LPS results in anti-inflammatory cytokine secretion (IL-10) and downregulation of pro-inflammatory cytokines, while data from other groups has shown an opposing function of Piezo1 where activation of Piezo1 in a murine *P. aeruginosa* pneumonia model is associated with an increase in pro-inflammatory cytokines (TNF-α, IL-6, IL-1β) (31, 32, 46, 49). We have summarized this data in **Figure 1**. Direct and indirect interactions and cross-talk between Piezo1 and TRPV4 is an area of active investigation.

Piezo1 and TRPV4 have been shown to work synergistically in several pathological states, such as osteoarthritis and pancreatitis. In osteoarthritis, chondrocytes sense physiologic levels of cyclical tensile strain (3% at 0.5 Hz for 8 hours) through TRPV4, while Piezo channels sense excessive, damaging levels of mechanical strain (18% at 0.5 Hz for 8 hours) (52). In pancreatic acinar cells, the activation of Piezo1 by shear stress on pancreatitis acinar cells resulted in a transient elevation of Ca^{2+} that was insufficient to result in the mitochondrial dysfunction and necrosis associated with pancreatitis. Only after activation of TRPV4 by Phospholipase A2 (PLA2) was there a sustained increase in Ca^{2+} which could result in cell death (53). Activation of TRPV4 by PLA2 generated through Piezo1 activation led to a synergistic increase in intracellular Ca^{2+} concentrations with the subsequent pathophysiologic consequences (53). These data demonstrate a complex relationship between Piezo1 and TRPV4. Future work is needed to fully uncover the Piezo1-TRPV4 interactions in inflammatory diseases.

ADHESION MOLECULES

Along with ion channels, other molecular families play important roles in mechanotransduction and mechano-responses in immune cells, such as the cytoskeletal proteins, actin and myosin, focal adhesions, selectins, and integrins. Due to the focused nature of this review, we direct you to more comprehensive reviews in this area (15, 54–56). The cytoskeletal-extracellular matrix interactions have an important role in mechanotransduction by enhancing intracellular signals, activating surface receptors, triggering migration, and cell-to-cell communication in macrophages and neutrophils. The cytoskeletal-extracellular matrix interaction is also necessary for cells to exert force (15). The generation of force is critical for several immune cell functions, such as leukocyte extravasation. Leukocytic integrins connect endothelial cell ligands to intracellular actin and myosin filaments through focal adhesions which serve as anchors to help leukocytes overcome vascular flow in order to initiate adhesion and rolling (15, 56, 57). However, looser associations between selectins and their ligands allow leukocytes to roll along the endothelial surface. These loose associations are characterized as "slip bonds," which weaken under increased tension (58). E-selectin ligands (ESL) allow neutrophils to transduce mechanical signals regarding blood flow and shear force that facilitate the slow rolling needed for effective immunosurveillance (59).

Integrins are transmembrane, heterodimeric proteins, with α and β subunits, which connect the extracellular matrix with the cytoskeleton and mediate intracellular signaling (54, 60). The tensegrity model suggests that integrins act as mechanotranducers by mediating force-induced rearrangements in the cytoskeleton (61). During leukocyte extravasation, chemokines and bacterial surface molecules (e.g. LPS), promote expression of integrins which strengthen the adhesion of leukocytes through the creation of "catch bonds" (60, 62). Catch bonds, unlike slip bonds, become stronger under tension until an optimal tension is exceeded. Cytoskeletal rearrangements mediated through integrins are necessary for the creation of pseudopodia which project between endothelial cells prior to transmigration for effective leukocyte recruitment to site of infection (63). In contrast, the first step of neutrophil extravasation in the lung is dependent on cytoskeletal rearrangements into submembrane F-actin rims in the neutrophil, resulting in neutrophil sequestration in response to lung infection (64).

Given the known interaction between TRPV4, integrins, and toll-like receptors (TLRs), it is worthy to mention the importance of epithelial/endothelial barrier function in the host response to infection. For example, integrin αvβ3 on epithelial/endothelial cells has been shown to be integral to the containment of herpes simplex virus (HSV). Integrin αvβ3 directs HSV to the acidic endosome pathway by re-localizing nectin-1, a cellular protein which mediates the entry of HSV (65). Integrin αvβ3 interactions with toll-like receptor 2 (TLR 2) and viral proteins lead to production of type 1 interferons and NF-kB which helps suppress HSV replication. These functions suggest αvβ3-integrin has an important role in mediating intracellular uptake of HSV and activation of innate immune signaling response (66).

Phagocytosis, the process by which a cell engulfs extracellular particles/pathogens *via* cytoskeletal rearrangement, is essential to

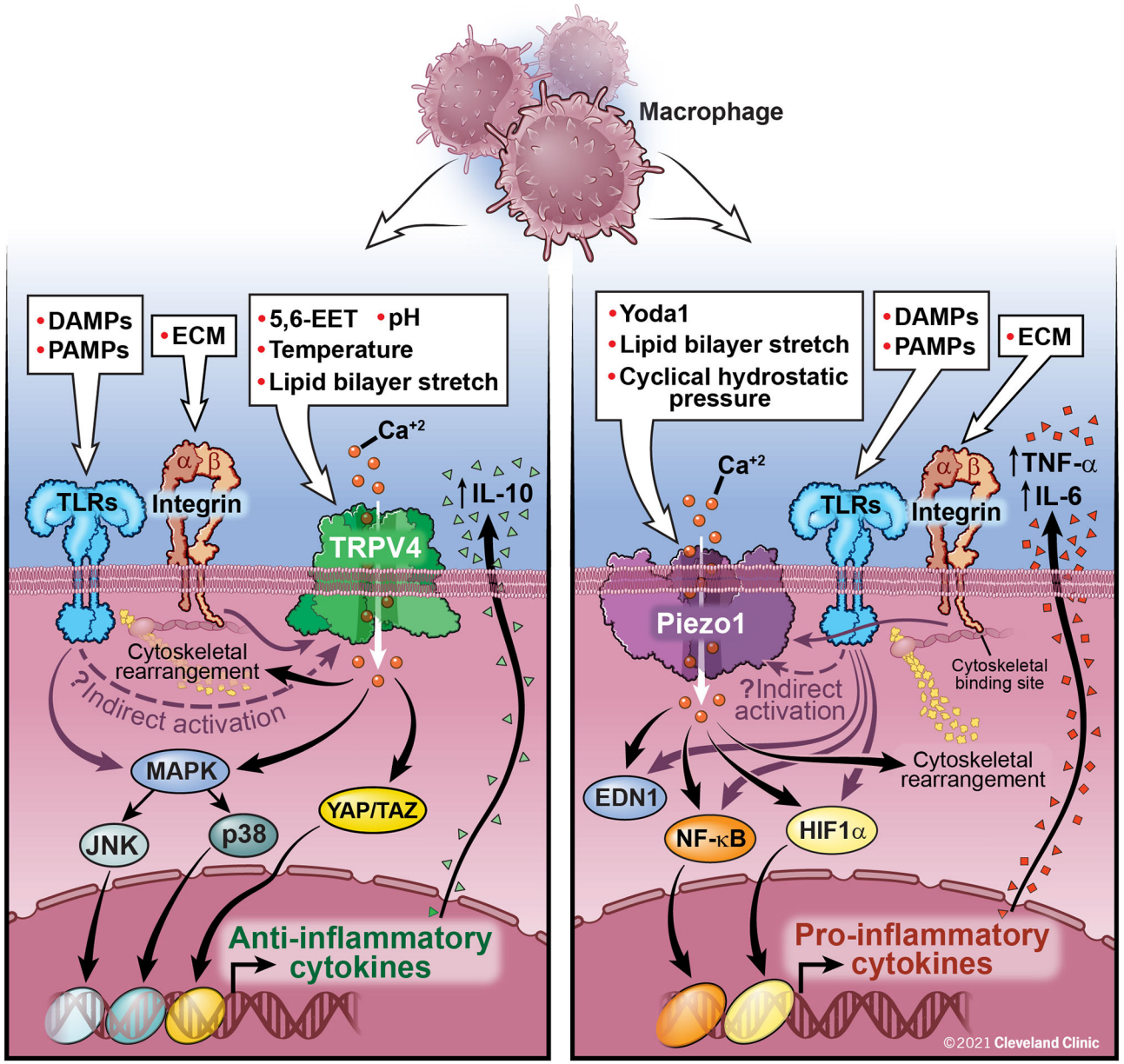

FIGURE 1 | Macrophage activation by TRPV4, Piezo1, and Integrins: TRPV4 is activated by both direct (chemical, mechanical) and indirect mechanisms (downstream signaling through interactions with integrins and TLRs, although the exact mechanism has yet to be elucidated). TRPV4 activation leads to Ca^{2+} influx and activation of several nuclear transcription factors, such as MAPK and YAP/TAZ leading to a decrease in pro-inflammatory cytokines and upregulation of anti-inflammatory cytokines, such as IL-10. Activation of Piezo1, either directly or through interaction with TLRs, leads to Ca^{2+} influx, AP-1 activation, production of EDN1, and nuclear translocation of HIF1α and NF-kB leading to an increase in pro-inflammatory cytokines, IL-6 and TNF-α. Feedback loops between Piezo1 and actin polymerization also contribute to macrophage function. Integrins traverse the cell membrane with an extracellular ligand binding site connecting to an intracellular cytoskeletal bind site. Integrins are important for control of viral and bacterial infections through interactions with TLRs. Further study is needed to fully understand the interactive functions of Piezo1 and TRPV4 and their ability to be activated by integrins and TLRs. These interactions are likely cell-type and context specific.

immune cell function. Upon activation of TLRs and G-protein coupled receptors (GPCR) by chemokines and LPS, phagocytes exit their resting state and undergo actin remodeling to become primed for interaction with phagocytic targets (55). Priming of phagocytes leads to the expression of phagocytotic receptors and growth of the phagocytotic cup (55). Similar to lamellipodial growth, expansion of the phagocytotic cup occurs by accumulation and arrangement of F-actin into a peripheral ring (15). Furthermore, during phagocytosis catch bonds form between the macrophage filopodia glycoprotein CD48 and the

adhesin FimH on the fimbrae of *Escherichia coli*. This stable connection triggers formation of a lamellipodium to scoop up the surface bound pathogens and shovel them into the phagocytotic cup (67). Once the pathogen is internalized, the phagosome undergoes maturation, preparing for pathogen killing and disposal. Fusion of the phagosome with proteolytic enzyme-rich granules and acidic lysosomes facilitates pathogen killing (68).

While the mechanism is not fully understood, the observation that constraints on macrophage cell shape induce changes to macrophage immune function suggests the important role of the cytoskeleton in determining macrophage inflammatory phenotype (69). This occurs through a dynamic bidirectional interaction, in which both outside-in signals (mechanical, physical, temperature, and chemical) and inside-out cytoskeletal modifications can affect macrophage function. Our lab has shown that matrix-stiffness is a critical factor in determining the effectiveness of phagocytosis and pathogen clearance, which is blocked in the absence of TRPV4 (46, 49). Improved overall pathogen clearance mediated by TRPV4 in the presence a stiff matrix is depends in part on cytoskeletal remodeling. That said, other processes including neutrophil recruitment and degranulation, reactive oxygen species generation, myeloperoxidase production, and cytokine and resolvin secretion contribute to overall pathogen clearance and resolution of infection.

CLINICAL IMPLICATIONS

Mechanotransduction in innate immune cells has been shown to have an impact on multiple disease states, including non-infectious (e.g. ventilator-associated and hydrochloric acid [HCl]) and infectious (e.g. pneumonia) inducers of lung injury (48, 70). In non-infectious inflammation, rapid influx of Ca^{2+} *via* TRPV4 in murine pulmonary endothelial cells undergoing mechanical ventilation with high peak inspiratory pressures (25 and 35 cmH_2O) leads to increased permeability, rapid accumulation of inflammatory cell infiltrates, and pulmonary edema (71, 72). These changes in surface tension on the alveolar surface can influence macrophage phagocytotic activity, with increasing alveolar surface tension associated with a reduction in effective macrophage phagocytosis (73). In a murine model of acute respiratory distress syndrome secondary to instillation of hydrochloric acid (HCl), mimicking aspiration-induced lung injury, TRPV4 KO lungs perfused with $TRPV4^{+/+}$ leukocytes had increased neutrophil activation, respiratory burst, and neutrophil adhesion and migration compared to TRPV4 KO lungs perfused with blood from TRPV4 KOs, suggesting that neutrophil TRPV4 mediates the acute cellular inflammatory response. On the other hand, vascular leak and histologic signs of lung injury were mediated by endothelial TRPV4, rather than neutrophil TRPV4 activation (70). Pharmacologic inhibition of TRPV4 attenuated the sequelae of acute lung injury secondary to HCl exposure, including the breakdown of the endothelial barrier, lung inflammation, and histologic signs of lung injury. This attenuation of lung injury occurred only if the TRPV4 inhibitor was given prior to the administration of HCl (70). On the other hand, post-exposure pharmacologic inhibition of TRPV4 suppressed pulmonary inflammation from chemically-induced lung injury through reductions in macrophages, neutrophils, and pro-inflammatory cytokines when given 30 minutes after HCl or chlorine gas administration (74).

In regards to infection-associated inflammation, TRPV4 has been noted to be activated by heat which may provide a mechanism for immune cell activation in response to changes in body temperature (43, 75). Febrile-range temperatures are associated with more effective recruitment and respiratory burst in neutrophils and increased bacterial clearance and cytokine secretion in macrophages (76). As previously discussed, both Piezo1 and TRPV4 activation leads to increased bacterial clearance. During cyclical hydrostatic pressure conditions, mice with absent Piezo1 in macrophages were shown to be unable to control infection after intranasal *P. aeruginosa* (31). Similarly, our work showed increased clearance of intrapulmonary *P. aeruginosa* in wild-type mice compared to TRPV4 KOs in a stiffness-dependent fashion (48). However, in a murine model of sepsis, pharmacologic inhibition of TRPV4 improved survival and reduced pro-inflammatory cytokines, including TNF-α and IL-6 (77). These studies demonstrate a context and model-system specificity and suggest that the role of TRPV4 in infection and inflammation remains to be fully understood.

Understanding the mechanisms by which immune cells sense and respond to mechanosensitive tissue signals presents potential targets to treat human disease. Limited clinical trials have been performed using pharmacologic inhibition of TRPV4 by GSK2798745 (GSK; GlaxoSmithKline, London, UK) (78). The safety and tolerability of the pharmacologic inhibitor of TRPV4, GSK, has been demonstrated in both healthy human subjects and in those with compensated heart failure (79). There have been clinical trials evaluating the potential therapeutic benefit of GSK for several conditions including: cardiogenic pulmonary edema, chronic cough, and LPS-induced lung injury, although the trials for lung injury and chronic cough were terminated early because they were unlikely to reach their primary end-points (80–82). The scientific basis for these trials is to inhibit TRPV4's role in vasodilation and vascular permeability, which is likely mediated by both endothelial and immune cell dysfunction (83). TRPV4 inhibition has even been proposed as a possible therapeutic agent preventing damage to the alveolar-capillary barrier associated with Coronavirus Disease 2019 (COVID-19) (84).

FUTURE DIRECTIONS

Ongoing study of mechanobiology in innate immune cells offers further understanding of human disease and opportunities for potential therapeutics. Future work is needed to target mechanosensitive channels or adhesion molecules to control intracellular signal transduction and modulate disease, with particular emphasis on examining Piezo1 and TRPV4 interactions during inflammation. While clinical trials in

humans have thus far failed to show efficacy, opportunities to target specific cell types or interacting partners may yield greater efficacy. Future therapeutic targets may be identified from further understanding of downstream signaling pathways, with important areas of future study including autoimmune, allergic, infectious, and malignant conditions. Research has only begun to elucidate the mechanisms involved in innate immune cell mechanotransduction and their potential involvement in a variety of human diseases leads to vast opportunities for ongoing study.

AUTHOR CONTRIBUTIONS

EMO, MAO, and RGS contributed to the conception and writing of the manuscript. AP, BDS, and LMG provided critical revisions to the article. All authors contributed to the article and approved the submitted version.

FUNDING

This work was supported by NIH grants (HL132079) to BDS, (R01HL-133721 and R01HL-158746) to MAO, and (K08HL-133380 and R01HL-155064) to RGS, the Ann Theodore Award to MAO and RGS, and the SMARRT T32 which is funded by the National Institutes of Heart, Lung, and Blood grant, T32HL-155005. The content is solely the responsibility of the authors and does not necessarily represent the official views of the NIH.

REFERENCES

1. Pageon SV, Govendir MA, Kempe D, Biro M. Mechanoimmunology: Molecular-Scale Forces Govern Immune Cell Functions. *Mol Biol Cell* (2018) 29(16):1919–26. doi: 10.1091/mbc.E18-02-0120
2. Rho JY, Ashman RB, Turner CH. Young's Modulus of Trabecular and Cortical Bone Material: Ultrasonic and Microtensile Measurements. *J Biomechanics* (1993) 26(2):111–9. doi: 10.1016/0021-9290(93)90042-D
3. Marinković A, Liu F, Tschumperlin DJ. Matrices of Physiologic Stiffness Potently Inactivate Idiopathic Pulmonary Fibrosis Fibroblasts. *Am J Respir Cell Mol Biol* (2013) 48(4):422–30. doi: 10.1165/rcmb.2012-0335OC
4. Humphrey JD, Dufresne ER, Schwartz MA. Mechanotransduction and Extracellular Matrix Homeostasis. *Nat Rev Mol Cell Biol* (2014) 15 (12):802–12. doi: 10.1038/nrm3896
5. Zhang X, Kim TH, Thauland TJ, Li H, Majedi FS, Ly C, et al. Unraveling the Mechanobiology of Immune Cells. *Curr Opin Biotechnol* (2020) 66:236–45. doi: 10.1016/j.copbio.2020.09.004
6. Zhu C, Chen W, Lou J, Rittase W, Li K. Mechanosensing Through Immunoreceptors. *Nat Immunol* (2019) 20(10):1269–78. doi: 10.1038/s41590-019-0491-1
7. McWhorter FY, Davis CT, Liu WF. Physical and Mechanical Regulation of Macrophage Phenotype and Function. *Cell Mol Life Sci* (2015) 72(7):1303–16. doi: 10.1007/s00018-014-1796-8
8. Meli VS, Atcha H, Veerasubramanian PK, Nagalla RR, Luu TU, Chen EY, et al. YAP-Mediated Mechanotransduction Tunes the Macrophage Inflammatory Response. *Sci Advances* (2020) 6(49):eabb8471. doi: 10.1126/sciadv.abb8471
9. Jain N, Vogel V. Spatial Confinement Downsizes the Inflammatory Response of Macrophages. *Nat Materials* (2018) 17(12):1134–44. doi: 10.1038/s41563-018-0190-6
10. Ekpenyong AE, Toepfner N, Fiddler C, Herbig M, Li W, Cojoc G, et al. Mechanical Deformation Induces Depolarization of Neutrophils. *Sci Advances* (2017) 3(6):e1602536. doi: 10.1126/sciadv.1602536
11. Wang SP, Chennupati R, Kaur H, Iring A, Wettschureck N, Offermanns S. Endothelial Cation Channel PIEZO1 Controls Blood Pressure by Mediating Flow-Induced ATP Release. *J Clin Invest* (2016) 126(12):4527–36. doi: 10.1172/JCI87343
12. Tsuchiya M, Hara Y, Okuda M, Itoh K, Nishioka R, Shiomi A, et al. Cell Surface Flip-Flop of Phosphatidylserine Is Critical for PIEZO1-Mediated Myotube Formation. *Nat Commun* (2018) 9(1):1–15. doi: 10.1038/s41467-018-04436-w
13. Zhou T, Gao B, Fan Y, Liu Y, Feng S, Cong Q, et al. Piezo1/2 Mediate Mechanotransduction Essential for Bone Formation Through Concerted Activation of NFAT-YAP1-ß-Catenin. *eLife* (2020) 9:e52779. doi: 10.7554/eLife.52779
14. Dustin ML. Integrins and Their Role in Immune Cell Adhesion. *Cell* (2019) 177(3):499–501. doi: 10.1016/j.cell.2019.03.038
15. Huse M. Mechanical Forces in the Immune System. *Nat Rev Immunol* (2017) 17(11):679–90. doi: 10.1038/nri.2017.74
16. Brown DM, Donaldson K, Stone V. Role of Calcium in the Induction of Tnfα Expression by Macrophages on Exposure to Ultrafine Particles. In: *Annals of Occupational Hygiene*, vol. 46. Oxford: Oxford Press (2002). p. 219–22. doi: 10.1093/annhyg/46.suppl-1.219
17. Lévêque M, Penna A, le Trionnaire S, Belleguic C, Desrues B, Brinchault G, et al. Phagocytosis Depends on TRPV2-Mediated Calcium Influx and Requires TRPV2 in Lipids Rafts: Alteration in Macrophages From Patients With Cystic Fibrosis. *Sci Rep* (2018) 8(1):1–13. doi: 10.1038/s41598-018-22558-5
18. Bréchard S, Melchior C, Plançon S, Schenten V, Tschirhart EJ. Store-Operated Ca2+ Channels Formed by TRPC1, TRPC6 and Orai1 and Non-Store-Operated Channels Formed by TRPC3 Are Involved in the Regulation of NADPH Oxidase in HL-60 Granulocytes. *Cell Calcium* (2008) 44(5):492–506. doi: 10.1016/j.ceca.2008.03.002
19. Immler R, Simon SI, Sperandio M. Calcium Signalling and Related Ion Channels in Neutrophil Recruitment and Function. *Eur J Clin Invest* (2018) 48:e12964. doi: 10.1111/eci.12964
20. Martinac B. Mechanosensitive Ion Channels: Molecules of Mechanotransduction. *J Cell Sci* (2004) 117(12):2449–60. doi: 10.1242/jcs.01232
21. *Nobel Prize in Medicine Awarded to David Julius and Ardem Patapoutian - the New York Times*. Available at: https://www.nytimes.com/2021/10/04/health/nobel-prize-medicine-physiology-temperature-touch.html (Accessed October 3, 2021).
22. Parpaite T, Coste B. Piezo Channels. *Curr Biol* (2017) 27(7):R250–2. doi: 10.1016/j.cub.2017.01.048
23. Faucherre A, Nargeot J, Mangoni ME, Jopling C. Piezo2b Regulates Vertebrate Light Touch Response. *J Neurosci* (2013) 33(43):17089–94. doi: 10.1523/JNEUROSCI.0522-13.2013
24. Woo SH, Lukacs V, de Nooij JC, Zaytseva D, Criddle CR, Francisco A, et al. Piezo2 Is the Principal Mechanotransduction Channel for Proprioception. *Nat Neurosci* (2015) 18(12):1756–62. doi: 10.1038/nn.4162
25. Kang SS, Shin SH, Auh CK, Chun J. Human Skeletal Dysplasia Caused by a Constitutive Activated Transient Receptor Potential Vanilloid 4 (TRPV4) Cation Channel Mutation. *Exp Mol Med* (2012) 44(12):707–22. doi: 10.3858/emm.2012.44.12.080
26. Coste B, Mathur J, Schmidt M, Earley TJ, Ranade S, Petrus MJ, et al. Piezo1 and Piezo2 are Essential Components of Distinct Mechanically Activated Cation Channels. *Science* (2010) 330(6000):55–60. doi: 10.1126/science.1193270
27. Zhao Q, Zhou H, Chi S, Wang Y, Wang J, Geng J, et al. Structure and Mechanogating Mechanism of the Piezo1 Channel. *Nature* (2018) 554 (7693):487–92. doi: 10.1038/nature25743
28. Botello-Smith WM, Jiang W, Zhang H, Ozkan AD, Lin Y-C, Pham CN, et al. A Mechanism for the Activation of the Mechanosensitive Piezo1 Channel by

the Small Molecule Yoda1. *Nat Commun* (2019) 10(1):1–10. doi: 10.1038/s41467-019-12501-1
29. Nourse JL, Pathak MM. How Cells Channel Their Stress: Interplay Between Piezo1 and the Cytoskeleton. *Semin Cell Dev Biol* (2017) 71:3–12. doi: 10.1016/j.semcdb.2017.06.018
30. Ellefsen KL, Holt JR, Chang AC, Nourse JL, Arulmoli J, Mekhdjian AH, et al. Myosin-II Mediated Traction Forces Evoke Localized Piezo1-Dependent Ca2+ Flickers. *Commun Biol* (2019) 2(1):1–13. doi: 10.1038/s42003-019-0514-3
31. Solis AG, Bielecki P, Steach HR, Sharma L, Harman CCD, Yun S, et al. Mechanosensation of Cyclical Force by PIEZO1 Is Essential for Innate Immunity. *Nature* (2019) 573(7772):69–74. doi: 10.1038/s41586-019-1485-8
32. Atcha H, Jairaman A, Holt JR, Meli VS, Nagalla RR, Veerasubramanian PK, et al. Mechanically Activated Ion Channel Piezo1 Modulates Macrophage Polarization and Stiffness Sensing. *Nat Commun* (2021) 12(1):3256. doi: 10.1038/s41467-021-23482-5
33. Geng J, Shi Y, Zhang J, Yang B, Wang P, Yuan W, et al. TLR4 Signalling *via* Piezo1 Engages and Enhances the Macrophage Mediated Host Response During Bacterial Infection. *Nat Commun* (2021) 12(1):1–14. doi: 10.1038/s41467-021-23683-y
34. Aykut B, Chen R, Kim JI, Wu D, Shadaloey SAA, Abengozar R, et al. Targeting Piezo1 Unleashes Innate Immunity Against Cancer and Infectious Disease. *Sci Immunol* (2020) 5(50):eabb5168. doi: 10.1126/SCIIMMUNOL.ABB5168
35. Ranade SS, Qiu Z, Woo SH, Hur SS, Murthy SE, Cahalan SM, et al. Piezo1, A Mechanically Activated Ion Channel, Is Required for Vascular Development in Mice. *Proc Natl Acad Sci USA* (2014) 111(28):10347–52. doi: 10.1073/pnas.1409233111
36. Partida-Sanchez S, Desai BN, Schwab A, Zierler S. Editorial: TRP Channels in Inflammation and Immunity. *Front Immunol* (2021) 12:684172. doi: 10.3389/fimmu.2021.684172
37. Liedtke W, Tobin DM, Bargmann CI, Friedman JM. Mammalian TRPV4 (VR-OAC) Directs Behavioral Responses to Osmotic and Mechanical Stimuli in Caenorhabditis Elegans. *Proc Natl Acad Sci USA* (2003) 100(24):14531–6. doi: 10.1073/pnas.2235619100
38. Michalick L, Kuebler WM. TRPV4—A Missing Link Between Mechanosensation and Immunity. *Front Immunol* (2020) 11:413. doi: 10.3389/fimmu.2020.00413
39. Deng Z, Paknejad N, Maksaev G, Sala-Rabanal M, Nichols CG, Hite RK, et al. Cryo-EM and X-Ray Structures of TRPV4 Reveal Insight Into Ion Permeation and Gating Mechanisms. *Nat Struct Mol Biol* (2018) 25(3):252–60. doi: 10.1038/s41594-018-0037-5
40. Christensen AP, Corey DP. TRP Channels in Mechanosensation: Direct or Indirect Activation? *Nat Rev Neurosci* (2007) 8(7):510–21. doi: 10.1038/nrn2149
41. Loukin S, Zhou X, Su Z, Saimi Y, Kung C. Wild-Type and Brachyolmia-Causing Mutant TRPV4 Channels Respond Directly to Stretch Force. *J Biol Chem* (2010) 285(35):27176–81. doi: 10.1074/jbc.M110.143370
42. White JPM, Cibelli M, Urban L, Nilius B, McGeown JG, Nagy I. TRPV4: Molecular Conductor of a Diverse Orchestra. *Physiol Rev* (2016) 96(3):911–73. doi: 10.1152/physrev.00016.2015
43. Watanabe H, Vriens J, Suh SH, Benham CD, Droogmans G, Nilius B. Heat-Evoked Activation of TRPV4 Channels in a HEK293 Cell Expression System and in Native Mouse Aorta Endothelial Cells. *J Biol Chem* (2002) 277(49):47044–51. doi: 10.1074/jbc.M208277200
44. Garcia-Elias A, Mrkonjić S, Pardo-Pastor C, Inada H, Hellmich UA, Rubio-Moscardó F, et al. Phosphatidylinositol-4,5-Biphosphate-Dependent Rearrangement of TRPV4 Cytosolic Tails Enables Channel Activation by Physiological Stimuli. *Proc Natl Acad Sci USA* (2013) 110(23):9553–8. doi: 10.1073/pnas.1220231110
45. Matthews BD, Thodeti CK, Tytell JD, Mammoto A, Overby DR, Ingber DE. Ultra-Rapid Activation of TRPV4 Ion Channels by Mechanical Forces Applied to Cell Surface β1 Integrins. *Integr Biol* (2010) 2(9):435–42. doi: 10.1039/c0ib00034e
46. Scheraga RG, Southern BD, Grove LM, Olman MA. The Role of TRPV4 in Regulating Innate Immune Cell Function in Lung Inflammation. *Front Immunol* (2020) 11:1211. doi: 10.3389/fimmu.2020.01211
47. Naik SK, Pattanaik K, Eich J, Sparr V, Hauptmann M, Kalsdorf B, et al. Differential Roles of the Calcium Ion Channel TRPV4 in Host Responses to Mycobacterium Tuberculosis Early and Late in Infection. *iScience* (2020) 23(6):101206. doi: 10.1016/j.isci.2020.101206
48. Scheraga RG, Abraham S, Niese KA, Southern BD, Grove LM, Hite RD, et al. TRPV4 Mechanosensitive Ion Channel Regulates Lipopolysaccharide-Stimulated Macrophage Phagocytosis. *J Immunol* (2016) 196(1):428–36. doi: 10.4049/jimmunol.1501688
49. Scheraga RG, Abraham S, Grove LM, Southern BD, Crish JF, Perelas A, et al. TRPV4 Protects the Lung From Bacterial Pneumonia *via* MAPK Molecular Pathway Switching. *J Immunol* (2020) 204(5):1310–21. doi: 10.4049/jimmunol.1901033
50. Sharma S, Goswami R, Zhang DX, Rahaman SO. TRPV4 Regulates Matrix Stiffness and Tgfβ1-Induced Epithelial-Mesenchymal Transition. *J Cell Mol Med* (2019) 23(2):761–74. doi: 10.1111/jcmm.13972
51. Yagi R, Chen LF, Shigesada K, Murakami Y, Ito Y. A WW Domain-Containing Yes-Associated Protein (YAP) Is a Novel Transcriptional Co-Activator. *EMBO J* (1999) 18(9):2551–62. doi: 10.1093/emboj/18.9.2551
52. Du G, Li L, Zhang X, Liu J, Hao J, Zhu J, et al. Roles of TRPV4 and Piezo Channels in Stretch-Evoked Ca2+ Response in Chondrocytes. *Exp Biol Med* (2020) 245(3):180–9. doi: 10.1177/1535370219892601
53. Swain SM, Romac JMJ, Shahid RA, Pandol SJ, Liedtke W, Vigna SR, et al. TRPV4 Channel Opening Mediates Pressure-Induced Pancreatitis Initiated by Piezo1 Activation. *J Clin Invest* (2020) 130(5):2527–41. doi: 10.1172/JCI134111
54. Hynes RO. Integrins: Bidirectional, Allosteric Signaling Machines. *Cell* (2002) 110(6):673–87. doi: 10.1016/S0092-8674(02)00971-6
55. Freeman SA, Grinstein S. Phagocytosis: Receptors, Signal Integration, and the Cytoskeleton. *Immunol Rev* (2014) 262(1):193–215. doi: 10.1111/imr.12212
56. Springer TA. Adhesion Receptors of the Immune System. *Nature* (1990) 346(6283):425–34. doi: 10.1038/346425a0
57. Geiger B, Spatz JP, Bershadsky AD. Environmental Sensing Through Focal Adhesions. *Nat Rev Mol Cell Biol* (2009) 10(1):21–33. doi: 10.1038/nrm2593
58. Beste MT, Hammer DA. Selectin Catch-Slip Kinetics Encode Shear Threshold Adhesive Behavior of Rolling Leukocytes. *Proc Natl Acad Sci USA* (2008) 105(52):20716–21. doi: 10.1073/pnas.0808213105
59. Chase SD, Magnani JL, Simon SI. E-Selectin Ligands as Mechanosensitive Receptors on Neutrophils in Health and Disease. *Ann Biomed Eng* (2012) 40(4):849–59. doi: 10.1007/s10439-011-0507-y
60. Meli VS, Veerasubramanian PK, Atcha H, Reitz Z, Downing TL, Liu WF. Biophysical Regulation of Macrophages in Health and Disease. *J Leukocyte Biol* (2019) 106(2):283–99. doi: 10.1002/JLB.MR0318-126R
61. Wang N, Butler JP, Ingber DE. Mechanotransduction Across the Cell Surface and Through the Cytoskeleton. *Science* (1993) 260(5111):1124–7. doi: 10.1126/science.7684161
62. Thelen M, Stein JV. How Chemokines Invite Leukocytes to Dance. *Nat Immunol* (2008) 9(9):953–9. doi: 10.1038/ni.f.207
63. Beekhuizen H, Furth Rv. Diapedesis. In: *Encyclopedia of Immunology*. Amsterdam: Elsevier (1998). p. 757–60. doi: 10.1006/rwei.1999.0200
64. Yoshida K, Kondo R, Wang Q, Doerschuk CM. Neutrophil Cytoskeletal Rearrangements During Capillary Sequestration in Bacterial Pneumonia in Rats. *Am J Respir Crit Care Med* (2006) 174(6):689–98. doi: 10.1164/rccm.200502-276OC
65. Gianni T, Campadelli-Fiume G. V 3-Integrin Relocalizes Nectin1 and Routes Herpes Simplex Virus to Lipid Rafts. *J Virology* (2012) 86(5):2850–5. doi: 10.1128/jvi.06689-11
66. Gianni T, Leoni V, Chesnokova LS, Hutt-Fletcher LM, Campadelli-Fiume G. αvβ3-Integrin Is a Major Sensor and Activator of Innate Immunity to Herpes Simplex Virus-1. *Proc Natl Acad Sci USA* (2012) 109(48):19792–7. doi: 10.1073/pnas.1212597109
67. Möller J, Lühmann T, Chabria M, Hall H, Vogel V. Macrophages Lift Off Surface-Bound Bacteria Using a Filopodium- Lamellipodium Hook-and-Shovel Mechanism. *Sci Rep* (2013) 3:2884. doi: 10.1038/srep02884
68. Lee WL, Harrison RE, Grinstein S. Phagocytosis by Neutrophils. *Microbes Infection* (2003) 5(14):1299–306. doi: 10.1016/j.micinf.2003.09.014
69. Rostam HM, Reynolds PM, Alexander MR, Gadegaard N, Ghaemmaghami AM. Image Based Machine Learning for Identification of Macrophage Subsets. *Sci Rep* (2017) 7(1):1–11. doi: 10.1038/s41598-017-03780-z
70. Yin J, Michalick L, Tang C, Tabuchi A, Goldenberg N, Dan Q, et al. Role of Transient Receptor Potential Vanilloid 4 in Neutrophil Activation and Acute Lung Injury. *Am J Respir Cell Mol Biol* (2016) 54(3):370–83. doi: 10.1165/rcmb.2014-0225OC

71. Parker JC, Hernandez LA, Peevy KJ. Mechanisms of Ventilator-Induced Lung Injury. *Crit Care Med* (1993) 21(1):131–43. doi: 10.1097/00003246-199301000-00024
72. Hamanaka K, Jian MY, Weber DS, Alvarez DF, Townsley MI, Al-Mehdi AB, et al. TRPV4 Initiates the Acute Calcium-Dependent Permeability Increase During Ventilator-Induced Lung Injury in Isolated Mouse Lungs. *Am J Physiol - Lung Cell Mol Physiol* (2007) 293(4):L923–32. doi: 10.1152/ajplung.00221.2007
73. Akei H, Whitsett JA, Buroker M, Ninomiya T, Tatsumi H, Weaver TE, et al. Surface Tension Influences Cell Shape and Phagocytosis in Alveolar Macrophages. *Am J Physiol - Lung Cell Mol Physiol* (2006) 291(4):L572–9. doi: 10.1152/ajplung.00060.2006
74. Balakrishna S, Song W, Achanta S, Doran SF, Liu B, Kaelberer MM, et al. TRPV4 Inhibition Counteracts Edema and Inflammation and Improves Pulmonary Function and Oxygen Saturation in Chemically Induced Acute Lung Injury. *Am J Physiol - Lung Cell Mol Physiol* (2014) 307(2):L158–72. doi: 10.1152/ajplung.00065.2014
75. Smith JB, Knowlton RP, Agarwal SS. Human Lymphocyte Responses are Enhanced by Culture at 40°C. *J Immunol* (1978) 121(2):691–4.
76. Evans SS, Repasky EA, Fisher DT. Fever and the Thermal Regulation of Immunity: The Immune System Feels the Heat. *Nat Rev Immunol* (2015) 15 (6):335–49. doi: 10.1038/nri3843
77. Dalsgaard T, Sonkusare SK, Teuscher C, Poynter ME, Nelson MT. Pharmacological Inhibitors of TRPV4 Channels Reduce Cytokine Production, Restore Endothelial Function and Increase Survival in Septic Mice. *Sci Rep* (2016) 6:33841. doi: 10.1038/srep33841
78. Home - ClinicalTrials.gov. Available at: https://clinicaltrials.gov/ (Accessed August 19, 2021).
79. Goyal N, Skrdla P, Schroyer R, Kumar S, Fernando F, Oughton A, et al. Clinical Pharmacokinetics, Safety, and Tolerability of a Novel, First-in-Class TRPV4 Ion Channel Inhibitor, GSK2798745, in Healthy and Heart Failure Subjects. *Am J Cardiovasc Drugs* (2019) 19(3):335–42. doi: 10.1007/s40256-018-00320-6
80. Stewart GM, Johnson BD, Sprecher DL, Reddy YNV, Obokata M, Goldsmith S, et al. Targeting Pulmonary Capillary Permeability to Reduce Lung Congestion in Heart Failure: A Randomized, Controlled Pilot Trial. *Eur J Heart Failure* (2020) 22(9):1641–5. doi: 10.1002/ejhf.1809
81. Mole S, Harry A, Fowler A, Hotee S, Warburton J, Waite S, et al. Investigating the Effect of TRPV4 Inhibition on Pulmonary-Vascular Barrier Permeability Following Segmental Endotoxin Challenge. *Pulmonary Pharmacol Ther* (2020) 64:101977. doi: 10.1016/j.pupt.2020.101977
82. Ludbrook VJ, Hanrott KE, Kreindler JL, Marks-Konczalik JE, Bird NP, Hewens DA, et al. Adaptive Study Design to Assess Effect of TRPV4 Inhibition in Patients With Chronic Cough. *ERJ Open Res* (2021) 7 (3):00269–2021. doi: 10.1183/23120541.00269-2021
83. Rosenbaum T, Benítez-Angeles M, Sánchez-Hernández R, Morales-Lázaro SL, Hiriart M, Morales-Buenrostro LE, et al. Trpv4: A Physio and Pathophysiologically Significant Ion Channel. *Int J Mol Sci* (2020) 21 (11):3837. doi: 10.3390/ijms21113837
84. Kuebler W, Jordt SE, Liedtke W. COVID-19: Urgent Reconsideration of Lung Edema as a Preventable Outcome: Inhibition of TRPV4 as a Promising and Feasible Approach. *SSRN* (2020) 3558887. doi: 10.2139/ssrn.3558887

Conflict of Interest: The authors declare that the research was conducted in the absence of any commercial or financial relationships that could be construed as a potential conflict of interest.

Publisher's Note: All claims expressed in this article are solely those of the authors and do not necessarily represent those of their affiliated organizations, or those of the publisher, the editors and the reviewers. Any product that may be evaluated in this article, or claim that may be made by its manufacturer, is not guaranteed or endorsed by the publisher.

frontiers in Immunology

ORIGINAL RESEARCH
published: 03 November 2021
doi: 10.3389/fimmu.2021.732029

The Roles of Transient Receptor Potential Vanilloid 1 and 4 in Pneumococcal Nasal Colonization and Subsequent Development of Invasive Disease

Masamitsu Kono[1†], Denisa Nanushaj[1†], Hideki Sakatani[1], Daichi Murakami[1], Masayoshi Hijiya[1], Tetsuya Kinoshita[1], Tatsuya Shiga[1], Fumie Kaneko[1], Keisuke Enomoto[1], Gen Sugita[1], Masayasu Miyajima[2], Yuka Okada[2], Shizuya Saika[2] and Muneki Hotomi[1]*

[1] Department of Otorhinolaryngology-Head and Neck Surgery, Wakayama Medical University, Wakayama, Japan, [2] Department of Ophthalmology, Wakayama Medical University, Wakayama, Japan

Transient receptor potential (TRP) channels, neuronal stimulations widely known to be associated with thermal responses, pain induction, and osmoregulation, have been shown in recent studies to have underlying mechanisms associated with inflammatory responses. The role of TRP channels on inflammatory milieu during bacterial infections has been widely demonstrated. It may vary among types of channels/pathogens, however, and it is not known how TRP channels function during pneumococcal infections. *Streptococcus pneumoniae* can cause severe infections such as pneumonia, bacteremia, and meningitis, with systemic inflammatory responses. This study examines the role of TRP channels (TRPV1 and TRPV4) for pneumococcal nasal colonization and subsequent development of invasive pneumococcal disease in a mouse model. Both TRPV1 and TRPV4 channels were shown to be related to regulation of the development of pneumococcal diseases. In particular, the influx of neutrophils (polymorphonuclear cells) in the nasal cavity and the bactericidal activity were significantly suppressed among TRPV4 knockout mice. This may lead to severe pneumococcal pneumonia, resulting in dissemination of the bacteria to various organs and causing high mortality during influenza virus coinfection. Regulating host immune responses by TRP channels could be a novel strategy against pathogenic microorganisms causing strong local/systemic inflammation.

Keywords: transient receptor potential (TRP), *Streptococcus pneumoniae* (pneumococcus), nasal colonization, pneumonia, sepsis, mouse model, influenza virus

OPEN ACCESS

Edited by:
Junji Xing,
Houston Methodist Research Institute, United States

Reviewed by:
Federico Iovino,
Karolinska Institutet (KI), Sweden
Vicky Sender,
Karolinska Institutet (KI), Sweden
Elizabeth Wohlfert,
University at Buffalo, United States

***Correspondence:**
Muneki Hotomi
mhotomi@wakayama-med.ac.jp

†These authors have contributed equally to this work and share first authorship

Specialty section:
This article was submitted to Molecular Innate Immunity, a section of the journal Frontiers in Immunology

Received: *28 June 2021*
Accepted: *07 October 2021*
Published: *03 November 2021*

Citation:
Kono M, Nanushaj D, Sakatani H, Murakami D, Hijiya M, Kinoshita T, Shiga T, Kaneko F, Enomoto K, Sugita G, Miyajima M, Okada Y, Saika S and Hotomi M (2021) The Roles of Transient Receptor Potential Vanilloid 1 and 4 in Pneumococcal Nasal Colonization and Subsequent Development of Invasive Disease. Front. Immunol. 12:732029. doi: 10.3389/fimmu.2021.732029

INTRODUCTION

Temperature is one of the most critical factors for organisms to maintain their lives. For maintenance of a suitable environment for survival, there are various temperature sensing mechanisms in many organisms. An environment of too high or low temperature is a life-threatening condition that is recognized as a sense of pain. The transient receptor potential vanilloid (TPRV) 1 channel was firstly identified in 1997 as one of the main molecules involved in temperature sensing systems (1). Transient receptor potential (TRP) channels are activated not only by temperature but also by multiple external stimuli such as taste, acidity, or pain and have a critical role in maintaining homeostasis. TRP channels have been shown in recent studies to be associated with various diseases, including infection by microorganisms (2–6).

TRPV channels are evolutionarily conserved and important in the signaling detection; they are activated by vanilloid-like compounds (7) and mostly expressed on the glial cells: microglia and astrocytes (8). However, some of the channels, such as TRPV1 and TRPV4, are found to be expressed in the upper respiratory tract and lungs. TRPV1 is a capsaicin-activated channel found in the peripheral nerves that is responsible for the burning pain in cases of inflammation (9), which is thought to have a strong relation with respiratory tract inflammatory diseases, asthma, and chronic obstructive pulmonary disease (10, 11). On the other hand, TRPV4 has been found to be activated by lipopolysaccharide (LPS), which is the main virulence factor of Gram-negative bacteria and a strong agonist of toll-like receptor 4 (3). TRPV4 is reported to be associated with the pathogenesis of chronic rhinosinusitis (12). The upper respiratory tract is the site where commensal bacterial flora is formed early in life. These bacteria sometimes invade deeper tissues or migrate to the other sites that cause local inflammation and tissue damage. TRP channels are thought to have potentially critical roles in the defense system by repairing the tissue in the upper respiratory tract damaged by infection, but the association between TRP and bacterial infections present in the upper respiratory tract is not well understood.

Streptococcus pneumoniae, a Gram-positive bacterium that does not have LPS, is a representative commensal of the nasopharynx that also can become pathogenic and cause diseases, such as otitis media, bacteremia, pneumonia, and meningitis in the cases of migration to the more sterile sites (13). It is also associated with potentially lethal secondary bacterial infection during viral infections, such as influenza virus (14). Despite the introduction of pneumococcal conjugate vaccines, there are still many outstanding problems to be resolved: the high evolution rate, serotype replacement, and the high risk of mortality by invasive pneumococcal infection within the immunologically immature population (15, 16). Our recent study revealed the invasion of *S. pneumoniae* into the cell-to-cell junction and the formation of clusters beneath the layer of human epithelial cells, suggesting the mechanism of pneumococcal colonization and invasion to deeper tissue (17). In this study, we hypothesized that TRPV channels have protective functions for the host by regulating inflammation and tissue damage in the course of pneumococcal nasal colonization and subsequent development of severe invasive infections. We evaluated the role of TRPV1 and TRPV4 channels on pneumococcal pathogenesis using a nasal colonization mouse model.

MATERIALS AND METHODS

Ethics Statement

This study was conducted according to the guidelines outlined by the National Science Foundation Animal Welfare Requirements and the Wakayama Medical University Animal Care and Use Committee. The study was approved by the Institutional Animal Care and Use Committee at Wakayama Medical University (Approval number: 901).

Bacterial Strain and Growth Conditions

A pneumococcal strain, P2431 (clinical isolate of serotype 6A), which can establish stable colonization and cause sepsis, was used in this study (18). The bacteria were grown in Todd–Hewitt broth containing 0.5% yeast extract (THY) at 37°C until the mid-log phase and stocked in aliquots at known CFU concentrations in THY broth containing 10% glycerol at −80°C until the experiment.

Mice

The mice used in this experiment were around 6 weeks old. C57BL/6J wild-type mice were purchased from Charles River Laboratories Japan, Inc. (Yokohama, Japan). TRPV1 KO mice were purchased from the Jackson Laboratory (Bar Harbor, ME, USA), and TRPV4 KO mice were introduced from RIKEN BRC (Tsukuba, Japan) (19, 20). All mice were maintained in a conventional animal facility at Wakayama Medical University.

Infection

The schematic of the experiments is shown in **Figure 1**. This study was designed to investigate a role of TRPV channels in the course of the development of invasive pneumococcal infections following nasal colonization. For the pneumococcal mono-infection group, the mice were intranasally administered with 10 μl of phosphate-buffered saline (PBS) on day −2, and with *S. pneumoniae* on day 0. For the influenza A virus (IAV) coinfection group, the mice were intranasally administered with 10 μl of IAV (HKx31, H3N2 strain) (2×10^3 $TCID_{50}$) on day −2, and with *S. pneumoniae* on day 0. To avoid the mice aspirating the bacteria to the lower respiratory tract and causing pneumonia directly, the mice were inoculated to colonize *S. pneumoniae* intranasally without anesthesia, as previously reported (21–23). The mice were sacrificed by isoflurane asphyxiation for sampling on the desired experimental day or monitored until the mice showed signs of lethal infection including sepsis and sustained bacteremia (decreased motor activity, shivering, and messy hair).

The upper respiratory tract was lavaged with 200 μl of sterile PBS from a needle (26 gauge) inserted into the trachea, and the

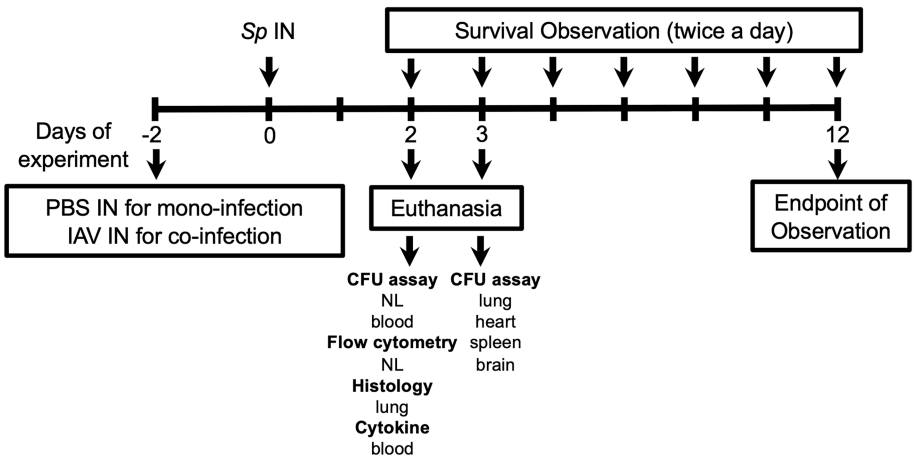

FIGURE 1 | Experimental schematic for this study. Mice were intranasally (IN) inoculated with PBS or IAV on day –2, and *S. pneumoniae* (*Sp*) on day 0. On day 2, nasal lavage (NL) for pneumococcal colony counts (CFU assay) and flow cytometry, lung for histology, blood for CFU assay, and cytokine quantification (ELISA) were collected. On day 3, lung, heart, spleen, and brain were collected for CFU assay. For evaluating the development of lethal infection, mice were monitored until they displayed signs of sick and confirmed bacteremia. NL, nasal lavage.

fluid was collected in a sterile tube. Twenty microliters of the lavage was serially diluted and incubated on a blood plate overnight so the colonies could be counted. Approximately 500 μl of blood was collected by cardiac puncture from each mouse. After taking 20 μl for colony counting, 480 μl of the blood was centrifuged and the serum was stocked for ELISA. The lungs, spleens, hearts, and brains were obtained after the removal of the blood by cardiac puncture. After washing thoroughly with sterile PBS, the organs were homogenized in 1 ml of PBS for counting colonies or were put in 4% of paraformaldehyde (PFA) for histology.

Histological Analyses

The spleens and the lungs were placed on the tubes consisting of 1 ml PFA. The organs were then placed in the automatic sample processor and dehydrated for 48 h. After the cooling process, the tissues were each cut 5 mm thick by microtome and were stored until hematoxylin and eosin (H & E) staining analysis.

The paraffin was fixed for 20 min in the incubator (67°C). The slides were cooled at room temperature for 15 min. The sections were deparaffinized with lemosol two times for 5 min each. The sections were then treated in the following order: 100% ethanol for 1 min × 2, 95% ethanol for 1 min × 2, 80% ethanol for 1 min, 70% ethanol for 1 min. The slides were soaked in Mayer's hematoxylin solution for 7 min and then rinsed in tap water. The slides were soaked in an eosin alcohol solution for 1.5 min and then rinsed in tap water. The tissues were dehydrated in the following order for 1 min each: 70%, 80%, 95%, 95%, 100%, and 100% ethanol). The tissues were cleaned in lemosol for 1 min two times. Then, the slides were coverslipped with Canada balsam mounting solution.

The severity of lung inflammation was quantified using the scoring system proposed in a previous report (24). In brief, the lung tissue was evaluated by five independent factors (neutrophils in the alveolar space, neutrophils in the interstitial space, hyaline membranes, proteinaceous debris filling the air spaces, alveolar septal thickening) indicating the degree of inflammation and calculated using the original formula (**Supplementary Table**). Six samples were evaluated for each group.

Flow Cytometry

Nasal lavages were pelleted at 1,500 rpm for 2 min and resuspended in 200 μl PBS containing 1% bovine serum albumin (BSA). After FcR blocking with a 1:200 dilution of anti-CD16/32 (BioLegend, San Diego, CA, USA) for 15 min, cells were stained for 30 min at 4°C with 25 μl of 1:150 dilution of the following antibodies: anti-CD11b-V450 (BD Biosciences, San Jose, CA, USA), anti-F4/80-PE (BioLegend), anti-Ly6G-PerCP-Cy (BD Biosciences), and anti-CD45-APC-Cy7 (BD Biosciences) for 30 min on ice in the dark. Cells were washed with PBS with 1% BSA, then fixed with 4% PFA. FACSVerse (BD) was used for flow cytometry analysis. After excluding dead cells and debris by gating with forward and side scatter, neutrophils (polymorphonuclear cells; PMNs) were detected as $CD11b^+$, $Ly6G^+$, and $CD45^+$ components. Macrophages were detected as $F4/80^+$, $Ly6G^-$, and $CD45^+$ components. The absolute number of cells in each sample was counted.

Enzyme-Linked Immunosorbent Assay (ELISA)

The blood samples were centrifuged at 5,000 rpm for 5 min and the sera were collected for enzyme-linked immunosorbent assay (ELISA). Quantitative evaluation of cytokines (TNF-α, IL-6, and IL-1β) in serum was performed by following the ELISA kit protocol (Proteintech, Rosemont, IL, USA).

Bactericidal Assay

To assess the impact of TRPV1 and TRPV4 on the neutrophil phagocytic function, we performed bactericidal assays using

murine PMNs ex vivo as previously reported (25). Bone marrow cells were flushed from the 6-week-old murine femora and tibia with RPMI 1640 (Thermo Fisher Scientific, Waltham, MA, USA) with 10% fetal bovine serum and 2 mM EDTA. By centrifugation for 30 min at 2,000 rpm, PMNs were isolated with a discontinuous gradient of Histopaque-1077 and -1119 (Sigma-Aldrich, St. Louis, MO, USA). The cells were then resuspended with Hank's Balanced Salt Solution (Thermo Fisher Scientific) and adjusted to the desired concentration. We confirmed that more than 90% of the $CD45^+$ cells isolated were $Ly6G^+$ and $CD11b^+$. The bacteria (10^2 CFU) were pre-opsonized with baby rabbit complement (Pel-Freez Biologicals, Rogers, AR, USA) for 30 min and applied to the PMNs in a bacterium: PMN ratio of 1:1,000. After 45 min of incubation at 37°C, the bacteria were incubated on the blood agar overnight and the number of colonies counted for quantification. The bacterial survival rate was calculated by dividing the number of bacteria in the experimental sample by those in the control that did not contain PMNs.

Statistical Analyses

All analyses were performed by GraphPad Prism 8.4.3 (GraphPad Software, San Diego, CA, USA). Analysis of the survival experiment was performed by the Kaplan–Meier log-rank test. The Kruskal–Wallis test with Dunn's multiple-comparison test was applied to compare the three groups. $p < 0.05$ was considered to indicate a significant difference.

RESULTS

Nasal Colonization and Development of Bacteremia After Intranasal Inoculation With a Virulent Strain 6A

To evaluate the role of TRPV1 and TRPV4 for pneumococcal carriage, mice (wild-type, TRPV1 KO, TRPV4 KO) were intranasally inoculated with two different doses (1×10^5 and 1×10^7 CFU/mouse) of *S. pneumoniae* 6A strain without anesthesia (**Figure 1**). *S. pneumoniae* was successful in establishing nasal colonization at the same level in all mouse strains (**Figures 2A, C**). The density of colonization was dose-dependently increased among all mouse strains. At the same timing as nasal lavages, the blood cultures were also evaluated for detection of bacteremia. In the low-dose group, bacteremia was not detected in any mouse strains (**Figure 2B**). On the other hand, a significantly higher ratio of bacteremia was observed in TRPV4 KO mice (15 out of 31 mice, 48.4%) compared with wild-type (3 out of 20 mice, 15%) and with TRPV1 KO mice (4 out of 14 mice, 28.6%) by high-dose inoculation (**Table 1**). The density of bacteremia in TRPV4

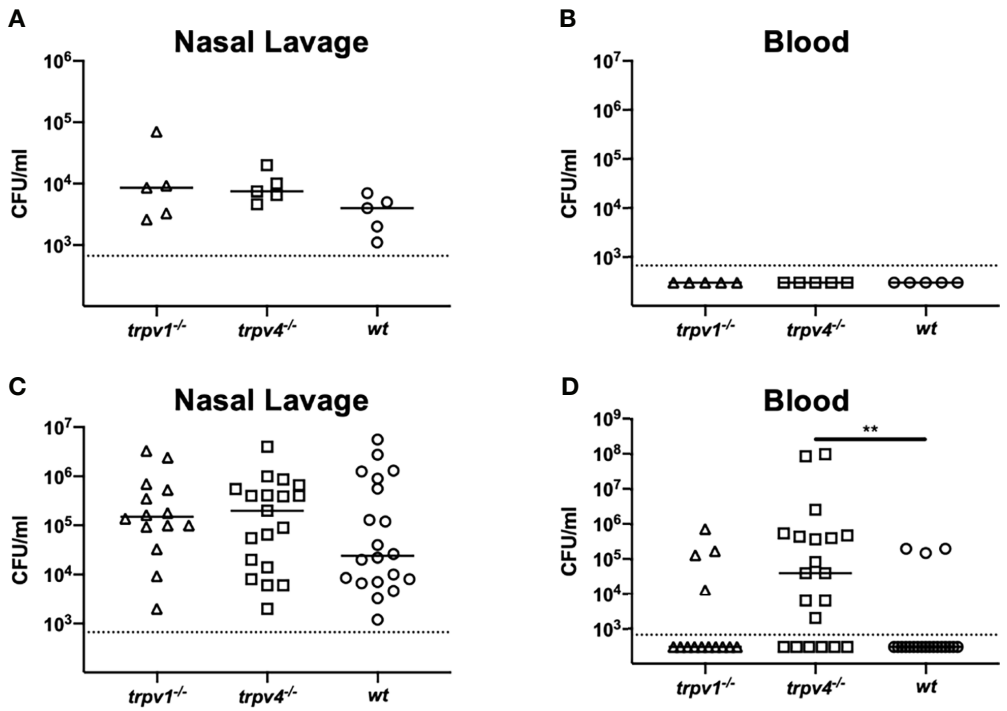

FIGURE 2 | Nasal colonization and bacteremia in the mono-infection model. Mice were intranasally inoculated with different two doses [1×10^5 for **(A, B)** and 1×10^7 CFU/mouse for **(C, D)**] of *S. pneumoniae* without anesthesia on day 0. Nasal lavage and blood were collected on day 2 for counting colonies. Each symbol represents individual data. For low-dose groups **(A, B)**, 5 of TRPV1 KO, 5 of TRPV4 KO, and 5 of wild-type mice were used. For high-dose groups **(C, D)**, 14 of TRPV1 KO, 20 of TRPV4 KO, and 20 of wild-type mice were used. **(A, C)** Nasal lavage and **(B, D)** blood. Horizontal lines indicate median values. The detection limit (the dotted line) is 666 CFU/ml. $^{**}p < 0.01$.

TABLE 1 | Summary of incidence of bacteremia.

	Bacteremia (ratio)	*p* value *vs*. wild type by Fisher's exact test
Mono-infection		
High dose		
Wild type	3/20 (15%)	–
TRPV1 KO	4/14 (28.6%)	Not significant (Ns)
TRPV4 KO	15/31 (48.4%)	$p < 0.05$
Coinfection		
Low dose		
Wild-type	0/12 (0%)	-
TRPV1 KO	2/9 (22.2%)	Ns
TRPV4 KO	4/9 (44.4%)	$p < 0.05$
High dose		
Wild-type	7/15 (46.7%)	–
TRPV1 KO	8/19 (42.1%)	Ns
TRPV4 KO	11/17 (64.7%)	Ns

mice was significantly higher than that of wild type by Kruskal–Wallis test ($p = 0.028$) (**Figure 2D**).

Next, we evaluated the impact of influenza virus coinfection, one of the most exacerbating factors of pneumococcal diseases, on nasal colonization and bacteremia. Even when the mice had been infected with influenza A virus (IAV), the density of nasal colonization was almost equal among all mouse strains, regardless of the dose of inoculum (**Figures 3A, C**). Unlike the pneumococcal mono-infection model, bacteremia was observed, even with the low-dose inoculum. Both the density and the incidence of bacteremia were significantly higher in TRPV4 mice than in wild-type mice ($p = 0.036$) (**Figure 3B**). Although bacteremia was detected at the same frequency in all mouse strains when the dose of inoculum was increased (**Table 1**), TRPV4 KO mice showed the highest density of bacteremia (**Figure 3D**). In this mouse model using a virulent pneumococcal strain, TRPV4 KO mice were more susceptible to development of bacteremia, although all mouse strains were colonized equally.

Local Inflammatory Responses in the Nasal Cavity After the Pneumococcal Inoculum

The local status of inflammation was analyzed with lavages of the upper respiratory tract. The number of PMNs in the nasal lavages on day 2 was counted by flow cytometry. The influx of PMNs was suppressed in TRPV4 KO mice compared to TRPV1 KO and wild-type mice (**Figures 4A, C**). Especially in the coinfection group, the number of PMNs was significantly lower in TRPV1 KO ($p = 0.043$) and TRPV4 KO ($p = 0.0002$)

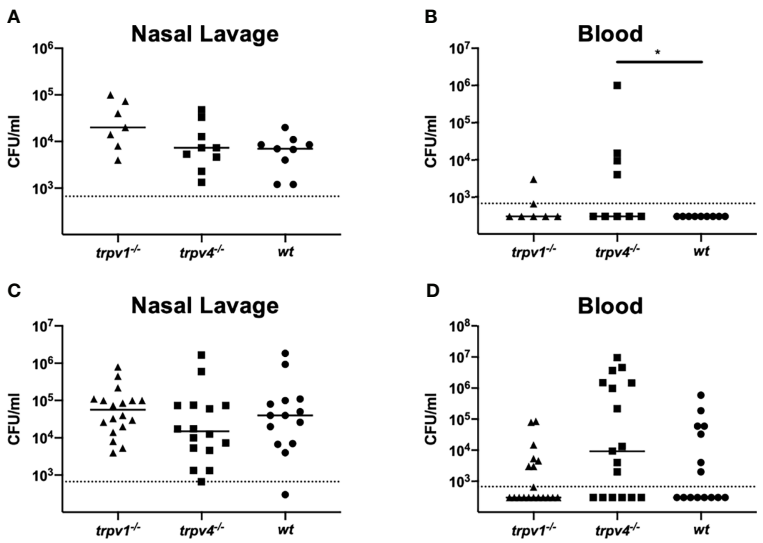

FIGURE 3 | Nasal colonization and bacteremia in the coinfection model. After inoculation of IAV on day –2, mice were intranasally inoculated with two different doses [1×10^5 CFU/mouse for **(A, B)** and 1×10^7 CFU/mouse for **(C, D)**] of *S. pneumoniae* without anesthesia on day 0. Nasal lavage and blood were collected on day 2 for counting colonies. Each symbol represents individual data. For low-dose groups **(A, B)**, 7 of TRPV1 KO, 9 of TRPV4 KO, and 9 of wild-type mice were used. For high-dose groups **(C, D)**, 19 of TRPV1 KO, 17 of TRPV4 KO, and 15 of wild-type mice were used. **(A, C)** Nasal lavage and **(B, D)** blood. Horizontal lines indicate median values. The detection limit (dotted line) is 666 CFU/ml. *$p < 0.05$.

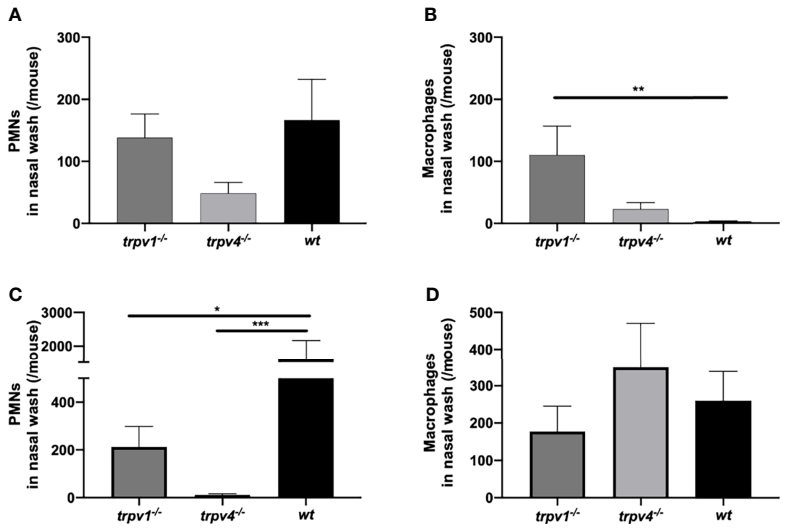

FIGURE 4 | The number of PMNs and macrophages in the nasal lavages. The nasal lavages were collected on day 2 from the mice in the mono-infection and coinfection model. The numbers of PMNs and macrophages were counted by flow cytometry. **(A, B)** The mono-infection model and **(C, D)** the coinfection model. **(A, C)** the number of PMNs and **(B, D)** the number of macrophages. The mean value with the standard error of the mean was represented by a line bar. For the mono-infection model **(A, B)**, 15 of TRPV1 KO, 10 of TRPV4 KO, and 10 of wild-type mice were used. For the coinfection model **(C, D)**, 11 of TRPV1 KO, 12 of TRPV4 KO, and 10 of wild-type mice were used. $^{*}p < 0.05$, $^{**}p < 0.01$, and $^{***}p < 0.001$.

than that of wild type. Among TRPV4 KO mice, the number of PMNs was significantly lower in the coinfection model than in the mono-infection model ($p = 0.018$ by Mann–Whitney's U test), which was the opposite result of an increase of PMNs in the coinfection model among wild-type mice.

We also counted the number of macrophages in the nasal lavages. There was a significant difference between TRPV1 KO and wild type in the mono-infection model (**Figure 4B**). In the coinfection model, there were no differences in the number of macrophages among the three mouse strains (**Figure 4D**).

Dissemination of the Pneumococcal Infection to the Other Organs

To see the spread of the pneumococcus to various organs after nasal colonization, the mice were sacrificed on day 3 and the hearts, spleens, lungs, and brains were collected for culture (**Figure 1**). In the pneumococcal mono-infection model, we could not find bacteria in any organs in any mouse strains (data not shown). Contrary to wild type, the bacteria were detected in most of the samples of TRPV1 KO and TRPV4 KO mice in the coinfection model (**Figure 5**). Especially in the TRPV4 KO mice, the density of bacteria in all organs examined was significantly increased as compared with the wild type.

To investigate the route of pneumococcal infection in the multiple organs, the lung tissues were histologically analyzed. In the mono-infection model, no inflammation was observed in the lungs among all mouse strains (**Figures 6A–F**). In the coinfection model, the lungs of TRPV4 KO mice showed inflammatory infiltrates with neutrophils and macrophages in the interstitium and hemorrhage in the alveoli (**Figures 6K, L**). Furthermore, the lung tissues of TRPV1 KO mice demonstrated alveolar walls showing capillary congestion and mild to moderate inflammatory infiltrate including inflammatory cells (**Figures 6I, J**). On the other hand, no evidence of apparent inflammation was observed in the lung tissues of wild-type mice (**Figures 6G, H**). The severity of inflammation was quantified using a previously reported scoring system (24). There was a significantly higher inflammation in TRPV4 KO mice than wildtype when the mice were infected with both S. pneumoniae and IAV (**Figure 6M**). We also evaluated the lung tissues of the mice infected only with IAV and confirmed no apparent findings of viral pneumonia (data not shown). Histological findings suggest that TRPV1 and TRPV4 may be involved in regulating the pneumococcus migration to the lower respiratory tract and dissemination to multiple organs.

Effect of TRPV on Pneumococcal Lethal Infection

To evaluate the role of TRPV1 and TRPV4 on pneumococcal invasive diseases, we established a spontaneous pneumococcal lethal infection model after nasal colonization. The mice were given the bacteria intranasally on day 0 of the experiment with the dose of 1×10^7/mouse. They were monitored every 12 h until they showed signs of lethal infection, such as decreased motor activity, shivering, and messy hair (**Figure 1**). Similar time courses were observed, and around 70% of mice finally developed lethal infection among all groups in the mono-infection model (wild type; 65%, TRPV1 KO; 62%, TRPV4 KO; 75%, respectively) (**Figure 7A**).

When the mice were pre-infected with IAV, more than 70% of TRPV1 KO mice eventually developed lethal infection. TRPV4 KO mice showed the worst course in the coinfection model, and

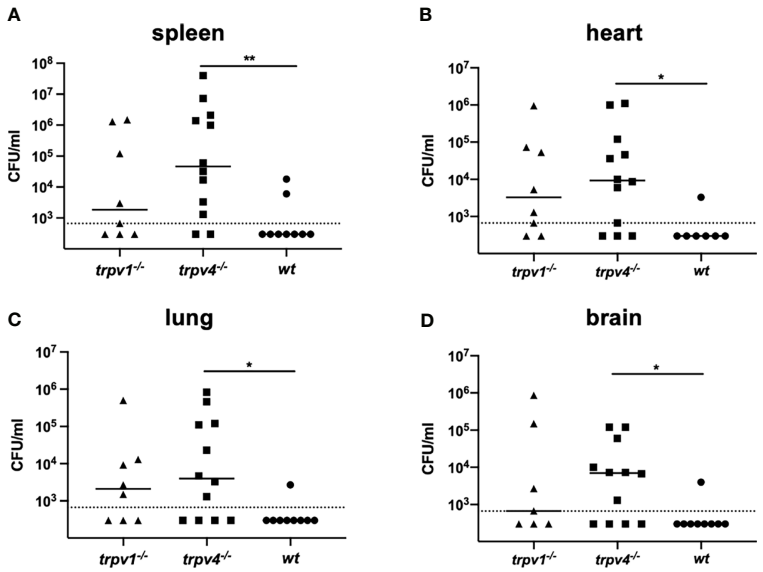

FIGURE 5 | The number of pneumococcal colonies detected in various organs. The spleen **(A)**, heart **(B)**, lung **(C)**, and brain **(D)** were collected on day 3 from the mice in the mono-infection and coinfection models. The data of the coinfection model were displayed. Each sample was thoroughly washed and homogenized in 1 ml of sterile PBS. Each symbol represents individual data. Eight of TRPV1 KO, 12 of TRPV4 KO, and 7 of wild-type mice were used. Horizontal lines indicate median values. The detection limit (the dotted line) is 666 CFU/ml. $^{*}p < 0.05$ and $^{**}p < 0.01$.

all mice developed lethal infection within 7 days after the pneumococcal challenge. Wild type showed significantly better survival (50%) than TRPV4 KO mice (**Figure 7B**). We also observed the mice infected with only IAV, and none of the mice in any of the three strains died during the observation period (data not shown).

Systemic Inflammatory Responses After the Pneumococcal Infection

Blood samples were collected from the colonized mice on day 2 of the experiment. The sera were separated by centrifugation, and the levels of cytokines—tumor necrosis factor-α (TNF-α), interleukin-6 (IL-6), and interleukin-1β (IL-1β)—were measured by ELISA. In the mono-infection model, the levels of TNF-α were significantly higher in TRPV4 KO mice than those of wild type and TRPV1 KO mice ($p < 0.05$ and $p < 0.001$, respectively) (**Figure 8A**). Similar levels of IL-6 and IL-1β were observed among wild-type and TRPV4 KO mice, whereas the production of IL-6 and IL-1β was low in TRPV1 KO mice (**Figures 8B, C**).

When coinfected with IAV, the production of TNF-α was greatly suppressed in TRPV4 KO mice compared with the mono-infection model (**Figure 8D**). The levels of IL-6 and IL-1β were lower in TRPV1 KO and TRPV4 KO mice than in wild-type mice, although without statistical differences (**Figures 8E, F**).

Effect of TRPV1 and TRPV4 on the Phagocytic Bactericidal Ability of Neutrophils

To evaluate the mechanism of protection against pneumococcal infection, we focused on the phagocytic bactericidal ability of neutrophils, which is one of the most effective systems for eliminating the pneumococcus. Neutrophils were isolated from each mouse strain and incubated with pre-opsonized bacteria with baby rabbit complement. The survival rate of the bacteria was compared between three groups. The experiment was repeated three times for each mouse strain, and the pooled data are displayed in **Figure 9**. Neutrophils derived from TRPV4 KO mice showed significantly lower bactericidal ability than those derived from wild type ($p < 0.0001$). TRPV1 KO mice showed a similar tendency, but no significant difference was observed.

DISCUSSION

In this report, we demonstrated for the first time that TRPV1 and TRPV4 were involved in the development of invasive pneumococcal infections after establishment of nasal colonization by using knockout mouse strains. Regarding nasal colonization, the pneumococcus could establish stable colonization at the same level among all three mouse strains with or without influenza virus coinfection. In previous studies, the role of TRP channels in infectious diseases has focused on a single-organ infection or a systemic infection (4–6), suggesting that TRP channels do not function positively in a carrier state that does not induce strong inflammation by *S. pneumoniae*.

On the other hand, knockout of TRPV channels showed a clear change in the development of pneumococcal infections. In the mono-infection model, the incidence of bacteremia significantly increased among TRPV4 KO mice by high-dose challenge. Even by low-dose challenge, TRPV4 KO mice

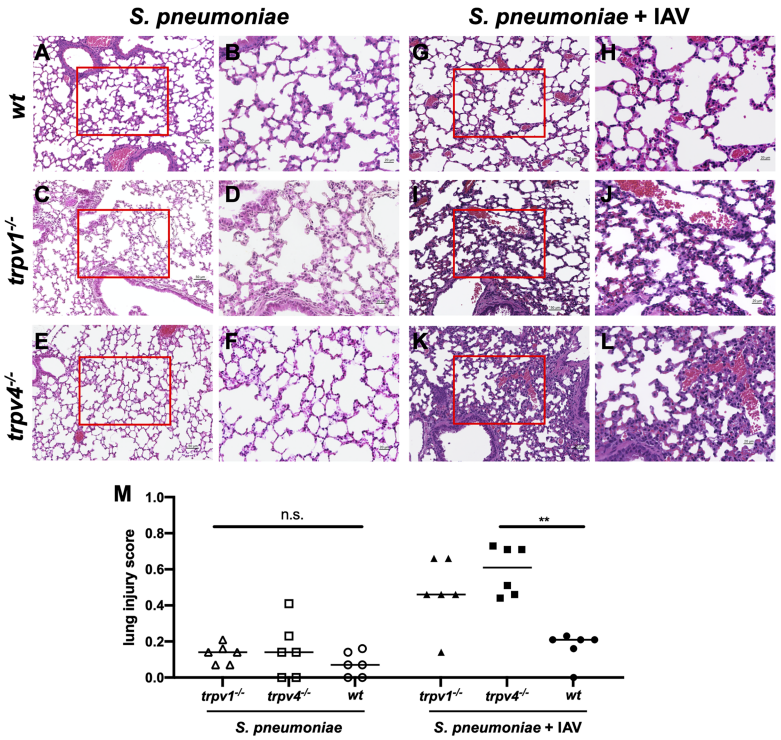

FIGURE 6 | The histology of the lung. The H&E staining of the lung was performed with three mice for each group. The representative images were displayed in this figure. **(A–F)** The mono-infection model. **(G, L)** The coinfection model. **(A, B, G, H)** Wild type **(C, D, I, J)**, TRPV1 KO, and **(E, F, K, L)** TRPV4 KO. **(A, C, E, G, I, K)** Low magnification (×200. Scale bar, 50 μm) and **(B, D, F, H, J, L)** high magnification of boxed sections of the low-magnification field (×400. Scale bar, 20 μm). **(M)** Lung injury score. The severity of lung inflammation was quantified using the scoring system. Each symbol represents individual data. Horizontal lines indicate median values. (N = 6 for each group). n.s., not significant, $^{**}p < 0.01$.

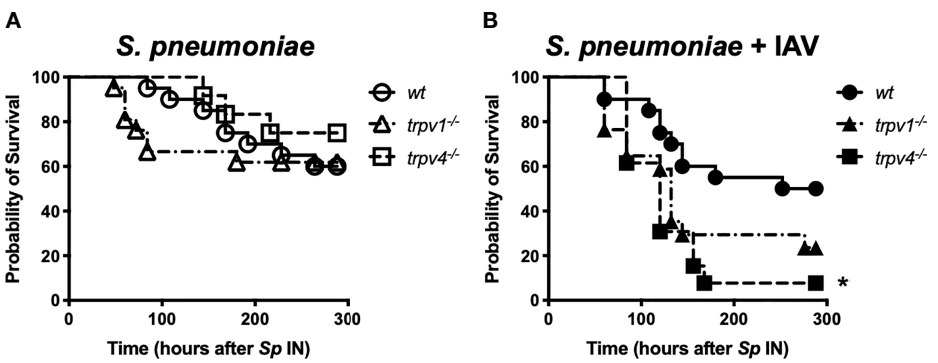

FIGURE 7 | The time course of development of lethal infection. After intranasal administration of *S. pneumoniae*, the mice were monitored every 12 h until day 12. When the mice were found to be sick (decreased motor activity, shivering, and messy hair), they were immediately euthanized and the blood was collected for confirmation of bacteremia. **(A)** The mono-infection model and **(B)** the coinfection model. Circle, triangle, and square indicate wild-type, TRPV1 KO, and TRPV4 KO mice, respectively. $^{*}p < 0.05$.

frequently developed bacteremia when the mice were precedingly infected with influenza virus. It is well known that influenza infection induces strong inflammation with neutrophil influx in the respiratory tract; however, the number of neutrophils in the nasal lavages from TRPV KO mice was significantly low, suggesting the possibility of defect of neutrophil recruitment during influenza infection without TRPV channels. Recent reports have shown that TRP channels are expressed in various cells including immune cells and protect lung infection of Gram-negative bacteria *via* MAPK activation

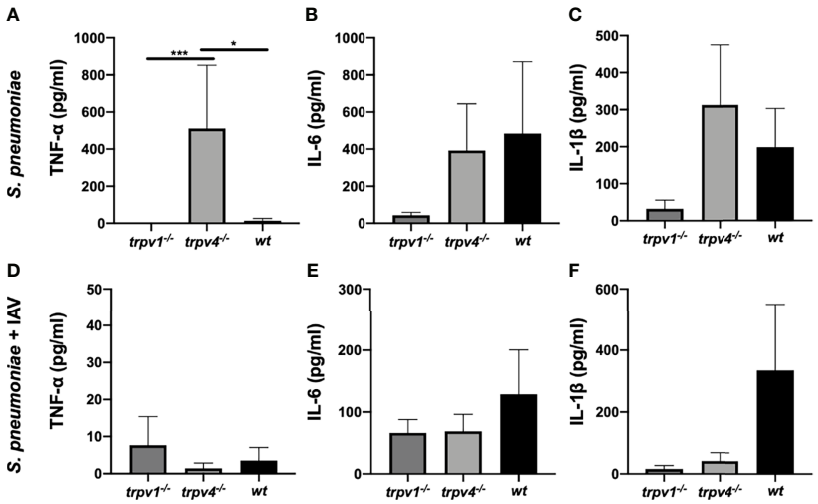

FIGURE 8 | The levels of cytokines in the sera. The levels of cytokines in the sera were measured on day 2 of the experiment. The data were displayed as mean with standard error of the mean. **(A, D)** TNF-α, **(B, E)** IL-6, and **(C, F)** IL-1β. **(A–C)** The mono- infection model and **(D–F)** the coinfection model. For the mono-infection model **(A–C)**, nine of TRPV1 KO, eight of TRPV4 KO, and eight of wild-type mice were used. For the coinfection model **(D–F)**, 13 of TRPV1 KO, 11 of TRPV4 KO, and 8 of wild-type mice were used. *$p < 0.05$, ***$p < 0.001$.

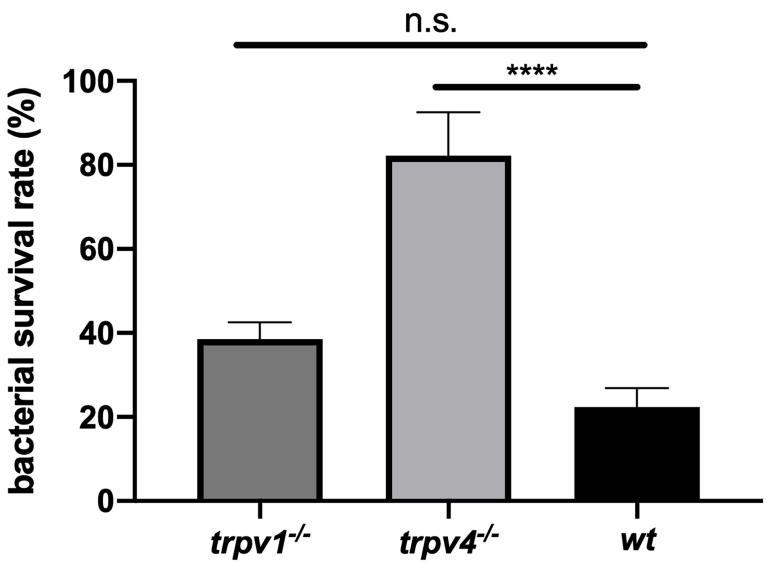

FIGURE 9 | The phagocytic bactericidal ability of PMNs. PMNs isolated from each mouse strain were incubated with the bacteria (10^2 CFU) pre-opsonized with baby rabbit complement for 45 min in a bacterium: PMN ratio of 1:1000. The bacterial survival rate was calculated by dividing the number of bacteria in the experimental sample by those in the control sample that did not contain PMNs. The assay was triplicated and repeated three times for each mouse strain. Pooled data were displayed (N = 9 for each group). The mean value with the standard error of the mean was represented by a line bar. n.s., not significant, ****$p < 0.0001$.

switching (6). We further investigated the bactericidal activity of neutrophils isolated from TRPV KO mice because phagocytosis of opsonized bacteria by neutrophil is one of the most important mechanisms for eliminating *S. pneumoniae*. Significantly impaired bactericidal function of neutrophils derived from both TRPV KO mice (especially TRPV4) ex vivo was observed, suggesting that the TRPV4 channel expressed on neutrophils would be one of the important factors that recognize the pneumococcus. Decreased local influx and phagocytosis of neutrophils might promote the migration of the pneumococcus to the lung and the development of invasion to the bloodstream. Little is known about the function of the TRPV4 channel during

influenza infection, but these results suggest that TRPV4 plays a key role for preventing the exacerbation of pneumococcal infections. In this study, the mechanism of decreased recruitment and impaired bactericidal function of neutrophils lacking TRPV4 are unrevealed. Future studies should be focused on investigating the interaction between TRP channels and pneumococcal virulence factors such as pneumolysin.

In TRPV KO mice (especially TRPV4 KO), bacterial dissemination was observed in multiple organs 3 days after pneumococcal infection, although it was unlikely among wild type. Together with the histological findings of the lungs, most of TRPV KO mice were in pre-sepsis state *via* pneumonia on day 3 after pneumococcal infection resulting in worse prognosis than the wild type. Because the strain used in this study was virulent, even wild-type mice eventually developed lethal infection at a similar rate, as previously reported using the same background strain (23).

The current results are consistent with the other studies related to TRPV4 and its role in the lungs, where the TRPV4 channel is important in the mediation of the phagocytosis, regulation of cytokines, and generation of reactive oxygen species (ROS). The TRPV4 channel may protect from bacterial pneumonia caused by *Pseudomonas aeruginosa* through mitogen-activated protein kinase (MAPK) switching (6). The TRPV4 channel has been shown to be expressed in macrophages of the lungs, and it may have a role in the activation by mechanical stress (26). Another mechanism has been demonstrated that the E3 ubiquitin ligase TRIM29 regulated the activation of alveolar macrophages and had a critical role in the protection against LPS-induced sepsis by *Haemophilus influenzae* (27). Macrophage is also thought to be critical for the clearance of *S. pneumoniae* (28, 29). Flow cytometry showed a similar number of macrophages among all three strains in the coinfection model, although the pneumococcus was detected in multiple organs among only TRPV KO mice. This discrepancy suggests that elimination of *S. pneumoniae* by macrophages may require a TRP-mediated cognitive mechanism, and the timing of evaluating macrophage recruitment was before the peak (30). Scheraga et al. reported that TRPV4 distributed the phenotypic change of macrophage that resulted in the promotion of phagocytosis and bacterial clearance (31).

Regarding the evaluation of cytokines, a significant elevation of TNF-α among TRPV4 KO mice during pneumococcal mono-infection is a good reflection of the relationship between TRPV4 and inflammatory mediators. Xu et al. reported an administration of the TRPV4 agonist inhibited TNF-α-induced monocyte and leukocyte adhesion to human epithelial cells, resulting in reduced atherosclerotic plaque formation in a mouse model (32). The stimulation of LPS to cultured rat microglia expressing TRPV4 controlled the release of TNF-α (33), suggesting that bacterial virulence factors can directly activate TRP channels. Mice lacking the TRPV4 channel could not suppress the production of TNF-α after the blood invasion of *S. pneumoniae*. Contrary to the mono-infection model, the level of TNF-α in the sera of TRPV4 KO mice was very low in the coinfection model. The relationship between influenza virus and TRPV4 channel has not been reported as far as we are aware. During a viral infection that causes strong inflammation in the respiratory tract, TRP channels may respond more strongly and differently, so further investigations are needed. The limitation of the cytokine assay in this study is that the evaluation timing was fixed on day 2 because the mice started developing lethal infection 48 h after the pneumococcal challenge. There should be mice in various conditions such as pneumonia, bacteremia, and sepsis, resulting in a huge variability of cytokine levels within each group.

The serotype 6A pneumococcal strain we used in this study usually develops bacteremia by direct invasion from nasal colonization (without pneumonia) (18). Mice lacking TRPV1 or TRPV4 channels, however, showed moderate to severe pneumonia 48 h after the super-infection of the pneumococcus. This finding is similar to secondary pneumococcal pneumonia, which sometimes occurs as a fatal complication during an influenza pandemic (14). TRPV1 and TRPV4 channels are suggested to contribute to the suppression of pneumococcal pneumonia in the coinfection model. The detailed mechanism of how TRPV channels protected the development pneumonia or lethal infection was not evaluated in the current study. We firstly aimed to investigate the role of TRPV channels on the development of invasive pneumococcal infections following nasal colonization, which the pneumococcus naturally acts within the host. To reveal the detailed mechanism of TRPV channels on each pneumococcal disease such as pneumonia or septicemia, a direct administration to the targeted organ (intra-tracheal injection or intravenous/intraperitoneal injection) should be conducted in the future study separately.

Although no significant difference in survival rate was observed in the lethal infection experiment, the pneumococcus was successful in disseminating to various organs by coinfection of influenza virus, and moderate pneumonia was found among TRPV1 KO mice. Taylor et al. reported that the influenza virus-infected lower respiratory tract inhibited capsaicin and substance P induced relaxation responses (34). The block of the TRPV1 channel may lead the loss of bronchoprotective response during viral infection, which results in exacerbation of pneumococcal super-infection.

The history is relatively short because the link between TRPV channels and infectious diseases remains controversial. Especially for TRPV1, there are a couple of reports concluding that inhibition of TRPV1 neurons during bacterial infection results in a better prognosis. A study of lung infection caused by *Staphylococcus aureus* showed that ablating the TRPV1 nociceptors increased the lung bacterial clearing rate, induced cytokines, and enhanced survival by suppression of the neutrophil activity and by mediation of immunosuppression due to the release of calcitonin gene-related peptide (CGRP) (4). Another study in the *Streptococcus pyogenes* infections demonstrated the role of TRPV1 in the clearance of the pathogen as TRPV1 neurons could be activated by streptolysin S and promoted by the release of CGRP in the infected tissues, therefore increasing the lethality by blocking the recruitment of neutrophils (5). To explain the discrepancy of the current result in TRPV1 KO mice, future studies will investigate how TRP

channels recognize the pneumococcal virulence factors and function positively or negatively within the host immune system.

In conclusion, both TRPV1 and TRPV4 channels regulated the development of pneumococcal infections arising from nasal colonization in an adult mouse model. The TRPV4 channel in particular may play an important role in the prevention of secondary pneumococcal pneumonia and its subsequent development of lethal infection during influenza virus infection. Regulating host immune responses with TRP channels would be a novel strategy against various pathogenic microorganisms.

DATA AVAILABILITY STATEMENT

The original contributions presented in the study are included in the article/**Supplementary Material**. Further inquiries can be directed to the corresponding author.

ETHICS STATEMENT

The animal study was reviewed and approved by the Institutional Animal Care and Use Committee at Wakayama Medical University.

AUTHOR CONTRIBUTIONS

MK, SS, and MHo conceived and designed the experiments. DN, MK, HS, DM, MHi, TK, TS, FK, KE, and MM performed the experiments. DN, MK, HS, DM, and GS analyzed the data. MK, DN, and MHo wrote the paper. YO and SS revised the manuscript. All authors contributed to the article and approved the submitted version.

FUNDING

This project was supported by JSPS KAKENHI Grant Number 19K08959 to GS and JSPS KAKENHI Grant Number 20K08825 to MK.

ACKNOWLEDGMENTS

We thank Prof. Jeffrey N. Weiser for providing the bacterial and viral strain. We thank Dr. Christopher B. Hergott for the technical support. We also thank Prof. Victor Nizet and Drs. Satoshi Uchiyama and Masanobu Hiraoka for the critical discussion and comments on the project. We acknowledge the editing and proofreading by Benjamin Phillis from the Clinical Study Support Center at Wakayama Medical University.

SUPPLEMENTARY MATERIAL

The Supplementary Material for this article can be found online at: https://www.frontiersin.org/articles/10.3389/fimmu.2021.732029/full#supplementary-material

REFERENCES

1. Caterina MJ, Schumacher MA, Tominaga M, Rosen TA, Levine JD, Julius D. The Capsaicin Receptor: A Heat-Activated Ion Channel in the Pain Pathway. *Nature* (1997) 389(6653):816–24. doi: 10.1038/39807
2. Rajan S, Schremmer C, Weber J, Alt P, Geiger F, Dietrich A. Ca^{2+} Signaling by TRPV4 Channels in Respiratory Function and Disease. *Cells* (2021) 10(4):822. doi: 10.3390/cells10040822
3. Mazgaeen L, Gurung P. Recent Advances in Lipopolysaccharide Recognition Systems. *Int J Mol Sci* (2020) 21(2):379. doi: 10.3390/ijms21020379
4. Baral P, Umans BD, Li L, Wallrapp A, Bist M, Kirschbaum T, et al. Nociceptor Sensory Neurons Suppress Neutrophil and Gammadelta T Cell Responses in Bacterial Lung Infections and Lethal Pneumonia. *Nat Med* (2018) 24(4):417–26. doi: 10.1038/nm.4501
5. Pinho-Ribeiro FA, Baddal B, Haarsma R, O'Seaghdha M, Yang NJ, Blake KJ, et al. Blocking Neuronal Signaling to Immune Cells Treats Streptococcal Invasive Infection. *Cell* (2018) 173(5):1083–1097.e22. doi: 10.1016/j.cell.2018.04.006
6. Scheraga RG, Abraham S, Grove LM, Southern BD, Crish JF, Perelas A, et al. TRPV4 Protects the Lung From Bacterial Pneumonia *via* MAPK Molecular Pathway Switching. *J Immunol* (2020) 204(5):1310–21. doi: 10.4049/jimmunol.1901033
7. Samanta A, Hughes TET, Moiseenkova-Bell VY. Transient Receptor Potential (TRP) Channels. *Subcell Biochem* (2018) 87:141–65. doi: 10.1007/978-981-10-7757-9_6
8. Caterina MJ. Transient Receptor Potential Ion Channels as Participants in Thermosensation and Thermoregulation. *Am J Physiol Regul Integr Comp Physiol* (2007) 292(1):R64–76. doi: 10.1152/ajpregu.00446.2006
9. White JP, Urban L, Nagy I. TRPV1 Function in Health and Disease. *Curr Pharm Biotechnol* (2011) 12(1):130–44. doi: 10.2174/138920111793937844
10. Grace MS, Baxter M, Dubuis E, Birrell MA, Belvisi MG. Transient Receptor Potential (TRP) Channels in the Airway: Role in Airway Disease. *Br J Pharmacol* (2014) 171(10):2593–607. doi: 10.1111/bph.12538
11. Abbott-Banner K, Poll C, Verkuyl JM. Targeting TRP Channels in Airway Disorders. *Curr Top Med Chem* (2013) 13(3):310–21. doi: 10.2174/1568026611313030008
12. Bhargave G, Woodworth BA, Xiong G, Wolfe SG, Antunes MB, Cohen NA. Transient Receptor Potential Vanilloid Type 4 Channel Expression in Chronic Rhinosinusitis. *Am J Rhinol* (2008) 22(1):7–12. doi: 10.2500/ajr.2008.22.3125
13. Weiser JN, Ferreira DM, Paton JC. *Streptococcus Pneumoniae*: Transmission, Colonization and Invasion. *Nat Rev Microbiol* (2018) 16(6):355–67. doi: 10.1038/s41579-018-0001-8
14. Smith AM, McCullers JA. Secondary Bacterial Infections in Influenza Virus Infection Pathogenesis. *Curr Top Microbiol Immunol* (2014) 385:327–56. doi: 10.1007/82_2014_394
15. Weinberger DM, Malley R, Lipsitch M. Serotype Replacement in Disease After Pneumococcal Vaccination. *Lancet* (2011) 378(9807):1962–73. doi: 10.1016/S0140-6736(10)62225-8
16. Chaguza C, Cornick JE, Everett DB. Mechanisms and Impact of Genetic Recombination in the Evolution of *Streptococcus Pneumoniae*. *Comput Struct Biotechnol J* (2015) 13:241–7. doi: 10.1016/j.csbj.2015.03.007
17. Takeda S, Kono M, Sugita G, Arai J, Briles DE, Hotomi M. Pneumococcal Capsular Phase Shift Is Associated With Invasion Into Cell-to-Cell Junctions and Is Inhibited by Macrolides. *Microb Pathog* (2021) 153:104787. doi: 10.1016/j.micpath.2021.104787
18. Kono M, Zafar MA, Zuniga M, Roche AM, Hamaguchi S, Weiser JN. Single Cell Bottlenecks in the Pathogenesis of *Streptococcus Pneumoniae*. *PloS Pathog* (2016) 12(10):e1005887. doi: 10.1371/journal.ppat.1005887
19. Suzuki M, Mizuno A, Kodaira K, Imai M. Impaired Pressure Sensation in Mice Lacking TRPV4. *J Biol Chem* (2003) 278(25):22664–8. doi: 10.1074/jbc.M302561200
20. Mizuno A, Matsumoto N, Imai M, Suzuki M. Impaired Osmotic Sensation in Mice Lacking TRPV4. *Am J Physiol Cell Physiol* (2003) 285(1):C96–101. doi: 10.1152/ajpcell.00559.2002

21. Nakamura S, Davis KM, Weiser JN. Synergic Stimulation of Type I Interferons During Influenza Virus Coinfection Promotes *Streptococcus Pneumoniae* Colonization in Mice. *J Clin Invest.* (2011) 121(9):3666–76. doi: 10.1172/JCI57761
22. Parker D, Martin FJ, Soong G, Harfenist BS, Aguilar JL, Ratner AJ, et al. *Streptococcus Pneumoniae* DNA Initiates Type I Interferon Signaling in the Respiratory Tract. *mBio* (2011) 2(3):e00016–11. doi: 10.1128/mBio.00016-11
23. Roche AM, King SJ, Weiser JN. Live Attenuated *Streptococcus Pneumoniae* Strains Induce Serotype-Independent Mucosal and Systemic Protection in Mice. *Infect Immun* (2007) 75(5):2469–75. doi: 10.1128/IAI.01972-06
24. Matute-Bello G, Downey G, Moore BB, Groshong SD, Matthay MA, Slutsky AS, et al. An Official American Thoracic Society Workshop Report: Features and Measurements of Experimental Acute Lung Injury in Animals. *Am J Respir Cell Mol Biol* (2011) 44(5):725–38. doi: 10.1165/rcmb.2009-0210st
25. Hergott CB, Roche AM, Naidu NA, Mesaros C, Blair IA, Weiser JN. Bacterial Exploitation of Phosphorylcholine Mimicry Suppresses Inflammation to Promote Airway Infection. *J Clin Invest.* (2015) 125(10):3878–90. doi: 10.1172/JCI81888
26. Pairet N, Mang S, Fois G, Keck M, Kühnbach M, Gindele J, et al. TRPV4 Inhibition Attenuates Stretch-Induced Inflammatory Cellular Responses and Lung Barrier Dysfunction During Mechanical Ventilation. *PloS One* (2018) 13 (4):e0196055. doi: 10.1371/journal.pone.0196055
27. Xing J, Weng L, Yuan B, Wang Z, Jia L, Jin R, et al. Identification of a Role for TRIM29 in the Control of Innate Immunity in the Respiratory Tract. *Nat Immunol* (2016) 17(12):1373–80. doi: 10.1038/ni.3580
28. Lemon JK, Miller MR, Weiser JN. Sensing of Interleukin-1 Cytokines During *Streptococcus Pneumoniae* Colonization Contributes to Macrophage Recruitment and Bacterial Clearance. *Infect Immun* (2015) 83(8):3204–12. doi: 10.1128/IAI.00224-15
29. Das R, LaRose MI, Hergott CB, Leng L, Bucala R, Weiser JN. Macrophage Migration Inhibitory Factor Promotes Clearance of Pneumococcal Colonization. *J Immunol* (2014) 193(2):764–72. doi: 10.4049/jimmunol.1400133
30. Siegel SJ, Tamashiro E, Weiser JN. Clearance of Pneumococcal Colonization in Infants Is Delayed Through Altered Macrophage Trafficking. *PloS Pathog* (2015) 11(6):e1004004. doi: 10.1371/journal.ppat.1004004
31. Scheraga RG, Abraham S, Niese KA, Southern BD, Grove LM, Hite RD, et al. TRPV4 Mechanosensitive Ion Channel Regulates Lipopolysaccharide-Stimulated Macrophage Phagocytosis. *J Immunol* (2016) 196(1):428–36. doi: 10.4049/jimmunol.1501688
32. Xu S, Liu B, Yin M, Koroleva M, Mastrangelo M, Ture S, et al. A Novel TRPV4-Specific Agonist Inhibits Monocyte Adhesion and Atherosclerosis. *Oncotarget* (2016) 7(25):37622–35. doi: 10.18632/oncotarget.9376
33. Konno M, Shirakawa H, Iida S, Sakimoto S, Matsutani I, Miyake T, et al. Stimulation of Transient Receptor Potential Vanilloid 4 Channel Suppresses Abnormal Activation of Microglia Induced by Lipopolysaccharide. *Glia* (2012) 60(5):761–70. doi: 10.1002/glia.22306
34. Taylor SJ, Mann TS, Henry PJ. Influence of Influenza a Infection on Capsaicin-Induced Responses in Murine Airways. *J Pharmacol Exp Ther* (2012) 340(2):377–85. doi: 10.1124/jpet.111.187872

Conflict of Interest: The authors declare that the research was conducted in the absence of any commercial or financial relationships that could be construed as a potential conflict of interest.

Publisher's Note: All claims expressed in this article are solely those of the authors and do not necessarily represent those of their affiliated organizations, or those of the publisher, the editors and the reviewers. Any product that may be evaluated in this article, or claim that may be made by its manufacturer, is not guaranteed or endorsed by the publisher.

frontiers in Immunology

REVIEW
published: 22 December 2021
doi: 10.3389/fimmu.2021.780451

Gateway Reflex and Mechanotransduction

Shiina Matsuyama[1], *Yuki Tanaka*[1,2], *Rie Hasebe*[1], *Shintaro Hojyo*[1,2] *and Masaaki Murakami*[1,2,3]*

[1] Molecular Psychoimmunology, Institute for Genetic Medicine, Graduate School of Medicine, Hokkaido University, Sapporo, Japan, [2] Group of Quantum Immunology, Institute for Quantum Life Science, National Institute for Quantum and Radiological Science and Technology (QST), Chiba, Japan, [3] Division of Neurommunology, National Institute for Physiological Sciences, Okazaki, Japan

Summary: The gateway reflex explains how autoreactive CD4+ T cells cause inflammation in tissues that have blood-barriers, such as the central nervous system and retina. It depends on neural activations in response to specific external stimuli, such as gravity, pain, stress, and light, which lead to the secretion of noradrenaline at specific vessels in the tissues. Noradrenaline activates NFkB at these vessels, followed by an increase of chemokine expression as well as a reduction of tight junction molecules to accumulate autoreactive CD4+ T cells, which breach blood-barriers. Transient receptor potential vanilloid 1 (TRPV1) molecules on sensory neurons are critical for the gateway reflex, indicating the importance of mechano-sensing. In this review, we overview the gateway reflex with a special interest in mechanosensory transduction (mechanotransduction).

Keywords: gateway reflex, mechanotransduction, inflammation, tissue specific autoimmune diseases, CD4+ T cells

OPEN ACCESS

Edited by:
Shaik O. Rahaman,
University of Maryland, United States

Reviewed by:
Hiroyuki Konishi,
Nagoya University, Japan
Gary Brenner,
Harvard Medical School, United States

***Correspondence:**
Masaaki Murakami
murakami@igm.hokudai.ac.jp

Specialty section:
This article was submitted to Molecular Innate Immunity, a section of the journal Frontiers in Immunology

Received: *21 September 2021*
Accepted: *30 November 2021*
Published: *22 December 2021*

Citation:
Matsuyama S, Tanaka Y, Hasebe R, Hojyo S and Murakami M (2021) Gateway Reflex and Mechanotransduction. Front. Immunol. 12:780451. doi: 10.3389/fimmu.2021.780451

MECHANO-SENSING RECEPTORS

Mechano-sensing is a general cellular phenomenon in which changes in membrane tension and the cytoskeletal structure induce intracellular signal transduction in response to an extracellular mechanical force (1). Many receptors are sensitive to mechanical forces. The list includes Twik-related K^+ channel (TREK) and Twik-related arachidonic acid-stimulated K^+ (TRAAK), both of which being two-pore domain K+ (K2p) channels, Piezo1/2, TMEM63/OSCA, and transmembrane channel-like (TMC)1 and TMC2. These mechanosensory ion channels (MSCs) all sense extracellular stimulations, such as pressure, gravity, acceleration, sound waves, tension, fluid flow, pain, light, temperature, and blood pressure (2–6). In addition, cells adhere to neighboring cells and to the extracellular matrix *via* transmembrane receptors of the cadherin (cell-to-cell) and integrin (cell-to-substrate) families. These molecules are related to cell adhesion but are also mechano-sensitive (7–9), suggesting they are mechano-sensing receptors in the broad sense of the term. The extracellular stimuli are converted by MSCs and adhesion molecules into intracellular signals *via* alterations in the intracellular ion concentration or intracellular cytoskeletal status in various cells including sensory neurons and endothelial cells (10).

MSCS AND ADHESION-RELATED MOLECULES IN MECHANOTRANSDUCTION

The above MSCs have been categorized as depolarizing cationic non-selective channels, such as Piezo1/2, and hyperpolarizing K+-selective stretch-activated channels, such as TREK/TRAAK K2p channels, TMEM63/OSCA, and TMC1/2. In mammalian cells, after the binding of a ligand or change in membrane tension around them, these channels change their structurers to shift the balance of the intracellular/extracellular ion concentration (2–5, 11). Piezo1/2 increase intracellular Ca^{2+}, while the other channels decrease intracellular K^{+}, thus augmenting the effects of intracellular Ca^{2+}. Degenerin channels (DEG), epithelial sodium channels (ENaC), acid-sensing ion channels (ASICS), and transient receptor potentials (TRP) channels are other MSCs. Recent electron cryo-microscopy structure studies for TRPs have revealed that a helical spring structure displaces intracellular cytoskeleton molecules to open the channels upon mechanical stress (11–13).

Endothelial cells in the blood vessels contact each other as a monolayer to pass essential factors, potential energy, and sometimes immune cells for the surveillance of tumor development and cells infected by pathogens from the blood to the tissues. Endothelial cells are constantly enduring mechanical stress from the blood flow, which is detected by transmembrane proteins, such as tyrosine kinase receptors, G protein-coupled receptors (GPCR), integrins, and cadherins, membrane structures, such as caveolae and primary cilia, glycocalyx, and cytoskeleton proteins, such as actin and tubulin, all of which transduce a mechanical signal to intracellular signals that cause transcriptional alterations to change the cellular status of endothelial cells (14–18)(**Figure 1**).

THE GATEWAY REFLEX

Endothelial cells in the central nervous system (CNS) represent a specific vessel structure named the blood-brain barrier (BBB), which prevents peripheral immune cells and other factors including immunoglobulins from infiltrating the CNS from the blood. The BBB is important for maintaining the CNS environment and depends on many of the mechano-sensing molecules described above. However, observations of neuroinflammation due to an accumulation of immune cells in many diseases, including autoimmune diseases, schizophrenia, and Alzheimer's disease, suggest the BBB can be compromised (19–24). To migrate past the BBB and into the CNS, peripheral immune cells particularly activated ones rely on adhesion molecules as well as chemokine molecules expressed by endothelial cells to affect mechanosensory pathways (25–29), because some signaling through adhesion molecules and chemokines directly increase molecules related to the mechanosensory pathways (25, 26, 30–32) and cytokines expressed from the immune cells accumulated also indirectly affect mechanosensory pathways (26–29). Because immune cells interact with endothelial cells in the BBB and affect the BBB structure and function, the status of the BBB is mechano-sensitive (30).

GRAVITY AND ELECTRIC GATEWAY REFLEXES

Space experiments have shown that gravity affects bone and muscle density (31, 32) and indicate that the body transduces gravity into mechanical signaling. We demonstrated that gravity

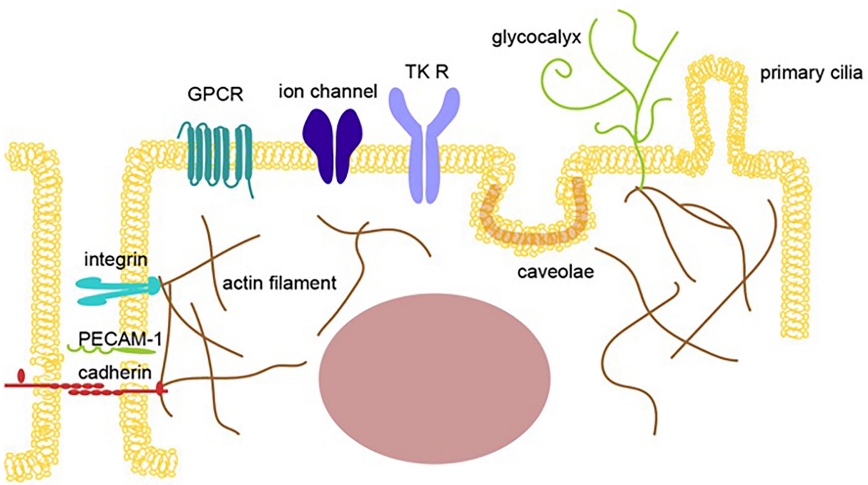

FIGURE 1 | Mechano-sensing receptors in endothelial cells. An illustration showing multiple mechano-sensing receptors, including mechanosensory ion channels and adhesion molecules, that can respond to extracellular stimulations, such as pressure, gravity, acceleration, sound, tension, fluid flow, pain, light, temperature, and blood pressure, to induce mechanotransduction in endothelial cells. The sensors shown include tyrosine kinase receptors (TK R), G protein-coupled receptors, ion channels, junction proteins, integrins, the cell membrane (caveolae), and glycocalyx.

regulates tissue-specific CNS inflammation by showing that autoreactive CD4+ T cells invade the specific sites of the CNS in experimental autoimmune encephalomyelitis (EAE), an animal model of multiple sclerosis (33). EAE mice are an invaluable tool for studying the pathogenesis of the BBB and the accumulation of immune cells in the CNS. One of the most popular murine models is EAE induced by a myelin-derived antigen, myelin oligodendrocyte glycoprotein 35-55 (MOG35–55), which is given emulsified in complete Freund's adjuvant (CFA) as a subcutaneous injection (34–37). The development of encephalomyelitis is observed as an ascending paralysis that begins with a drooping tail and progresses to paralysis of the lower limbs. The adoptive transfer of MOG-specific CD4+ T cells (pathogenic CD4+ T cells) from donor mice that were actively immunized by the MOG peptide with CFA to naïve recipient mice can also induce EAE. This adoptive transfer EAE model allows study of the autoimmune CNS inflammation induced specifically by pathogenic CD4+ T cells (38).

We found that in EAE mice transferred with pathogenic CD4+ T cells, the cells accumulated in the dorsal vascular sites of the fifth lumbar (L5) cord. Dorsal vascular endothelial cells of the L5 cord in EAE mice show an inflammation status including the expression of chemokines and growth factors followed by the accumulation of immune cells and proliferation of tissue nonimmune cells due to NFκB signaling. Pathogenic CD4+ T cells, but mainly Th17 ones, accumulate in the vascular endothelium and flow into the CNS using CCL20 as a chemotactic factor. After pathogenic CD4+ T cell accumulates, the BBB is breached due to various cytokines including NFκB and STAT stimulators from pathogenic CD4+ T cells, resulting in the accumulation of various immune cells from the blood to the L5 cord. This accumulation increases mechanical stress because of the increased cell density.

In a later experiment, we focused on sensory nerve input from the soleus muscles. The main anti-gravity muscles are the soleus muscles in both mice and human, and the sensory pathway from soleus muscles connects to the L5 dorsal root ganglion (DRG), which is the largest DRG and is activated by anti-gravity responses (33). Indeed, when the same experiment was performed on mice with their tails suspended to model a microgravity environment on the hind legs, CNS inflammation was induced in the cervical vessels but not the L5 vessels. Furthermore, electrically stimulating the soleus muscles, which mimics gravity stimulation, induced CCL20 at the L5 vessels. Moreover, electrically stimulating the quadriceps, whose afferent sensory nerves come from the L3 DRG, and the epitrochlearis/triceps brachii, whose afferent nerves come from between the fifth cervical and fifth thoracic DRG, caused CCL20 expression to increase in the L3 vessels and between the fifth cervical and fifth thoracic vessels, respectively.

Sympathetic ganglions of the L5 level, but not other levels, were activated by gravity responses in the soleus muscles, and treatment with the norepinephrine antagonist atenolol significantly suppressed CCL20 mRNA expression, NFκB activation, and pathogenic CD4+ T cell accumulation around the L5 vessels and abrogated EAE development. These experiments indicate that sensory nerves in the soleus muscles that receive a gravity stimulus activate the sympathetic pathway at the L5 level, resulting in the production of noradrenaline, which upregulates CCL20 expression at the L5 dorsal vessels, although a detail crosstalk between sensory-sympatheic pathway in the L5 level has not been demonstrated. The resulting chemokine expression triggered inflammation around the vascular endothelium in the L5 cord, causing the accumulation of pathogenic CD4+ T cells from the blood and the development of neuroinflammation. These mechanisms, by which the nervous system regulates CNS inflammation in response to gravity stimulation or electric stimulation *via* the alteration of specific vessels, have been named the gravity gateway reflex and electric gateway reflex, respectively (**Figure 2**) (33).

Gravity maintains the appropriate body state under healthy conditions. However, depending on the immune status of the individual, including the numbers of autoreactive T cells in the blood, it may also allow immune cells to invade the CNS and initiate autoimmune disease development *via* the gateway reflex. The receptors of sensory nerves that perceive gravity stimuli are still unclear, and the mechanosensory mechanism by which gravity stimuli activate the sensory nerves needs further investigation during both the gravity gateway reflex and electric gateway reflex.

PAIN GATEWAY REFLEX

Two-thirds of patients with multiple sclerosis and particularly those with a relapse-remittent type will experience flare-ups (39). In contrast, in EAE mice transfected with pathogenic CD4+ T cells, the symptoms disappear within 2-3 weeks. Normally, EAE mice in remission show no relapse for more than 300 days after the transfer, but if pain stimulation is added, the symptoms relapse (40). The mouse trigeminal nerve is composed mainly of sensory nerve (41). Trigeminal neuropathic pain causes activation of the anterior cingulate cortex (ACC) and sensory neurons in the thalamus (42). A positive correlation has been reported between ACC activity, pain-induced sympathetic vasoconstrictor reflexes, and sympathetic responses to pain in humans, suggesting a functional link between the ACC, central sympathetic pathways, and pain experience (43). In remission EAE mice, trigeminal nerve ligation caused a relapse of the EAE symptoms, but a sham-operation did not. Capsaicin stimulation also induced the relapse, indicating that the pain-sensing TPRV1 channel activates sensory nerves and causes ACC activation. To confirm this hypothesis, pain stimulation was performed in TRPV1 knockout mice, but no relapse was observed. TRP channels are MSCs but also activated by heat, which alters the membrane tension and the status of intracellular cytoskeletal molecules (13). These results suggested that not only pain but also mechanical stimulations, such as compression, can induce the relapse *via* a similar neural pathway.

Mechanistically, pain sensation caused an accumulation of MHC2+CD11b+ myeloid cells at the ventral vascular blood vessels of the L5 cord, which triggered the accumulation of

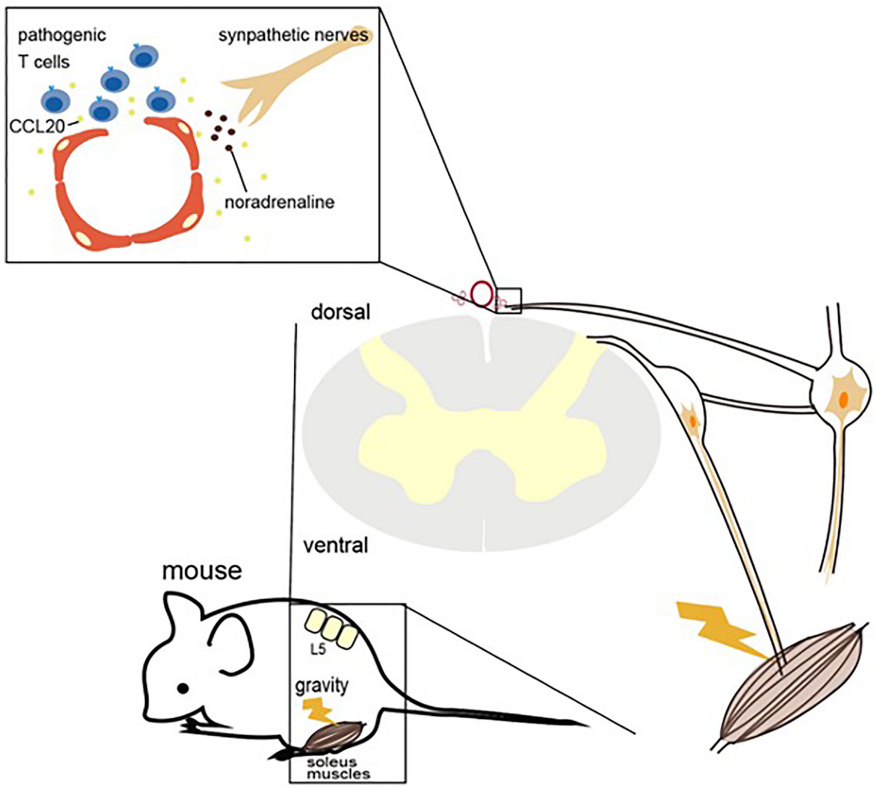

FIGURE 2 | Light gateway reflex. The light gateway reflex. Photopic light stimulates a high expression of noradrenaline and adrenaline to downregulate a1A-adrenoceptor (a $_{1A}$AR) expression on the retinal vessels in mice with autoreactive T cells against photoreceptors. The downregulation of a_{1A}AR inhibits the noradrenaline-mediated activation of NFκB and STAT3, suppressing the IL-6 amplifier and retinal inflammation.

pathogenic CD4+ T cells in the blood and ultimately the infiltration of other immune cells into the spinal cord after breaching the BBB there. MHC class II+CD11b+ cells in EAE-recovered mice expressed not only MHC class II molecules but also co-stimulatory molecules, such as CD80, CD86, and intercellular adhesion molecule-1 (ICAM-1), which is a ligand of integrins and a mechano-sensing receptor. Importantly, MHC class II+CD11b+ cells have the ability to stimulate pathogenic CD4+ T cells without the addition of MOG peptide, suggesting they presented self-antigen peptides that stimulated pathogenic CD4+ T cells. We found that MHC2+CD11b+ cells increased the expression of CX3CR1 and its ligand CX3CL1 from L5 vessels in response to sympathetic noradrenaline. When CX3CL1 was inhibited with a neutralizing antibody, the relapse symptoms caused by pain stimulation were suppressed. Moreover, the inhibition of sympathetic nerve function by a β1-adrenagic receptor antagonist, atenolol, or the sympathectomy regent 6-hydroxydopamine (6-OHDA) suppressed the upregulated CX3CL1 expression and relapse, suggesting that not only the TRPV1+ sensory pathway but also the sympathetic pathway is critical for the pain gateway reflex (40).

Thus, pain induction first causes an accumulation of MHC class II+CD11b+ cells at the ventral vessels of the L5 cord *via* sensory-sympathetic crosstalk. Then, an MHC class II+CD11b+ cell-mediated accumulation and activation of pathogenic CD4+ T cells in the blood occurs, leading to EAE relapse. Because the activated pathogenic CD4+ T cells in the L5 cord express various cytokines, including NFkB and STAT3 stimulators like IL-17, TNFa, and IL-6, the chemokines were induced in the L5 ventral vessels by activation of the IL-6 amplifier, a local chemokine inducer in endothelial cells (44). In other words, pain induction causes sympathetic activation *via* the sensory pathway, which depends on TRPV1 channels, and noradrenaline produced by the sympathetic nerves induces local inflammation in the L5 cord by accumulating immune cells (**Figure 3**).

STRESS GATEWAY REFLEX

Stress is involved in many diseases. We have identified a stress-related nerve circuit that causes gastrointestinal failure and sudden death when pathogenic CD4+ T cells migrate to the CNS from the blood (45). We again employed transfer EAE mice under two stress conditions that have no obviously significant negative effect on the body: light sleep and wet bed environments. Severe gastrointestinal inflammation and heart failure were observed in mice with either stress in the presence of pathogenic CD4+ T cells. A mechanistic analysis showed that the

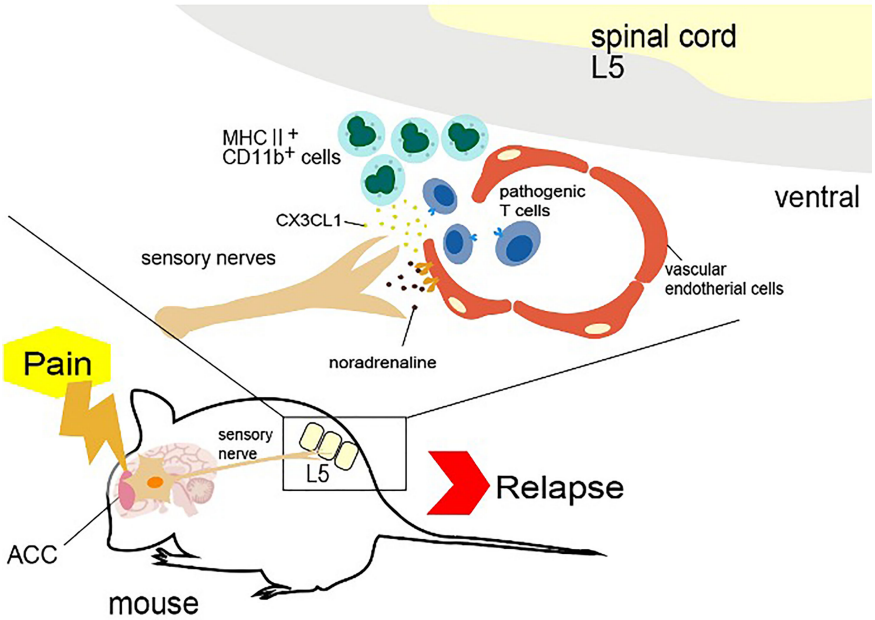

FIGURE 3 | Gravity gateway reflex. Gravity stimulation induces the activation of sensory nerves in the soleus muscles, which connects the fifth lumbar vertebra (L5) dorsal root ganglion, followed by the activation of L5 sympathetic ganglion neurons. Norepinephrine (also known as noradrenaline) from the sympathetic nerves induces the IL-6 amplifier and the infiltration of autoreactive T cells into the spinal cord by upregulating CCL20 at the dorsal vessels of the L5 cord.

stress stimulation activated noradrenergic neurons in the paraventricular nucleus of the hypothalamus (PVN), which relates to stress and projects to two specific blood vessels surrounded by the third ventricle, dentate gyrus and thalamus, establishing the gateways for the pathogenic CD4+ T cells (45). We named this phenomenon the "stress gateway reflex". Considering that the dentate gyrus and PVN are stress-related brain regions (46, 47), the stress gateway reflex could play a role even under the steady state. We hypothesized permeability around the specific vessels was increased even in the absence of pathogenic CD4+ T cells, i.e. in the physiological condition that suppresses stress responses, by the activation of neurons in the dorsomedial hypothalamic nucleus (DMH)/anterior hypothalamic nucleus (AHN) (48).

On the other hand, during the stress gateway reflex in the presence of pathogenic CD4+ T cells in the blood, PVN-derived noradrenergic neurons upregulate CCL5 expression at the blood vessels in a manner dependent on noradrenaline-mediated NFkB activation, thus recruiting pathogenic CD4+ T cells and MHC class II^+ monocytes from the blood followed by the activation of pathogenic CD4+ T cells there. Cytokines expressed by activated pathogenic CD4+ T cells accelerated the NFkB activation in endothelial cells and triggered micro-inflammation *via* the IL-6 amplifier (45). Locally, adenosine triphosphate (ATP) produced by the micro-inflammation functioned as a neurotransmitter (49, 50). Indeed, ATP directly activated neurons in the DMH/AHN to activate neurons in the dorsal motor vagal nucleus (DMX) (45). The enhanced activation of the efferent vagus nerve projected to the upper gastrointestinal tract from the DMX to yield severe gastrointestinal inflammation *via* massive acetylcholine secretion followed by hyperkalemia with sudden death (45) (**Figure 4**).

Because the accumulation of immune cells including pathogenic CD4+ T cells at brain-specific vessels should increase the density and pressure between cells followed by an increase of the mechanistic signaling, not only ATP signaling but also mechanical stress activates NFkB in the blood vessels and stimulates the neural pathway to the DMH/AHP.

LIGHT GATEWAY REFLEX

We showed that photopic light stimulation suppresses the establishment of experimental autoimmune uveroretinitis (EAU), a model of uveroretinitis, in mice (51–53). We noticed a pathological difference between mice kept in photopic light and in mesopic light conditions. A gateway at retinal vascular endothelial cells can be established by NFkB-mediated chemokine expression in retinal endothelial cells to accelerate the infiltration of pathogenic CD4+ T cells against photoreceptors through the blood-retina barrier from the blood (51). EAU mice kept in mesopic light showed more $CD4^+$, $CD8^+$ and $CD11b^+$ cells in the retina than mice kept in photopic light (51). Similar to the other four gateway reflexes, the light gateway reflex includes the activation of sympathetic/noradrenergic neurons in its nerve pathway. Exposure to photopic light downregulated the noradrenergic pathway in retinal vessels by excessive noradrenaline and adrenaline levels

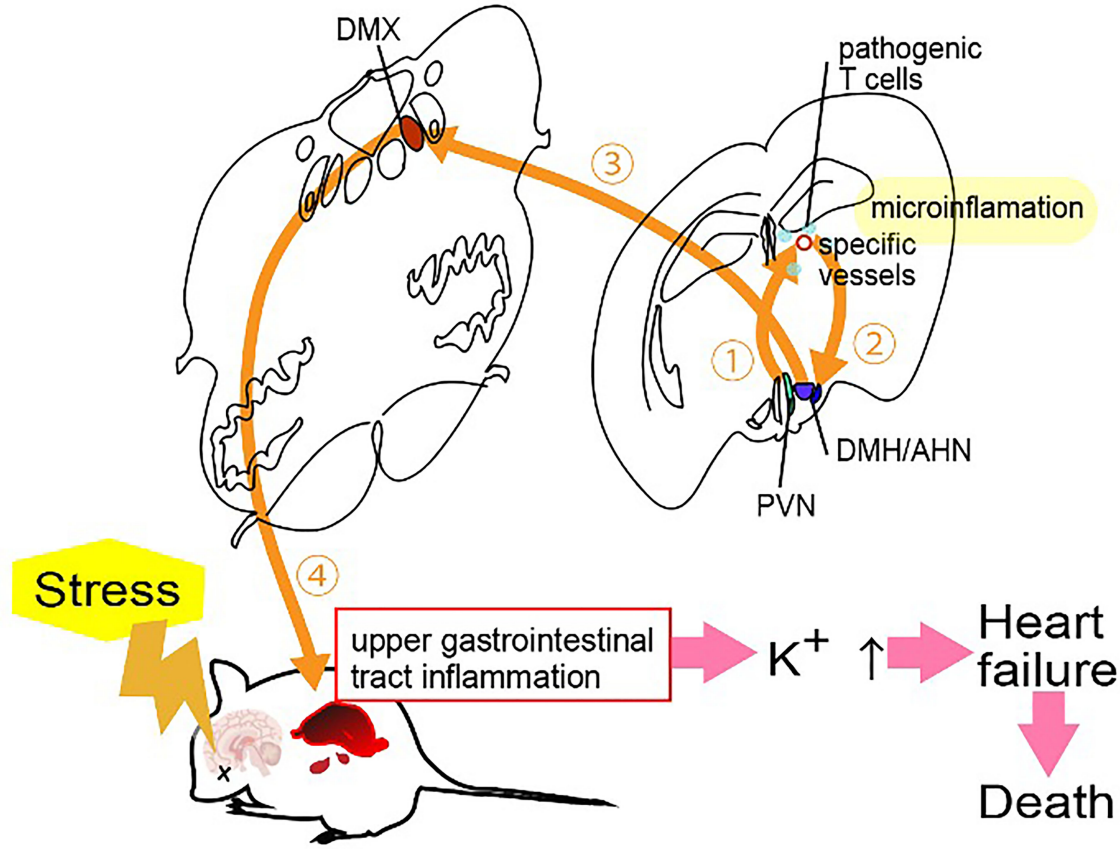

FIGURE 4 | Pain gateway reflex. Pain-induced sensory nerve activation stimulates the anterior cingulate cortex (ACC), which activates specific sympathetic nerves distributed at two ventral vessels of the spinal cord. Because there are many major histocompatibility complex (MHC) class II$^+$ monocytes around the L5 cord, norepinephrine secretion at the ventral blood vessels of the fifth lumbar vertebra (L5) cord stimulates the production of CX3CL1 from endothelial cells *via* the IL-6 amplifier. CX3CL1 accumulates MHC class II$^+$ monocytes and increases the permeability of blood vessels. Autoreactive T cells in the blood flow accumulate at the vessels to induce experimental autoimmune encephalomyelitis relapse.

from neural terminal in the retina, disrupting the expression of a1A-adrenagic receptor (a $_{1A}$AR) and subsequently suppressing NFkB activation in the retinal vessels (51) (**Figure 5**). The light gateway reflex can be observed not only in uveitis and retinitis, but also in autoimmune intraocular diseases such as retinal vasculitis and ischemic retinopathy. Moreover, activation of the sympathetic pathway can also be observed in autoimmune diseases that present intraocular inflammation such as human leukocyte antigen-B27 (HLA-B27) spondyloarthropathies, sarcoidosis, and juvenile chronic arthritis (54–56). These findings suggest that excessive activation of the sympathetic pathway suppresses the establishment of the gateways for autoreactive T cells in the blood-barrier including in blood-retina one by downregulating adrenergic receptors on the vessels, thus inhibiting tissue-specific inflammation.

Finally, during the pathology of EAU, we noticed an abnormal spatial alignment of neural terminal in the retina due to an accumulation of immune cells and proliferation of retinal nonimmune cells, including fibroblasts. This abnormal alignment likely caused an increase in tension and/or pressure in the retinal lesion. Thus, the mechanosensory pathway affects the pathogenesis of retinal inflammation.

CONCLUDING REMARKS

In summary, we here focused on the gateway reflex, in which mechanical forces, such as gravity, changes the microvascular structure of blood barriers to allow immune cells to invade associated organs, such as the CNS and retina. Inflammation caused by the gateway reflex is different from whole organ inflammation, because autoreactive T cells invade from specific blood vessels in the organs. Pain stimuli induces the accumulation of MHC class II+ CD11b+ myeloid cells at specific ventral vessels of the L5 cord *via* activation of TPRV1 receptor-positive sensory nerves to cause relapse of CNS-inflammation (pain gateway reflex). Although other peripheral-derived CD11b+ myeloid cells in the CNS do not show any obvious function after the pathogenesis, environmental stimuli, including pain sensation, can accumulate them *via* the activation of specific neural circuits by changing the

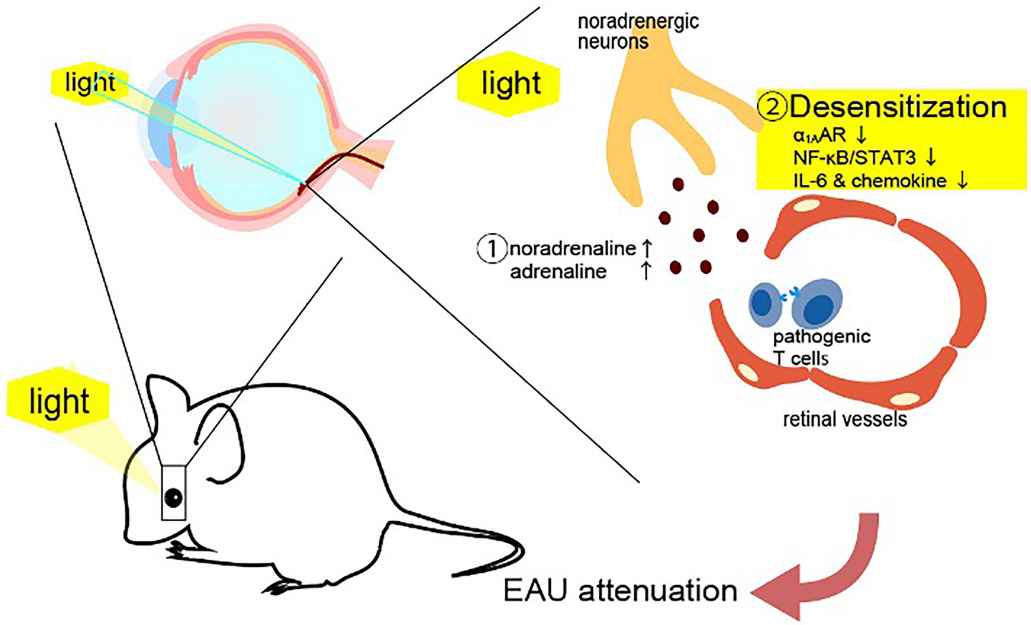

FIGURE 5 | Stress gateway reflex. Chronic stresses including light sleep activate noradrenergic neurons in the paraventricular nucleus (PVN) to establish gateways for immune cells at specific blood vessels in the brain, particularly in the presence of myelin-specific $CD4^+$ T cells in the blood. Myelin-specific $CD4^+$ T cells accumulate at the specific vessels together with major histocompatibility complex class II^+ monocytes to develop micro-inflammation there. ATP produced by the micro-inflammation functions as a neurotransmitter to directly activate neurons in the dorsomedial hypothalamic nucleus (DMH)/anterior hypothalamic nucleus (AHN), followed by the activation of neurons of the dorsal motor vagal nucleus (DMX). The resulting activated efferent vagus nerve causes acetylcholine-dependent gastrointestinal inflammation followed by hyperkalemia with heart failure and sudden death.

status of specific blood vessels. Regarding, tissue-specific autoimmune diseases, the adaptive immune system, such as T cells and B cells in the blood, plus neural circuits activated by environmental stimulations are critical for the gateway reflex. Autoimmune diseases always commence with the accumulation of immune cells at specific vessels, which increases pressure and tension on the tissue cells as well as the immune cells themselves. Therefore, it is reasonable that mechanotransduction contributes to these diseases. Further elucidation of this transduction as well as immune cells is important for understanding the pathogenesis of various diseases and establishing new treatments.

AUTHOR CONTRIBUTIONS

All authors read and discussed the paper. All authors contributed to the article and approved the submitted version.

FUNDING

This work was supported by KAKENHI and AMED (MM), the Grant for the Joint Research Program of the Institute for Genetic Medicine, Hokkaido University (MM), the Photo-excitonix Project at Hokkaido University (MM), and the Promotion Project for Young Investigators at Hokkaido University (MM).

ACKNOWLEDGMENTS

We thank Dr P. Karagiannis (CiRA, Kyoto University, Kyoto, Japan) for carefully reading the manuscript and important discussion. We are grateful to Ms. Chiemi Nakayama, Ms. Satomi Fukumoto, and Ms. Mari Osawa for their excellent administrative assistance.

REFERENCES

1. Ingber DE. Mechanical Control of Tissue Morphogenesis During Embryological Development. *Int J Dev Biol* (2006) 50:255–66. doi: 10.1387/ijdb.052044di
2. Du G, Li L, Zhang X, Liu J, Hao J, Zhu J, et al. Roles of TRPV4 and Piezo Channels in Stretch-Evoked Ca(2+) Response in Chondrocytes. *Exp Biol Med (Maywood)* (2020) 245:180–9. doi: 10.1177/1535370219892601
3. Murthy SE, Dubin AE, Whitwam T, Jojoa-Cruz S, Cahalan SM, Mousavi SAR, et al. OSCA/TMEM63 Are an Evolutionarily Conserved Family of Mechanically Activated Ion Channels. *Elife* (2018) 7:e41844. doi: 10.7554/eLife.41844
4. Noel J, Zimmermann K, Busserolles J, Deval E, Alloui A, Diochot S, et al. The Mechano-Activated K+ Channels TRAAK and TREK-1 Control Both Warm and Cold Perception. *EMBO J* (2009) 28:1308–18. doi: 10.1038/emboj.2009.57

5. Maingret F, Fosset M, Lesage F, Lazdunski M, Honore E. TRAAK is a Mammalian Neuronal Mechano-Gated K+ Channel. *J Biol Chem* (1999) 274:1381–7. doi: 10.1074/jbc.274.3.1381
6. Pan B, Akyuz N, Liu XP, Asai Y, Nist-Lund C, Kurima K, et al. TMC1 Forms the Pore of Mechanosensory Transduction Channels in Vertebrate Inner Ear Hair Cells. *Neuron* (2018) 99:736–53.e6. doi: 10.1016/j.neuron.2018.07.033
7. Izawa Y, Gu YH, Osada T, Kanazawa M, Hawkins BT, Koziol JA, et al. Beta1-Integrin-Matrix Interactions Modulate Cerebral Microvessel Endothelial Cell Tight Junction Expression and Permeability. *J Cereb Blood Flow Metab* (2018) 38:641–58. doi: 10.1177/0271678X17722108
8. Luis Alonso J, Goldmann WH. Cellular Mechanotransduction. *AIMS Biophysics* (2016) 3:50–62. doi: 10.3934/biophy.2016.1.50
9. Rubsam M, Mertz AF, Kubo A, Marg S, Jungst C, Goranci-Buzhala G, et al. E-Cadherin Integrates Mechanotransduction and EGFR Signaling to Control Junctional Tissue Polarization and Tight Junction Positioning. *Nat Commun* (2017) 8:1250. doi: 10.1038/s41467-017-01170-7
10. Arnadottir J, Chalfie M. Eukaryotic Mechanosensitive Channels. *Annu Rev Biophys* (2010) 39:111–37. doi: 10.1146/annurev.biophys.37.032807.125836
11. Retailleau K, Duprat F, Arhatte M, Ranade SS, Peyronnet R, Martins JR, et al. Piezo1 in Smooth Muscle Cells Is Involved in Hypertension-Dependent Arterial Remodeling. *Cell Rep* (2015) 13:1161–71. doi: 10.1016/j.celrep.2015.09.072
12. Winkler PA, Huang Y, Sun W, Du J, Lu W. Electron Cryo-Microscopy Structure of a Human TRPM4 Channel. *Nature* (2017) 552:200–4. doi: 10.1038/nature24674
13. Jin P, Bulkley D, Guo Y, Zhang W, Guo Z, Huynh W, et al. Electron Cryo-Microscopy Structure of the Mechanotransduction Channel NOMPC. *Nature* (2017) 547:118–22. doi: 10.1038/nature22981
14. Zhou J, Li YS, Chien S. Shear Stress-Initiated Signaling and Its Regulation of Endothelial Function. *Arterioscler Thromb Vasc Biol* (2014) 34:2191–8. doi: 10.1161/ATVBAHA.114.303422
15. Vion AC, Alt S, Klaus-Bergmann A, Szymborska A, Zheng T, Perovic T, et al. Primary Cilia Sensitize Endothelial Cells to BMP and Prevent Excessive Vascular Regression. *J Cell Biol* (2018) 217:1651–65. doi: 10.1083/jcb.201706151
16. Li YS, Haga JH, Chien S. Molecular Basis of the Effects of Shear Stress on Vascular Endothelial Cells. *J Biomech* (2005) 38:1949–71. doi: 10.1016/j.jbiomech.2004.09.030
17. Malek AM, Izumo S. Mechanism of Endothelial Cell Shape Change and Cytoskeletal Remodeling in Response to Fluid Shear Stress. *J Cell Sci* (1996) 109:713–26. doi: 10.1242/jcs.109.4.713
18. Fu BM, Tarbell JM. Mechano-Sensing and Transduction by Endothelial Surface Glycocalyx: Composition, Structure, and Function. *Wiley Interdiscip Rev Syst Biol Med* (2013) 5:381–90. doi: 10.1002/wsbm.1211
19. Cai HQ, Catts VS, Webster MJ, Galletly C, Liu D, O'Donnell M, et al. Increased Macrophages and Changed Brain Endothelial Cell Gene Expression in the Frontal Cortex of People With Schizophrenia Displaying Inflammation. *Mol Psychiatry* (2020) 25:761–75. doi: 10.1038/s41380-018-0235-x
20. Harry GJ. Microglia During Development and Aging. *Pharmacol Ther* (2013) 139:313–26. doi: 10.1016/j.pharmthera.2013.04.013
21. Nitta T, Hata M, Gotoh S, Seo Y, Sasaki H, Hashimoto N, et al. Size-Selective Loosening of the Blood-Brain Barrier in Claudin-5-Deficient Mice. *J Cell Biol* (2003) 161:653–60. doi: 10.1083/jcb.200302070
22. Ortiz GG, Pacheco-Moises FP, Macias-Islas MA, Flores-Alvarado LJ, Mireles-Ramirez MA, Gonzalez-Renovato ED, et al. Role of the Blood-Brain Barrier in Multiple Sclerosis. *Arch Med Res* (2014) 45:687–97. doi: 10.1016/j.arcmed.2014.11.013
23. Romanitan MO, Popescu BO, Winblad B, Bajenaru OA, Bogdanovic N. Occludin is Overexpressed in Alzheimer's Disease and Vascular Dementia. *J Cell Mol Med* (2007) 11:569–79. doi: 10.1111/j.1582-4934.2007.00047.x
24. Zlokovic BV. The Blood-Brain Barrier in Health and Chronic Neurodegenerative Disorders. *Neuron* (2008) 57:178–201. doi: 10.1016/j.neuron.2008.01.003
25. Larochelle C, Alvarez JI, Prat A. How do Immune Cells Overcome the Blood-Brain Barrier in Multiple Sclerosis? *FEBS Lett* (2011) 585:3770–80. doi: 10.1016/j.febslet.2011.04.066
26. Wong D, Dorovini-Zis K, Vincent SR. Cytokines, Nitric Oxide, and cGMP Modulate the Permeability of an *In Vitro* Model of the Human Blood-Brain Barrier. *Exp Neurol* (2004) 190:446–55. doi: 10.1016/j.expneurol.2004.08.008
27. Chui R, Dorovini-Zis K. Regulation of CCL2 and CCL3 Expression in Human Brain Endothelial Cells by Cytokines and Lipopolysaccharide. *J Neuroinflamm* (2010) 7:1. doi: 10.1186/1742-2094-7-1
28. Holman DW, Klein RS, Ransohoff RM. The Blood-Brain Barrier, Chemokines and Multiple Sclerosis. *Biochim Biophys Acta* (2011) 1812:220–30. doi: 10.1016/j.bbadis.2010.07.019
29. Lombardi A, Cantini G, Mello T, Francalanci M, Gelmini S, Cosmi L, et al. Molecular Mechanisms Underlying the Pro-Inflammatory Synergistic Effect of Tumor Necrosis Factor Alpha and Interferon Gamma in Human Microvascular Endothelium. *Eur J Cell Biol* (2009) 88:731–42. doi: 10.1016/j.ejcb.2009.07.004
30. Wang X, Xue GX, Liu WC, Shu H, Wang M, Sun Y, et al. Melatonin Alleviates Lipopolysaccharide-Compromised Integrity of Blood-Brain Barrier Through Activating AMP-Activated Protein Kinase in Old Mice. *Aging Cell* (2017) 16:414–21. doi: 10.1111/acel.12572
31. Prasad B, Grimm D, Strauch SM, Erzinger GS, Corydon TJ, Lebert M, et al. Influence of Microgravity on Apoptosis in Cells, Tissues, and Other Systems *In Vivo* and *In Vitro*. *Int J Mol Sci* (2020) 21:9373. doi: 10.3390/ijms21249373
32. Arfat Y, Xiao WZ, Iftikhar S, Zhao F, Li DJ, Sun YL, et al. Physiological Effects of Microgravity on Bone Cells. *Calcif Tissue Int* (2014) 94:569–79. doi: 10.1007/s00223-014-9851-x
33. Arima Y, Harada M, Kamimura D, Park JH, Kawano F, Yull FE, et al. Regional Neural Activation Defines a Gateway for Autoreactive T Cells to Cross the Blood-Brain Barrier. *Cell* (2012) 148:447–57. doi: 10.1016/j.cell.2012.01.022
34. Farooqi N, Gran B, Constantinescu CS. Are Current Disease-Modifying Therapeutics in Multiple Sclerosis Justified on the Basis of Studies in Experimental Autoimmune Encephalomyelitis? *J Neurochem* (2010) 115:829–44. doi: 10.1111/j.1471-4159.2010.06982.x
35. Steinman L, Zamvil SS. Virtues and Pitfalls of EAE for the Development of Therapies for Multiple Sclerosis. *Trends Immunol* (2005) 26:565–71. doi: 10.1016/j.it.2005.08.014
36. Gold R, Linington C, Lassmann H. Understanding Pathogenesis and Therapy of Multiple Sclerosis *via* Animal Models: 70 Years of Merits and Culprits in Experimental Autoimmune Encephalomyelitis Research. *Brain* (2006) 129:1953–71. doi: 10.1093/brain/awl075
37. Ogura H, Murakami M, Okuyama Y, Tsuruoka M, Kitabayashi C, Kanamoto M, et al. Interleukin-17 Promotes Autoimmunity by Triggering a Positive-Feedback Loop *via* Interleukin-6 Induction. *Immunity* (2008) 29:628–36. doi: 10.1016/j.immuni.2008.07.018
38. Stromnes IM, Goverman JM. Passive Induction of Experimental Allergic Encephalomyelitis. *Nat Protoc* (2006) 1:1952–60. doi: 10.1038/nprot.2006.284
39. Steinman L. A Molecular Trio in Relapse and Remission in Multiple Sclerosis. *Nat Rev Immunol* (2009) 9:440–7. doi: 10.1038/nri2548
40. Arima Y, Kamimura D, Atsumi T, Harada M, Kawamoto T, Nishikawa N, et al. A Pain-Mediated Neural Signal Induces Relapse in Murine Autoimmune Encephalomyelitis, a Multiple Sclerosis Model. *Elife* (2015) 4:e08733. doi: 10.7554/eLife.08733
41. Thygesen TH, Baad-Hansen L, Svensson P. Sensory Action Potentials of the Maxillary Nerve: A Methodologic Study With Clinical Implications. *J Oral Maxillofac Surg* (2009) 67:537–42. doi: 10.1016/j.joms.2008.02.015
42. Critchley HD. Neural Mechanisms of Autonomic, Affective, and Cognitive Integration. *J Comp Neurol* (2005) 493:154–66. doi: 10.1002/cne.20749
43. Li X-Y, Chen T, Descalzi G, Koga K, Wang H, Kim SS, et al. Alleviating Neuropathic Pain Hypersensitivity by Inhibiting PKMz in the Anterior Cingulate Cortex. *Science* (2010) 330:1400–4. doi: 10.1126/science.1191792
44. Murakami M, Kamimura D, Hirano T. Pleiotropy and Specificity: Insights From the Interleukin 6 Family of Cytokines. *Immunity* (2019) 50:812–31. doi: 10.1016/j.immuni.2019.03.027
45. Arima Y, Ohki T, Nishikawa N, Higuchi K, Ota M, Tanaka Y, et al. Brain Micro-Inflammation at Specific Vessels Dysregulates Organ-Homeostasis *via* the Activation of a New Neural Circuit. *Elife* (2017) 6:e25517. doi: 10.7554/eLife.25517
46. Yun S, Reynolds RP, Petrof I, White A, Rivera PD, Segev A, et al. Stimulation of Entorhinal Cortex-Dentate Gyrus Circuitry is Antidepressive. *Nat Med* (2018) 24:658–66. doi: 10.1038/s41591-018-0002-1
47. Moretto JN, Duffy Á M, Scharfman HE. Acute Restraint Stress Decreases C-Fos Immunoreactivity in Hilar Mossy Cells of the Adult Dentate Gyrus. *Brain Struct Funct* (2017) 222:2405–19. doi: 10.1007/s00429-016-1349-z

48. Ulrich-Lai YM, Herman JP. Neural Regulation of Endocrine and Autonomic Stress Responses. *Nat Rev Neurosci* (2009) 10:397–409. doi: 10.1038/nrn2647
49. Verkhratsky A, Krishtal OA. Adenosine Triphosphate(ATP) as a Neurotransmitter. In: *Encyclopaedia of Neuroscience 4th Edition* Cambridge: Academic Press, (2009) p. 115–23.
50. Sabharwal L, Kamimura D, Meng J, Bando H, Ogura H, Nakayama C, et al. The Gateway Reflex, Which Is Mediated by the Inflammation Amplifier, Directs Pathogenic Immune Cells Into the CNS. *J Biochem* (2014) 156:299–304. doi: 10.1093/jb/mvu057
51. Stofkova A, Kamimura D, Ohki T, Ota M, Arima Y, Murakami M. Photopic Light-Mediated Down-Regulation of Local α(1A)-Adrenergic Signaling Protects Blood-Retina Barrier in Experimental Autoimmune Uveoretinitis. *Sci Rep* (2019) 9:2353. doi: 10.1038/s41598-019-38895-y
52. Stofkova A, Kamimura D, Ohki T, Ota M, Arima Y, Murakami M. Photopic Light-Mediated Down-Regulation of Local Alpha1a-Adrenergic Signaling Protects Blood-Retina Barrier in Experimental Autoimmune Uveoretinitis. *Sci Rep* (2019) 9:2353. doi: 10.1038/s41598-019-38895-y
53. Ughi N, Hervey SA, Gualtierotti R, Silvana Z, Herrick AL, Ingegnoli F, et al. Sparing Effect of Hemiplegia on Skin Fibrosis and Microvascular Involvement: Reports of Two Cases of Systemic Sclerosis and Review of the Literature. *Semin Arthritis Rheum* (2015) 44:597–601. doi: 10.1016/j.semarthrit.2014.10.011
54. Smith JR, Rosenbaum JT. Management of Uveitis: A Rheumatologic Perspective. *Arthritis Rheum* (2002) 46:309–18. doi: 10.1002/art.503
55. Pras E, Neumann R, Zandman-Goddard G, Levy Y, Assia EI, Shoenfeld Y, et al. Intraocular Inflammation in Autoimmune Diseases. *Semin Arthritis Rheum* (2004) 34:602–9. doi: 10.1016/j.semarthrit.2004.05.002
56. Keyszer G, Langer T, Kornhuber M, Taute B, Horneff G. Neurovascular Mechanisms as a Possible Cause of Remission of Rheumatoid Arthritis in Hemiparetic Limbs. *Ann Rheum Dis* (2004) 63:1349–51. doi: 10.1136/ard.2003.016410

Conflict of Interest: The authors declare that the research was conducted in the absence of any commercial or financial relationships that could be construed as a potential conflict of interest.

Publisher's Note: All claims expressed in this article are solely those of the authors and do not necessarily represent those of their affiliated organizations, or those of the publisher, the editors and the reviewers. Any product that may be evaluated in this article, or claim that may be made by its manufacturer, is not guaranteed or endorsed by the publisher.

frontiers in Immunology

MINI REVIEW
published: 20 January 2022
doi: 10.3389/fimmu.2021.828115

Diverse Roles of TRPV4 in Macrophages: A Need for Unbiased Profiling

Thanh-Nhan Nguyen[1,2], *Ghizal Siddiqui*[3], *Nicholas A. Veldhuis*[1,2*] *and Daniel P. Poole*[1,2*]

[1] Drug Discovery Biology Theme, Monash Institute of Pharmaceutical Sciences, Monash University, Parkville, VIC, Australia, [2] Australian Research Council (ARC) Centre of Excellence in Convergent Bio-Nano Science & Technology, Monash University, Parkville, VIC, Australia, [3] Drug Delivery, Disposition and Dynamics Theme, Monash Institute of Pharmaceutical Sciences, Monash University, Parkville, VIC, Australia

Transient receptor potential vanilloid 4 (TRPV4) is a non-selective mechanosensitive ion channel expressed by various macrophage populations. Recent reports have characterized the role of TRPV4 in shaping the activity and phenotype of macrophages to influence the innate immune response to pathogen exposure and inflammation. TRPV4 has been studied extensively in the context of inflammation and inflammatory pain. Although TRPV4 activity has been generally described as pro-inflammatory, emerging evidence suggests a more complex role where this channel may also contribute to anti-inflammatory activities. However, detailed understanding of how TRPV4 may influence the initiation, maintenance, and resolution of inflammatory disease remains limited. This review highlights recent insights into the cellular processes through which TRPV4 contributes to pathological conditions and immune processes, with a focus on macrophage biology. The potential use of high-throughput and omics methods as an unbiased approach for studying the functional outcomes of TRPV4 activation is also discussed.

Keywords: TRP channels, mechanosensation, macrophage, inflammation, transient receptor potential vanilloid 4 (TRPV4)

OPEN ACCESS

Edited by:
Chaofeng Han,
Second Military Medical University, China

Reviewed by:
Rishov Goswami,
Dana-Farber Cancer Institute, United States
Laura Michalick,
Charité University Medicine Berlin, Germany
Ammar Boudaka,
Sultan Qaboos University, Oman

***Correspondence:**
Daniel P. Poole
Daniel.Poole@monash.edu
Nicholas A. Veldhuis
Nicholas.Veldhuis@monash.edu

Specialty section:
This article was submitted to Molecular Innate Immunity, a section of the journal Frontiers in Immunology

Received: *03 December 2021*
Accepted: *24 December 2021*
Published: *20 January 2022*

Citation:
Nguyen T-N, Siddiqui G, Veldhuis NA and Poole DP (2022) Diverse Roles of TRPV4 in Macrophages: A Need for Unbiased Profiling. Front. Immunol. 12:828115. doi: 10.3389/fimmu.2021.828115

INTRODUCTION

Inflammation is an essential defense mechanism generated by the immune system to protect the body from harmful stimuli or pathogen infection (1). Normally, inflammation is actively resolved to prevent tissue damage. This tightly regulated process involves the spatially and temporally controlled production of mediators leading to dilution of chemokine gradients to ensure that inflammatory responses subside in a timely fashion. Processes which resolve inflammation and rectify tissue homeostasis include reduction or cessation of tissue infiltration by neutrophils, apoptosis of spent neutrophils, down-regulation of chemokines and cytokines, macrophage transformation, and the initiation of healing (2, 3). Disruption of the control mechanisms that underlie these processes results in prolonged or uncontrolled inflammation, which is associated with chronic disease including inflammatory arthritis (4), inflammatory bowel disease (5), pulmonary diseases (6), atherosclerosis (7), foreign body response (8) and fibrosis (9).

The transient receptor potential (TRP) superfamily of ion channels plays important and emerging roles in inflammatory and immune-mediated diseases (10). One of the best

characterized members is transient receptor potential vanilloid 4 (TRPV4), which is expressed by immune cells including macrophages (11–14), neutrophils (15), and dendritic cells. TRPV4 is a tetrameric ion channel with each subunit containing 6 transmembrane domains, a pore-forming loop, and 6 highly conserved ankyrin repeat domains in the cytoplasmic N-terminus (16). The functional role of TRPV4 and involvement in pathophysiology is most extensively defined for macrophages (12, 13, 17, 18). TRPV4 is expressed by various macrophage populations including tissue-resident macrophages located in the lung, gut, brain, liver, and skin (11–14, 19–21). Although TRPV4 has long been associated with pro-inflammatory roles, recent studies propose that TRPV4 activity can also influence macrophage function to promote the reduction or resolution of inflammatory damage (12, 13, 22). This raises a key question: *how can a single ion channel regulate two opposing processes?* In this review, we first highlight emerging evidence for the involvement of TRPV4 as a mechanosensitive channel in pathological conditions and immune responses, with a specific focus on macrophages. We then explore how the use of high-throughput omics approaches could reveal greater insight into the complex network of cellular pathways associated with TRPV4 activation.

TRPV4: A POLYMODAL ION CHANNEL AND KEY EFFECTOR OF RECEPTOR SIGNALING

TRPV4 was first identified as an osmosensitive channel due to its activation by hypotonicity (23, 24). It has since been shown to function as a polymodal non-selective cation channel that can be activated by a diverse array of stimuli including mechanical stress (25–28), warm temperature (above 27°C) (29, 30), endogenous polyunsaturated fatty acids (PUFAs) (31–33) and receptor-operated signaling (34). TRPV4 integrates cellular responses to these various stimuli, enabling this channel to influence a broad range of signaling and associated transcriptional events (11–14, 35–52), as summarized in **Figure 1**, and previously reviewed in detail (53).

TRPV4 is activated by hypoosmolarity, shear stress or direct deflection at cell-substrate contact points. Activation of TRPV4 by cellular indentation or membrane stretch is also commonly reported (25, 54), although the relative importance and generality of this mode of gating has recently been questioned based on electrophysiological studies (27, 28). This suggests that TRPV4 may only respond directly to specific mechanical cues. It is also evident that TRPV4 activation by hypotonic conditions and shear stress can indirectly modulate channel gating *via* production of lipid metabolites such as arachidonic acid and its metabolite 5′,6′-EET. This process requires PLA2 and cytochrome P450 epoxygenase activity (33, 55), suggesting that there are parallels between TRPV4 mechanosensitivity and its function as a receptor-operated channel. For example, G protein-coupled receptors (GPCRs) can also promote PLA2 and P450 activity to increase production of the same anandamide and arachidonic acid-derived lipid species. GPCRs, including members of the protease-activated, muscarinic, serotonin, and histamine receptor families, converge on TRPV4 through lipid signaling pathways, presumably as a mechanism to amplify specific signaling and transcriptional events (34). GPCR signaling can also sensitize and enhance the responsiveness of TRPV4 to these lipid metabolites by promoting direct phosphorylation of residues in its cytoplasmic N- and C-terminal domains by PKA, PKC and Src family tyrosine kinases (34). TRPV4 is proposed to be a key effector and 'amplifier' of sensory afferent nerve signaling. GPCR- and protein kinase-dependent sensitization of TRPV4 is associated with increased pain transmission and the peripheral release of neuropeptides and other mediators that promote neurogenic inflammation (56).

Recent studies have extended our understanding of how TRPV4 functions as an effector for receptor signaling and a broader integrator of mechanical cues in different cell types. Integrins are ubiquitously expressed transmembrane mechanoreceptors that are responsible for cell-cell interactions and cell adhesion (57). In endothelial cells, mechanical strain activates TRPV4-mediated Ca^{2+} influx *via* the β1 integrin-CD98hc axis, which is hypothesized to occur through a direct, physical interaction (58, 59). In this model, mechanical strain is sensed by β1 integrin, which initiates ultra-rapid signal transduction. The signal is transmitted from the cytoplasmic C terminus of β1 integrin to the N-terminal cytoplasmic ankyrin domain of TRPV4 *via* the transmembrane glycoprotein CD98hc, resulting in increased channel gating (59) (**Figure 1**).

Swain et al. have also recently demonstrated that TRPV4 is an effector protein for other ion channels (60, 61). Shear stress and mechanical pushing of pancreatic acinar cells indirectly activated TRPV4 *via* the fast-inactivating mechanosensitive ion channel Piezo1 (61). Piezo1 activation initiated a transient Ca^{2+} influx followed by a sustained elevation of intracellular Ca^{2+}, an effect that was inhibited by the TRPV4 antagonist HC-067047 and mediated by PLA2 (60, 61).

The precise mechanisms involved in the TRPV4-dependent inflammatory response are not fully understood. However, it is speculated that changes to the extracellular matrix stiffness during inflammation can activate TRPV4. Scheraga et al. reported that TRPV4 is required for expression of dual-specificity phosphatase 1 (DUSP1) in response to LPS under pathophysiological matrix stiffness (>8kPa), but not under subthreshold matrix stiffness (1kPa) (12). DUSP1 is an inflammatory regulator, which inhibits c-Jun N-terminal kinases (JNK) and promotes p38 mitogen-activated protein kinases (MAPK) (12). In addition, calcium influx *via* TRPV4 also activates calcineurin which promotes nuclear factor of activated T-cells (NFAT) and nuclear factor kappa B (NF-kB) expression (62, 63). These studies illustrate an important role for TRPV4 in LPS-induced macrophage activation. Further detail outlining the involvement of TRPV4 in phenotypic switch by macrophages is provided in subsequent sections.

These established and emerging roles of TRPV4 as a key integrator and amplifier of mechano- and receptor-mediated signaling have been demonstrated for a range of distinct cell types including sensory neurons and endothelial cells. This is

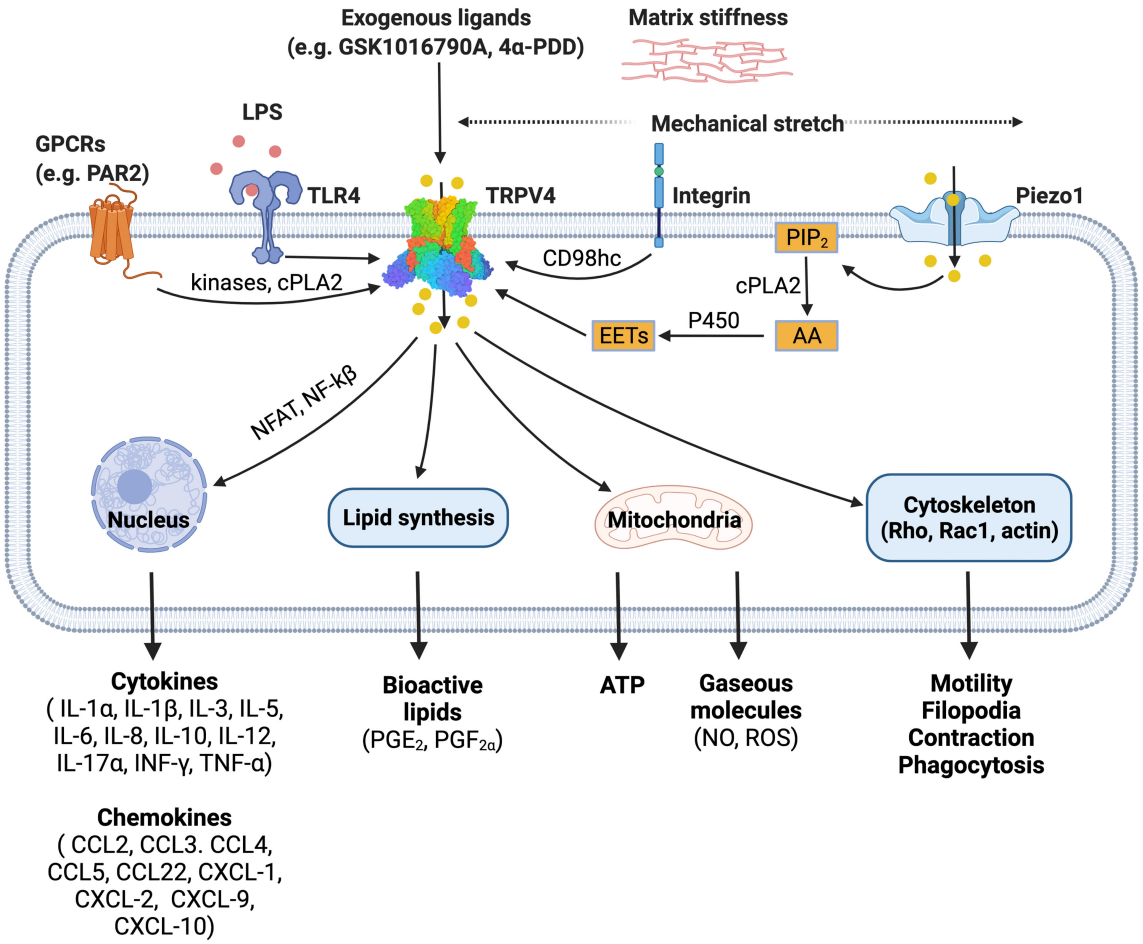

FIGURE 1 | TRPV4 is a polymodal ion channel which can be activated directly or indirectly by a diverse range of stimuli including mechanical force, endogenous mediators, and pharmacological tools. TRPV4 signals through multiple pathways leading to a range of downstream effects on cellular function. The figure illustrates published activation pathways and associated outcomes. *TRPV4, transient receptor potential vanilloid 4; GPCRs, G protein-coupled receptors; TLR4, toll-like receptor 4; LPS, lipopolysaccharide; PIP_2, phosphatidylinositol biphosphate; AA, arachidonic acid; cPLA2, cytosolic phospholipase A_2; P450, cytochrome P450 epoxygenase; EETs, epoxyeicosatrienoic acids; NFAT, nuclear factor of activated T-cells; NF-kB, nuclear factor kappa B*. Figure created with BioRender.com.

consistent with the generality of this function and highlights the associated challenges and opportunities when considering TRPV4 signaling and function as a potential therapeutic target.

TRPV4-EXPRESSING MACROPHAGES AS A THERAPEUTIC TARGET FOR RESOLVING INFLAMMATION

TRPV4 mRNA or protein has been detected in most organs and tissues (23, 24, 30, 31, 64–70) and is expressed by a broad range of cell types including neurons, urothelia, epithelia, immune cells, endothelial cells and aortic and airway smooth muscle (35, 65, 68, 71–73). This widespread expression pattern, coupled with multiple activating modalities, underlies the diverse roles of TRPV4 in physiological processes including volume- and osmo-sensing, thermoregulation, mechanosensation in the vasculature and urinary tract, cell barrier function, bone formation, metabolic disorders, pain, neurogenic inflammation, and gut motility (23, 29, 34, 53, 74–77). TRPV4 also performs critical pro-fibrotic roles and can detect and influence changes to the extracellular matrix (78). TRPV4 antagonists have been pursued and patented for several therapeutic applications including treatment or prevention of lung injury, heart failure, ischemic heart disease, and pain (79). Furthermore, pre-clinical and clinical studies have investigated TRPV4 inhibition as a therapeutic approach for treatment of osteoarthritis (80, 81), atherosclerosis (82), and cancer (83–85). More recently, the use of TRPV4 antagonists for managing comorbidities associated with SARS-CoV-2 infection such as lung edema has also been proposed (86). Despite these extensive efforts to define the importance of TRPV4 in cardiovascular, pulmonary, and inflammatory diseases, there is currently only one drug candidate (GSK2798745) approved for phase II clinical trials (87, 88). This clinical candidate is a small molecule, orally available inhibitor with low nanomolar potency (87).The apparent

lack of therapeutic advancement may reflect limitations to our mechanistic understanding of the precise involvement of TRPV4 in inflammatory and protective processes.

In chronic disease, such as arthritis and joint pain, there are persistent changes to lipid production, osmolarity, increased presence of GPCR ligands (e.g., immune-derived peptides and proteases) and exposure to mechanical cues such as those associated with fibrosis. All these factors have the potential to promote sustained inflammatory signaling, edema, sprouting of nerve fibers, and angiogenesis, and most importantly, influence TRPV4 function (89). Studies using pharmacological tools and *trpv4*$^{-/-}$ mice have consistently shown that inhibition or loss of TRPV4 function reduces inflammatory processes and tissue edema. Accordingly, TRPV4 is often described as a pro-inflammatory mediator and a therapeutic target for treating inflammatory disease. However, most of these studies are acute in nature, and may not always adequately reflect proposed resolving roles for TRPV4. Macrophages are of particular interest for targeting inflammation and associated diseases. These cells orchestrate both inflammation and resolution, as summarized in **Table 1**, and recent evidence supports the dichotomous nature of

TABLE 1 | Summary of factors that are secreted in response to mechanical or pharmacological activation of TRPV4.

Secreted factors	Experimental conditions	Study models	Related conditions or physiological functions	Ref.
↑ IL-1α, IL-1β, IL-6, IL-8 & CCL2	Stretch (cyclic 30%, 1.25 Hz)	M1 (GM-CSF induced) - hMDM	Lung injury	(44)
↑ TNF-α & CCL2	Stretch (cyclic 30%, 1.25 Hz)	M2 (M-CSF induced) - hMDM	Lung injury	(44)
↑ IL-1α, IL-6, IL-8 & CCL22	GSK101 (3 nM) or Stretch (cyclic 30%, 1.25 Hz)	NCI-H292	Lung injury	(44)
↑ IL-6 & CXCL1	Mechanical ventilation (30 ml/kg T_V)	Balb/c mice (bronchoalveolar lavage fluid)	Lung injury	(44)
↓ IL-6, TNF-α & ROS	LPS (100 ng/mL)	TRPV4 siRNA RAW267.4	Lung injury	(62)
↑ NO & ROS	4α-PDD (10 μM)	mAM	Lung injury	(11)
↑ ROS	4α-PDD (10 μM)	Endothelial cells	Lung injury	(36)
↑ IL-6, CXCL1 & CXCL2	LPS (100 ng/mL) clinical strain of *Pseudomonas aeruginosa* embedded in agarose beads	*trpv4*$^{-/-}$ mBMDM *trpv4*$^{-/-}$ C57BL6 mice (whole lung lavage fluid)	Pulmonary infection and injury in murine pneumonia model	(12)
↑ IL-1β ↓ IL-10	LPS (100 ng/mL) & pathological matrix stiffness (25kPa)	*trpv4*$^{-/-}$ mBMDM	Pulmonary infection, injury, and fibrosis	(13)
↓ IL-1α, IL-1β, IL-3, IL-5, IL-6, IL-12p40, IL-12p70, IL-13, IL- 17α, INF-γ, TNF-α, CCL2, CCL3, CCL4, CCL5 & GM-CSF	LPS (50 mg/kg) + GSK219 (1 mg/kg)	C57BL6/J mice (blood concentration)	Sepsis	(45)
↑ IL-6, CCL2, CCL5 & CXCL1	Intracolonic administration of 4α-PDD (200 μg in 40% ethanol)	Mouse colonic tissue	Colitis	(35)
↑ IL-8, CCL2, CXCL9 & CXCL10	4α-PDD (100μM)	Caco-2	Colitis	(35)
↑ IL-8, CCL5 CXCL9 & CXCL10	4α-PDD (100μM)	T84	Colitis	(35)
↑ CCL2	GSK101 (10nM) or Hypotonic stimuli (200 mOsm/kg)	Muller glia	Acute retinal detachment	(46)
↑ Prostaglandin $F_{2\alpha}$	GSK101 (100 nM)	Aorta from high-salt diet-fed mouse	Hypertension	(43)
↑ Prostaglandin E2	GSK101 (300 nM)	mMM	GI motility	(14)
↑ ATP	GSK101 (100 nM) or Heat (25 -35.8°C)	Mouse esophageal keratinocytes	GERD, wound healing	(37, 47)
	GSK101 (100 nM) or 5,6-EET (500 nM) or mechanical stretch (120% lateral stretch)	RGE1-01	Gastric emptying	(48)
	GSK101 (0.01 mL, 50 nM)	Rat corneal epithelium + stroma, endothelium, cornea	Acute ocular hypertension	(49)
	GSK101 (10 nM – 10 μM)	Human bronchial epithelial cells	COPD (cigarette smoking-related)	(38)
	4α-PDD (3 μM, 10 μM)	HET-1A	Esophagitis and GERD	(39)
	GSK101 (100 nM)	Mouse cholangiocytes	Cholestatic liver disorders	(40)
	Stretch (400 μm/s) or 4α-PDD (10 μM)	Mouse urothelial cells	Bladder function	(41)
	4α-PDD (10 μM)	Astrocyte	N/A	(42)

mBMDM, mouse bone marrow-derived macrophages; hMDM, human blood monocyte-derived macrophages; mAM, mouse alveolar macrophages; mMM, mouse muscularis macrophages; GI, gastrointestinal; GERD, gastroesophageal reflux disease; COPD, chronic obstructive pulmonary disease; GSK101, GSK1016790A; GSK219, GSK2193874; 4α-PDD, 4α-Phorbol 12,13-didecanoate; N/A, not available.

↑ = increased; ↓ = decreased.

TRPV4 in both homeostatic or protective roles and in pathophysiological pathways (12, 13). This includes roles in phagocytosis and cytokine production, both of which can be influenced by changes to the cellular environment in which the macrophages are located (11–13, 62).

TRPV4 ACTIVITY INFLUENCES MACROPHAGE POLARIZATION AND METABOLISM

i) TRPV4 and Macrophage Polarization

Macrophages are a heterogeneous population of cells with the capability to change phenotype and perform specific roles in response to their microenvironment. For many years, the two main extremes of macrophage phenotype were widely accepted as M1 (so-called 'classical' pro-inflammatory phenotype) and M2 ('non-classical' anti-inflammatory phenotype). In reality, macrophages are highly versatile and the distinction between subsets is less clear. Metabolic reprogramming of macrophages is essential for phenotypic switch and immune responses. The M1 and M2 phenotypes have unique metabolic hallmarks (90–92). The manipulation of metabolic pathways in macrophages can alter their functions (93) and targeting of immunometabolism is a promising approach for blocking inflammatory signaling. For example, some anti-inflammatory drugs (e.g., dimethyl fumarate, metformin, methotrexate, and rapamycin) limit inflammation through targeting metabolic events in immune cells including macrophages (90).

TRPV4 activation is associated with phenotypic switch by macrophages (12, 13, 17, 51, 94). Current understanding of macrophage polarization is based largely on the use of biochemical cues such as cytokines or LPS to alter cellular phenotype. However, it is important to consider other biophysical factors originating from the microenvironment that may influence phenotype, such as exposure to shear stress and alterations in extracellular matrix stiffness. Several studies have explored how physical stimuli can affect macrophage phenotype, including the involvement of TRPV4 (see **Table 1**). Moderate cyclic stretch (7%, 0.8 Hz) applied to human peripheral blood mononuclear cells over a 7-day period increased the relative proportion of M2 cells ($CD206^+$), whereas higher stretch (12%, 0.8 Hz) increased the M1-like ($CCR7^+$) phenotype (95). In addition, cyclic or static stretch also triggered production of cytokines, chemokines, and enzymes by macrophages. This included expression of mRNA for iNOS, IL-6, MCP-1, and IL-10 (95, 96). Changes in stiffness of the surrounding extracellular matrix can affect surface protein expression and the secretion profile of macrophages. Previtera et al. (97) cultured murine BMDMs on 0.3–230 kPa polyacrylamide hydrogels and observed that macrophages grown on high stiffness substrates produced elevated levels of pro-inflammatory mediators relative to macrophages grown on softer substrates (97). However, a different study led by Chen et al. (98) showed that murine BMDMs cultured in polyacrylamide hydrogels at a low matrix stiffness (2.55 ± 0.32 kPa) displayed an M1-like phenotype, with enhanced CD86 cell surface expression and higher production of ROS, IL-1β and TNF-α. In contrast, a higher matrix stiffness (34.88 ± 4.22 kPa) drove the cells toward an M2-like phenotype with higher CD206 expression, and production of IL-4 and TGF-β (98). Direct comparison of these studies is complicated by the differences in the experimental design. In addition, although both used polyacrylamide hydrogels, Previtera et al. (97) pre-treated the gel with laminin (97), which has been shown to promote expression of pro-inflammatory factors in microglia (99) and reduce IL-10 secretion by THP-1 cells (100). However, these studies suggest that mechanosensitive receptors, such as TRPV4 (17), play a critical role in macrophage phenotypic switch in response to the biophysical properties of their environment. This is consistent with other non-TRPV4-related studies demonstrating that matrix stiffness has a profound influence on macrophage polarization states (100, 101) and warrants further investigation, as discussed by other manuscripts within this special issue.

ii) TRPV4 and Macrophage Metabolism

Beyond expression of specific markers, macrophage phenotypes can also be differentiated based on their metabolic profiles, especially those associated with central carbon metabolism. Pro-inflammatory macrophages utilize glycolysis and the pentose phosphate pathway (PPP) to generate sufficient energy to meet higher ATP requirements. Fatty acid synthesis is increased, as this is required both as an energy production pathway and for synthesis of pro-inflammatory lipids, such as prostaglandins. At the same time, oxygen consumption is reduced, and the tricarboxylic acid (TCA) cycle and oxidative phosphorylation (OXPHOS) are suppressed. In contrast, macrophages with a protective phenotype have a normal TCA cycle and higher fatty acid oxidation rate (93).

Greater understanding of how TRPV4 influences macrophage phenotype at the metabolic level will provide further insight into the role of this channel in inflammation and inflammatory diseases. Although this has not been defined in detail, there is some evidence to suggest that TRPV4 can regulate central carbon metabolism, cellular respiration, and lipid metabolism. Several studies report that TRPV4 activation can increase production of reactive oxygen species (ROS) and nitric oxide (NO) (11, 36, 102) and evoke ATP release (37–42). In macrophages, ROS is largely generated through the NADPH oxidase pathway, while NO is mainly produced from arginine *via* the iNOS pathway. Both require NADPH as a co-factor. The high glycolytic flux of activated macrophages provides glucose-6-phosphate for the PPP, which is the main source of NADPH (93). Furthermore, the TRPV4 activator 4α-PDD reduces mitochondrial bioenergetics and oxygen consumption in pulmonary arterial endothelial cells after a 3 h incubation period (36). TRPV4 can also negatively regulate expression of peroxisome proliferator-activated receptor γ (PPARγ) coactivator 1α (PGC1α), mitochondrial uncoupling protein 1 (UCP1), and cellular respiration in adipocytes (103). PGC-1α is a transcriptional coregulator of pPPARγ, controlling the UCP1 promoter, which is involved in mitochondrial biogenesis and oxidative metabolism.

PPARγ is an important transcription factor of M2 macrophages and is associated with fatty acid uptake and oxidation.

Pharmacological activation of TRPV4 also triggers secretion of pro-inflammatory lipid mediators including prostaglandins, suggesting a potential link between this ion channel and fatty acid biosynthesis (14, 43). Collectively, the metabolic profile of TRPV4-activated cells shares some similarities with the profile of the pro-inflammatory macrophage phenotype including high glycolysis, low OXPHOS activity and increased synthesis of pro-inflammatory lipids.

INVESTIGATING PLEIOTROPIC ROLES OF TRPV4 USING A SYSTEMS BIOLOGY APPROACH

This approach utilizes high-throughput omics platforms to interrogate complex biological systems. In contrast to most targeted studies outlined above, systems biology can comprehensively characterize molecular profiles at the level of the genome, transcriptome, proteome, peptidome, metabolome and lipidome in an unbiased manner (104–109). These approaches are well suited to the study of TRPV4 function in macrophages as these cells secrete mediators and their metabolic activity is highly regulated and linked to the inflammatory state.

i) Metabolic Profiling in Mechanobiology and Immunology

Metabolomic methods have revealed novel biological pathways and important metabolites in inflammatory responses and have identified signature metabolites associated with different macrophage phenotypes (110–112). This includes the distinct metabolomic profiles of central carbon metabolism between M1 and M2 macrophages, as outlined above.

There are relatively few studies that examine the role of TRPV4 at a metabolic level (11, 36–42, 102). Furthermore, these are limited to targeted pathways including cellular respiration, NO production, and bioactive lipids, such as prostaglandins (**Table 1**). For example, targeted studies of isolated mouse alveolar macrophages have shown that 4-αPDD activates TRPV4 to promote Ca^{2+} influx and subsequent release of NO and superoxide (11). The combination of NO and superoxide can produce peroxynitrite, a strong oxidant involved in pathogen defense and inflammation (113, 114). Untargeted global profiling of TRPV4-induced macrophage phenotypes could help to address important questions of how and why TRPV4 can have both pro- and anti-inflammatory responses, and further understand the underlying mechanisms involved.

ii) Profiling TRPV4-Mediated Lipid Synthesis and Metabolism

Macrophages are an important source of bioactive lipid mediators which are important determinants of the magnitude and duration of inflammatory signaling. In the onset phase of acute inflammation, eicosanoid lipid mediators (leukotrienes and prostaglandins) are released to promote inflammation (115, 116). At the resolution phase, cells switch to production of specialized pro-resolving mediators, such as lipoxins, resolvins, protectins, and maresins to resolve inflammation (115, 116). The imbalance of pro-inflammatory and pro-resolving mediators results in chronic inflammation (115, 116). Although TRPV4 activity can affect lipid metabolism in macrophages, including prostaglandin E2 (PGE2) production (14), this process has not been examined in detail and remains poorly characterized. The release of prostaglandins at the early stages of acute inflammation is important for a protective response. However, excessive production can promote chronic inflammation (115, 117, 118).

There is a clear need for more detailed investigation into how TRPV4 may influence lipid metabolism in the context of inflammatory disease. A comprehensive and unbiased lipidomics approach will provide mechanistic insight beyond that provided by current studies and significantly advance understanding of how TRPV4-mediated secretion of bioactive lipid mediators contributes to the initiation and resolution of inflammation.

iii) Profiling the Protein Interactome

TRPV4 can directly or indirectly interact with a broad range of proteins (53, 56, 119). Mass spectrometry-based proteomics has become the core technology for large-scale investigation of protein-protein interactions with high confidence. Many purification methods have been developed to enable single protein complex characterization through to global interactome profiling (120). Commonly used workflows for purification of the target protein and its interactors include antibody-based affinity-purification mass spectrometry (AP-MS) (121), quantitative immunoprecipitation combined with knock-down (QUICK) (122), and proximity-ligation techniques such as BioID (123). The global interactome profiling requires biochemical techniques including fractionation by size-exclusion chromatography (SEC), ion-exchange chromatography (IEX), or perturbation co-behavior approach. The pros and cons of each of these workflows are covered elsewhere (120). Comprehensive analysis of the protein-protein interaction network will enable novel insight into the contribution of TRPV4 to cellular biology beyond what is possible with currently used methodology. Furthermore, this approach may facilitate identification of new avenues and targets to enable therapeutic modulation of TRPV4-dependent inflammatory signaling.

CONCLUDING REMARKS

This review provides an overview of how TRPV4 influences macrophage function in pathological conditions and highlights the dual roles that this channel has in promoting and preventing inflammation. There is little doubt that TRPV4 is important for maintaining homeostasis and immune responses. This includes: 1) responses to pathogens and changes in biophysical factors including mechanical stress and matrix stiffness, 2) mediating

inflammatory responses (phagocytosis, cytokine secretion) and balancing pro- and anti-inflammatory cytokine secretion, and 3) facilitating cell-cell communication *via* secreted factors. However, the underlying mechanisms involved in each role are not fully understood. In addition, cytokines and bioactive lipids secreted by macrophages are essential mediators of the inflammatory response. The importance of TRPV4 for macrophage polarization and associated production of cytokines is well documented. In contrast, current understanding of how TRPV4 regulates synthesis of bioactive lipids, protein expression, and protein-protein interactions is limited. This suggests that a focus on this specific research area using more comprehensive analysis methods is required. Application of high-throughput omics approaches to definitively characterize the effects of TRPV4 modulation on macrophages may reveal novel functions and pathways important for understanding the precise involvement of TRPV4 in inflammatory and protective processes. Similar methods have been widely applied in the immunology field, which has helped to further differentiate pro- and anti-inflammatory macrophage phenotypes (107, 124, 125). This information is critical for understanding how TRPV4 can influence both inflammatory and resolving processes and will contribute to future therapeutic targeting of TRPV4 in inflammatory diseases.

AUTHOR CONTRIBUTIONS

T-NN, GS, NV, and DP reviewed the literature and wrote the manuscript. All authors contributed to the article and approved the submitted version.

FUNDING

ARC Centre of Excellence in Convergent Bio-Nano Science and Technology (CE14100036).

REFERENCES

1. Medzhitov R. Inflammation 2010: New Adventures of an Old Flame. *Cell* (2010) 140(6):771–6. doi: 10.1016/j.cell.2010.03.006
2. Reville K, Crean JK, Vivers S, Dransfield I, Godson C. Lipoxin A4 Redistributes Myosin IIA and Cdc42 in Macrophages: Implications for Phagocytosis of Apoptotic Leukocytes. *J Immunol* (2006) 176(3):1878–88. doi: 10.4049/jimmunol.176.3.1878
3. Serhan CN, Savill J. Resolution of Inflammation: The Beginning Programs the End. *Nat Immunol* (2005) 6(12):1191–7. doi: 10.1038/ni1276
4. McInnes IB, Schett G. Pathogenetic Insights From the Treatment of Rheumatoid Arthritis. *Lancet* (2017) 389(10086):2328–37. doi: 10.1016/S0140-6736(17)31472-1
5. Nielsen OH, Ainsworth MA. Tumor Necrosis Factor Inhibitors for Inflammatory Bowel Disease. *N Engl J Med* (2013) 369(8):754–62. doi: 10.1056/NEJMct1209614
6. Barnes PJ. Targeting Cytokines to Treat Asthma and Chronic Obstructive Pulmonary Disease. *Nat Rev Immunol* (2018) 18(7):454–66. doi: 10.1038/s41577-018-0006-6
7. Wolf D, Ley K. Immunity and Inflammation in Atherosclerosis. *Circ Res* (2019) 124(2):315–27. doi: 10.1161/CIRCRESAHA.118.313591
8. Veiseh O, Vegas AJ. Domesticating the Foreign Body Response: Recent Advances and Applications. *Adv Drug Deliv Rev* (2019) 144:148–61. doi: 10.1016/j.addr.2019.08.010
9. Jun JI, Lau LF. Resolution of Organ Fibrosis. *J Clin Invest* (2018) 128(1):97–107. doi: 10.1172/JCI93563
10. Santoni G, Morelli MB, Amantini C, Santoni M, Nabissi M, Marinelli O, et al. "Immuno-Transient Receptor Potential Ion Channels": The Role in Monocyte- and Macrophage-Mediated Inflammatory Responses. *Front Immunol* (2018) 9:1273. doi: 10.3389/fimmu.2018.01273
11. Hamanaka K, Jian MY, Townsley MI, King JA, Liedtke W, Weber DS, et al. TRPV4 Channels Augment Macrophage Activation and Ventilator-Induced Lung Injury. *Am J Physiol Lung Cell Mol Physiol* (2010) 299(3):L353–62. doi: 10.1152/ajplung.00315.2009
12. Scheraga RG, Abraham S, Grove LM, Southern BD, Crish JF, Perelas A, et al. TRPV4 Protects the Lung From Bacterial Pneumonia *via* MAPK Molecular Pathway Switching. *J Immunol* (2020) 204(5):1310–21. doi: 10.4049/jimmunol.1901033
13. Scheraga RG, Abraham S, Niese KA, Southern BD, Grove LM, Hite RD, et al. TRPV4 Mechanosensitive Ion Channel Regulates Lipopolysaccharide-Stimulated Macrophage Phagocytosis. *J Immunol* (2016) 196(1):428–36. doi: 10.4049/jimmunol.1501688
14. Luo J, Qian A, Oetjen LK, Yu W, Yang P, Feng J, et al. TRPV4 Channel Signaling in Macrophages Promotes Gastrointestinal Motility *via* Direct Effects on Smooth Muscle Cells. *Immunity* (2018) 49(1):107–19.e4. doi: 10.1016/j.immuni.2018.04.021
15. Yin J, Michalick L, Tang C, Tabuchi A, Goldenberg N, Dan Q, et al. Role of Transient Receptor Potential Vanilloid 4 in Neutrophil Activation and Acute Lung Injury. *Am J Respir Cell Mol Biol* (2016) 54(3):370–83. doi: 10.1165/rcmb.2014-0225OC
16. Naert R, Lopez-Requena A, Voets T, Talavera K, Alpizar YA. Expression and Functional Role of TRPV4 in Bone Marrow-Derived CD11c(+) Cells. *Int J Mol Sci* (2019) 20(14):3378. doi: 10.3390/ijms20143378
17. Dutta B, Goswami R, Rahaman SO. TRPV4 Plays a Role in Matrix Stiffness-Induced Macrophage Polarization. *Front Immunol* (2020) 11:570195. doi: 10.3389/fimmu.2020.570195
18. Dutta B, Arya RK, Goswami R, Alharbi MO, Sharma S, Rahaman SO. Role of Macrophage TRPV4 in Inflammation. *Lab Invest* (2020) 100(2):178–85. doi: 10.1038/s41374-019-0334-6
19. Luo J, Feng J, Yu G, Yang P, Mack MR, Du J, et al. Transient Receptor Potential Vanilloid 4-Expressing Macrophages and Keratinocytes Contribute Differentially to Allergic and Nonallergic Chronic Itch. *J Allergy Clin Immunol* (2018) 141(2):608–19.e7. doi: 10.1016/j.jaci.2017.05.051
20. Seth RK, Das S, Dattaroy D, Chandrashekaran V, Alhasson F, Michelotti G, et al. TRPV4 Activation of Endothelial Nitric Oxide Synthase Resists Nonalcoholic Fatty Liver Disease by Blocking CYP2E1-Mediated Redox Toxicity. *Free Radic Biol Med* (2017) 102:260–73. doi: 10.1016/j.freeradbiomed.2016.11.047
21. Liu M, Liu X, Wang L, Wang Y, Dong F, Wu J, et al. TRPV4 Inhibition Improved Myelination and Reduced Glia Reactivity and Inflammation in a Cuprizone-Induced Mouse Model of Demyelination. *Front Cell Neurosci* (2018) 12:392. doi: 10.3389/fncel.2018.00392
22. Naik SK, Pattanaik K, Eich J, Sparr V, Hauptmann M, Kalsdorf B, et al. Differential Roles of the Calcium Ion Channel TRPV4 in Host Responses to Mycobacterium Tuberculosis Early and Late in Infection. *iScience* (2020) 23(6):101206. doi: 10.1016/j.isci.2020.101206
23. Strotmann R, Harteneck C, Nunnenmacher K, Schultz G, Plant TD. OTRPC4, a Nonselective Cation Channel That Confers Sensitivity to Extracellular Osmolarity. *Nat Cell Biol* (2000) 2(10):695–702. doi: 10.1038/35036318
24. Liedtke W, Choe Y, Marti-Renom MA, Bell AM, Denis CS, Sali A, et al. Vanilloid Receptor-Related Osmotically Activated Channel (VR-OAC), a Candidate Vertebrate Osmoreceptor. *Cell* (2000) 103(3):525–35. doi: 10.1016/s0092-8674(00)00143-4

25. Loukin S, Zhou X, Su Z, Saimi Y, Kung C. Wild-Type and Brachyolmia-Causing Mutant TRPV4 Channels Respond Directly to Stretch Force. *J Biol Chem* (2010) 285(35):27176–81. doi: 10.1074/jbc.M110.143370
26. Ryskamp DA, Frye AM, Phuong TT, Yarishkin O, Jo AO, Xu Y, et al. TRPV4 Regulates Calcium Homeostasis, Cytoskeletal Remodeling, Conventional Outflow and Intraocular Pressure in the Mammalian Eye. *Sci Rep* (2016) 6:30583. doi: 10.1038/srep30583
27. Servin-Vences MR, Moroni M, Lewin GR, Poole K. Direct Measurement of TRPV4 and PIEZO1 Activity Reveals Multiple Mechanotransduction Pathways in Chondrocytes. *Elife* (2017) 6. doi: 10.7554/eLife.21074
28. Sianati S, Schroeter L, Richardson J, Tay A, Lamande SR, Poole K. Modulating the Mechanical Activation of TRPV4 at the Cell-Substrate Interface. *Front Bioeng Biotechnol* (2020) 8:608951. doi: 10.3389/fbioe.2020.608951
29. Guler AD, Lee H, Iida T, Shimizu I, Tominaga M, Caterina M. Heat-Evoked Activation of the Ion Channel, TRPV4. *J Neurosci* (2002) 22(15):6408–14. doi: 10.1523/JNEUROSCI.22-15-06408.2002
30. Chung MK, Lee H, Caterina MJ. Warm Temperatures Activate TRPV4 in Mouse 308 Keratinocytes. *J Biol Chem* (2003) 278(34):32037–46. doi: 10.1074/jbc.M303251200
31. Everaerts W, Nilius B, Owsianik G. The Vanilloid Transient Receptor Potential Channel TRPV4: From Structure to Disease. *Prog Biophys Mol Biol* (2010) 103(1):2–17. doi: 10.1016/j.pbiomolbio.2009.10.002
32. Vriens J, Owsianik G, Fisslthaler B, Suzuki M, Janssens A, Voets T, et al. Modulation of the Ca2 Permeable Cation Channel TRPV4 by Cytochrome P450 Epoxygenases in Vascular Endothelium. *Circ Res* (2005) 97(9):908–15. doi: 10.1161/01.RES.0000187474.47805.30
33. Watanabe H, Vriens J, Prenen J, Droogmans G, Voets T, Nilius B. Anandamide and Arachidonic Acid Use Epoxyeicosatrienoic Acids to Activate TRPV4 Channels. *Nature* (2003) 424(6947):434–8. doi: 10.1038/nature01807
34. Veldhuis NA, Poole DP, Grace M, McIntyre P, Bunnett NW. The G Protein-Coupled Receptor-Transient Receptor Potential Channel Axis: Molecular Insights for Targeting Disorders of Sensation and Inflammation. *Pharmacol Rev* (2015) 67(1):36–73. doi: 10.1124/pr.114.009555
35. D'Aldebert E, Cenac N, Rousset P, Martin L, Rolland C, Chapman K, et al. Transient Receptor Potential Vanilloid 4 Activated Inflammatory Signals by Intestinal Epithelial Cells and Colitis in Mice. *Gastroenterology* (2011) 140(1):275–85. doi: 10.1053/j.gastro.2010.09.045
36. Lu Q, Zemskov EA, Sun X, Wang H, Yegambaram M, Wu X, et al. Activation of the Mechanosensitive Ca(2+) Channel TRPV4 Induces Endothelial Barrier Permeability *via* the Disruption of Mitochondrial Bioenergetics. *Redox Biol* (2021) 38:101785. doi: 10.1016/j.redox.2020.101785
37. Mihara H, Boudaka A, Sugiyama T, Moriyama Y, Tominaga M. Transient Receptor Potential Vanilloid 4 (TRPV4)-Dependent Calcium Influx and ATP Release in Mouse Oesophageal Keratinocytes. *J Physiol* (2011) 589(Pt 14):3471–82. doi: 10.1113/jphysiol.2011.207829
38. Baxter M, Eltom S, Dekkak B, Yew-Booth L, Dubuis ED, Maher SA, et al. Role of Transient Receptor Potential and Pannexin Channels in Cigarette Smoke-Triggered ATP Release in the Lung. *Thorax* (2014) 69(12):1080–9. doi: 10.1136/thoraxjnl-2014-205467
39. Ueda T, Shikano M, Kamiya T, Joh T, Ugawa S. The TRPV4 Channel is a Novel Regulator of Intracellular Ca2+ in Human Esophageal Epithelial Cells. *Am J Physiol Gastrointest Liver Physiol* (2011) 301(1):G138–47. doi: 10.1152/ajpgi.00511.2010
40. Li Q, Kresge C, Boggs K, Scott J, Feranchak A. Mechanosensor Transient Receptor Potential Vanilloid Member 4 (TRPV4) Regulates Mouse Cholangiocyte Secretion and Bile Formation. *Am J Physiol Gastrointest Liver Physiol* (2020) 318(2):G277–G87. doi: 10.1152/ajpgi.00176.2019
41. Mochizuki T, Sokabe T, Araki I, Fujishita K, Shibasaki K, Uchida K, et al. The TRPV4 Cation Channel Mediates Stretch-Evoked Ca2+ Influx and ATP Release in Primary Urothelial Cell Cultures. *J Biol Chem* (2009) 284(32):21257–64. doi: 10.1074/jbc.M109.020206
42. Shibasaki K, Ikenaka K, Tamalu F, Tominaga M, Ishizaki Y. A Novel Subtype of Astrocytes Expressing TRPV4 (Transient Receptor Potential Vanilloid 4) Regulates Neuronal Excitability *via* Release of Gliotransmitters. *J Biol Chem* (2014) 289(21):14470–80. doi: 10.1074/jbc.M114.557132
43. Zhang P, Sun C, Li H, Tang C, Kan H, Yang Z, et al. TRPV4 (Transient Receptor Potential Vanilloid 4) Mediates Endothelium-Dependent Contractions in the Aortas of Hypertensive Mice. *Hypertension* (2018) 71(1):134–42. doi: 10.1161/HYPERTENSIONAHA.117.09767
44. Pairet N, Mang S, Fois G, Keck M, Kuhnbach M, Gindele J, et al. TRPV4 Inhibition Attenuates Stretch-Induced Inflammatory Cellular Responses and Lung Barrier Dysfunction During Mechanical Ventilation. *PloS One* (2018) 13(4):e0196055. doi: 10.1371/journal.pone.0196055
45. Dalsgaard T, Sonkusare SK, Teuscher C, Poynter ME, Nelson MT. Pharmacological Inhibitors of TRPV4 Channels Reduce Cytokine Production, Restore Endothelial Function and Increase Survival in Septic Mice. *Sci Rep* (2016) 6:33841. doi: 10.1038/srep33841
46. Matsumoto H, Sugio S, Seghers F, Krizaj D, Akiyama H, Ishizaki Y, et al. Retinal Detachment-Induced Muller Glial Cell Swelling Activates TRPV4 Ion Channels and Triggers Photoreceptor Death at Body Temperature. *J Neurosci* (2018) 38(41):8745–58. doi: 10.1523/JNEUROSCI.0897-18.2018
47. Boudaka A, Saito CT, Tominaga M. Deletion of TRPV4 Enhances *In Vitro* Wound Healing of Murine Esophageal Keratinocytes. *Sci Rep* (2020) 10(1):11349. doi: 10.1038/s41598-020-68269-8
48. Mihara H, Suzuki N, Boudaka AA, Muhammad JS, Tominaga M, Tabuchi Y, et al. Transient Receptor Potential Vanilloid 4-Dependent Calcium Influx and ATP Release in Mouse and Rat Gastric Epithelia. *World J Gastroenterol* (2016) 22(24):5512–9. doi: 10.3748/wjg.v22.i24.5512
49. Sun L, Yao K, Zhang H, Chen W. Activation of the ATP-P2X Pathway by TRPV4 in Acute Ocular Hypertension. *Int J Ophthalmol* (2020) 13(11):1697–704. doi: 10.18240/ijo.2020.11.03
50. Jay SM, Skokos E, Laiwalla F, Krady MM, Kyriakides TR. Foreign Body Giant Cell Formation is Preceded by Lamellipodia Formation and can be Attenuated by Inhibition of Rac1 Activation. *Am J Pathol* (2007) 171(2):632–40. doi: 10.2353/ajpath.2007.061213
51. Ou-Yang Q, Li B, Xu M, Liang H. TRPV4 Promotes the Migration and Invasion of Glioma Cells *via* AKT/Rac1 Signaling. *Biochem Biophys Res Commun* (2018) 503(2):876–81. doi: 10.1016/j.bbrc.2018.06.090
52. Arya RK, Goswami R, Rahaman SO. Mechanotransduction *via* a TRPV4-Rac1 Signaling Axis Plays a Role in Multinucleated Giant Cell Formation. *J Biol Chem* (2021) 296:100129. doi: 10.1074/jbc.RA120.014597
53. White JP, Cibelli M, Urban L, Nilius B, McGeown JG, Nagy I. TRPV4: Molecular Conductor of a Diverse Orchestra. *Physiol Rev* (2016) 96(3):911–73. doi: 10.1152/physrev.00016.2015
54. Soya M, Sato M, Sobhan U, Tsumura M, Ichinohe T, Tazaki M, et al. Plasma Membrane Stretch Activates Transient Receptor Potential Vanilloid and Ankyrin Channels in Merkel Cells From Hamster Buccal Mucosa. *Cell Calcium* (2014) 55(4):208–18. doi: 10.1016/j.ceca.2014.02.015
55. Vriens J, Watanabe H, Janssens A, Droogmans G, Voets T, Nilius B. Cell Swelling, Heat, and Chemical Agonists Use Distinct Pathways for the Activation of the Cation Channel TRPV4. *Proc Natl Acad Sci USA* (2004) 101(1):396–401. doi: 10.1073/pnas.0303329101
56. Poole DP, Amadesi S, Veldhuis NA, Abogadie FC, Lieu T, Darby W, et al. Protease-Activated Receptor 2 (PAR2) Protein and Transient Receptor Potential Vanilloid 4 (TRPV4) Protein Coupling is Required for Sustained Inflammatory Signaling. *J Biol Chem* (2013) 288(8):5790–802. doi: 10.1074/jbc.M112.438184
57. Kechagia JZ, Ivaska J, Roca-Cusachs P. Integrins as Biomechanical Sensors of the Microenvironment. *Nat Rev Mol Cell Biol* (2019) 20(8):457–73. doi: 10.1038/s41580-019-0134-2
58. Matthews BD, Thodeti CK, Tytell JD, Mammoto A, Overby DR, Ingber DE. Ultra-Rapid Activation of TRPV4 Ion Channels by Mechanical Forces Applied to Cell Surface Beta1 Integrins. *Integr Biol (Camb)* (2010) 2(9):435–42. doi: 10.1039/c0ib00034e
59. Potla R, Hirano-Kobayashi M, Wu H, Chen H, Mammoto A, Matthews BD, et al. Molecular Mapping of Transmembrane Mechanotransduction Through the Beta1 Integrin-CD98hc-TRPV4 Axis. *J Cell Sci* (2020) 133(20). doi: 10.1242/jcs.248823
60. Swain SM, Liddle RA. Piezo1 Acts Upstream of TRPV4 to Induce Pathological Changes in Endothelial Cells Due to Shear Stress. *J Biol Chem* (2021) 296:100171. doi: 10.1074/jbc.RA120.015059

61. Swain SM, Romac JM, Shahid RA, Pandol SJ, Liedtke W, Vigna SR, et al. TRPV4 Channel Opening Mediates Pressure-Induced Pancreatitis Initiated by Piezo1 Activation. *J Clin Invest* (2020) 130(5):2527–41. doi: 10.1172/JCI134111
62. Li M, Fang XZ, Zheng YF, Xie YB, Ma XD, Liu XT, et al. Transient Receptor Potential Vanilloid 4 is a Critical Mediator in LPS Mediated Inflammation by Mediating Calcineurin/NFATc3 Signaling. *Biochem Biophys Res Commun* (2019) 513(4):1005–12. doi: 10.1016/j.bbrc.2019.04.020
63. Rayees S, Joshi JC, Tauseef M, Anwar M, Baweja S, Rochford I, et al. PAR2-Mediated cAMP Generation Suppresses TRPV4-Dependent Ca(2+) Signaling in Alveolar Macrophages to Resolve TLR4-Induced Inflammation. *Cell Rep* (2019) 27(3):793–805.e4. doi: 10.1016/j.celrep.2019.03.053
64. Fernandez-Fernandez JM, Nobles M, Currid A, Vazquez E, Valverde MA. Maxi K+ Channel Mediates Regulatory Volume Decrease Response in a Human Bronchial Epithelial Cell Line. *Am J Physiol Cell Physiol* (2002) 283 (6):C1705–14. doi: 10.1152/ajpcell.00245.2002
65. Jia Y, Wang X, Varty L, Rizzo CA, Yang R, Correll CC, et al. Functional TRPV4 Channels are Expressed in Human Airway Smooth Muscle Cells. *Am J Physiol Lung Cell Mol Physiol* (2004) 287(2):L272–8. doi: 10.1152/ajplung.00393.2003
66. Wissenbach U, Bodding M, Freichel M, Flockerzi V. Trp12, a Novel Trp Related Protein From Kidney. *FEBS Lett* (2000) 485(2-3):127–34. doi: 10.1016/S0014-5793(00)02212-2
67. Delany NS, Hurle M, Facer P, Alnadaf T, Plumpton C, Kinghorn I, et al. Identification and Characterization of a Novel Human Vanilloid Receptor-Like Protein, VRL-2. *Physiol Genomics* (2001) 4(3):165–74. doi: 10.1152/physiolgenomics.2001.4.3.165
68. Birder L, Kullmann FA, Lee H, Barrick S, de Groat W, Kanai A, et al. Activation of Urothelial Transient Receptor Potential Vanilloid 4 by 4alpha-Phorbol 12,13-Didecanoate Contributes to Altered Bladder Reflexes in the Rat. *J Pharmacol Exp Ther* (2007) 323(1):227–35. doi: 10.1124/jpet.107.125435
69. Gevaert T, Vriens J, Segal A, Everaerts W, Roskams T, Talavera K, et al. Deletion of the Transient Receptor Potential Cation Channel TRPV4 Impairs Murine Bladder Voiding. *J Clin Invest* (2007) 117(11):3453–62. doi: 10.1172/JCI31766
70. Shen J, Harada N, Kubo N, Liu B, Mizuno A, Suzuki M, et al. Functional Expression of Transient Receptor Potential Vanilloid 4 in the Mouse Cochlea. *Neuroreport* (2006) 17(2):135–9. doi: 10.1097/01.wnr.0000199459.16789.75
71. Groot-Kormelink PJ, Fawcett L, Wright PD, Gosling M, Kent TC. Quantitative GPCR and Ion Channel Transcriptomics in Primary Alveolar Macrophages and Macrophage Surrogates. *BMC Immunol* (2012) 13:57. doi: 10.1186/1471-2172-13-57
72. Rajasekhar P, Poole DP, Veldhuis NA. Role of Nonneuronal TRPV4 Signaling in Inflammatory Processes. *Adv Pharmacol* (2017) 79:117–39. doi: 10.1016/bs.apha.2017.03.002
73. Filosa JA, Yao X, Rath G. TRPV4 and the Regulation of Vascular Tone. *J Cardiovasc Pharmacol* (2013) 61(2):113–9. doi: 10.1097/FJC.0b013e318279ba42
74. Toft-Bertelsen TL, Krizaj D, MacAulay N. When Size Matters: Transient Receptor Potential Vanilloid 4 Channel as a Volume-Sensor Rather Than an Osmo-Sensor. *J Physiol* (2017) 595(11):3287–302. doi: 10.1113/JP274135
75. Watanabe H, Davis JB, Smart D, Jerman JC, Smith GD, Hayes P, et al. Activation of TRPV4 Channels (hVRL-2/Mtrp12) by Phorbol Derivatives. *J Biol Chem* (2002) 277(16):13569–77. doi: 10.1074/jbc.M200062200
76. Hartmannsgruber V, Heyken WT, Kacik M, Kaistha A, Grgic I, Harteneck C, et al. Arterial Response to Shear Stress Critically Depends on Endothelial TRPV4 Expression. *PloS One* (2007) 2(9):e827. doi: 10.1371/journal.pone.0000827
77. Nilius B, Voets T. The Puzzle of TRPV4 Channelopathies. *EMBO Rep* (2013) 14(2):152–63. doi: 10.1038/embor.2012.219
78. Rahaman SO, Grove LM, Paruchuri S, Southern BD, Abraham S, Niese KA, et al. TRPV4 Mediates Myofibroblast Differentiation and Pulmonary Fibrosis in Mice. *J Clin Invest* (2014) 124(12):5225–38. doi: 10.1172/JCI75331
79. Lawhorn BG, Brnardic EJ, Behm DJ. TRPV4 Antagonists: A Patent Review (2015-2020). *Expert Opin Ther Pat* (2021) 31:773–84. doi: 10.1080/13543776.2021.1903432
80. Atobe M. Activation of Transient Receptor Potential Vanilloid (TRPV) 4 as a Therapeutic Strategy in Osteoarthritis. *Curr Top Med Chem* (2019) 19 (24):2254–67. doi: 10.2174/1568026619666191010162850
81. Atobe M, Nagami T, Muramatsu S, Ohno T, Kitagawa M, Suzuki H, et al. Discovery of Novel Transient Receptor Potential Vanilloid 4 (TRPV4) Agonists as Regulators of Chondrogenic Differentiation: Identification of Quinazolin-4(3 H)-Ones and in Vivo Studies on a Surgically Induced Rat Model of Osteoarthritis. *J Med Chem* (2019) 62(3):1468–83. doi: 10.1021/acs.jmedchem.8b01615
82. Xu S, Liu B, Yin M, Koroleva M, Mastrangelo M, Ture S, et al. A Novel TRPV4-Specific Agonist Inhibits Monocyte Adhesion and Atherosclerosis. *Oncotarget* (2016) 7(25):37622–35. doi: 10.18632/oncotarget.9376
83. Thoppil RJ, Adapala RK, Cappelli HC, Kondeti V, Dudley AC, Gary Meszaros J, et al. TRPV4 Channel Activation Selectively Inhibits Tumor Endothelial Cell Proliferation. *Sci Rep* (2015) 5:14257. doi: 10.1038/srep14257
84. Adapala RK, Thoppil RJ, Ghosh K, Cappelli HC, Dudley AC, Paruchuri S, et al. Activation of Mechanosensitive Ion Channel TRPV4 Normalizes Tumor Vasculature and Improves Cancer Therapy. *Oncogene* (2016) 35 (3):314–22. doi: 10.1038/onc.2015.83
85. Peters AA, Jamaludin SYN, Yapa K, Chalmers S, Wiegmans AP, Lim HF, et al. Oncosis and Apoptosis Induction by Activation of an Overexpressed Ion Channel in Breast Cancer Cells. *Oncogene* (2017) 36(46):6490–500. doi: 10.1038/onc.2017.234
86. Kuebler WM, Jordt SE, Liedtke WB. Urgent Reconsideration of Lung Edema as a Preventable Outcome in COVID-19: Inhibition of TRPV4 Represents a Promising and Feasible Approach. *Am J Physiol Lung Cell Mol Physiol* (2020) 318(6):L1239–43. doi: 10.1152/ajplung.00161.2020
87. Goyal N, Skrdla P, Schroyer R, Kumar S, Fernando D, Oughton A, et al. Clinical Pharmacokinetics, Safety, and Tolerability of a Novel, First-In-Class TRPV4 Ion Channel Inhibitor, GSK2798745, in Healthy and Heart Failure Subjects. *Am J Cardiovasc Drugs* (2019) 19(3):335–42. doi: 10.1007/s40256-018-00320-6
88. Stewart GM, Johnson BD, Sprecher DL, Reddy YNV, Obokata M, Goldsmith S, et al. Targeting Pulmonary Capillary Permeability to Reduce Lung Congestion in Heart Failure: A Randomized, Controlled Pilot Trial. *Eur J Heart Fail* (2020) 22(9):1641–5. doi: 10.1002/ejhf.1809
89. McNulty AL, Leddy HA, Liedtke W, Guilak F. TRPV4 as a Therapeutic Target for Joint Diseases. *Naunyn Schmiedebergs Arch Pharmacol* (2015) 388 (4):437–50. doi: 10.1007/s00210-014-1078-x
90. Palsson-McDermott EM, O'Neill LAJ. Targeting Immunometabolism as an Anti-Inflammatory Strategy. *Cell Res* (2020) 30(4):300–14. doi: 10.1038/s41422-020-0291-z
91. Spiller KL, Koh TJ. Macrophage-Based Therapeutic Strategies in Regenerative Medicine. *Adv Drug Deliv Rev* (2017) 122:74–83. doi: 10.1016/j.addr.2017.05.010
92. O'Neill LA, Pearce EJ. Immunometabolism Governs Dendritic Cell and Macrophage Function. *J Exp Med* (2016) 213(1):15–23. doi: 10.1084/jem.20151570
93. Viola A, Munari F, Sanchez-Rodriguez R, Scolaro T, Castegna A. The Metabolic Signature of Macrophage Responses. *Front Immunol* (2019) 10:1462. doi: 10.3389/fimmu.2019.01462
94. Lee WH, Choong LY, Jin TH, Mon NN, Chong S, Liew CS, et al. TRPV4 Plays a Role in Breast Cancer Cell Migration *via* Ca(2+)-Dependent Activation of AKT and Downregulation of E-Cadherin Cell Cortex Protein. *Oncogenesis* (2017) 6(5):e338. doi: 10.1038/oncsis.2017.39
95. Ballotta V, Driessen-Mol A, Bouten CV, Baaijens FP. Strain-Dependent Modulation of Macrophage Polarization Within Scaffolds. *Biomaterials* (2014) 35(18):4919–28. doi: 10.1016/j.biomaterials.2014.03.002
96. Wehner S, Buchholz BM, Schuchtrup S, Rocke A, Schaefer N, Lysson M, et al. Mechanical Strain and TLR4 Synergistically Induce Cell-Specific Inflammatory Gene Expression in Intestinal Smooth Muscle Cells and Peritoneal Macrophages. *Am J Physiol Gastrointest Liver Physiol* (2010) 299(5):G1187–97. doi: 10.1152/ajpgi.00452.2009

97. Previtera ML, Sengupta A. Substrate Stiffness Regulates Proinflammatory Mediator Production Through TLR4 Activity in Macrophages. *PloS One* (2015) 10(12):e0145813. doi: 10.1371/journal.pone.0145813
98. Chen M, Zhang Y, Zhou P, Liu X, Zhao H, Zhou X, et al. Substrate Stiffness Modulates Bone Marrow-Derived Macrophage Polarization Through NF-kappaB Signaling Pathway. *Bioact Mater* (2020) 5(4):880–90. doi: 10.1016/j.bioactmat.2020.05.004
99. Pietrogrande G, Mabotuwana N, Zhao Z, Abdolhoseini M, Johnson SJ, Nilsson M, et al. Chronic Stress Induced Disturbances in Laminin: A Significant Contributor to Modulating Microglial Pro-Inflammatory Tone? *Brain Behav Immun* (2018) 68:23–33. doi: 10.1016/j.bbi.2017.09.012
100. Sridharan R, Cavanagh B, Cameron AR, Kelly DJ, O'Brien FJ. Material Stiffness Influences the Polarization State, Function and Migration Mode of Macrophages. *Acta Biomater* (2019) 89:47–59. doi: 10.1016/j.actbio.2019.02.048
101. Blakney AK, Swartzlander MD, Bryant SJ. The Effects of Substrate Stiffness on the *In Vitro* Activation of Macrophages and *In Vivo* Host Response to Poly(Ethylene Glycol)-Based Hydrogels. *J BioMed Mater Res A* (2012) 100 (6):1375–86. doi: 10.1002/jbm.a.34104
102. Alpizar YA, Boonen B, Sanchez A, Jung C, Lopez-Requena A, Naert R, et al. TRPV4 Activation Triggers Protective Responses to Bacterial Lipopolysaccharides in Airway Epithelial Cells. *Nat Commun* (2017) 8 (1):1059. doi: 10.1038/s41467-017-01201-3
103. Ye L, Kleiner S, Wu J, Sah R, Gupta RK, Banks AS, et al. TRPV4 is a Regulator of Adipose Oxidative Metabolism, Inflammation, and Energy Homeostasis. *Cell* (2012) 151(1):96–110. doi: 10.1016/j.cell.2012.08.034
104. Lee WC, Reuben A, Hu X, McGranahan N, Chen R, Jalali A, et al. Multiomics Profiling of Primary Lung Cancers and Distant Metastases Reveals Immunosuppression as a Common Characteristic of Tumor Cells With Metastatic Plasticity. *Genome Biol* (2020) 21(1):271. doi: 10.1186/s13059-020-02175-0
105. Wilson JL, Nagele T, Linke M, Demel F, Fritsch SD, Mayr HK, et al. Inverse Data-Driven Modeling and Multiomics Analysis Reveals Phgdh as a Metabolic Checkpoint of Macrophage Polarization and Proliferation. *Cell Rep* (2020) 30(5):1542–52.e7. doi: 10.1016/j.celrep.2020.01.011
106. Yang X. Multitissue Multiomics Systems Biology to Dissect Complex Diseases. *Trends Mol Med* (2020) 26(8):718–28. doi: 10.1016/j.molmed.2020.04.006
107. Hsieh WY, Zhou QD, York AG, Williams KJ, Scumpia PO, Kronenberger EB, et al. Toll-Like Receptors Induce Signal-Specific Reprogramming of the Macrophage Lipidome. *Cell Metab* (2020) 32(1):128–43.e5. doi: 10.1016/j.cmet.2020.05.003
108. Lagerborg KA, Watrous JD, Cheng S, Jain M. High-Throughput Measure of Bioactive Lipids Using Non-Targeted Mass Spectrometry. *Methods Mol Biol* (2019) 1862:17–35. doi: 10.1007/978-1-4939-8769-6_2
109. Masoodi M, Eiden M, Koulman A, Spaner D, Volmer DA. Comprehensive Lipidomics Analysis of Bioactive Lipids in Complex Regulatory Networks. *Anal Chem* (2010) 82(19):8176–85. doi: 10.1021/ac1015563
110. Tannahill GM, Curtis AM, Adamik J, Palsson-McDermott EM, McGettrick AF, Goel G, et al. Succinate is an Inflammatory Signal That Induces IL-1beta Through HIF-1alpha. *Nature* (2013) 496(7444):238–42. doi: 10.1038/nature11986
111. O'Neill LAJ, Artyomov MN. Itaconate: The Poster Child of Metabolic Reprogramming in Macrophage Function. *Nat Rev Immunol* (2019) 19 (5):273–81. doi: 10.1038/s41577-019-0128-5
112. De Souza DP, Achuthan A, Lee MK, Binger KJ, Lee MC, Davidson S, et al. Autocrine IFN-I Inhibits Isocitrate Dehydrogenase in the TCA Cycle of LPS-Stimulated Macrophages. *J Clin Invest* (2019) 129(10):4239–44. doi: 10.1172/JCI127597
113. Pacher P, Beckman JS, Liaudet L. Nitric Oxide and Peroxynitrite in Health and Disease. *Physiol Rev* (2007) 87(1):315–424. doi: 10.1152/physrev.00029.2006
114. Salvemini D, Doyle TM, Cuzzocrea S. Superoxide, Peroxynitrite and Oxidative/Nitrative Stress in Inflammation. *Biochem Soc Trans* (2006) 34 (Pt 5):965–70. doi: 10.1042/BST0340965
115. Buckley CD, Gilroy DW, Serhan CN. Proresolving Lipid Mediators and Mechanisms in the Resolution of Acute Inflammation. *Immunity* (2014) 40 (3):315–27. doi: 10.1016/j.immuni.2014.02.009
116. Serhan CN, Chiang N, Dalli J, Levy BD. Lipid Mediators in the Resolution of Inflammation. *Cold Spring Harb Perspect Biol* (2014) 7(2):a016311. doi: 10.1101/cshperspect.a016311
117. Serhan CN. Pro-Resolving Lipid Mediators are Leads for Resolution Physiology. *Nature* (2014) 510(7503):92–101. doi: 10.1038/nature13479
118. Flower RJ. Prostaglandins, Bioassay and Inflammation. *Br J Pharmacol* (2006) 147 Suppl 1:S182–92. doi: 10.1038/sj.bjp.0706506
119. Peng S, Grace MS, Gondin AB, Retamal JS, Dill L, Darby W, et al. The Transient Receptor Potential Vanilloid 4 (TRPV4) Ion Channel Mediates Protease Activated Receptor 1 (PAR1)-Induced Vascular Hyperpermeability. *Lab Invest* (2020) 100(8):1057–67. doi: 10.1038/s41374-020-0430-7
120. Smits AH, Vermeulen M. Characterizing Protein-Protein Interactions Using Mass Spectrometry: Challenges and Opportunities. *Trends Biotechnol* (2016) 34(10):825–34. doi: 10.1016/j.tibtech.2016.02.014
121. Morris JH, Knudsen GM, Verschueren E, Johnson JR, Cimermancic P, Greninger AL, et al. Affinity Purification-Mass Spectrometry and Network Analysis to Understand Protein-Protein Interactions. *Nat Protoc* (2014) 9 (11):2539–54. doi: 10.1038/nprot.2014.164
122. Ge F, Li WL, Bi LJ, Tao SC, Zhang ZP, Zhang XE. Identification of Novel 14-3-3zeta Interacting Proteins by Quantitative Immunoprecipitation Combined With Knockdown (QUICK). *J Proteome Res* (2010) 9(11):5848–58. doi: 10.1021/pr100616g
123. Ummethum H, Hamperl S. Proximity Labeling Techniques to Study Chromatin. *Front Genet* (2020) 11:450. doi: 10.3389/fgene.2020.00450
124. Yang W, Zhao X, Tao Y, Wu Y, He F, Tang L. Proteomic Analysis Reveals a Protective Role of Specific Macrophage Subsets in Liver Repair. *Sci Rep* (2019) 9(1):2953. doi: 10.1038/s41598-019-39007-6
125. Court M, Petre G, Atifi ME, Millet A. Proteomic Signature Reveals Modulation of Human Macrophage Polarization and Functions Under Differing Environmental Oxygen Conditions. *Mol Cell Proteomics* (2017) 16(12):2153–68. doi: 10.1074/mcp.RA117.000082

Conflict of Interest: The authors declare that the research was conducted in the absence of any commercial or financial relationships that could be construed as a potential conflict of interest.

frontiers in Immunology

ORIGINAL RESEARCH
published: 16 March 2022
doi: 10.3389/fimmu.2022.779888

Cytotoxic T Lymphocyte Activation Signals Modulate Cytoskeletal Dynamics and Mechanical Force Generation

Aashli Pathni[1†], Altuğ Özçelikkale[2,3†], Ivan Rey-Suarez[2], Lei Li[4], Scott Davis[5], Nate Rogers[5], Zhengguo Xiao[1,4] and Arpita Upadhyaya[1,2,5]*

[1] Biological Sciences Graduate Program, University of Maryland, College Park, MD, United States, [2] Institute for Physical Science and Technology, University of Maryland, College Park, MD, United States, [3] Department of Mechanical Engineering, Middle East Technical University, Ankara, Turkey, [4] Department of Animal and Avian Sciences, University of Maryland, College Park, MD, United States, [5] Department of Physics, University of Maryland, College Park, MD, United States

OPEN ACCESS

Edited by:
Shizuya Saika,
Wakayama Medical University Hospital, Japan

Reviewed by:
Nadine Varin-Blank,
Institut National de la Santé et de la Recherche Médicale (INSERM), France
Yuri Sykulev,
Thomas Jefferson University, United States

***Correspondence:**
Arpita Upadhyaya
arpitau@umd.edu

[†]These authors have contributed equally to this work and share first authorship

Specialty section:
This article was submitted to Molecular Innate Immunity, a section of the journal Frontiers in Immunology

Received: 20 September 2021
Accepted: 23 February 2022
Published: 16 March 2022

Citation:
Pathni A, Özçelikkale A, Rey-Suarez I, Li L, Davis S, Rogers N, Xiao Z and Upadhyaya A (2022) Cytotoxic T Lymphocyte Activation Signals Modulate Cytoskeletal Dynamics and Mechanical Force Generation. Front. Immunol. 13:779888. doi: 10.3389/fimmu.2022.779888

Cytotoxic T lymphocytes (CTLs) play an integral role in the adaptive immune response by killing infected cells. Antigen presenting cells (APCs), such as dendritic cells, present pathogenic peptides to the T cell receptor on the CTL surface and co-stimulatory signals required for complete activation. Activated CTLs secrete lytic granules containing enzymes that trigger target cell death at the CTL-target contact, also known as the immune synapse (IS). The actin and microtubule cytoskeletons are instrumental in the killing of CTL targets. Lytic granules are transported along microtubules to the IS, where granule secretion is facilitated by actin depletion and recovery. Furthermore, actomyosin contractility promotes target cell death by mediating mechanical force exertion at the IS. Recent studies have shown that inflammatory cytokines produced by APCs, such as interleukin-12 (IL-12), act as a third signal for CTL activation and enhance CTL proliferation and effector function. However, the biophysical mechanisms mediating such enhanced effector function remain unclear. We hypothesized that the third signal for CTL activation, IL-12, modulates cytoskeletal dynamics and force exertion at the IS, thus potentiating CTL effector function. Here, we used live cell total internal reflection fluorescence (TIRF) microscopy to study actomyosin and microtubule dynamics at the IS of murine primary CTLs activated in the presence of peptide-MHC and co-stimulation alone (two signals), or additionally with IL-12 (three signals). We found that three signal-activated CTLs have altered actin flows, myosin dynamics and microtubule growth rates as compared to two signal-activated CTLs. We further showed that lytic granules in three-signal activated CTLs are less clustered and have lower velocities than in two-signal activated CTLs. Finally, we used traction force microscopy to show that three signal-activated CTLs exert greater traction forces than two signal-activated CTLs. Our results demonstrate that activation of CTLs in the presence of IL-12 leads to differential modulation of the cytoskeleton, thereby augmenting the mechanical response of CTLs to their targets.

This indicates a potential physical mechanism *via* which the third signal can enhance the CTL response.

Keywords: CD8+ cytotoxic T lymphocyte, cytoskeleton, traction force, IL-12 cytokine, actin, microtubule, lytic granule, myosin

INTRODUCTION

CD8+ T cells or cytotoxic T lymphocytes (CTLs) play an integral role in the adaptive immune response triggered by pathogens and in tumor surveillance. Antigen presenting cells (APCs) process and present pathogenic peptides bound to class I major histocompatibility complex (MHC) molecules on their cell membranes. The T cell receptor (TCR) on naïve CD8+ T cells is stimulated after recognition of a cognate peptide-MHC complex on the APC membrane. A second co-stimulatory signal is required for complete CTL activation and is provided by binding of B7-1/2 proteins expressed on the APC surface to the CD28 receptor on the naïve T cell membrane (1). Once activated, CTLs recognize and kill infected or damaged host cells by secreting lytic granules containing perforins and granzymes, which collectively act to promote target cell apoptosis.

Inflammatory cytokines, such as interleukin-12 (IL-12) and interferons α and β (IFN-α/β), have been recently characterized as a third signal for T cell activation. *In vitro* studies have shown that IL-12 is able to drive naïve CD8+ T cells to differentiate into potent effector CTLs (1). CD8+ T cells activated with peptide-MHC and co-stimulatory proteins in the presence of IL-12 (**three signal**, or **3SI**) exhibit increased IL-2 signaling and enhanced proliferation as compared to CD8+ T cells activated in the presence of peptide-MHC and co-stimulation alone (**two signal**, or **2SI**) (1–4). While both 2SI and 3SI CTLs produce effector proteins and are able to lyse target cells, 3SI CTLs have increased expression of granzymes and perforin, contributing to increased cytolytic efficiency both *in vitro* and *in vivo* (2–8). Target cell killing by 3SI CTLs is also potentially augmented by increased efficiency of synapse formation as compared to 2SI CTLs (9). While the above studies have used population-scale experiments such as flow cytometry and microarray analysis to study the enhancement of effector function in 3SI CTLs, the mechanisms by which the third signal may modulate cytotoxic efficiency have not been explored at the cellular scale.

At the single-cell level, the T cell cytoskeleton is intricately involved during activation and cytolytic function at the CTL-target synapse, also known as the immunological synapse (IS) (10). Following initial contact of a CTL with a target cell, TCR engagement triggers a downstream signaling cascade which results in dramatic cytoskeletal rearrangements beginning with initial actin polymerization at the contact site (11–14). The cytoskeletal motor proteins dynein and myosin II act in tandem to promote translocation of the centrosome towards the IS (15–18). Centrosome translocation is followed by docking at the synapse, which is required for the transport of lytic granules along microtubules towards the target cell (19, 20). The microtubule motors dynein and kinesin facilitate granule transport towards the minus or plus end of microtubules respectively, aiding in the approach of lytic granules towards the contact site (19, 21, 22). An increase in intracellular calcium flux following TCR activation is also required for granule transport and release (23–25).

Actin dynamics regulate secretion of lytic granules at the IS: within the first minute of contact with the target cell, actin rapidly depletes across the center of the IS, allowing lytic granules to dock and fuse with the CTL plasma membrane. Granule secretion is halted within a few minutes by the recovery of cortical actin, which acts as a physical barrier to granule release (14, 26, 27). Additionally, T cells exert mechanical forces during activation and IS formation (28–34). These forces are known to be actomyosin and microtubule-dependent (30, 32–34). Force exertion by CTLs is spatiotemporally correlated with lytic granule secretion at the IS and potentiates the efficacy of target cell killing by creating local hotspots of increased membrane tension, which promotes pore formation by the effector protein perforin (31).

The current paradigm for the role of the cytoskeleton in CTL function has been informed by studies performed in CTLs activated in the absence of the third signal. Recent work has shown that IL-12 treatment modulates the expression of cytoskeletal regulators such as Rho GTPases and Rho-GTPase-activating proteins (Rho-GAPs) in CD4+ and CD8+ T cells (4, 35–37). Furthermore, IL-12 treatment activates central signaling pathways that regulate actin depletion and recovery at the IS (4, 8, 26, 27, 38) and are required for cytoskeletal force generation in CTLs (29, 31). Together, these studies suggest that activation of CD8+ T cells in the presence of IL-12 may enhance CTL function by modulating cytoskeletal dynamics and forces, suggesting a mechanochemical pathway that links cytokine stimulation to CTL effector function.

Here, we examine the role for the third signal for CTL activation, IL-12, in modulating cytoskeletal dynamics and mechanical force generation at the IS. We use high resolution microscopy to study cytoskeletal dynamics and force generation in murine CTLs activated in the presence and absence of IL-12. Our data show that CTL activation in the presence of the third signal results in altered cytoskeletal repatterning at the CTL-target interface, leading to a larger actin depletion zone, slower actin speeds and faster microtubule growth rates. We also find differences in lytic granule dynamics with three-signal activated CTLs exhibiting a higher number of lytic granules and slower granule speeds. Finally, using traction force microscopy (TFM), we show that three-signal activated CTLs generate higher traction forces at the IS. Thus, by regulating the cytoskeleton, cytokine stimulation of CTLs may provide a potential mechanism for augmenting their killing response during the immune response.

MATERIALS AND METHODS

Plasmids

pEGFP-C1 F-tractin-EGFP was a gift from Dyche Mullins (Addgene plasmid #58473). Lamp1-RFP was a gift from Walther Mothes (Addgene plasmid #1817). The EGFP-EB3 and MLC-EGFP plasmids were gifts from Dr. Robert Fischer, National Heart, Lung, and Blood Institute.

Purification of Naïve OT-I CD8+ T Cells

Isolation of naïve OT-I CD8+ T cells was performed as described before (39). Briefly, peripheral lymph nodes were collected from euthanized OT-I mice and homogenized in 15 mL glass grinders (DWK Life Sciences, Millville, NJ), to become single cell suspension. The cells were washed with complete Allos medium, followed by filtering through a 70 μm filter (VWR, Radnor, PA). Cells were incubated with FITC-labeled antibodies specific to B220, CD4, CD44, CD11c, and I-Ab (BioLegend, San Diego, CA) for 25 minutes at 4°C. After washing with Allos, the resuspended cells were incubated for 20 minutes at 4°C with anti-FITC conjugated magnetic MicroBeads (Miltenyi Biotech, Auburn CA). The cells were washed and passed through separation columns inserted in a MACS magnet. Cells that flowed through the columns were collected, which were > 94% CD8+ and <0.5% CD25. Allos medium is RPMI-1640 supplemented with fetal calf serum (10%), HEPES (10 mM), MEM non-essential amino acid (1×), sodium pyruvate (1 mM), penicillin and streptomycin (100 U/mL), and 2-mercaptoethanol (50 μM) (Mediatech, Manassas, VA).

Activation of Naïve OT-I CD8+ T Cells by 2SI and 3SI

Flat-bottom microtiter wells in 24-well plates were coated with Dimer X-2Kb:Ig fusion protein loaded with OVA257–264 peptide (BD Pharmingen, San Jose, CA) and recombinant B7-1/Fc chimeric protein (R&D Systems, Minneapolis, MN) as previously described (42). For two signal (2SI) stimulation, purified naive OT-I CD8+ T cells were plated at a density of 3×10^5 cells in 1.5 mL Allos medium in each well of a coated plate with 2.5 U/mL recombinant human IL-2 (R&D Systems, Minneapolis, MN). For three signal (3SI) stimulation, naive OT-I CD8 T cells were plated under 2SI conditions as described above and additionally supplemented with 2 U/mL of murine rIL-12 (R&D Systems, Minneapolis, MN). The cells were incubated for three days before further analysis.

Killing Assay

The CellTiter-Glo® (CTG) killing assay is based on the number of viable cells left in the culture after cytotoxic T lymphocyte killing of the target cells (39, 40). B16.OVA melanoma cells adhere to plastic surfaces and can efficiently present $OVA_{257-264}$ peptide; activated OT-I T cells recognize H-$2K^b$/$OVA_{257-264}$ and initiate specific killing of these B16.OVA cells (41, 42). B16.OVA cells were seeded onto 96-well white plates at 30,000 cells/well in 100 μL Allos medium, and activated OT-I cells were added to each well as effectors to target cells (B16.OVA cells) at a ratio of 1:1, 5:1, and 20:1. After overnight incubation, T cell suspensions (both OT-I cells and B16.OVA) were removed by washing three times with Allos medium. Luminescent signals (relative luminescent unit, RLU) from a 96-well plate were measured by the addition of 200 μL of 50% Cell Titer Glo (Promega, Madison, WI) followed by measurement of luminesce using a plate reader (Bio-Rad). The kill percentage of the B16.OVA cells by effector OT-I cells was calculated according to the following equation: Killed % = 100% x (RLU of untreated B16.OVA cells – RLU of B16.OVA cells cultured with OT-I cells)/RLU of untreated B16.OVA.

Cell Culture and Transient Transfections

The Neon electroporation system (Invitrogen, Waltham, MA) was used for transient transfection of activated CTLs. Transfections were performed two days prior to the experiment according to the following protocol: $1.5\text{-}2 \times 10^5$ cells were resuspended in 10 μL of R buffer with 0.5-2 μg of plasmid. The cells were electroporated under the following conditions: 1325V/10ms/3 pulses. Transfected cells were transferred to fresh pre-warmed Allos medium and incubated at 37°C with 5% CO_2 for 36-48 hours prior to imaging.

Substrate Preparation

8-well chambers (Cellvis, Mountain View, CA) were incubated with 0.01% poly-L-lysine (PLL) diluted in distilled water for 10 mins at room temperature. PLL was aspirated from each well and the chambers were allowed to dry for 1 hour at 37°C. PLL-coated dishes were subsequently incubated with a 10 μg/mL solution of purified anti-mouse CD3 antibody (Clone 17A2, BioLegend, San Diego, CA) in 1x Dulbecco's phosphate-buffered saline (DPBS) for 2 hours at 37°C or overnight at 4°C. The coated wells were washed with Leibovitz's L-15 (L-15) imaging medium prior to the experiment.

Immunofluorescence

Activated CTLs were stimulated on anti-CD3 coated coverslips and fixed at 3 and 6 minutes after stimulation using 3.5% paraformaldehyde for 10 minutes. Fixed cells were washed thoroughly with 1X DPBS. Cells were permeabilized for 8 minutes with a 0.15% Triton-X solution. Blocking was performed using 0.02g/mL bovine serum albumin (BSA) and 0.3M Glycine in 1X DPBS solution for 1 hour at room temperature. Acti-stain 488 phalloidin (Cytoskeleton, Inc., Denver, CO) was used to label F-actin according to the manufacturer's instructions.

Total Internal Reflection Fluorescence (TIRF) Microscopy

Imaging was performed on an inverted microscope (Nikon Ti-E PFS, Melville NY) equipped with a 60x objective for IRM and TFM, and a 100× objective lens TIRF imaging respectively using a Prime BSI camera (Photometrics, Tucson AZ). Imaging protocols were implemented using Nikon Elements and images were cropped in Fiji before further analysis using MATLAB scripts. For live cell imaging, activated CTLs in L-15 medium were seeded on anti-CD3 coated surfaces equilibrated to 37°C in

a stage-top Okolab Incubator (Okolab S. R. L., Pozzuoli, NA, Italy). IRM time-lapse images were acquired every 5 s. TIRF images were acquired every 0.5-1 s for imaging of F-Tractin-EGFP transfected cells and every 1 s for imaging of EGFP-EB3 transfected cells.

Fast imaging of lytic granules: Rapid TIRF imaging of lytic granules was performed using a 100x objective and an electron multiplying charge coupled device (emCCD) camera (Andor iXon 897). Activated CTLs expressing Lamp1-RFP were imaged between 1 to 15 minutes after being added to an anti-CD3-coated coverslip. For each cell, timelapse images were acquired every 100 ms for 100 s (1000 frames).

Traction Force Microscopy

Coverslip activation, polyacrylamide gel fabrication and gel surface functionalization were performed as described previously (43). Briefly, 35 mm glass bottom dishes with No. 1.5 coverslips (Cellvis, Mountain View, CA) were activated by incubating with 2% 3-aminopropyltrimethoxysilane (Sigma-Aldrich, St. Louis, MO) followed by thorough washing, drying and incubation with 1% glutaraldehyde (Fisher Scientific, Hampton, NH). Dried coverslips were used for fabrication of two-layer polyacrylamide gels with a thin layer of fluorescent beads on top. A ratio of 3% acrylamide to 0.1% bis-acrylamide was used for preparation of polyacrylamide gels with individual gel stiffnesses in the range of 0.7-1.2 kPa. Indentation by stainless steel spheres was used to quantify gel stiffness as before (30). Prepared polyacrylamide gels were functionalized using hydrazine hydrate and coated with 0.01% poly-L-lysine. Functionalized gels were washed with 1x DPBS and incubated with 10 µg/mL purified anti-mouse CD3 antibody for 2 hours at 37°C or overnight at 4°C, followed by washing with 1xDPBS. PBS was replaced with pre-warmed L-15 medium prior to imaging.

Activated CTLs were added to anti-CD3 coated polyacrylamide gels. The cells were allowed to adhere to the substrate and imaging was initiated within 5 minutes of addition of cells. Images of CTLs in brightfield and the fluorescent bead field were acquired every 15 s for a total of 15 minutes using widefield microscopy. CTLs were detached from the substrate using 2 mL each of 0.25% trypsin-EDTA and 1x DPBS. A final image of the fluorescent bead field was acquired after detachment of CTLs to be used as a reference frame.

For inhibitor treatments, activated CTLs were added to anti-CD3 coated polyacrylamide gels and were imaged as above until 15 minutes after addition of cells. Y27632 was added to the imaging medium at a final concentration of 100 µM, and imaging was performed for another 15 minutes. CTLs were detached using trypsin-EDTA and 1x DPBS as before, and a final reference image of the fluorescent bead field was captured.

Image Analysis

Area Calculation From IRM Images

Edge detection using the Canny operator in MATLAB was implemented to segment IRM images to obtain a binary mask of the cell. The area over time curves were fit to a hyperbolic tangent function $A(t) \sim A_0 \tanh(\alpha t)$ to obtain the cell spreading rate α.

Intensity Analysis of Fixed Cells

Edge detection was implemented as above to segment images of phalloidin-labeled CTLs. The binary mask of the cell was eroded with a disk of radius 0.3*radius of the cell to define a 'central' and an 'annular' region. The ratio of total actin intensity in the cell center to total actin intensity in the annulus was calculated to quantify actin depletion at the cell center. The Wilcoxon rank sum test was used to test the null hypothesis of actin intensity ratios being derived from the same population.

Spatio-Temporal Image Correlation Spectroscopy (STICS)

STICS analysis (44, 45) was run to generate actin and myosin flow vector maps after the cell had achieved maximum spread area for up to five minutes after the start of imaging. STICS was run with a subregion size of 16 x 16 pixels with a shift of 4 pixels between subregions. For analysis of actin flows, the time of interest (TOI) window was selected to be 20 seconds, with a TOI shift of 2 seconds. For analysis of myosin flows, the time of interest (TOI) window was selected to be 60 seconds, with a TOI shift of 6 seconds. Directionality was defined as the cosine of the angle between a given actin flow vector and a vector from the same region of the cell pointing toward the cell center. All vectors with directionality greater than 0.9 were defined as inward flows. The two-sample Kolmogorov Smirnov test was used to test the null hypothesis of actin flow speeds originating from the same distribution. The proportions test was used to test the null hypothesis of the two proportions of inward flow being identical.

Tracking of EB3 Tips

Analysis of EB3 tips was performed after the cell had achieved maximum spread area for up to five minutes after the start of imaging. EB3 tips were tracked using the comet detection routine of the MATLAB-based software u-track (46). A Brownian search radius of 1 to 6 pixels (corresponding to 0.06-0.39 µm) was used for frame-to-frame linking.

Analysis of Granule Distribution

To quantify granule distribution four frames (30 seconds apart) from the live imaging of Lamp1-RFP cells were chosen to detect and measure bright spots corresponding to individual granules or granule clumps. The cell edge was detected from the maximum intensity projection of the live cell movie. The individual frames were binarized and granules were segmented using the function *imbinarize* from MATLAB. Thresholding values used for each image were defined based on the mean of the distribution of pixel intensities in an automated manner to account for photobleaching and differences in Lamp1-RFP expression. Detected objects smaller than 3 pixels (~ 0.5 µm) were discarded and granule area fraction was calculated as the ratio of number of pixels within the granule and the total number of pixels in the cell.

Tracking of Lytic Granules

Individual lytic granules were detected and tracked using the Fiji plugin TrackMate (47). The following parameters were used for detection and tracking of lytic granules: estimated blob diameter

= 1 μm, threshold = 0.5, maximum linking distance = 0.6 μm, maximum gap closing distance = 0.6 μm, maximum gap closing frames = 2. Tracks with a duration lower than 2 seconds were excluded from further analysis. MSD curves were calculated for each track using the MATLAB per-value class @msdanalyzer (48). A one-degree polynomial fit was performed for the log-log of the MSD curves to obtain a value of α for each curve. Only tracks with fits with an r-squared value greater than 0.8 were retained for further analysis.

Traction Force Analysis

Microscopy images were registered using ImageJ/Fiji (descriptor-based registration) and cropped into 600 x 600 pixel-sized regions of interests (ROIs) each containing a single cell at the center. Traction force microscopy analysis was conducted on the single-cell ROIs based on Regularized Fourier Transform Traction Cytometry (FTTC) (49) using a open-source package implemented in MATLAB (50). The displacement field was estimated using a template matching algorithm with a template size of 32 pixels and maximum displacement of 16 pixels. The values for elastic modulus and gel height were obtained by indentation experiments mentioned above. Regularization parameter for stress estimation was 0.0001. Calculated stress fields at each time point were integrated over the entire ROI and reported as traction force applied by each cell. Traction force metrics including the maximum, mean and median force during the 15-minute imaging period were considered for comparison of 2SI and 3SI CTLs. For inhibitor experiments on 3SI CTL, the effect of treatment was quantified by the ratio of traction force at the end of treatment to the traction force at the onset of treatment for each cell. Statistical comparisons of traction force and force ratio were based on Wilcoxon rank sum test.

RESULTS

CTL Activation Conditions Influence the Size and Organization of the Immune Synapse

TCR triggering by APCs leads to rapid cytoskeletal reorganization at the cell-cell interface, which is essential for proper CTL function (14). Cytoskeletal remodeling leads to the rapid spreading of CTLs on the target cell or on stimulatory surfaces (11). We sought to investigate how the presence of inflammatory cytokines as a third activating signal impacts CD8+ T cell cytoskeletal dynamics upon TCR restimulation. We purified naïve CD8+ T cells from lymph nodes of OT-I mice (**Figure S1A**) and activated these *in vitro* under 2SI or 3SI conditions. We verified that 3SI activated cells expressed increased levels of CD25 and similar CD62L levels as compared to 2SI activated cells (**Figure S1B**). Next, we confirmed the functional activity of 2SI and 3SI CTLs by measuring effector molecule production and cytolytic efficiency. Consistent with the typical phenotype of effectors generated by 2SI and 3SI, we found that 3SI CTLs exhibited increased IFN-γ and granzyme B production, accompanied by enhanced cytolytic efficiency (**Figures S1C, D**) (3, 4, 51).

To visualize the contact interface, activated CTLs were imaged during interaction with an anti-CD3-coated stimulatory glass coverslip using interference reflection microscopy (IRM) (**Figures 1A** and **S2A**). Upon contact with the coverslip, cells started spreading on the surface, forming an extended contact zone or immune synapse. To compare spreading dynamics between 2SI and 3SI CTLs, the cell area was calculated using segmented images (see Methods). The change in area over time was fit to a hyperbolic tangent function, which has been previously used to describe T cell spreading (52, 53). Fitted curves were used to calculate the rate of cell spreading (**Figure S2B**). We find that 2SI and 3SI CTLs have comparable spreading rates (**Figure 1B**). We further measured the contact area from images of CTLs fixed at 6 minutes, a timepoint at which most CTLs achieved the maximum spread area in our experiments, and found that 3SI CTLs display a larger IS area than 2SI CTLs (**Figure 1C**).

TCR stimulation on anti-CD3 coated surfaces in activated CTLs induces rapid actin depletion at the immune synapse, followed by actin recovery (14, 26). This depletion of cortical actin at immune synapse is required for secretion of lytic granules and release of granule contents towards the target cell (14, 26). To study the formation and recovery of this actin 'ring', we next compared the organization of the actin cytoskeleton in 2SI and 3SI CTLs. Activated 2SI and 3SI CTLs stimulated on anti-CD3-coated glass coverslips were fixed at 3 and 6 minutes after stimulation to capture 'early' and 'late' stages of actin reorganization at the IS. To study F-actin distribution, cells were stained with phalloidin and imaged using TIRF microscopy (**Figure 1D**). Qualitatively, we observed a larger actin depletion zone in 3SI cells, with this effect enhanced at early timepoints (**Figure 1D**). From the fluorescent images, we defined two regions – the cell 'center' and 'annulus' as shown in **Figure 1E**. The mean fluorescence intensity (MFI), which measures the total fluorescence intensity in a given region divided by the area of the region, was calculated for these two regions. The ratio of actin MFI at the cell center to actin MFI in the annulus (henceforth referred to as the 'actin intensity ratio') was compared across activation conditions. An actin intensity ratio equal to 1 would signify a relatively homogenous distribution of actin at the synapse, while a ratio greater than or lesser than 1 could arise due to central actin accumulation or depletion respectively. We found that 3SI CTLs consistently displayed enhanced actin depletion at the center of the IS as compared to 2SI CTLs at both early and late timepoints. (**Figure 1F**). Importantly, the observed difference in actin intensity ratio is due to reduced actin MFI at the center of 3SI CTLs at both 3 and 6 minutes (**Figure S2C**).

3SI CTLs Exhibit Altered Lytic Granule Distribution and Dynamics as Compared to 2SI CTLs

Activated CTLs kill target cells by secreting lytic granules containing perforin and granzymes that trigger target cell

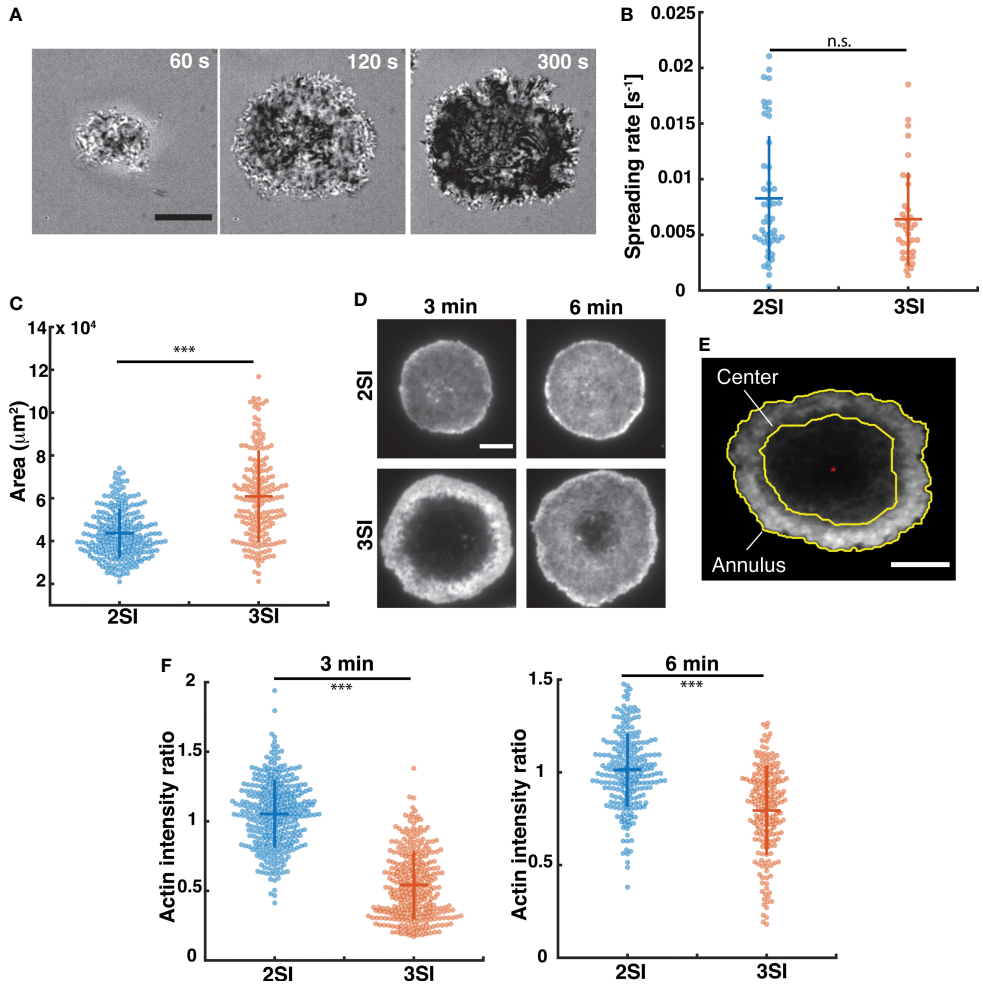

FIGURE 1 | Spreading kinetics and actin distribution in activated CTLs. **(A)** Representative time-lapse images of a 3SI CTL spreading on an anti-CD3-coated coverslip and imaged using IRM. Scale bar = 10 μm. **(B)** Spreading rates of 2SI (n=48 cells), 3SI (n=36 cells) CTLs from at least 3 independent experiments. **(C)** Representative TIRF images of 2SI and 3SI CTLs fixed at 3 and 6 minutes and stained with phalloidin to visualize F-actin. **(D)** Immune synapse area obtained from TIRF images of phalloidin-stained 2SI and 3SI CTLs fixed at 6 min. **(E)** Depiction of the erosion of a binary mask to define central and annular regions in the cell. Red asterisk indicates the cell centroid. **(F)** Actin intensity ratio at 3 and 6 min. Actin intensity ratio was defined at the ratio of actin MFI at the center to the actin MFI at the annulus. Scale bar = 5 um for panels **(D, E)**. Data taken from at least 150 cells from 3 independent experiments. Wilcoxon rank-sum test performed to calculate p-values. ***p<0.001, n.s. - not significant.

apoptosis. Lytic granule secretion occurs in zones of actin depletion in both CTLs and natural killer cells (14, 26, 54, 55). Furthermore, lytic granule movement in natural killer cells is modulated by the cytoskeleton – inhibiting various elements of the cytoskeleton using small molecular inhibitors of actin or microtubules leads to altered granule mobility patterns (56, 57). In CTLs, depolymerization of actin using Latrunculin A leads to continued granule release (26). Given that the cytoskeleton regulates lytic granule dynamics, enhanced actin depletion in 3SI CTLs may be associated with altered granule dynamics at the interface, potentially resulting in increased lytic granule secretion as compared to 2SI CTLs. We therefore studied lytic granule dynamics in 2SI and 3SI activated CTLs co-transfected with F-Tractin-EGFP and Lamp1-RFP (Lysosomal-associated membrane protein 1) to label F-actin and lytic granules respectively. While Lamp1 is a lysosomal membrane marker, previous studies have shown that over 90% of Lamp1-labeled lysosomes in CTLs contain cathepsin-D and granzymes found in lytic granules (58). Lamp1 tagging has also been previously used to track lytic granule mobility and release in CTLs and natural killer cells (14, 26, 55, 58). Transfected CTLs were stimulated on anti-CD3 coated glass coverslips and imaged with TIRF every 1 second (**Figure S3A**). In agreement with previous work, both 2SI and 3SI CTLs show characteristic actin ring formation and recovery, with granule secretion occurring in areas of the synapse where actin is transiently depleted (**Figures S3B, C**).

To capture lytic granule dynamics near the plasma membrane prior to release, we performed rapid TIRF imaging of activated CTLs transfected with Lamp1-RFP at intervals of 100 ms (**Supplementary Movie 1**). Fast imaging of Lamp1-RFP-

labeled lytic granules showed a variety of mobility patterns, with a larger fraction exhibiting low mobility, while others displayed fast directed motion – likely the result of transport along microtubules. Qualitatively, 3SI CTLs appeared to have a greater number of lytic granules at the synapse than 2SI CTLs. Furthermore, lytic granules in 2SI CTLs appeared to be more clustered towards the center of the synapse, while 3SI CTLs displayed a relatively homogenous distribution of granules across the synapse (**Figure 2A**). To quantify these differences, we used thresholding to detect individual granule-sized objects in the captured images. Consistent with our qualitative observations, a higher number of structures were detected per cell for 3SI CTLs than for 2SI CTLs (**Figure 2B**). From the detected structures, we calculated the mean granule fluorescence intensity and granule area as a fraction of the cell area. This data was then summarized in five bins based on radial position of the granule from the cell center, where a radial position of 0 corresponds to the cell centroid. We found that for 2SI CTLs, granules tend to occupy a larger fraction of the cell area closer to the cell center (corresponding to radial position bins 0-0.2 and 0.2-0.4) (**Figure 2C**). In 3SI CTLs, granules were distributed more evenly across the synapse compared to the more clustered appearance in 2SI cells. Furthermore, granules closer to the cell center in 2SI CTLs tended to have a higher MFI than in 3SI, reflecting a high degree of granule accumulation at the center of the synapse (**Figure 2D**).

We then tracked granule movements at the synapse (**Figure 2E**) and calculated instantaneous and median granule

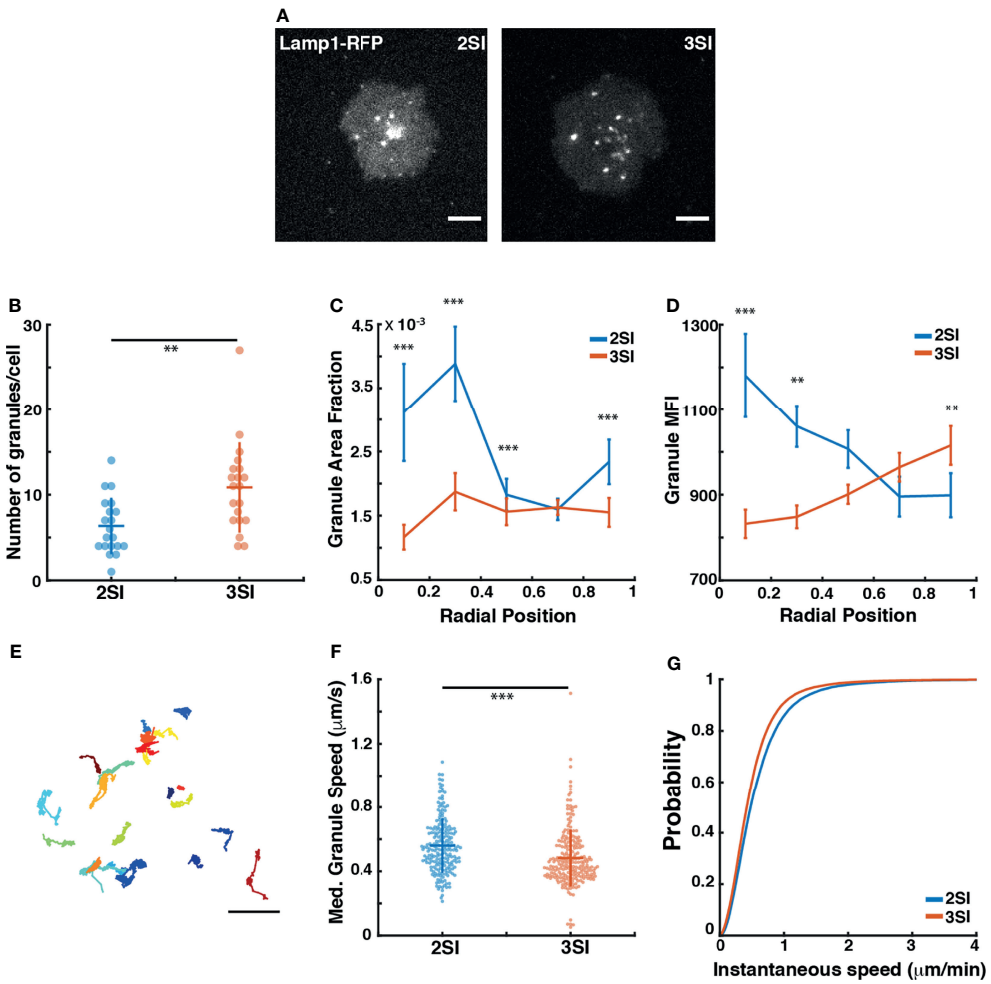

FIGURE 2 | 3SI CTLs exhibit altered lytic granule distribution and dynamics: **(A)** Representative snapshots of a 2SI and 3SI CTL expressing Lamp1-RFP interacting with an anti-CD3-coated coverslip imaged using TIRF microscopy after reaching maximum spread area. Scale bar = 5 μm. **(B)** Number of granules for 2SI and 3SI CTLs detected per cell using thresholding. For granule number, p=0.002 (Wilcoxon rank-sum test). **(C)** Fraction of the complete cell area occupied by lytic granules granules and **(D)** Granule MFI binned according to granule radial position. Data is presented as mean ± SEM. **(E)** Full lytic tracks for a representative 3SI CTL. Scale bar = 2 μm. **(F)** Median granule speeds and **(G)** cumulative distribution function of instantaneous granule speeds obtained from tracking of lytic granules. For median granule speeds, p=6.762793e-08 (Wilcoxon rank-sum test). For instantaneous granule speeds, p=0.005 (two-sample Kolmogorov-Smirnov test). Data taken from 20 cells each for 2SI (n=205 tracks) and 3SI (n=226 tracks) from 2 independent experiments. ***p<0.001, **p<0.01.

speeds. We found that 3SI CTLs exhibit significantly slower granule speeds across the synapse as compared to 2SI CTLs (**Figures 2F, G**). Finally, the mean-squared displacement (MSD) was calculated for each track to capture the degree of overall granule movement. The first 25% of each MSD curve was fit according to the relationship $MSD(t) = Bt^{\alpha}$ to obtain a value of α for each track (48, 59). The resulting α values for each track were used to classify the track as exhibiting super-diffusion ($\alpha > 1.2$), normal diffusion ($1.2 > \alpha > 0.8$) or sub-diffusion ($\alpha < 0.8$). 2SI and 3SI CTLs both show similar fractions of super-diffusive, normal, and sub-diffusive tracks (**Figure S3E**). Classified tracks were also used to construct ensemble MSDs for both 2SI and 3SI CTLs, with the resultant ensemble MSD curves showing similar behavior regardless of activation condition (**Figure S3D**). In summary, these results show that, while activation conditions do not influence overall lytic granule mobility patterns, 3SI CTLs exhibit altered granule distribution and speeds as compared to 2SI CTLs.

Cytokine Stimulation Alters Actomyosin Dynamics

Actin clearance at the center of the immune synapse is accompanied by extensive actin flow at the periphery of the synapse. Actin flows drive the centripetal movement of TCR signaling microclusters towards the center of the synapse and trigger downstream signaling resulting in sustained calcium flux (11, 60–66). Having observed differences in actin organization at the IS in 2SI and 3SI CTLs, we next investigated actin flow dynamics using high-resolution live-cell imaging methods. We transfected activated CTLs with F-Tractin-EGFP to label F-actin. Transfected CTLs were stimulated on anti-CD3 coated glass coverslips as described above and imaged using TIRF microscopy every 1 second (**Figure 3A** and **Figure S4A**, **Supplementary Movie 2**). Live TIRF imaging of activated CTLs expressing F-Tractin-EGFP revealed dynamic protrusions and retractions at the lamellipodial edge. Both 2SI and 3SI CTLs exhibited transient actin depletion at the center of the synapse, followed by recovery of cortical actin (as seen in the last panel of **Figure 3A** and **Figure S3A**) which coincides with termination of granule fusion (26).

Actin flows during the first 5 minutes after the cell had achieved its maximum spread area were analyzed using Spatio-Temporal Image Correlation Spectroscopy (STICS). STICS is a technique that quantifies spatiotemporal changes in protein dynamics based on fluorescence intensity correlations across spatial and temporal interrogation windows (44, 45). A representative output image depicting actin flow velocity vectors color-coded for magnitude overlaid on an image of an activated CTL is shown in **Figure 3B**. We decomposed actin flow velocity vectors into heatmaps of speed magnitudes and directionalities (**Figures 3C** and **S4B**). Actin flow directionality was defined as the cosine of the angle between an actin flow vector and a vector from the same region of the cell pointing towards the cell center.

To quantify differences in actin flows between 2SI and 3SI CTLs, we constructed the cumulative distribution function (CDF) of actin speeds calculated using STICS. We found that 3SI CTLs exhibited significantly slower actin flow speeds at the synapse as compared to 2SI CTLs (**Figures 3D** and **S4C**). We further constructed probability density functions (PDFs) of actin flow directions to compare directionalities between conditions. All vectors with directionality greater than 0.9 were classified as 'inward flows'. Our analysis showed that while directionalities for 2SI and 3SI CTLs followed a similar distribution, 3SI CTLs had significantly higher inward flows (**Figure S4D**).

High-resolution imaging of the IS has implicated myosin II in forming arc-like structures at the base of the peripheral regions of the contact zone (60) that were shown to drive the inward movement of engaged TCR clusters. We next examined whether cytokine stimulation alters myosin dynamics. We transfected activated CTLs with EGFP-tagged myosin light chain (MLC) to label myosin II. Transfected CTLs were stimulated on anti-CD3 coated glass coverslips as described above and imaged using TIRF microscopy every 1 second (**Supplementary Movie 3**). STICS analysis of myosin II dynamics revealed that 3SI stimulated cells showed more coherent and higher overall myosin speeds compared to 2SI stimulated cells (**Figure S4E**, **Figures 3E, F**).

3SI CTLs Display Faster Microtubule Growth Rates As Compared To 2SI CTLs

Contact formation between CTLs and target cells induces centrosome reorientation towards the IS with lytic granules being transported along microtubules (MTs) to the CTL-target cell synapse (19, 20). Our prior work has demonstrated that actin flow patterns at the IS further influence MT dynamics at the IS (32, 67). Having observed differences in lytic granule distribution and actin flows, we decided to investigate whether the activation of CTLs in the presence of inflammatory cytokines would also affect MT distribution and dynamics. We first used immunofluorescence to study microtubule organization at the IS of 2SI and 3SI CTLs. Activated CTLs stimulated on anti-CD3-coated glass coverslips were fixed at 3 and 6 minutes after stimulation, similar to the methodology used to study actin distribution. Fixed cells were stained with antibodies to tubulin and imaged using TIRF microscopy (**Figure 4A**). Comparison of tubulin MFI in central and annular regions of the cell revealed that 3SI CTLs had a higher ratio of tubulin intensity at the cell center to annulus at both timepoints (**Figure 4B**). This effect arises due to a lower MFI of tubulin intensity at the annulus of 3SI CTLs, likely caused by a higher accumulation of actin in the same region (**Figures S5B** and **Figures 1D**, **3A**).

To study microtubule growth rates, we transfected activated CTLs with EGFP-EB3, a construct that labels EB3 (end-binding protein 3). EB3 binds to the ends of growing microtubules and is frequently used to study microtubule growth (68). Transfected CTLs were stimulated on anti-CD3 coated glass coverslips as above and imaged using TIRF at 1 second intervals (**Figure 4C** and **Figure S5A**, **Supplementary Movie 4**). We tracked EB3 comets during the first 5 minutes after the cell had achieved its maximum spread area using the MATLAB-based software,

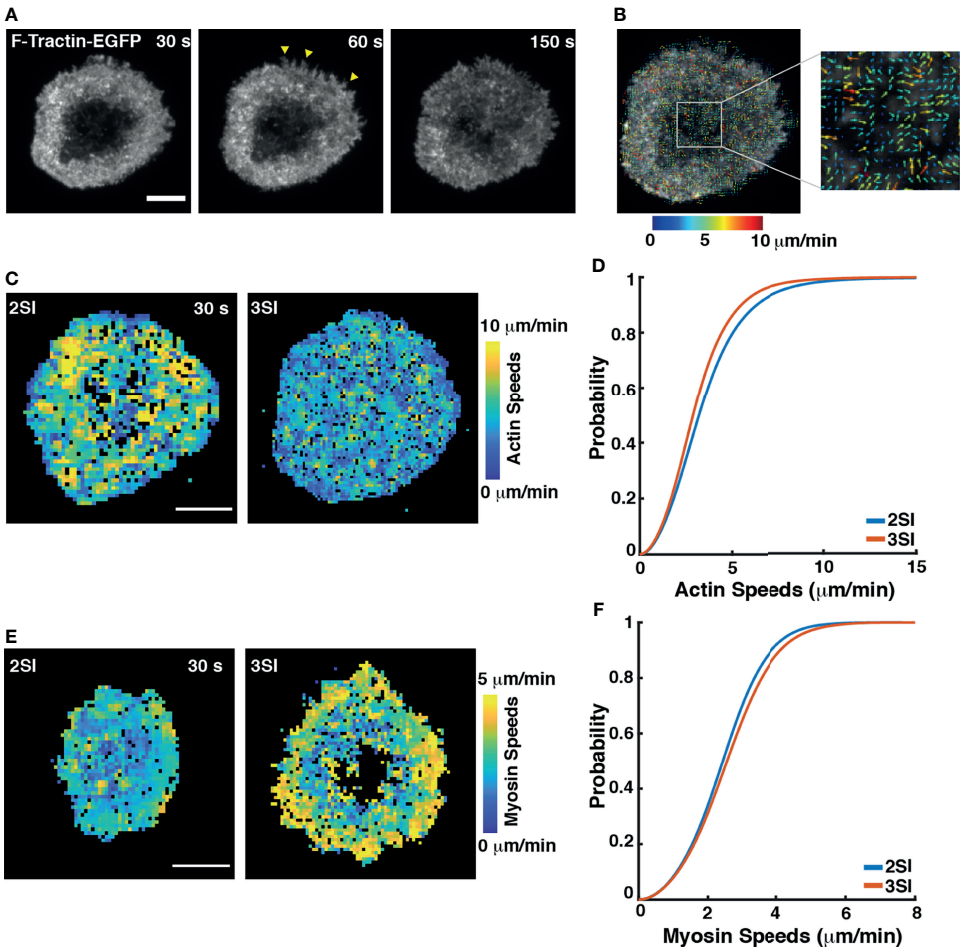

FIGURE 3 | 3SI stimulation alters actomyosin flow speeds in CTLs: **(A)** Representative time-lapse images of a 3SI CTL expressing F-tractin-EGFP spreading on an anti-CD3-coated coverslip and imaged using TIRF microscopy. Yellow arrows show actin protrusions. **(B)** Output from STICS analysis showing actin flow vectors at the immune synapse. The color of actin flow vectors corresponds to the magnitude of actin speeds, as represented by the color bar. **(C)** Heat maps showing magnitudes of actin flow speeds over the synapse at the indicated timepoint for 2SI and 3SI CTLs. Colors correspond to speeds as indicated by the color bar. **(D)** Cumulative distribution function of actin flow speeds obtained from STICS analysis of 2SI and 3SI CTLs. n=15 cells for 2SI and 12 cells for 3SI from 6 independent experiments. For actin speeds, p= 8.09e-06, two sample Kolmogorov-Smirnov test. Scale bars = 5 μm. **(E)** Heat maps showing myosin flow speeds at the indicated time point in 2SI and 3SI cells. **(F)** Cumulative distribution function of myosin flow speeds obtained from STICS analysis of 2SI and 3SI CTLs. n=11 cells for 2SI and 17 cells for 3SI from 3 independent experiments. For myosin speeds, p=8e-04, two sample Kolmogorov-Smirnov test. Scale bars = 5 μm.

uTrack (46) (**Figure 4D**). The instantaneous speed of a microtubule tip was defined as the inter-frame tip displacement between two consecutive images divided by the imaging interval (1 second) (67). We constructed the CDF of instantaneous EB3 speeds to compare the distributions of microtubule tip speeds between activation conditions and found that 3SI CTLs exhibited significantly faster EB3 speeds than 2SI CTLs (**Figure 4E**). These results indicate faster microtubule growth rates in 3SI CTLs as compared to 2SI CTLs.

Traction Force Microscopy Reveals 3SI CTLs Generate Stronger Traction Forces Than 2SI CTLs

The extensive actin flows and MT dynamics during the formation of the IS mediate force generation at the CTL-target contact site. These forces enhance target cell killing, potentially by altering the membrane and cytoskeletal tension of the target cell, thereby facilitating perforin activity and target cell lysis (30–33). Given our above results on differences in actin and microtubule dynamics in 3SI CTLs and to further investigate the role of the third signal in modulating cytoskeletal dynamics, we proceeded to examine mechanical force generation by activated CTLs.

We used traction force microscopy (TFM) to measure forces generated by 2SI and 3SI CTLs during stimulation by a biomimetic stimulatory surface. We prepared polyacrylamide (PA) hydrogel substrates of approximately 1.0 kPa stiffness embedded with fluorescent nanoparticles and coated with anti-CD3. The chosen stiffness level for the hydrogel substrates matches the range of stiffness reported for various cancer cell lines and was considered appropriate for modeling the target cell (69–71). Activated CTLs

were plated on PA gels and the fluorescent nanoparticle field was imaged every 15 seconds using widefield microscopy during the interaction of CTLs with the gel surface (**Figure 5A** and **Supplementary Movie 5**). A reference image of the nanoparticle field was obtained by detaching the cells with trypsin-EDTA and washing the gel with PBS after the end of imaging. Force exertion by CTLs on the PA hydrogel substrate causes displacement of fluorescent nanoparticles. Displacement fields were obtained for each cell by comparing the locations of fluorescent nanoparticles with respect to the reference image (**Figure 5B**). The measured displacements were used to calculate the traction stresses exerted by the cell based on the linear elastic theory for a homogenous isotropic material of known stiffness and thickness (**Figure 5C**, **Methods**).

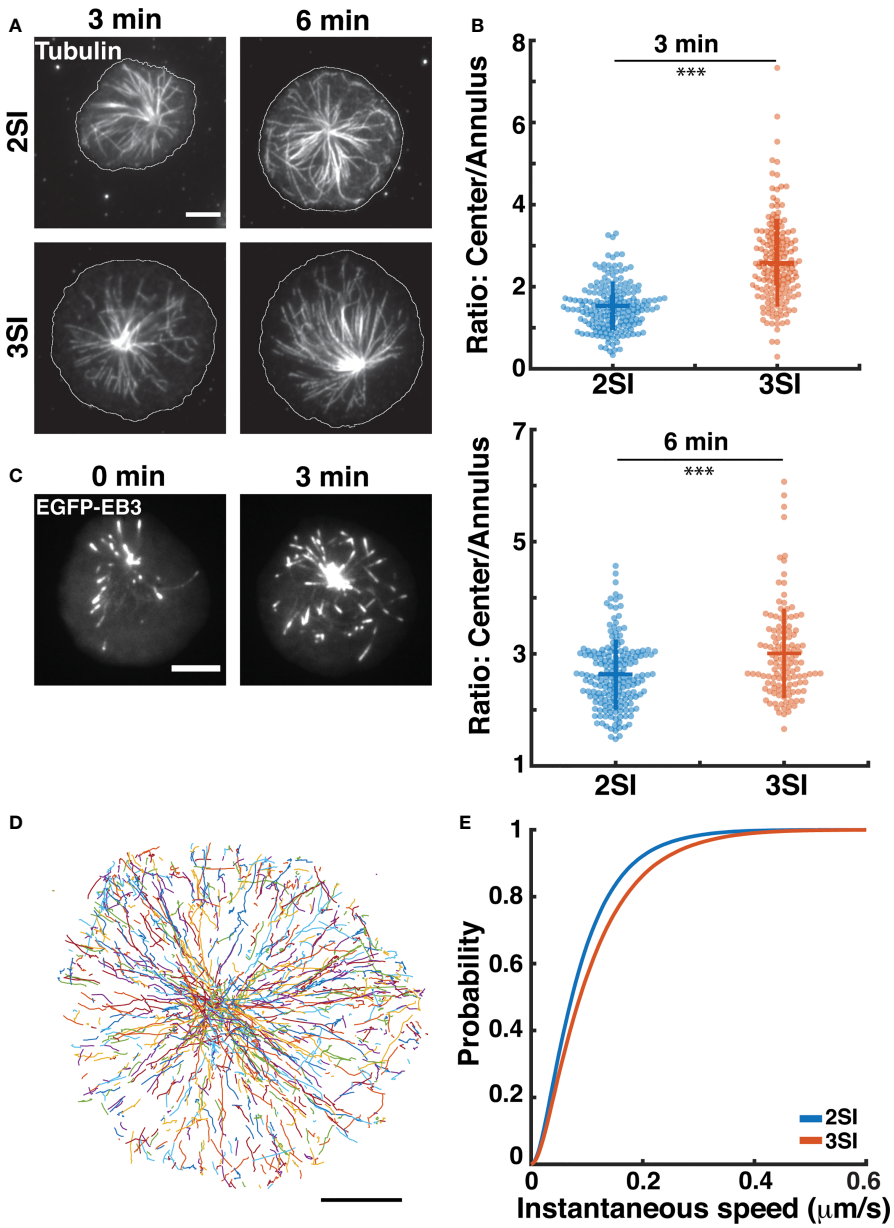

FIGURE 4 | 3SI CTLs display altered microtubule growth rates: **(A)** Representative TIRF images of 2SI and 3SI CTLs fixed at 3 and 6 min and stained with anti-β-tubulin to visualize microtubules. Cell outline is shown in white. **(B)** Ratio of tubulin fluorescence intensity at the center to the annulus at 3 and 6 min. Data taken from at least 130 cells from 3 independent experiments. Wilcoxon rank-sum test performed to calculate p-values. ***p<0.001. **(C)** Representative time-lapse images of a 3SI CTL expressing EGFP-EB3 spreading on an anti-CD3-coated coverslip and imaged using TIRF microscopy. **(D)** All EB3 tracks for a representative 3SI cell. **(E)** Cumulative distribution function of instantaneous microtubule tip. n=12 cells for 2SI, 16 cells for 3SI from 4 independent experiments. For EB3 speeds, p=0.009 (two sample Kolmogorov-Smirnov test). All scale bars represent 5 μm.

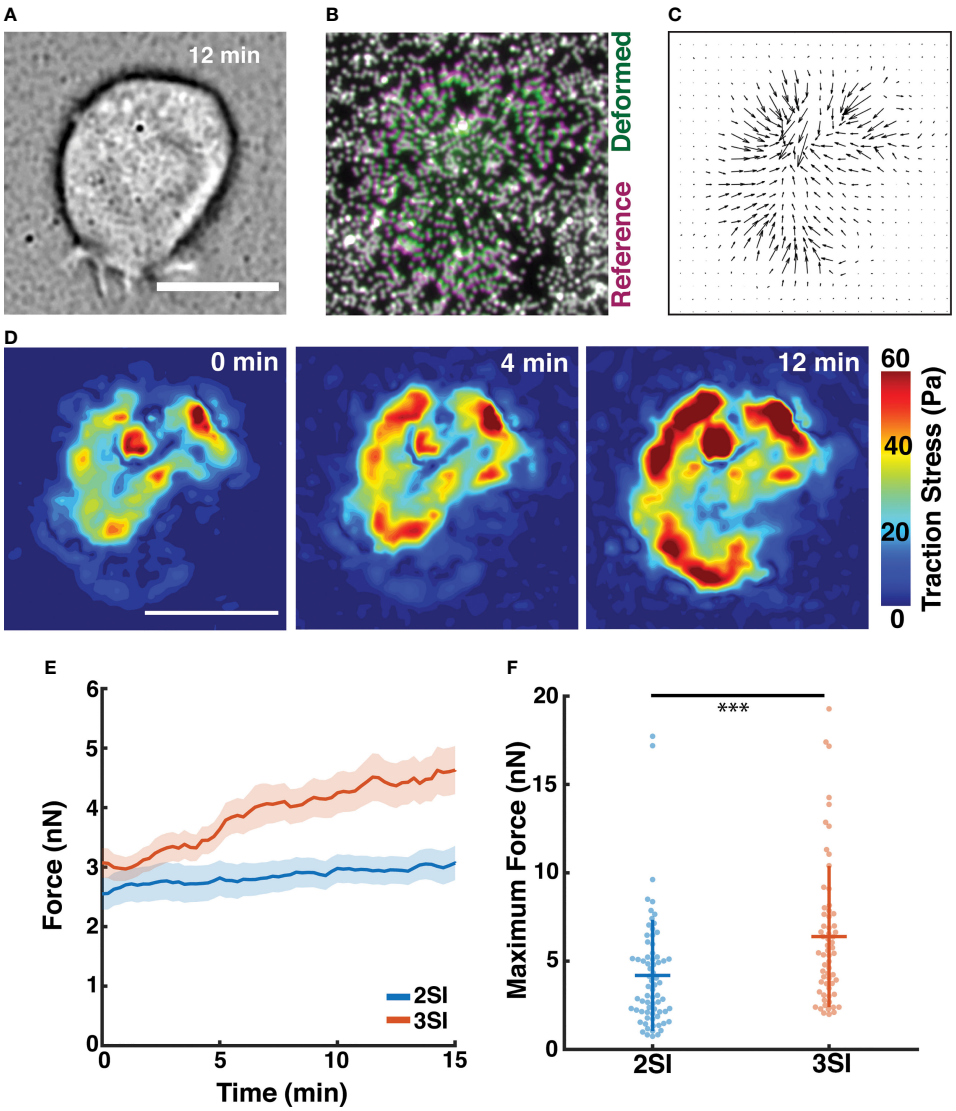

FIGURE 5 | Traction force microscopy reveals 3SI CTLs generate stronger traction forces. **(A)** Brightfield image of a 3SI CTL spreading on a polyacrylamide hydrogel substrate at 12 minutes of imaging. **(B)** Composite fluorescence image showing displacement of fluorescent beads embedded in the gel surface during spreading of the cell in **(A)**. Bead positions for deformed and undeformed (reference) states of the hydrogel are indicated by green and magenta, respectively. Undisplaced beads are indicated by white. **(C)** Traction stress vectors calculated for the cell in **(A)**. **(D)** Spatial distribution of traction stress magnitude associated with the cell in **(A)** at time points between 0 and 12 minutes of imaging. **(E)** Evolution of integrated traction force over the course of imaging for 2SI and 3SI CTLs. The trends are reported as mean ± sem. **(F)** Maximum traction force generated by 2SI and 3SI cells during the imaging period. n = 72 cells for 2SI and 63 cells for 3SI. Data taken from 4 independent experiments. *** p-value < 0.0001. All scale bars indicate 10 μm.

2SI and 3SI CTLs rapidly begin to exert a force after contact with the stimulatory PA gel building up to saturating levels (~10-15 min, **Figure 5D** and **Supplementary Figure S6A**). Enhanced traction stresses were observed in an annular region at the cell periphery, likely corresponding to the actomyosin ring. The baseline level of force at 0 min resulted from a finite time lag between addition of cells on the substrate and the start of imaging. The total forces exerted by primary CTLs were in the nano-newton (nN) range, comparable to previously measured values (31, 33) (**Figure 5E**). Intriguingly, our results show that 3SI CTLs exert significantly greater traction forces than 2SI CTLs (**Figures 5E, F** and **Figure S6B**). Previous work has shown that myosin II is required for force generation in T cells (30, 31). Analogous to previous observations, we found that force exertion by 3SI CTLs was reduced after treatment with the Rho-kinase inhibitor Y27632 which reduces myosin II activity (72) (**Figure S6C**). Observed differences in force generation between 2SI and 3SI CTLs are potentially indicative of differential modulation of the cytoskeletal machinery by third signal cytokines such as IL-12.

DISCUSSION

Optimal function of effector CD8+ T cells requires integration of multiple signals, including cytokine stimulation as a third signal (73). A number of studies have led to the well-established paradigm that third signal cytokines such as IL-12 induce the optimal accumulation of activated CD8+ T cell populations *in vivo* by regulating their division and survival (74) or by conferring a proliferative advantage (38, 51, 75). In addition, prior exposure to third signal cytokines leads to rewiring of TCR signaling pathways (76) and increased expression of perforin and granzymes (3, 4), potentially mediating their enhanced effector function.

In this work, we used a combination of high resolution TIRF imaging and traction force microscopy to delineate an additional mechanism by which third signal cytokines enhance effector function by regulation of the CTL cytoskeleton. We showed that 3SI CTLs exhibit higher actin depletion as compared to 2SI CTLs. This is accompanied by larger numbers of lytic granules and decreased clustering of lytic granules towards the center of the synapse in 3SI CTLs. Given that actin depletion regulates secretion of lytic granules in $CD8^+$ T cells (14, 26), these results likely indicate an improved ability of 3SI CTLs to secrete lytic granules, hence contributing to enhanced cytotoxic efficiency.

We further found that activation in the presence of IL-12 leads to changes in cytoskeletal dynamics, with 3SI CTLs exhibiting slower actin flows compared to 2SI CTLs. Intriguingly, we found that myosin speeds are higher in 3SI CTLs at the synaptic interface. Actin retrograde flow is a result of the 'superimposition' of two processes - actin assembly and myosin-based filament retraction (77, 78). Previous studies have found that myosin-II has a larger influence on flows in primary T cells, where flows are mostly localized to the lamellar region of the cell (79). Of note, we observed that activated CTLs show coherent myosin retrograde flow whereas inward actin flow is not as organized.

Actomyosin dynamics are known to drive cellular force generation in T cells. Our results showed that 3SI CTLs exert higher traction forces than 2SI CTLs with higher myosin-II speeds being an important contributor toward the exertion of traction forces in CD8+ T cells. Overall, our observations that slower actin flow rates in the distal region of the IS are correlated with higher traction forces are broadly consistent with prior work on adherent cells (80). These differences in mechanical force exertion between 2SI and 3SI CTLs have important functional implications. Basu et al. have shown that mechanical force exertion across the CTL-target interface facilitates perforin pore formation, thereby suggesting a correlation between actomyosin generated forces and cytotoxic potential (31). The enhanced force generation by 3SI CTLs may provide an additional mechanism by which cytokines augment effector function.

A central question that remains is the mechanism by which the actin cytoskeleton may be differentially regulated in 3SI CTLs. Previous work comparing gene expression in 2SI and 3SI CTLs at timepoints similar to those used in our study may shed light on potential molecular players (4). Primary among these are the Rho-family GTPases RhoA, Rac and Cdc42. 3SI CTLs exhibit lower expression of GTPase-activating proteins Rho-GAP1 and Rac-GAP1 which participate in GTPase 'molecular switching' by triggering GTPase behavior of Rho, leading to GTP dissociation and conversion to an 'off' state. This is consistent with our results showing increased myosin speeds and cellular forces which would be expected with enhanced Rho activity. Additionally, IL-12 treatment results in decreased expression of Cdc42 and its effector proteins in CD4+ and CD8+ T cells (35), which could lead to the decreased actin flows that we observed. Finally, expression of the Cdc42 effector protein IQGAP1 is differentially modulated in 3SI CTLs. IQGAP1 links microtubule plus ends with the actin cortex and is cleared along with actin at the time of granule secretion delivery (20).

Another important cytoskeletal regulatory pathway that may be involved is *via* phosphatidylinositol-3-kinase (PI3K). IL-12 treatment activates the PI3K signaling pathway in CD8+ T cells (8, 38) and in CD4+ T cells (81, 82). Class IA PI3K isoforms generate the second messenger PIP3 which controls actin ring formation (37). PI3K regulatory subunit p85alpha, which is expressed at higher levels in 3SI CTLs, is recruited to TCR microclusters (4, 37). PI3K signaling is also required for force exertion and IS formation: inhibition of PI3K antagonist PTEN leads to higher forces (31), and an increase in IS size and killing efficiency (37). Examining the connection between IL-12 regulation of the PI3K pathway and enhanced effector function of CTLs will be the subject of future work.

We further found that 3SI CTLs have a higher density of microtubules at the cell center. One possible mechanism regulating reorganization of the MT cytoskeleton in 3SI CTLs may involve differential diacylglycerol (DAG) concentrations. DAG accumulates in the cSMAC and is required for centrosome docking at the IS. Diacylglycerol kinase-α (DGK-α) localizes to the dSMAC and is required to focus DAG in the cSMAC for proper centrosome polarization (83). DGK-α is expressed at lower levels in 3SI CTLs which may result in differential DAG concentrations across the synapse, thus modulating centrosome polarization and reorganization of the MT cytoskeleton (4). We also found that 3SI CTLs have faster microtubule growth rates. It has been previously reported that actin acts as a physical barrier for MT growth (84). Actomyosin dynamics further regulate MT filament curvature and dynamics (67, 85). Furthermore, we have previously shown that actin retrograde flow in T cells is negatively correlated with MT tip influx (32). Thus, faster MT tip speeds in 3SI CTLs may serve to slow actin retrograde flow and augment force generation. These results also underscore the importance of exploring the roles played by different proteins involved in actin-microtubule crosstalk such as IQGAP1 (86), CLIP-170 (87) and Apc (88).

We note that the experimental system used in our studies did not include ICAM-1, the ligand for the T cell integrin LFA-1. LFA-1 localizes to the peripheral supramolecular activation cluster - an annular region of the IS located at an intermediate distance between the cell center and the cell edge (89). The interaction of LFA-1 with ICAM-1 mediates adhesion of a CTL

to a target cell, and is required in addition to antigenic stimulation for granule secretion and IS formation on planar lipid bilayers (37, 90–92), LFA-1 engagement further regulates actin assembly and flows (93–96). While anti-CD3 acts as a strong stimulatory signal to induce cytoskeletal reorganization, whether additional LFA-1 engagement would alter the differential cytoskeletal remodeling patterns observed in our study remains an open question.

The cytoskeleton acts as a dynamic framework for the transmission of mechanochemical signals to regulate T cell signaling and gene expression. At the receptor level, the cytoskeleton is intricately linked to the TCR (13, 93), which has been characterized as a mechanosensor (97–101). Not only can forces activate signaling *via* the TCR, piconewton-level actomyosin forces applied through the TCR allow for the formation of catch bonds with cognate ligands and thus participate in peptide discrimination (100–104). At the cellular level, the cytoskeleton allows the T cell to sample mechanical properties, such as stiffness, of the antigen presenting surface, and modulate force generation (30). While our current work involved CTL activation and force measurements on a hydrogel of physiologically relevant stiffness, an important open question is whether three-signal activation conditions prime CD8+ T cells to better recognize and respond to a range of substrate stiffnesses, thus augmenting T cell function.

In conclusion, the results from our current study indicate that three-signal activation conditions modulate cytoskeletal dynamics and forces in CD8+ T cells. Given that the cytoskeleton is an established regulator of T cell signaling and effector function, differential modulation of the cytoskeletal machinery may be a potential mechanism by which IL-12 enhances CTL effector function. Our results provide novel biophysical insights into the role of IL-12 in improving T cell function at the single cell level.

DATA AVAILABILITY STATEMENT

The raw data supporting the conclusions of this article will be made available by the authors, without undue reservation.

ETHICS STATEMENT

The animal study was reviewed and approved by Institutional Animal Care and Use Committee, University of Maryland, College Park.

AUTHOR CONTRIBUTIONS

AP, AO, and AU designed the experiments with input from ZX. AP and AO performed the experiments. AP, AO, and IR-S analyzed the data with help from SD. NR, IR-S, and AU provided guidance on data analysis. LL performed the purification and characterization of naïve and activated murine CD8+ T cells. AP and AU wrote the manuscript, with input from AO, IR-S, and ZX. AU supervised the project. All authors contributed to the article and approved the submitted version.

FUNDING

AU and ZX acknowledge support from the grant NIH R01 GM131054. AU acknowledges support from NSF PHY 1806903. AP's contribution to this research was supported in part by NSF award DGE-1632976. IR-S would like to acknowledge support from the Fulbright-Colciencias scholarship.

ACKNOWLEDGMENTS

We would like to thank Kaustubh Wagh (UMD) and Jared Cunanan (UMD) for their help with image analysis.

SUPPLEMENTARY MATERIAL

The Supplementary Material for this article can be found online at: https://www.frontiersin.org/articles/10.3389/fimmu.2022.779888/full#supplementary-material

REFERENCES

1. Curtsinger JM, Schmidt CS, Mondino A, Lins DC, Kedl RM, Jenkins MK, et al. Inflammatory Cytokines Provide a Third Signal for Activation of Naive CD4+ and CD8+ T Cells. *J Immunol* (1999) 162:3256–62.
2. Curtsinger JM, Johnson CM, Mescher MF. CD8 T Cell Clonal Expansion and Development of Effector Function Require Prolonged Exposure to Antigen, Costimulation, and Signal 3 Cytokine. *J Immunol* (2003) 171:5165–71. doi: 10.4049/jimmunol.171.10.5165
3. Curtsinger JM, Lins DC, Johnson CM, Mescher MF. Signal 3 Tolerant CD8 T Cells Degranulate in Response to Antigen But Lack Granzyme B to Mediate Cytolysis. *J Immunol* (2005) 175:4392–9. doi: 10.4049/jimmunol.175.7.4392
4. Agarwal P, Raghavan A, Nandiwada SL, Curtsinger JM, Bohjanen PR, Mueller DL, et al. Gene Regulation and Chromatin Remodeling by IL-12 and Type I IFN in Programming for CD8 T Cell Effector Function and Memory. *J Immunol* (2009) 183:1695–704. doi: 10.4049/jimmunol.0900592
5. Curtsinger JM, Gerner MY, Lins DC, Mescher MF. Signal 3 Availability Limits the CD8 T Cell Response to a Solid Tumor. *J Immunol* (2007) 178:6752–60. doi: 10.4049/jimmunol.178.11.6752
6. Gerner MY, Heltemes-Harris LM, Fife BT, Mescher MF. Cutting Edge: IL-12 and Type I IFN Differentially Program CD8 T Cells for Programmed Death 1 Re-Expression Levels and Tumor Control. *J Immunol* (2013) 191:1011–5. doi: 10.4049/jimmunol.1300652
7. Xiao Z, Casey KA, Jameson SC, Curtsinger JM, Mescher MF. Programming for CD8 T Cell Memory Development Requires IL-12 or Type I IFN. *J Immunol* (2009) 182:2786–94. doi: 10.4049/jimmunol.0803484
8. Rao RR, Li Q, Odunsi K, Shrikant PA. The mTOR Kinase Determines Effector Versus Memory CD8+ T Cell Fate by Regulating the Expression of Transcription Factors T-Bet and Eomesodermin. *Immunity* (2010) 32:67–78. doi: 10.1016/j.immuni.2009.10.010
9. Markiewicz MA, Wise EL, Buchwald ZS, Cheney EE, Hansen TH, Suri A, et al. IL-12 Enhances CTL Synapse Formation and Induces Self-Reactivity 1. *J Immunol* (2009) 182(3):1351–61. doi: 10.4049/jimmunol.182.3.1351

10. Poenie M, Kuhn J, Combs J. Real-Time Visualization of the Cytoskeleton and Effector Functions in T Cells. *Curr Opin Immunol* (2004) 16:428–38. doi: 10.1016/J.COI.2004.05.016
11. Bunnell SC, Kapoor V, Trible RP, Zhang W, Samelson LE. Dynamic Actin Polymerization Drives T Cell Receptor-Induced Spreading: A Role for the Signal Transduction Adaptor LAT. *Immunity* (2001) 14:315–29. doi: 10.1016/S1074-7613(01)00112-1
12. Bunnell SC, Hong DI, Kardon JR, Yamazaki T, McGlade CJ, Barr VA, et al. T Cell Receptor Ligation Induces the Formation of Dynamically Regulated Signaling Assemblies. *J Cell Biol* (2002) 158:1263–75. doi: 10.1083/jcb.200203043
13. Burkhardt JK, Carrizosa E, Shaffer MH. The Actin Cytoskeleton in T Cell Activation. *Annu Rev Immunol* (2008) 26:233–59. doi: 10.1146/annurev.immunol.26.021607.090347
14. Ritter AT, Asano Y, Stinchcombe JC, Dieckmann NMG, Chen BC, Gawden-Bone C, et al. Actin Depletion Initiates Events Leading to Granule Secretion at the Immunological Synapse. *Immunity* (2015) 42:864–76. doi: 10.1016/j.immuni.2015.04.013
15. Kuhn JR, Poenie M. Dynamic Polarization of the Microtubule Cytoskeleton During CTL-Mediated Killing. *Immunity* (2002) 16:111–21. doi: 10.1016/S1074-7613(02)00262-5/ATTACHMENT/07CBFE25-B73E-4D14-AB80-8D22B067C19F/MMC12.AVI
16. Combs J, Kim SJ, Tan S, Ligon LA, Holzbaur ELF, Kuhn J, et al. Recruitment of Dynein to the Jurkat Immunological Synapse. *Proc Natl Acad Sci* (2006) 103:14883–8. doi: 10.1073/PNAS.0600914103
17. Liu X, Kapoor TM, Chen JK, Huse M. Diacylglycerol Promotes Centrosome Polarization in T Cells via Reciprocal Localization of Dynein and Myosin II. *Proc Natl Acad Sci USA* (2013) 110:11976–81. doi: 10.1073/pnas.1306180110
18. Yi J, Wu X, Chung AH, Chen JK, Kapoor TM, Hammer JA. Centrosome Repositioning in T Cells Is Biphasic and Driven by Microtubule End-on Capture-Shrinkage. *J Cell Biol* (2013) 202:779–92. doi: 10.1083/jcb.201301004
19. Burkhardt JK, McIlvain JMJ, Sheetz MP, Argon Y. Lytic Granules From Cytotoxic T Cells Exhibit Kinesin-Dependent Motility on Microtubules In Vitro. *J Cell Sci* (1993) 104:151–62. doi: 10.1242/jcs.104.1.151
20. Stinchcombe JC, Majorovits E, Bossi G, Fuller S, Griffiths GM. Centrosome Polarization Delivers Secretory Granules to the Immunological Synapse. *Nature* (2006) 443:462–5. doi: 10.1038/nature05071
21. Kurowska M, Goudin N, Nehme NT, Court M, Garin J, Fischer A, et al. Terminal Transport of Lytic Granules to the Immune Synapse Is Mediated by the Kinesin-1/Slp3/Rab27a Complex. *Blood* (2012) 119:3879–89. doi: 10.1182/BLOOD-2011-09-382556
22. Mentlik AN, Sanborn KB, Holzbaur EL, Orange JS. Rapid Lytic Granule Convergence to the MTOC in Natural Killer Cells Is Dependent on Dynein But Not Cytolytic Commitment. *Mol Biol Cell* (2010) 21:2241–56. doi: 10.1091/MBC.E09-11-0930/ASSET/IMAGES/LARGE/ZMK0131094880009.JPEG
23. Beal AM, Anikeeva N, Varma R, Cameron TO, Vasiliver-Shamis G, Norris PJ, et al. Kinetics of Early T Cell Receptor Signaling Regulate the Pathway of Lytic Granule Delivery to the Secretory Domain. *Immunity* (2009) 31:632–42. doi: 10.1016/J.IMMUNI.2009.09.004/ATTACHMENT/C3B35A36-2B16-4DF4-8530-10B9F0DED128/MMC3.MOV
24. Maul-Pavicic A, Chiang SCC, Rensing-Ehl A, Jessen B, Fauriat C, Wood SM, et al. ORAI1-Mediated Calcium Influx is Required for Human Cytotoxic Lymphocyte Degranulation and Target Cell Lysis. *Proc Natl Acad Sci USA* (2011) 108:3324–9. doi: 10.1073/PNAS.1013285108/-/DCSUPPLEMENTAL
25. Davis LC, Morgan AJ, Chen JL, Snead CM, Bloor-Young D, Shenderov E, et al. NAADP Activates Two-Pore Channels on T Cell Cytolytic Granules to Stimulate Exocytosis and Killing. *Curr Biol* (2012) 22:2331–7. doi: 10.1016/J.CUB.2012.10.035/ATTACHMENT/D714AAC4-32B1-4CAD-A054-8CC8D65EA175/MMC1.PDF
26. Ritter AT, Kapnick SM, Murugesan S, Schwartzberg PL, Griffiths GM, Lippincott-Schwartz J. Cortical Actin Recovery at the Immunological Synapse Leads to Termination of Lytic Granule Secretion in Cytotoxic T Lymphocytes. *Proc Natl Acad Sci USA* (2017) 114:E6585–94. doi: 10.1073/pnas.1710751114
27. Gawden-Bone CM, Frazer GL, Richard AC, Ma CY, Strege K, Griffiths GM. PIP5 Kinases Regulate Membrane Phosphoinositide and Actin Composition for Targeted Granule Secretion by Cytotoxic Lymphocytes. *Immunity* (2018) 49:427–437.e4. doi: 10.1016/j.immuni.2018.08.017
28. Husson J, Chemin K, Bohineust A, Hivroz C, Henry N. Force Generation Upon T Cell Receptor Engagement. *PloS One* (2011) 6(5):e19680. doi: 10.1371/journal.pone.0019680
29. Bashour KT, Gondarenko A, Chen H, Shen K, Liu X, Huse M, et al. CD28 and CD3 Have Complementary Roles in T-Cell Traction Forces. *Proc Natl Acad Sci USA* (2014) 111:2241–6. doi: 10.1073/pnas.1315606111
30. Hui KL, Balagopalan L, Samelson LE, Upadhyaya A. Cytoskeletal Forces During Signaling Activation in Jurkat T-Cells. *Mol Biol Cell* (2015) 26:685–95. doi: 10.1091/mbc.E14-03-0830
31. Basu R, Whitlock BM, Husson J, Le Floc'h A, Jin W, Oyler-Yaniv A, et al. Cytotoxic T Cells Use Mechanical Force to Potentiate Target Cell Killing. *Cell* (2016) 165:100–10. doi: 10.1016/j.cell.2016.01.021
32. Hui KL, Upadhyaya A. Dynamic Microtubules Regulate Cellular Contractility During T-Cell Activation. *Proc Natl Acad Sci USA* (2017) 114(21):E4175–E4183. doi: 10.1073/pnas.1614291114
33. Tamzalit F, Wang MS, Jin W, Tello-Lafoz M, Boyko V, Heddleston JM, et al. Interfacial Actin Protrusions Mechanically Enhance Killing by Cytotoxic T Cells. *Sci Immunol* (2019) 4(33):eaav5445. doi: 10.1126/sciimmunol.aav5445
34. Tamzalit F, Tran D, Jin W, Boyko V, Bazzi H, Kepecs A, et al. Centrioles Control the Capacity, But Not the Specificity, of Cytotoxic T Cell Killing. *Proc Natl Acad Sci USA* (2020) 117:4310–9. doi: 10.1073/pnas.1913220117/-/DCSupplemental
35. Rosengren AT, Nyman TA, Lahesmaa R. Proteome Profiling of Interleukin-12 Treated Human T Helper Cells. *Proteomics* (2005) 5:3137–41. doi: 10.1002/pmic.200401151
36. Sit ST, Manser E. Rho GTPases and Their Role in Organizing the Actin Cytoskeleton. *J Cell Sci* (2011) 124:679–83. doi: 10.1242/jcs.064964
37. Floc'h A, Tanaka Y, Bantilan NS, Voisinne G, Altan-Bonnet G, Fukui Y, et al. Annular PIP3 Accumulation Controls Actin Architecture and Modulates Cytotoxicity at the Immunological Synapse. *J Exp Med* (2013) 210:2721–37. doi: 10.1084/jem.20131324
38. Starbeck-Miller GR, Xue HH, Harty JT. IL-12 and Type I Interferon Prolong the Division of Activated CD8 T Cells by Maintaining High-Affinity IL-2 Signaling In Vivo. *J Exp Med* (2014) 211:105–20. doi: 10.1084/jem.20130901
39. Wu SW, Li L, Wang Y, Xiao Z. CTL-Derived Exosomes Enhance the Activation of CTLs Stimulated by Low-Affinity Peptides. *Front Immunol* (2019) 10:1274. doi: 10.3389/fimmu.2019.01274
40. Zhang L, Manirarora JN, Wei CH. Evaluation of Immunosuppressive Function of Regulatory T Cells Using a Novel *In Vitro* Cytotoxicity Assay. *Cell Biosci* (2014) 4(1):1–5. doi: 10.1186/2045-3701-4-51
41. Gerner MY, Casey KA, Mescher MF. Defective MHC Class II Presentation by Dendritic Cells Limits CD4 T Cell Help for Antitumor CD8 T Cell Responses. *J Immunol* (2008) 181:155–64. doi: 10.4049/JIMMUNOL.181.1.155
42. Gerner MY, Mescher MF. Antigen Processing and MHC-II Presentation by Dermal and Tumor-Infiltrating Dendritic Cells. *J Immunol* (2009) 182:2726–37. doi: 10.4049/JIMMUNOL.0803479
43. Rey I, Garcia DA, Wheatley BA, Song W, Upadhyaya A. Biophysical Techniques to Study B Cell Activation: Single-Molecule Imaging and Force Measurements. *Methods Mol Biol* (2018) 1707:51–68. doi: 10.1007/978-1-4939-7474-0_4
44. Hebert B, Costantino S, Wiseman PW. Spatiotemporal Image Correlation Spectroscopy (STICS) Theory, Verification, and Application to Protein Velocity Mapping in Living CHO Cells. *Biophys J* (2005) 88:3601–14. doi: 10.1529/biophysj.104.054874
45. Ashdown GW, Owen DM. Spatio-Temporal Image Correlation Spectroscopy and Super-Resolution Microscopy to Quantify Molecular Dynamics in T Cells. *Methods* (2018) 140–141:112–8. doi: 10.1016/j.ymeth.2018.01.017
46. Jaqaman K, Loerke D, Mettlen M, Kuwata H, Grinstein S, Schmid SL, et al. Robust Single-Particle Tracking in Live-Cell Time-Lapse Sequences. *Nat Methods* (2008) 5:695–702. doi: 10.1038/nmeth.1237

47. Tinevez JY, Perry N, Schindelin J, Hoopes GM, Reynolds GD, Laplantine E, et al. TrackMate: An Open and Extensible Platform for Single-Particle Tracking. *Methods* (2017) 115:80–90. doi: 10.1016/J.YMETH.2016.09.016
48. Tarantino N, Tinevez J-Y, Crowell EF, Boisson B, Henriques R, Mhlanga M, et al. TNF and IL-1 Exhibit Distinct Ubiquitin Requirements for Inducing NEMO–IKK Supramolecular Structures. *J Cell Biol* (2014) 204:231–45. doi: 10.1083/JCB.201307172
49. Butler JP, Tolić-Nørrelykke IM, Fabry B, Fredberg JJ. Traction Fields, Moments, and Strain Energy That Cells Exert on Their Surroundings. *Am J Physiol Cell Physiol* (2002) 282:595–605. doi: 10.1152/AJPCELL.00270.2001
50. Han SJ, Oak Y, Groisman A, Danuser G. Traction Microscopy to Identify Force Modulation in Subresolution Adhesions. *Nat Methods* (2015) 12:653–6. doi: 10.1038/nmeth.3430
51. Valenzuela J, Schmidt C, Mescher M. The Roles of IL-12 in Providing a Third Signal for Clonal Expansion of Naive CD8 T Cells. *J Immunol* (2002) 169:6842–9. doi: 10.4049/JIMMUNOL.169.12.6842
52. Lam Hui K, Wang C, Grooman B, Wayt J, Upadhyaya A. Membrane Dynamics Correlate With Formation of Signaling Clusters During Cell Spreading. *Biophys J* (2012) 102:1524. doi: 10.1016/J.BPJ.2012.02.015
53. Wagh K, Wheatley BA, Traver MK, Hussain I, Schaefer BC, Upadhyaya A. Bcl10 Is Associated With Actin Dynamics at the T Cell Immune Synapse. *Cell Immunol* (2020) 356:104161. doi: 10.1016/j.cellimm.2020.104161
54. Rak GD, Mace EM, Banerjee PP, Svitkina T, Orange JS. Natural Killer Cell Lytic Granule Secretion Occurs Through a Pervasive Actin Network at the Immune Synapse. *PloS Biol* (2011) 9:e1001151. doi: 10.1371/journal.pbio.1001151
55. Carisey AF, Mace EM, Saeed MB, Davis DM, Orange JS. Nanoscale Dynamism of Actin Enables Secretory Function in Cytolytic Cells. *Curr Biol* (2018) 28(4):489–502. doi: 10.1016/j.cub.2017.12.044
56. Liu D, Meckel T, Long EO. Distinct Role of Rab27a in Granule Movement at the Plasma Membrane and in the Cytosol of NK Cells. *PloS One* (2010) 5: e12870. doi: 10.1371/JOURNAL.PONE.0012870
57. Johnson JL, Monfregola J, Napolitano G, Kiosses WB, Catz SD. Vesicular Trafficking Through Cortical Actin During Exocytosis Is Regulated by the Rab27a Effector JFC1/Slp1 and the RhoA-GTPase-Activating Protein Gem-Interacting Protein. *Mol Biol Cell* (2012) 23:1902–16. doi: 10.1091/MBC.E11-12-1001/ASSET/IMAGES/LARGE/1902FIG8.JPEG
58. Martina JA, Wu XS, Catalfamo M, Sakamoto T, Yi C, Hammer JAIII. Imaging of Lytic Granule Exocytosis in CD8+ Cytotoxic T Lymphocytes Reveals a Modified Form of Full Fusion. *Cell Immunol* (2011) 271:267. doi: 10.1016/J.CELLIMM.2011.07.004
59. Saxton MJ. Modeling 2D and 3D Diffusion. *From Methods Mol Biol* (2007) 400:295–321. doi: 10.1007/978-1-59745-519-0_20
60. Murugesan S, Hong J, Yi J, Li D, Beach JR, Shao L, et al. Formin-Generated Actomyosin Arcs Propel T Cell Receptor Microcluster Movement at the Immune Synapse. *J Cell Biol* (2016) 215:383–99. doi: 10.1083/jcb.201603080
61. Babich A, Li S, O'Connor RS, Milone MC, Freedman BD, Burkhardt JK. F-Actin Polymerization and Retrograde Flow Drive Sustained Plcγ1 Signaling During T Cell Activation. *J Cell Biol* (2012) 197:775–87. doi: 10.1083/jcb.201201018
62. Kumari S, Depoil D, Martinelli R, Judokusumo E, Carmona G, Gertler FB, et al. Actin Foci Facilitate Activation of the Phospholipase C-γ in Primary T Lymphocytes *via* the WASP Pathway. *Elife* (2015) 2015:1–31. doi: 10.7554/eLife.04953
63. Blumenthal D, Burkhardt JK. Multiple Actin Networks Coordinate Mechanotransduction at the Immunological Synapse. *J Cell Biol* (2020) 219(2):e201911058. doi: 10.1083/jcb.201911058
64. Campi G, Varma R, Dustin ML. Actin and Agonist MHC–peptide Complex–Dependent T Cell Receptor Microclusters as Scaffolds for Signaling. *J Exp Med* (2005) 202:1031–6. doi: 10.1084/JEM.20051182
65. Varma R, Campi G, Yokosuka T, Saito T, Dustin ML. T Cell Receptor-Proximal Signals Are Sustained in Peripheral Microclusters and Terminated in the Central Supramolecular Activation Cluster. *Immunity* (2006) 25:117–27. doi: 10.1016/J.IMMUNI.2006.04.010/ATTACHMENT/8CD3EE26-CE73-4C66-9A54-565816C034AE/MMC7.MOV
66. Kaizuka Y, Douglass AD, Varma R, Dustin ML, Vale RD. Mechanisms for Segregating T Cell Receptor and Adhesion Molecules During Immunological Synapse Formation in Jurkat T Cells. *Proc Natl Acad Sci* (2007) 104:20296–301. doi: 10.1073/PNAS.0710258105
67. Rey-Suarez I, Rogers N, Kerr S, Shroff H, Upadhyaya A. Actomyosin Dynamics Modulate Microtubule Deformation and Growth During T Cell Activation. *Mol Biol Cell* (2021) 32(18):1641–53. doi: 10.1091/mbc.E20-10-0685
68. Akhmanova A, Hoogenraad CC. Microtubule Plus-End-Tracking Proteins: Mechanisms and Functions. *Curr Opin Cell Biol* (2005) 17:47–54. doi: 10.1016/J.CEB.2004.11.001
69. Alibert C, Goud B, Manneville J-B. Are Cancer Cells Really Softer Than Normal Cells? *Biol Cell* (2017) 109:167–89. doi: 10.1111/boc.201600078
70. Watanabe T, Kuramochi H, Takahashi A, Imai K, Katsuta N, Nakayama T, et al. Higher Cell Stiffness Indicating Lower Metastatic Potential in B16 Melanoma Cell Variants and in (–)-Epigallocatechin Gallate-Treated Cells. *J Cancer Res Clin Oncol* (2012) 138(5):859–66. doi: 10.1007/S00432-012-1159-5
71. Xu W, Mezencev R, Kim B, Wang L, McDonald J, Sulchek T. Cell Stiffness Is a Biomarker of the Metastatic Potential of Ovarian Cancer Cells. *PloS One* (2012) 7:e46609. doi: 10.1371/JOURNAL.PONE.0046609
72. Uehata M, Ishizaki T, Satoh H, Ono T, Kawahara T, Morishita T, et al. Calcium Sensitization of Smooth Muscle Mediated by a Rho-Associated Protein Kinase in Hypertension. *Nat* (1997) 389(6654):990–4. doi: 10.1038/40187
73. Curtsinger JM, Mescher MF. Inflammatory Cytokines as a Third Signal for T Cell Activation. *Curr Opin Immunol* (2010) 22:333–40. doi: 10.1016/j.coi.2010.02.013
74. Valenzuela JO, Hammerbeck CD, Mescher MF. Cutting Edge: Bcl-3 Up-Regulation by Signal 3 Cytokine (IL-12) Prolongs Survival of Antigen-Activated CD8 T Cells. *J Immunol* (2005) 174:600–4. doi: 10.4049/jimmunol.174.2.600
75. Pipkin ME, Sacks JA, Cruz-Guilloty F, Lichtenheld MG, Bevan MJ, Rao A. Interleukin-2 and Inflammation Induce Distinct Transcriptional Programs That Promote the Differentiation of Effector Cytolytic T Cells. *Immunity* (2010) 32:79. doi: 10.1016/J.IMMUNI.2009.11.012
76. Vacaflores A, Freedman SN, Chapman NM, Houtman JCD. Pretreatment of Activated Human CD8 T Cells With IL-12 Leads to Enhanced TCR-Induced Signaling and Cytokine Production. *Mol Immunol* (2017) 81:1–15. doi: 10.1016/j.molimm.2016.11.008
77. Lin CH, Espreafico EM, Mooseker MS, Forscher P. Myosin Drives Retrograde F-Actin Flow in Neuronal Growth Cones. *Neuron* (1996) 16:769–82. doi: 10.1016/S0896-6273(00)80097-5
78. Wilson CA, Tsuchida MA, Allen GM, Barnhart EL, Applegate KT, Yam PT, et al. Myosin II Contributes to Cell-Scale Actin Network Treadmilling Through Network Disassembly. *Nat* (2010) 465(7296):373–7. doi: 10.1038/nature08994
79. Colin-York H, Javanmardi Y, Skamrahl M, Kumari S, Chang VT, Khuon S, et al. Cytoskeletal Control of Antigen-Dependent T Cell Activation. *Cell Rep* (2019) 26:3369–3379.e5. doi: 10.1016/j.celrep.2019.02.074
80. Gardel ML, Sabass B, Ji L, Danuser G, Schwarz US, Waterman CM. Traction Stress in Focal Adhesions Correlates Biphasically With Actin Retrograde Flow Speed. *J Cell Biol* (2008) 183:999–1005. doi: 10.1083/jcb.200810060
81. Yoo JK, Cho JH, Lee SW, Sung YC. IL-12 Provides Proliferation and Survival Signals to Murine CD4 + T Cells Through Phosphatidylinositol 3-Kinase/Akt Signaling Pathway. *J Immunol* (2002) 169:3637–43. doi: 10.4049/jimmunol.169.7.3637
82. Garcia CA, Wang H, Benakanakere MR, Barrett E, Kinane DF, Martin M. C-Jun Controls the Ability of IL-12 to Induce IL-10 Production From Human Memory CD4+ T Cells. *J Immunol* (2009) 183:4475–82. doi: 10.4049/JIMMUNOL.0901283
83. Chauveau A, Floc'h A, Bantilan NS, Koretzky GA, Huse M. Diacylglycerol Kinase α Establishes T Cell Polarity by Shaping Diacylglycerol Accumulation at the Immunological Synapse. *Sci Signal* (2014) 7:ra82–2. doi: 10.1126/SCISIGNAL.2005287
84. Colin A, Singaravelu P, Théry M, Blanchoin L, Gueroui Z. Actin-Network Architecture Regulates Microtubule Dynamics. *Curr Biol* (2018) 28:2647–2656.e4. doi: 10.1016/J.CUB.2018.06.028
85. Dogterom M, Koenderink GH. Actin–Microtubule Crosstalk in Cell Biology. *Nat Rev Mol Cell Biol* (2018) 20(1):38–54. doi: 10.1038/s41580-018-0067-1

86. Gorman JA, Babich A, Dick CJ, Schoon RA, Koenig A, Gomez TS, et al. The Cytoskeletal Adaptor Protein IQGAP1 Regulates TCR-Mediated Signaling and Filamentous Actin Dynamics. *J Immunol* (2012) 188:6135–44. doi: 10.4049/JIMMUNOL.1103487
87. Lim WM, Ito Y, Sakata-Sogawa K, Tokunaga M. CLIP-170 Is Essential for MTOC Repositioning During T Cell Activation by Regulating Dynein Localisation on the Cell Surface. *Sci Rep* (2018) 8(1):1–12. doi: 10.1038/s41598-018-35593-z
88. Juzans M, Cuche C, Rose T, Mastrogiovanni M, Bochet P, Di Bartolo V, et al. Adenomatous Polyposis Coli Modulates Actin and Microtubule Cytoskeleton at the Immunological Synapse to Tune CTL Functions. *ImmunoHorizons* (2020) 4:363–81. doi: 10.4049/IMMUNOHORIZONS.2000044
89. Monks CRF, Freiberg BA, Kupfer H, Sciaky N, Kupfer A. Three-Dimensional Segregation of Supramolecular Activation Clusters in T Cells. *Nat* (1998) 395(6697):82–6. doi: 10.1038/25764
90. Somersalo K, Anikeeva N, Sims TN, Thomas VK, Strong RK, Spies T, et al. Cytotoxic T Lymphocytes Form an Antigen-Independent Ring Junction. *J Clin Invest* (2004) 113:49–57. doi: 10.1172/JCI19337
91. Doh J, Irvine DJ. Immunological Synapse Arrays: Patterned Protein Surfaces That Modulate Immunological Synapse Structure Formation in T Cells. *Proc Natl Acad Sci USA* (2006) 103:5700–5. doi: 10.1073/pnas.0509404103
92. Anikeeva N, Somersalo K, Sims TN, Thomas VK, Dustin ML, Sykulev Y. Distinct Role of Lymphocyte Function-Associated Antigen-1 in Mediating Effective Cytolytic Activity by Cytotoxic T Lymphocytes. *Proc Natl Acad Sci* (2005) 102:6437–42. doi: 10.1073/PNAS.0502467102
93. Tabdanov E, Gondarenko S, Kumari S, Liapis A, Dustin ML, Sheetz MP, et al. Micropatterning of TCR and LFA-1 Ligands Reveals Complementary Effects on Cytoskeleton Mechanics in T Cells. *Integr Biol (United Kingdom)* (2015) 7:1272–84. doi: 10.1039/c5ib00032g
94. Jankowska KI, Williamson EK, Roy NH, Blumenthal D, Chandra V, Baumgart T, et al. Integrins Modulate T Cell Receptor Signaling by Constraining Actin Flow at the Immunological Synapse. *Front Immunol* (2018) 9:25. doi: 10.3389/fimmu.2018.00025
95. Roy NH, MacKay JL, Robertson TF, Hammer DA, Burkhardt JK. Crk Adaptor Proteins Mediate Actin-Dependent T Cell Migration and Mechanosensing Induced by the Integrin LFA-1. *Sci Signal* (2018) 11 (560):eaat3178. doi: 10.1126/scisignal.aat3178
96. Comrie WA, Burkhardt JK. Action and Traction: Cytoskeletal Control of Receptor Triggering at the Immunological Synapse. *Front Immunol* (2016) 7:68:68. doi: 10.3389/fimmu.2016.00068
97. Blumenthal D, Chandra V, Avery L, Burkhardt JK. Mouse T Cell Priming Is Enhanced by Maturation-Dependent Stiffening of the Dendritic Cell Cortex. *Elife* (2020) 9:1–44. doi: 10.7554/eLife.55995
98. Judokusumo E, Tabdanov E, Kumari S, Dustin ML, Kam LC. Mechanosensing in T Lymphocyte Activation. *Biophys J* (2012) 102:L5–7. doi: 10.1016/j.bpj.2011.12.011
99. Wahl A, Dinet C, Dillard P, Nassereddine A, Puech PH, Limozin L, et al. Biphasic Mechanosensitivity of T Cell Receptor-Mediated Spreading of Lymphocytes. *Proc Natl Acad Sci USA* (2019) 116:5908–13. doi: 10.1073/pnas.1811516116
100. Kim ST, Takeuchi K, Sun ZYJ, Touma M, Castro CE, Fahmy A, et al. The αβ T Cell Receptor Is an Anisotropic Mechanosensor. *J Biol Chem* (2009) 284:31028–37. doi: 10.1074/jbc.M109.052712
101. Liu B, Chen W, Evavold BD, Zhu C. Accumulation of Dynamic Catch Bonds Between TCR and Agonist Peptide-MHC Triggers T Cell Signaling. *Cell* (2014) 157:357–68. doi: 10.1016/j.cell.2014.02.053
102. Li Y-C, Chen B-M, Wu P-C, Cheng T-L, Kao L-S, Tao M-H, et al. Cutting Edge: Mechanical Forces Acting on T Cells Immobilized *via* the TCR Complex Can Trigger TCR Signaling. *J Immunol* (2010) 184:5959–63. doi: 10.4049/jimmunol.0900775
103. Das DK, Feng Y, Mallis RJ, Li X, Keskin DB, Hussey RE, et al. Force-Dependent Transition in the T-Cell Receptor β-Subunit Allosterically Regulates Peptide Discrimination and pMHC Bond Lifetime. *Proc Natl Acad Sci USA* (2015) 112:1517–22. doi: 10.1073/pnas.1424829112
104. Liu Y, Blanchfield L, Pui-Yan Ma V, Andargachew R, Galior K, Liu Z, et al. DNA-Based Nanoparticle Tension Sensors Reveal That T-Cell Receptors Transmit Defined pN Forces to Their Antigens for Enhanced Fidelity. *Proc Natl Acad Sci USA* (2016) 113:5610–5. doi: 10.1073/pnas.1600163113

Conflict of Interest: The authors declare that the research was conducted in the absence of any commercial or financial relationships that could be construed as a potential conflict of interest.

frontiers in Immunology

ORIGINAL RESEARCH
published: 31 March 2022
doi: 10.3389/fimmu.2022.805076

Emergent Temporal Signaling in Human Trabecular Meshwork Cells: Role of TRPV4-TRPM4 Interactions

Oleg Yarishkin[1†], Tam T. T. Phuong[1†], Felix Vazquez-Chona[1], Jacques Bertrand[2], Joseph van Battenburg-Sherwood[2], Sarah N. Redmon[1], Christopher N. Rudzitis[1,3], Monika Lakk[1], Jackson M. Baumann[1,4], Marc Freichel[5], Eun-Mi Hwang[6], Darryl Overby[2] and David Križaj[1,3,4,7]*

[1] Department of Ophthalmology and Visual Sciences, University of Utah School of Medicine, Salt Lake City, United States, [2] Department of Bioengineering, Imperial College London, London, United Kingdom, [3] Interdepartmental Program in Neuroscience, University of Utah, Salt Lake City, United States, [4] Department of Bioengineering, University of Utah, Salt Lake City, United States, [5] Institute of Pharmacology, Heidelberg University, Heidelberg, Germany, [6] Center for Functional Connectomics, Korea Institute of Science and Technology (KIST), Seoul, South Korea, [7] Department of Neurobiology, University of Utah, Salt Lake City, United States

OPEN ACCESS

Edited by:
Ruchi Bansal,
University of Twente, Netherlands

Reviewed by:
Günther Schlunck,
University of Freiburg, Germany
Jonathan Soboloff,
Temple University, United States

***Correspondence:**
David Križaj
david.krizaj@hsc.utah.edu

†These authors have contributed equally to this work

Specialty section:
This article was submitted to Molecular Innate Immunity, a section of the journal Frontiers in Immunology

Received: *29 October 2021*
Accepted: *02 March 2022*
Published: *31 March 2022*

Citation:
Yarishkin O, Phuong TTT, Vazquez-Chona F, Bertrand J, van Battenburg-Sherwood J, Redmon SN, Rudzitis CN, Lakk M, Baumann JM, Freichel M, Hwang EM, Overby D and Križaj D (2022) Emergent Temporal Signaling in Human Trabecular Meshwork Cells: Role of TRPV4-TRPM4 Interactions. Front. Immunol. 13:805076. doi: 10.3389/fimmu.2022.805076

Trabecular meshwork (TM) cells are phagocytic cells that employ mechanotransduction to actively regulate intraocular pressure. Similar to macrophages, they express scavenger receptors and participate in antigen presentation within the immunosuppressive milieu of the anterior eye. Changes in pressure deform and compress the TM, altering their control of aqueous humor outflow but it is not known whether transducer activation shapes temporal signaling. The present study combines electrophysiology, histochemistry and functional imaging with gene silencing and heterologous expression to gain insight into Ca^{2+} signaling downstream from TRPV4 (Transient Receptor Potential Vanilloid 4), a stretch-activated polymodal cation channel. Human TM cells respond to the TRPV4 agonist GSK1016790A with fluctuations in intracellular Ca^{2+} concentration ($[Ca^{2+}]_i$) and an increase in $[Na^+]_i$. $[Ca^{2+}]_i$ oscillations coincided with monovalent cation current that was suppressed by BAPTA, Ruthenium Red and the TRPM4 (Transient Receptor Potential Melastatin 4) channel inhibitor 9-phenanthrol. TM cells expressed TRPM4 mRNA, protein at the expected 130-150 kDa and showed punctate TRPM4 immunoreactivity at the membrane surface. Genetic silencing of TRPM4 antagonized TRPV4-evoked oscillatory signaling whereas TRPV4 and TRPM4 co-expression in HEK-293 cells reconstituted the oscillations. Membrane potential recordings suggested that TRPM4-dependent oscillations require release of Ca^{2+} from internal stores. 9-phenanthrol did not affect the outflow facility in mouse eyes and eyes from animals lacking TRPM4 had normal intraocular pressure. Collectively, our results show that TRPV4 activity initiates dynamic calcium signaling in TM cells by stimulating TRPM4 channels and intracellular Ca^{2+} release. It is possible that TRPV4-TRPM4 interactions downstream from the tensile and compressive impact of intraocular pressure contribute to homeostatic regulation and pathological remodeling within the conventional outflow pathway.

Keywords: Trabecular meshwork, TRPV4, TRPM4, calcium oscillations, glaucoma, conventional outflow facility, GSK1016790, immune

INTRODUCTION

Biomechanical factors such as intraocular pressure (IOP) are an important determinant of the ocular environment, with roles in growth, cellular signaling that subserve ocular health and pathology (1). IOP is homeostatically regulated by the trabecular meshwork (TM), a mechanosensitive phagocytic tissue composed of smooth muscle-, macrophage- and fibroblast-like cells that function as an adaptive valve for outflow of aqueous humor from the anterior eye (1, 2). In healthy cells, acute IOP elevations engender an increase in outflow resistance that is followed by an adaptive response that guides gradual recovery of tissue permeability to fluid flow (3) whereas chronic mechanical stress triggers transdifferentiation of TM cells into stiff and contractile myofibroblasts that subserve a lasting increase in outflow resistance (4–6). TM cells express major histocompatibility complex proteins and Toll-like receptor 4 receptors (TLR4) and help maintain the immune privilege in the anterior eye *via* phagocytosis and TGFβ2 signaling (7). TLR4 expression is increased in glaucoma, TGFβ-TLR4 crosstalk is involved in production of ECM and regulation of IOP, whereas a mutation in TLR4 inhibited TGFβ2-induced ocular hypertension in mice (7). These observations suggest that the innate immune system might be involved in pressure-dependent differentiation of TM cells into profibrogenic myofibroblasts (8) yet the molecular mechanisms that underlie pressure-dependent TRL4 activation, TGFβ signaling and ECM remodeling remain unknown. Recent studies showed that TM cells sense acute and chronic mechanical stressors *via* arrays of mechanosensitive proteins that include integrins, the cytoskeleton, and stretch-activated ion channels (SACs) (9–11) such as TRPV4. This nonselective cation channel responds to TM substrate deformation with Ca^{2+} influx that regulates cytoskeletal and lipid dynamics, Rho signaling and cell-ECM interactions to facilitate myofibroblast differentiation (12–14). Excessive TRPV4 activity was suggested to drive the pressure-induced increase in TM stiffness and contractility (5, 14, 15) but it is not known how the channel responds to sustained activation.

The human TRPV4 gene contains 16 exons that encode a protein consisting of a proline-rich (PRD) domain, phosphoinositide binding site, ankyrin repeats and a helix-turn-helix (HTH) linker domain within the N-terminus, six transmembrane domains with the pore between S5-S6, and modulatory sites (TRP domain, MAP7-binding domain, CaM/IP3R-binding domain, PDZ domain) in the C-terminus that endow the channel with sensitivity to temperature, metabolites of arachidonic acid, nociceptive and mechanical stimuli (16, 17). Gain- and loss-of-function mutations in the TRPV4 gene cause debilitating skeletal abnormalities, sensorimotor neuropathies and vision loss (18), indicating that the channel is required for homeostatic transduction of sensory information. TRPV4 overactivation and exposure to TGFβ induce transdifferentiation of epithelial, endothelial, and smooth muscle cells into hypersecretory and contractile myofibroblasts (19, 20). Interactions with a wide array of proteins (aquaporins, BK channels, kinases, actin) and processes (Ca^{2+} release from intracellular stores, receptor-operated and store-operated Ca^{2+} influx) (13, 21–24) indicate that TRPV4 exerts its functions within a multiplicity of biological contexts.

The aim of this study was to simulate sustained application of mechanical stress in the absence of confounding effects of the *in situ* milieu and attendant activation of auxiliary stretch-activated channels (SACs) such as TREK-1 and Piezo1 (10, 11). We report that continual chemical stimulation of TRPV4 channels [P_{Ca}/P_{Na} = 10 (25)] induces $[Ca^{2+}]_i$ fluctuations that require TRPM4, a Ca^{2+}-activated monovalent cation channel [P_{Ca}/P_{Na} = 0.12 (26)] that has been linked to hypertension and Ca^{2+} oscillations and Ca^{2+} release from intracellular compartments in lymphocytes and macrophages (27–30). TRPV4 and TRPM4 were also implicated in the maturation of phagocytic function, with disruption of either TRPV4 or TRPM4 signaling in monocytes and macrophages resulting in profound dysregulation of Ca^{2+} homeostasis, LPS-stimulated phagocytosis and survival (31, 32). These findings identify a mechanism that couples TM mechanosensing to endogenous oscillatory activity, with potential functions in innate immune regulation and outflow resistance in the anterior eye.

MATERIALS AND METHODS

Primary Cell Isolation and Culture

Primary trabecular meshwork cells (pTM) were isolated from juxtacanalicular and corneoscleral regions of the human donors' eyes (56 years-old male, 62 years-old female) with no recorded history of eye disease as described (10, 11, 13). The tissues were obtained through the Lions Eye Bank at the Moran Eye Center at the University of Utah and were used in concordance with the tenets of the WMA Declaration of Helsinki and the Department of Health and Human Services Belmont Report. A subset of biochemical experiments was conducted in parallel with immortalized cells (hTM), isolated from the juxtacanalicular region of the human eye (ScienCell Research Laboratories, Carlsbad, CA, USA). The cell phenotype was periodically profiled for expression of *MYOC, TIMP3, AQP1, MGP, ACTA2* (α-smooth muscle actin, αSMA) genes and DEX-induced upregulation of myocilin protein (11, 14).

Passage 2 – 6 cells were seeded onto Collagen I-coated coverslips and grown in Trabecular Meshwork Cell Medium (ScienCell, Catalog#6591; Carlsbad, CA, USA) supplemented with 2% fetal bovine serum (FBS), 100 units/ml penicillin, 100 ug/ml streptomycin, at 37°C and pH 7.4. Cells were transfected with scrambled shRNA (Sc-shRNA) or *Trpm4* shRNA using Lipofectamin™ 3000 (5 μg per 25 cm^2 tissue culture flask). shRNA -transfected cells were identified by green (GFP) or red (mCherry) fluorescence. Knockdown efficiency of TRPM4 shRNA was validated in HEK 293T cells overexpressing GFP-hTRPM4, scrambled shRNA or one of three *TRPM4* shRNA constructs. shRNA1 and shRNA2, with target sequences GGACATTGCCCAGAGTGAACT (1218–1238) and GGAAAGACCTGGCGTTCAAGT (1835–1855), showed >65% knockdown efficiency (**Supplementary Figure 1**). Experiments were conducted 3 - 4 days post- transfection.

Reagents

GSK1016790A (GSK101) is a highly specific agonist (16, 17, 23) and HC067047 (HC-06) antagonist, of TRPV4 channels. Both were

purchased from Sigma (St. Louis, MO) or Cayman Chemical (Ann Arbor, MI). Salts were purchased from Sigma (St. Louis, MO) or VWR (Radnor, PA), CBA (4-chloro-2-[[2-(2-chlorophenoxy) acetyl aminobenzoic acid from Tocris Bioscience (Minneapolis, MN), and BAPTA (1,2-Bis(2-aminophenoxy)ethane-N,N,N',N'-tetraacetic acid) from Alfa Aesar (Tewksbury, MA). The TRPM4 antagonist 9-phenanthrol (9-PA) was from Tocris Bioscience (Bristol, UK). GSK101 (1 mM), and HC-06 (20 mM) DMSO stocks were diluted in extracellular saline (98.5 mM NaCl, 5 mM KCl, 3 mM $MgCl_2$, 2 mM $CaCl_2$, 10 mM HEPES, 10 mM D-glucose, 93 mM mannitol), with final DMSO concentration not exceeding 0.1%.

Immunocytochemistry

Cells

Cells were plated on collagen Type 1-coated glass cover slip 1 day prior to fixation with the 4% PFA for 10 minutes at RT. The samples were blocked with phosphate-buffered saline containing 0.3% Triton X-100 and 5% FBS for 30 minutes at a room temperature (RT). The primary polyclonal rabbit antibody was diluted 1:1000 in PBS (2% BSA and 0.2% Triton X-100) and incubated overnight at 4°C (32). After rinsing, cells were incubated for 1 hour at RT with goat anti-mouse and goat anti-rabbit IgG (H + L) secondary antibodies conjugated to fluorophores (Alexa Fluor 488 nm, 568 nm and/or 594 nm; 1:500; Life Technologies, Carlsbad, CA, USA). Unbound antibody was rinsed, and conjugated fluorophores protected with Fluoromount-G (Southern Biotech, Birmingham, AL, USA) prior to mounting coverslips. Images were acquired on a confocal microscope (FV1200; Olympus, Center Valley, PA) at 1024 x 1024 pixels with a 20x water superobjective (1.00 N.A.; field size: 158.565 x 158.565 μm; 0.155 μm/pixel; sampling speed: 10.0 us/pixel; 12 bits/pixel). ≥50 cells per experiment were acquired for at least 4 independent experiments (n ≥ 200 in total; N ≥ 4).

Tissue Immunohistochemistry

Anterior chambers were fixed in 4% paraformaldehyde for 1 hour, cryoprotected in 15 and 30% sucrose gradients, embedded in Tissue-Tek® O.C.T. (Sakura, 4583), and cryosectioned at 12 μm, as described (13, 30). Sections were probed with a polyclonal rabbit TRPM4 antibody (1:100 (32); and aquaporin-1 mouse monoclonal antibody (1:1000; Santa Cruz Biotechnology Sc-25287). Secondary antibodies were anti-rabbit IgG DyLight 488 (Invitrogen, 35552) and anti-mouse IgG DyLight 594 (Invitrogen, 35511). Sections were coverslipped with DAPI-Fluoromount-G (Electron Microscopy Sciences, Hatfield, PA, 17984-24) and imaged with a confocal microscope. Images were acquired using identical (HV, gain, offset) parameters.

Semiquantitative Real Time-PCR

Total RNA was extracted using Arcturus PicoPure RNA Isolation Kit (ThermoFisher, Cat. No.: KIT0204) (33, 34). 100 ng of total RNA was used for reverse transcription. First-strand cDNA synthesis and PCR amplification of cDNA were performed using qScript™ XLT cDNA Supermix (Quanta Biosciences, Cat. No. 95161). The samples were run on 2% agarose gels using ethidium bromide staining along with the 100-bp DNA ladder (ThermoFisher Scientific, Waltham, MA, Cat. No.: S0323). The primers used in the study are listed in **Table 1**.

Western Blot

TM cells were detached from culture flasks by trypsinization and centrifuged at 2000 rpm for 3 minutes. The cell pellet was washed with PBS and lysed in a RIPA Buffer System (Santa Cruz Biotechnology, Dallas, TX). Cell lysates were separated by 10% SDS-PAGE followed by electrophoretic transfer to polyvinylidene difluoride membranes (Bio-Rad, Hercules CA). Membranes were blocked with 5% skim milk in PBS containing 0.1% Tween 20 and incubated at 4°C overnight with the TRPM4 antibody, following by 3 washes with PBS containing 0.1% Tween-20, blotted with HRP-conjugated GAPDH antibody for 30 min at room temperature and washed with PBS containing 0.1% Tween 20. The signals were visualized with an enhanced chemiluminescence system (FluorChem Q, Cell Biosciences, Santa Clara, CA).

Ion Imaging

Pharmacological experiments were conducted on a microscope stage in a fast-flow chamber (RC26GLP, Warner Instruments, Hamden CT) connected to a gravity-fed perfusion system. The flow rate of the solution was regulated *via* individual pinch valves (VC-6; Warner Instruments; Holliston, MA). Primary cells were loaded with Fura-2 AM (3 μM; Invitrogen/ThermoFisher Scientific) for 45 min at RT. The cells were perfused with extracellular solution containing (mM): 135 NaCl, 2.5 KCl, 1.5 $MgCl_2$, 1.8 $CaCl_2$, 10 HEPES, 5.6 D-glucose (pH = 7.4, osmolarity = 300 - 303 mOsm). Epifluorescence imaging was performed on Nikon microscopes using 40x (1.3 N.A., oil or 0.80 N.A., water) objectives, 340 nm and 380 nm excitation filters (Semrock, Lake Forest, IL, USA) and a Xenon arc lamp (DG4, Sutter Instruments). Fluorescence emission at 510 nm, in response to alternating 340/340 excitation, was captured with cooled

TABLE 1 | Primer sequences used for PCR analysis.

Name	Forward primer	Reverse primer	Product size (bp)	NCBI reference number
TRPM4	GATGCACACCACGGAGAA	AGAGCCGGAGGAAATTGCTG	91	NM_017636.4
TRPV1	GCCCAGCATGTTCCCAAATC	TGTCCCAGTAGAGACTGACCA	169	NM_080704.3
TRPV4	TCCCATTCTTGCTGACCCAC	AGGGCTGTCTGACCTCGATA	217	NM_021625.4
MYOC	CCACGTGGAGAATCGACACA	TCCAGTGGCCTAGGCAGTAT	118	NM_000261.1
AQP1	TGGAGCAAGCTCTTCCCTTG	CTGTCCTTGGGCTGCAACTA	174	NM_198098.3
GAPDH	CTCCTGTTCGACAGTCAGCC	GACTCCGACCTTCACCTTCC	89	NM_002046.5

EMCCD or CMOS cameras (Photometrics, Tucson, AZ). Data acquisition was controlled by NIS Elements 3.22 software (Nikon). Typically, ~5-10 cells per slide were averaged across ~3-6 slides per experiments, with at least 3 independent experiments ($n \geq 50$; $N \geq 3$). The experiments were performed at room temperature (20 - 22°C).

Ca^{2+} imaging. Cells were loaded with 3 μM Fura-2 AM (Invitrogen/ThermoFisher) (K_d at RT = 225 nM) for 45 min. ΔR/R (peak F_{340}/F_{380} ratio – baseline/baseline) was used to quantify the amplitude of Ca^{2+} signals (e.g (13, 35). Only transient Ca^{2+} events with amplitudes exceeding three standard deviations of baseline fluctuations were included in analysis.

Intracellular Na^+ imaging. Cells were loaded with 3 μM NaTRIUM Green™-2 AM (TEFLabs Austin, TX) for 50 – 60 min in a cell culture incubator at 37°C. Fluorescence was acquired at 484 nm excitation and 520 nm emission (Semrock, Rochester, NY). Na^+ signals were normalized to the average baseline (F/F_o) obtained at the beginning of the experiments.

Electrophysiology

Whole cell and single-channel techniques were used to record membrane currents (voltage clamp) or voltage (current clamp) (11, 35, 36). Borosilicate patch pipettes (WPI, Sarasota, FL) were pulled to resistances of 5 - 8 MΩ (P-2000; Sutter Instruments, Novato CA). The standard pipette solution contained (in mM): 125 NaCl, 10 KCl, 10 HEPES, 1 $MgCl_2$, 2 ethylene glycol-bis(β-aminoethyl ether)-N,N,N',N"-tetraacetic acid (EGTA), 0.3 Na-GTP (pH 7.3) The pipette solution for recording Ca^{2+}-activated current contained (in mM): 125 Na-gluconate, 10 HEPES, 1 $MgCl_2$, 0.01 $CaCl_2$, 0.3 Na-GTP (pH 7.3). Nominally Ca^{2+}-free pipette solution (standard) contained (in mM): 125 Na-gluconate, 10 HEPES, 1 $MgCl_2$, 5 BAPTA, 0.3 Na-GTP (pH 7.3). The standard extracellular solution contained (in mM): 135 NaCl, 2.5 KCl, 1.5 $MgCl_2$, 1.8 $CaCl_2$, 10 HEPES, 5 D-glucose (pH 7.4). The extracellular solution for recording Ca^{2+}-activated current contained (in mM): 135 Na-gluconate, 10 HEPES, 1 $MgCl_2$, 1.8 $CaCl_2$, 0.3 Na-GTP (pH 7.3). The bathing solution for excised (inside-out) patch clamp experiments contained (mM): 140 NaCl, 2.5 KCl, 1.5 $MgCl_2$, 1.8 Ca^{2+} or 10 EGTA, 5.6 D-glucose, 10 HEPES (pH 7.4, adjusted with NaOH). The pipette solution used in excised patch recordings contained 140 NaCl, 2.5 KCl, 1.5 $MgCl_2$, 1.8 $CaCl_2$, 5.6 D-glucose, 10 HEPES (pH 7.4, adjusted with NaOH). Experiments were performed at room temperature of 21-22°C.

Patch clamp data in whole-cell and single-channel configurations was acquired with a Multiclamp 700B amplifier and a Digidata 1550 interface, and controlled by Clampex 10.7 (Molecular Devices, Union City, CA). Cells were held at -100 mV or +100 mV, with currents sampled at 5 kHz, filtered at 2 kHz with an 8-pole Bessel filter and analyzed with Clampfit 10.7 (Molecular Devices) and Origin 8 Pro (Origin Lab, Northampton, MA). Whole-cell currents were elicited by voltage ramps ascending from -100 mV to 100 mV (0.2 V/sec) from the holding potential of 0 mV. The time course of Ca^{2+}-activated currents was obtained by subtracting voltage ramp-evoked currents traces recorded 40 s after obtaining the whole-cell configuration from preceding and following traces. I-V curves of Ca^{2+}-activated currents were assessed by subtracting currents recorded 40 s after obtaining the whole-cell configuration from steady state currents recorded 4 min after obtaining the whole-cell configuration.

Patch clamp combined with fluorescent imaging. Cells were loaded with a calcium indicator Fluo-4 (Invitrogen/ThermoFisher) through a patch pipette. Fluorescence signals in voltage-clamped cells were detected using the excitation filter 484 nm and the emission filter 520 nm (Semrock, Lake Forest, IL). VOCC-mediated current was recorded in the extracellular solution containing as following (mM): 115 NaCl, 2.5 KCl, 20 $BaCl_2$, 1.5 $MgCl_2$, 10 HEPES, 5.6 D-glucose.

Outflow Facility Measurement: iPerfusion

Procedures on living mice were carried out under the authority of a UK Home Office project license and adhered to the ARVO Statement for the Use of Animals in Ophthalmic and Vision Research. The outflow facility in enucleated eyes from C57BL/6J mice (N = 5 mice; 11-week-old males; Charles River UK Ltd., Margate, UK) was measured using *iPerfusion*, a custom-made microfluidic setup (37, 38). Following cervical dislocation, eyes were enucleated and affixed to a support platform using tissue glue. Eyes were submerged in a PBS bath kept at 35°C throughout the perfusion. Using a micro-manipulator under a dissection microscope, the anterior chamber was cannulated within 10 minutes of death using a glass micropipette pulled to have a 100 μm diameter beveled tip. The perfusion fluid was Dulbecco's PBS containing divalent cations and 5.5 mM glucose (DBG) that was sterile filtered (0.25 μm) prior to use.

One eye was perfused with 9-PA (25 μM) whilst the contralateral eye was perfused with vehicle (perfusion fluid containing the same concentration of DMSO). IOP was set to 9 mmHg for 1 hour to pressurize and acclimatize the eye to the perfusion environment and to allow sufficient time for 9-PA to reach the outflow tissues. Flow into the eye was then measured over 8 increasing pressure steps from 6.5 to 17 mmHg. Steady state for each step was evaluated when the ratio of the flow rate to pressure changed by less than 0.1 nl/min/mmHg per minute over a 5-minute window (37). The stable pressure, P, and flow rate, Q, were calculated over the last 4 minutes of each step, and a power-law relationship of the form

$$Q = C_r \left(\frac{P}{P_r}\right)^{\beta} P \quad \text{Eq. 1}$$

was fit to the $Q - P$ data. The reference outflow facility, C_r, represents the value of outflow facility at a reference pressure P_r of 8 mmHg, and β characterizes the non-linearity of the Q-P relationship (37). The relative difference in C_r between treated and untreated contralateral eyes was then calculated as the ratio of C_r in the treated eye relative to that in the contralateral control eye minus unity. We evaluated whether the relative difference in facility was statistically different from zero using a weighted t-test on the log-transformed data, as previously described (37). Facility values and relative changes in facility are reported in terms of the geometric mean and the 95% confidence interval on the mean.

IOP Measurement

Male and female C57BL/6J mice (JAX; Bar Harbor, ME) and homozygous pan-TRPM4 KO mice (39) were maintained in a pathogen-free facility with a 12-hour light/dark cycle and *ad libitum* access to food and water. The experimental protocol was approved by the animal ethics committee at the University of Utah and adhered to the tenets of the ARVO Statement for the Use of Animals in Ophthalmic and Vision Research. No sex differences were noted in the data, which were pooled. A TonoLab rebound tonometer was used to measure IOP in mice between noon and 2 PM, as described (13). In animals habituated to handling for several days preceding the IOP measurement. An IOP reading represents an average of 10 to 20 tonometer readings.

Statistical Analysis

Student's paired t-test or two-sample t-test (OriginPro 9.0; OriginLab, Northampton, MA) were applied to estimate statistical significance of results. $P < 0.05$ was considered statistically significant. Results are presented as the means ± S.E.M. A preprint of this article was submitted at https://biorxiv.org/cgi/content/short/2021.12.15.472700v1.

RESULTS

Activation of TRPV4 Induces Fluctuations of $[Ca^{2+}]_i$

Unstimulated TM cells from healthy donors have low basal $[Ca^{2+}]_i$ and rarely show Ca^{2+} fluctuations (13) but previous studies of mechanically evoked Ca^{2+} signaling in TM cells have been limited to short stimulation paradigms (5-10 min) (11, 13) and little is known about how the TM regulates $[Ca^{2+}]_i$ in the presence of sustained TRPV4 activity. To investigate the mechanisms that underlie Ca^{2+} signaling downstream from the channel, Fura-2-loaded human TM cells were stimulated for 30 – 45 min with bath-applied agonist GSK101 (25 nM). Agonist-evoked $[Ca^{2+}]_i$ increases peaked within 2-3 min, followed by a gradual decline to a steady plateau at ~27% of the peak (**Figures 1**, **2**). A subset (~50%) of cells showed an increase in the frequency of Ca^{2+} fluctuations during the plateau phase whereas cells treated with the TRPV4 antagonist HC067047 (HC-06; 5 μM) (**Figures 1B, C**), broad-spectrum inhibitors of TRP channels such as Ruthenium Red, or Ca^{2+} -free saline (**Figure 2**), did not exhibit this time-dependent behavior.

Oscillatory Ca^{2+} signals can reflect activation of voltage-operated mechanisms within the membrane and/or release from internal compartments. Voltage-dependent mechanisms were tested by stimulating the cells in the current-clamp mode. The agonist evoked a ~15 mV shift in the membrane potential (**Figures 3A, C**) that was maintained over the course of the experiment (e.g., 40 min after agonist application; red trace in **Figure 3B**) and was not associated with changes in temporal behavior.

L-type voltage-operated Ca^{2+} channels have been implicated in calcium oscillations and pressure-dependent contractility in smooth muscle cells (40). To test their involvement, we combined imaging in Fluo-4-loaded cells with whole-cell recording. As shown in **Figure 3D**, stepping the holding potential from the holding potential of -70 mV to 0 mV had no detectable effect on the Ca^{2+} signal. Similarly, extracellular $BaCl_2$ (20 mM) which permeates voltage-operated Ca^{2+} channels without inactivating the channel pore or stimulating Ca^{2+} release from ER stores (41–43) did not induce depolarization-evoked inward currents or Ca^{2+} spiking (**Figure 3Ei**) whereas retinal ganglion cells responded with an inward current (**Figures 3Eii, F**) that was blocked by the L-type channel blocker nimodipine (1 μM) (**Figure 3Fii**). These data suggest that TRPV4-dependent Ca^{2+} oscillations in human TM cells do not involve L-type voltage-operated Ca^{2+} channels activity.

TRPV4-Induced Ca^{2+} Fluctuations Require TRPM4

To further investigate the mechanism that underlies TRPV4-induced calcium oscillations, cells were loaded with the Na^+-sensitive indicator NaTRIUM Green-2 and exposed to GSK101. The agonist stimulated an increase in $[Na^+]_i$ in 54% (39/73) cells (5.96 ± 0.81% above baseline; $p < 0.0001$; $n = 39$). The increase in Na^+ concentration was not associated with an oscillatory component, indicating that TRPV4-induced Na^+ influx is distinct from mechanisms that subserve Ca^{2+} oscillations. We tested the potential involvement TRPM4, a Ca^{2+}-activated channel permeable to monovalent ions that has been implicated in $[Ca^{2+}]_i$ oscillations in T cells, cardiomyocytes, and smooth muscle cells (27, 28, 40) but with no known functions in the eye by exposing the cells to GSK101 in the presence of 9-phenanthrol (9-PA, 40 μM), an intracellularly acting benzoquinolizinium inhibitor of the channel (44, 45). 9-PA reversibly attenuated the increase in $[Na^+]_i$ evoked by GSK101 ($P < 0.001$) (**Figures 4A, B**), and obliterated Ca^{2+} fluctuations during the plateau response phase (**Figures 4C, D**) ($P < 0.0001$).

Histology: TM Cells Express TRPM4

Transcriptional profiling of immortalized (hTM) and primary (pTM) cells showed robust expression of TRPM4 and TRPV4 transcripts (**Figure 5A**) together with TM markers myocilin and aquaporin 1, at bp sizes that matched expected sizes for their respective DNAs. The overall levels of TRPM4 transcripts in hTM cells were comparable to TRPV4 mRNA, and ~35% of TRPV4 mRNA in primary cells (**Figure 5B**). In both cell lines, a validated antibody (32) labeled a Western blot band at ~130 kDa (**Figure 5C**), corresponding to the known M.W. of the TRPM4b protein variant (46). Confocal examination of TRPV4-immunol reactive cells and intact tissue further showed labeling of the plasma membrane and cytosolic puncta (**Figure 5Dii**) and cytosolic puncta. In the preparation from the mouse anterior eye, TRPM4-ir was distributed across the juxtacanalicular and corneoscleral TM regions (green), where it colocalized with the TM marker Collagen IV. Additional, albeit more modest, TRPM4-ir signals were also detected in the ciliary body and the retina.

Electrophysiology: TM Cells Functionally Express TRPM4

We next assessed the properties of the TRPM4-mediated current in voltage-clamped cells by probing for a Ca^{2+}-sensitive monovalent

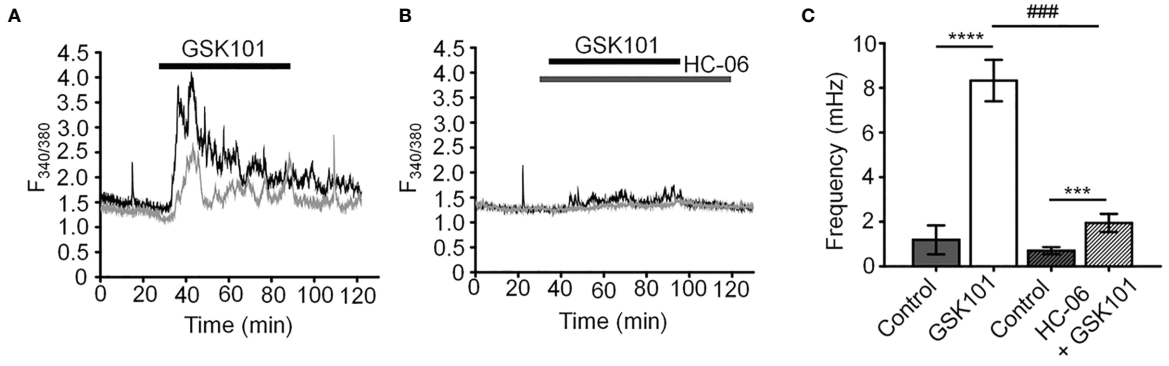

FIGURE 1 | GSK101 triggers intracellular Ca^{2+} oscillations in hTM cells. **(A)** Representative traces of $[Ca^{2+}]_i$ oscillations in GSK101 treated TM cells. **(B)** GSK101-induced oscillations are absent in cells pretreated with HC-06. **(C)** Quantification of results shown in **(A, B)**, shown as average ± S.E.M. ****P < 0.0001, ***P < 0.001 (paired-sample t-test), ###P < 0.001 (two-sample t-test), n = 49 cells and n = 38 cells for control/GSK101 and control/HC06+GSK101 groups, respectively.

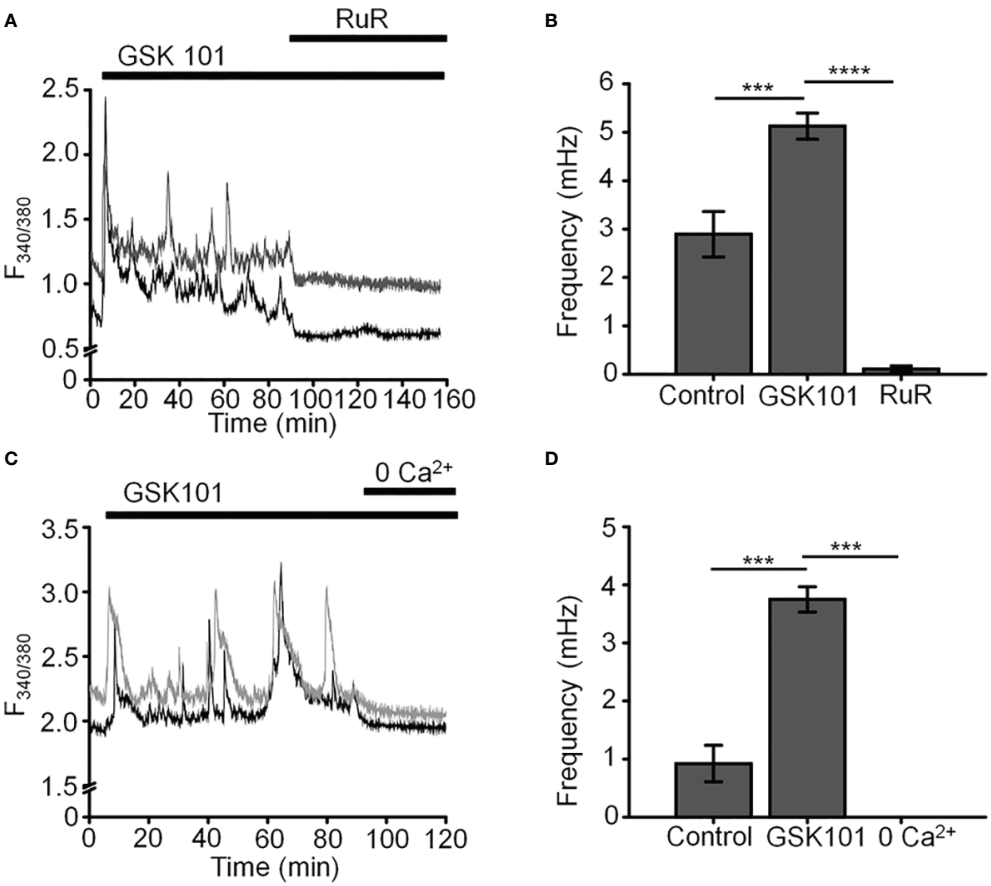

FIGURE 2 | GSK101-induced $[Ca^{2+}]_i$ oscillations requires activity of Ca^{2+} -permeable and Ca^{2+} -dependent TRP channels. Shown are representative traces. **(A, C)** GSK101-induced $[Ca^{2+}]_i$ fluctuations are abolished by the nonselective TRP blocker Ruthenium Red (RuR; 10 μM) and in the absence of free extracellular Ca^{2+}. **(B, D)** RuR and Ca^{2+}-free solution abolish GSK101 induced $[Ca^{2+}]_i$ oscillations. Mean ± S.E.M. ***P < 0.001, ****P < 0.0001, paired t-test, n = 51 and n = 43 cells for **(B, D)**, respectively.

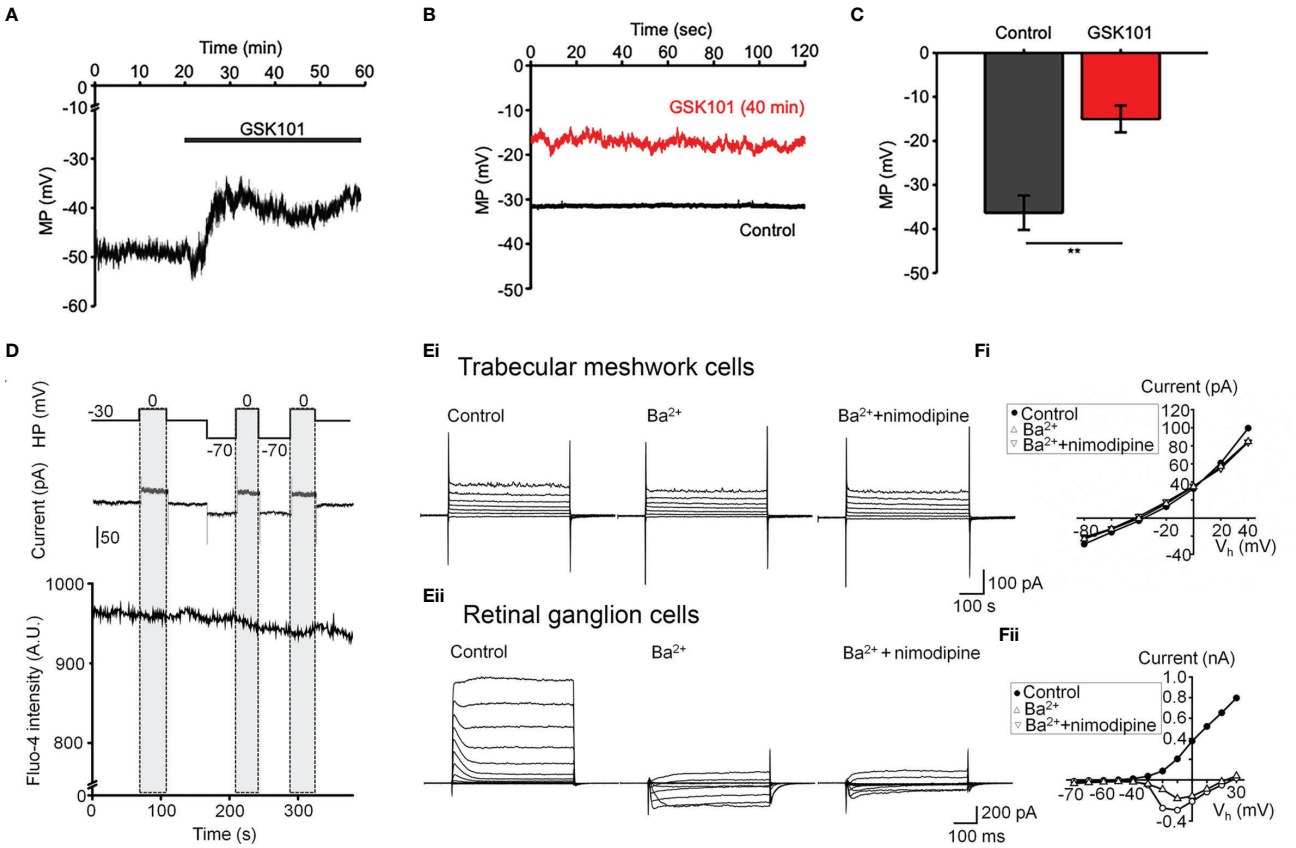

FIGURE 3 | GSK101 depolarizes TM cells, but they lack functional L-type voltage-operated Ca^{2+} channels **(A–C)** Current clamp. GSK101 depolarizes the cells, with the effect maintained over 40 min (red trace vs. black trace denoting the unstimulated control in B). **(D)** Combined whole cell recording and calcium imaging. The voltage protocol (upper trace), depolarization-evoked whole-cell current (middle trace), time-lapse of Fluo-4 fluorescence (lower trace). Shadowed bars indicate the depolarizing steps. **(E, F)** Representative whole-cell currents elicited by voltage steps in TM cells (Ei; n = 15) **(B)** and mouse retinal ganglion cells (Eii; n = 5), respectively. **(F)** Voltage-current relationships derived from cells shown in **(E)**. The current was measured at the end of each voltage pulse.

current (47, 48). Cells were dialyzed with pipette solutions containing 10 μM or zero Ca^{2+} and Ca^{2+}-activated K^+ and Cl^- conductances were minimized by replacing extra/intracellular K^+ ions (with Na^+) and Cl^- ions with gluconate (47). ~50% of cells dialyzed with the Ca^{2+}-containing solution showed time-dependent increases in inward and outward whole-cell currents. The current-voltage relationship of the Ca^{2+}-dependent current showed modest outward rectification and peaked within ~4 min after obtaining the whole-cell configuration (**Figure 6A**), had a reversal potential of 1.6 ± 2.9 mV and amplitudes of -122.7 ± 61.5 pA and 211.2 ± 93.7 pA at holding potentials of -100 mV and 100 mV, respectively, (**Figure 6B**). The current was inhibited by 9-PA (20 μM; n=7/7) and was not observed in cells dialyzed with Ca^{2+}-free solutions or exposed to bath-applied Ruthenium Red (10 μM) (n = 5/5) (**Figure 6A**).

Single channel properties of the Ca^{2+}-activated current were additionally investigated in inside-out membrane patches using symmetrical Na^+ gluconate-based pipette and extracellular solutions. Patch excision in 1.8 mM Ca^{2+}-containing saline triggered a rapidly inactivating channel with a linear current-voltage relationship (n = 15/85 patches; **Figures 6C, F**). The slope conductance of the unitary current was 18.9 ± 0.6 pS and the amplitude at 100 mV was 2.05 ± 0.04 pA (**Figures 6D–F**). The channel was facilitated at positive membrane potentials, inhibited by 9-PA (**Figures 6C, D**), and typically inactivated within ~5 min after patch excision. Its activity was abolished in Ca^{2+}-free saline (**Figure 6C**). Both whole-cell and single channel properties of the Ca^{2+}-induced current in TM cells are consistent with TRPM4 activity.

TRPM4 Is Required for TRPV4-Dependent Ca^{2+} Oscillations

To more specifically test the role of TRPM4 in $[Ca^{2+}]_i$ fluctuations, we transfected the cells with TRPM4-specific short-hairpin (shTRPM4-GFP) or "scrambled" (Sc-GFP) control shRNAs (**Figure 7A**). Of the 3 TRPM4-shRNA constructs, we utilized Sh#1 which downregulated TRPM4 mRNA by 80% (**Supplementary Figure 1**). Compared to Sc-shRNA-expressing controls, TRPM4 shRNA-transfected cells showed ~80% reduction in the frequency of TRPV4-induced Ca^{2+} fluctuations (**Figures 7B–D**).

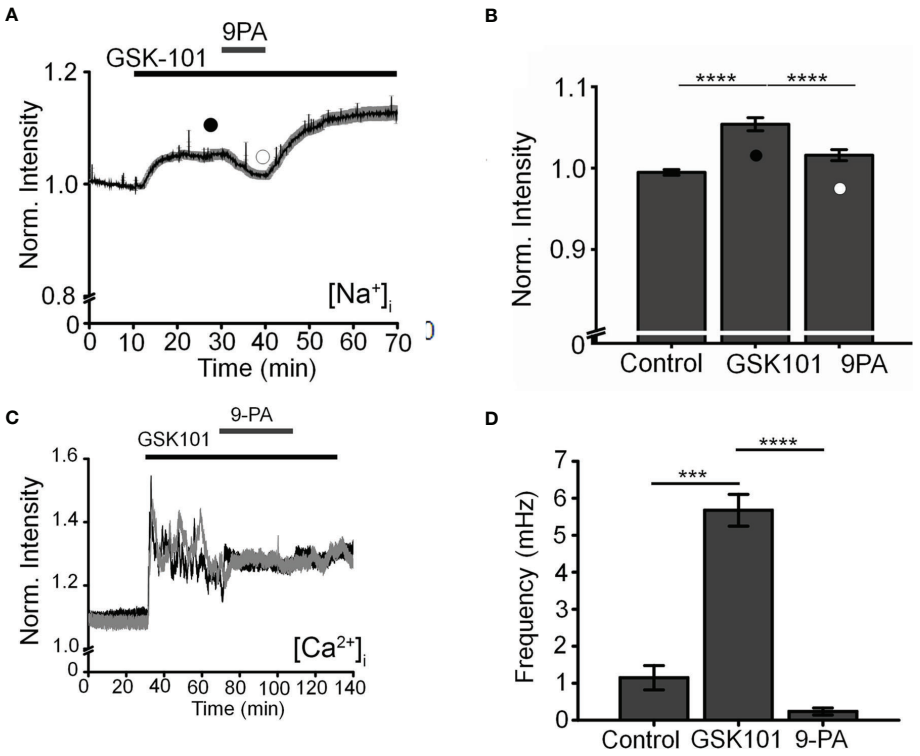

FIGURE 4 | TRPM4 mediates TRPV4-induced Na^+ influx and facilitates Ca^{2+} fluctuations. **(A).** Averaged time lapse ratio in NaTRIUM Green-loaded TM cells. GSK101-evoked increase in $[Na^+]_i$ is partially and reversibly suppressed by 9-PA. **(B)** Mean ± S.E.M. values for the experiment in A (n = 10). Black and white symbols represent time at which the intensity was measured. **(C)** GSK101-evoked $[Ca^{2+}]_i$ oscillations are suppressed by 9-PA (n = 39). **(D)** Summary of the data shown in **(C)**, as mean ± S.E.M. *** = P < 0.001, **** = p < 0.0001, paired-sample t-test.

We also tested the TRPM4-dependence of TRPV4-induced calcium signals by transfecting HEK293 cells with TRPV4 and/or TRPM4 DNA. TRPV4 only-transfected cells responded to GSK101 with a peak $[Ca^{2+}]_i$ increase that inactivated to a plateau without showing time-dependent Ca^{2+} oscillations whereas cells co-transfected with TRPV4 + TRPM4 DNA displayed robust oscillations in the presence of GSK101 (**Supplementary Figure 2**).

TRPM4 Does Not Regulate Trabecular Outflow or Steady-State Intraocular Pressure

Chronic TRPV4 activation was suggested to suppress aqueous humor drainage in hypertensive mouse eyes (13). Given that 9-PA inhibits TRPV4-dependent Ca^{2+} oscillations *in vitro* (**Figures 8A, B**), we tested whether it influences the trabecular component of pressure-induced fluid outflow ("outflow facility"). The effect of 9-PA on outflow facility was examined in enucleated mouse eyes using the *iPerfusion* system (37, 38). In response to 25 μM 9-PA, outflow facility decreased by -5% [-23%, 18%] (geometric mean [95% CI]; **Figure 8A**) relative to contralateral eyes that were perfused with vehicle, but this difference was not statistically significant (p=0.38, n=5 pairs). C_r for 9-PA treated eyes was 5.4 [4.2, 6.9] nl/min/mmHg and 5.5 [4.6, 6.7] nl/min/mmHg for vehicle-treated eyes (**Figure 8A**).

Finally, we investigated whether genetic deletion of TRPM4 channels affects intraocular pressure homeostasis in the mouse eye. $TRPM4^{-/-}$ eyes showed intraocular pressure levels (11.86 ± 0.14 mm Hg that were comparable to controls (12.10 ± 0.16 mm Hg; p > 0.05; n = 14 eyes and n = 36 eyes for WT and $TRPM4^{-/-}$, respectively), indicating that TRPM4 may not be required for steady-state intraocular pressure regulation **(Figure 8C)**. Overall, these results suggest that TRPM4 signaling is not required for step-induced fluid drainage across the or for steady-state intraocular pressure regulation.

DISCUSSION

The goal of this study was to define the properties of calcium homeostasis during sustained stimulation of TRPV4, a transducer of mechanical stimuli that has been implicated in the regulation of conventional outflow and intraocular pressure (13). We show that long-term TRPV4 stimulation evokes Ca^{2+} oscillations that are independent of the membrane potential and require expression of TRPM4. Both TRPV4 and TRPM4 were strongly expressed in primary and immortalized TM cells, with functional coupling between the two cation channels revealed by the rise of the Ca^{2+}-activated monovalent current and loss of oscillatory response

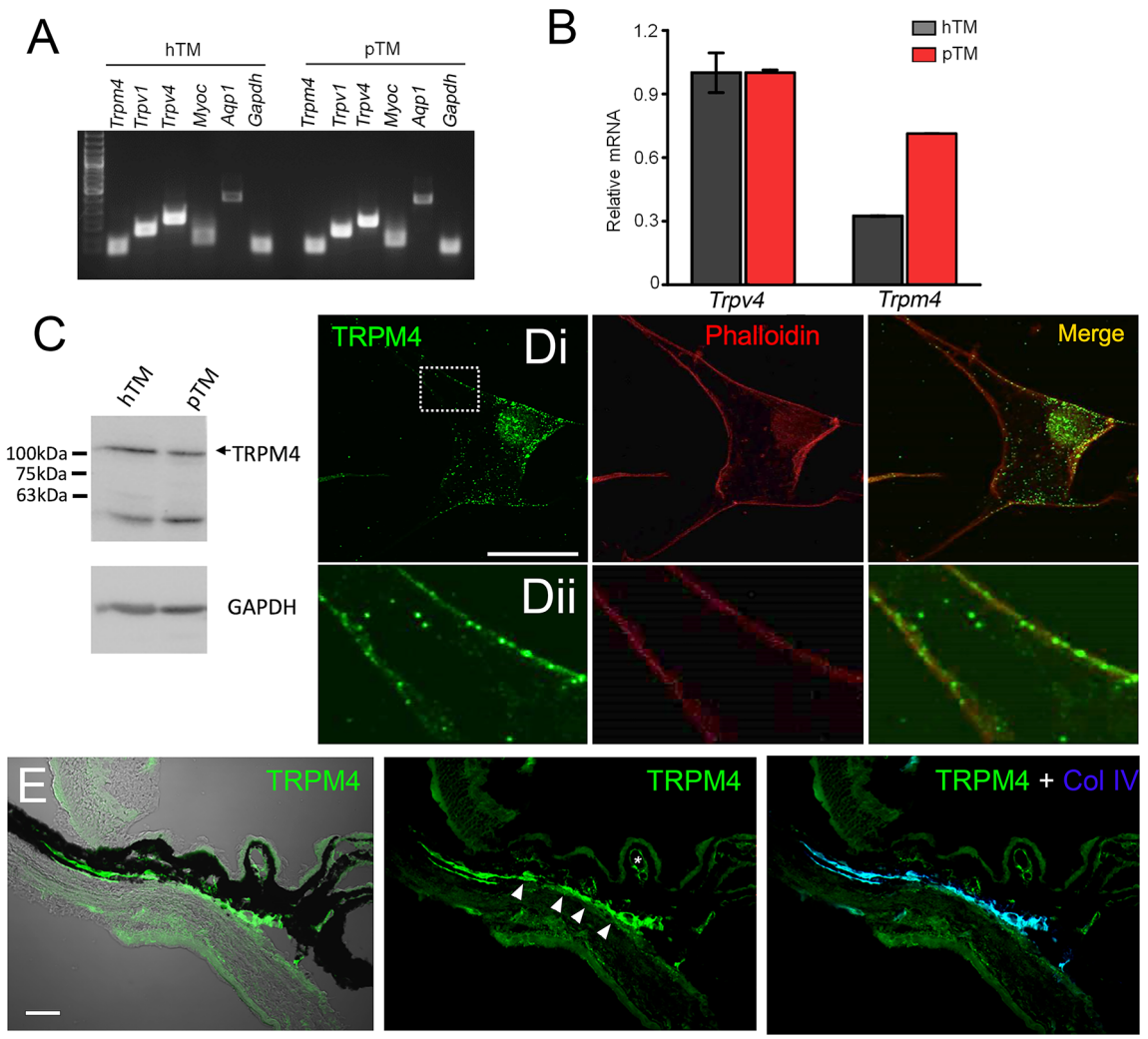

FIGURE 5 | TRPM4 is expressed in TM cells. **(A)** Representative PCR gels show expression of TRPM4 and TRPV4 transcripts together with markers aquaporin 1 (AQP1), TRPV1, and myocilin (MYOC) in immortalized (hTM) and primary (pTM) cells. **(B)** Semiquantitative qRT-PCR. Relative mRNA abundance of TRPM4 vs. TRPV4; expression is normalized to hTM TRPM4; mean ± S.E.M, N = 3. **(C)** Western blot. hTM and pTM cells show a TRPM4 band at the expected M.W. [**(D)**, upper panel] Cultured cells immunolabeled for TRPM4, with a magnified image of the region selected by the square (*inset*) showing punctate signals within the plasma membrane. Scale bar = 50 µm. **(E)** Anterior eye section from a wild type C57 mice, labeled with TRPM4. The TM region shows pronounced TRPM4-ir (arrows) that colocalizes with the marker Collagen IV (Col IV, blue). Moderate signal is seen in the ciliary body (arrows) and ciliary vasculature (asterisk).

following TRPM4 knockdown. Our findings identify novel interactions between TRPV4, TRPM4 and intracellular calcium stores and build a new working model that may help increase our understanding of homeostatic and time-dependent signaling within the primary outflow pathway.

Changes in $[Ca^{2+}]_i$ represent one of the earliest responses of nonexcitable cells to mechanical stress. Resting human TM cells do not exhibit spontaneous calcium activity whereas sustained stimulation of TRPV4 channels produced three types of time-dependent calcium behavior. (i) The initial increase in $[Ca^{2+}]_i$ evoked by GSK101 peaked within 2-4 min and showed slow onset kinetics that was likely shaped by the messenger pathway involving obligatory activation of phospholipase A2 and production of epoxyeicosatrienoic messengers that bind the pocket formed by S2-S3/S4-S5 linker residues (13, 17). (ii) The subsequent relaxation to the steady-state plateau phase reflects Ca^{2+}-dependent channel inactivation, internalization, interactions with modulatory sites within N- and C-termini (16) or negative regulation of Ca^{2+} influx by TRPM4 (44). (iii) The relaxation phase was associated with Ca^{2+} fluctuations in a frequency range similar to signals reported in glaucomatous TM (45) and pressure-, stretch- and GSK101- stimulated fibroblasts and chondrocytes (49, 50).

Several pieces of evidence suggest that the oscillatory response requires TRPM4 signaling. (i) TRPV4-induced fluctuations were suppressed by 9-PA, which also induced a reversible decrease in $[Na^+]_i$; (ii) TRPM4 knockdown in TM cells preserved the GSK101

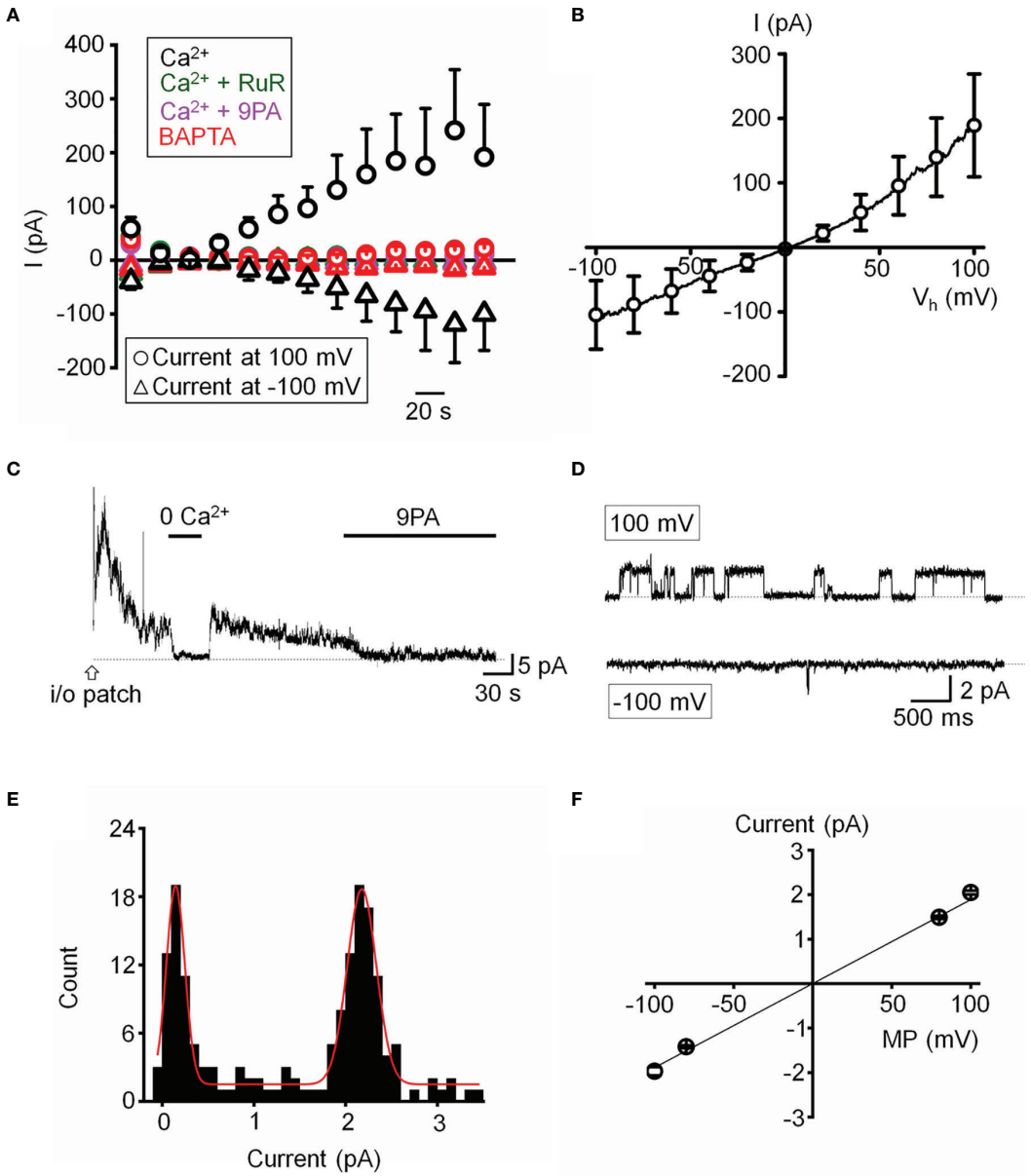

FIGURE 6 | Functional expression of a calcium-activated non-selective cation channels. **(A)** Time course of the whole-cell current recorded at the holding potentials 100 and -100 mV. The pipette solution contained 10 μM Ca^{2+} in the standard saline (*black*, n = 5), with addition of Ruthenium Red (RuR; 10 μM*; olive*, n = 11), 9-PA (20 μM*; magenta*, n = 15) in extracellular solution, or Ca^{2+}-free pipette solution (*red*, n = 15). **(B)** Averaged current-voltage relationship of the Ca^{2+} activated current in A subtracted by the Ca^{2+}-free component (n = 6). **(C)** Representative trace demonstrating the activity of a Ca^{2+}-activated channel in an inside-out patch preparation at +100 mV. **(D)** Representative traces of single channel activity. **(E)** Histogram of unitary current amplitude, fit with Gaussian function (red trace; R-Square = 96.6%). The data were binned at 0.02 pA. **(F)** Current-voltage relationship of single channel current, n = 6 patches. **(A, B, F)** show mean ± S.E.M.

response but eliminated the oscillatory calcium component, and (iii) Heterologous expression of TRPV4 and TRPM4 channels reconstituted fluctuations in HEK293 cells. TRPM4 expression in TM cells was confirmed by transcriptional profiling and immunohistochemistry, with *TRPM4* mRNA levels reaching ~30-70% of *TRPV4* mRNA, and immunoblots showing a band at the predicted M.W. As in other cell types (51, 52), the TRPM4 antibody labeled plasma membrane and intracellular compartments. The former corresponds to full-length TRPM4b variant which forms the Ca^{2+}-activated Ca^{2+}-impermeant cation channel and appears to congregate into punctate clusters within the cell membrane (**Figure 5Dii**) whereas intracellular puncta may correspond to truncated N-terminal variants with unknown functions that localize to the ER (32, 53, 54). The aggregation of TRPM4-ir

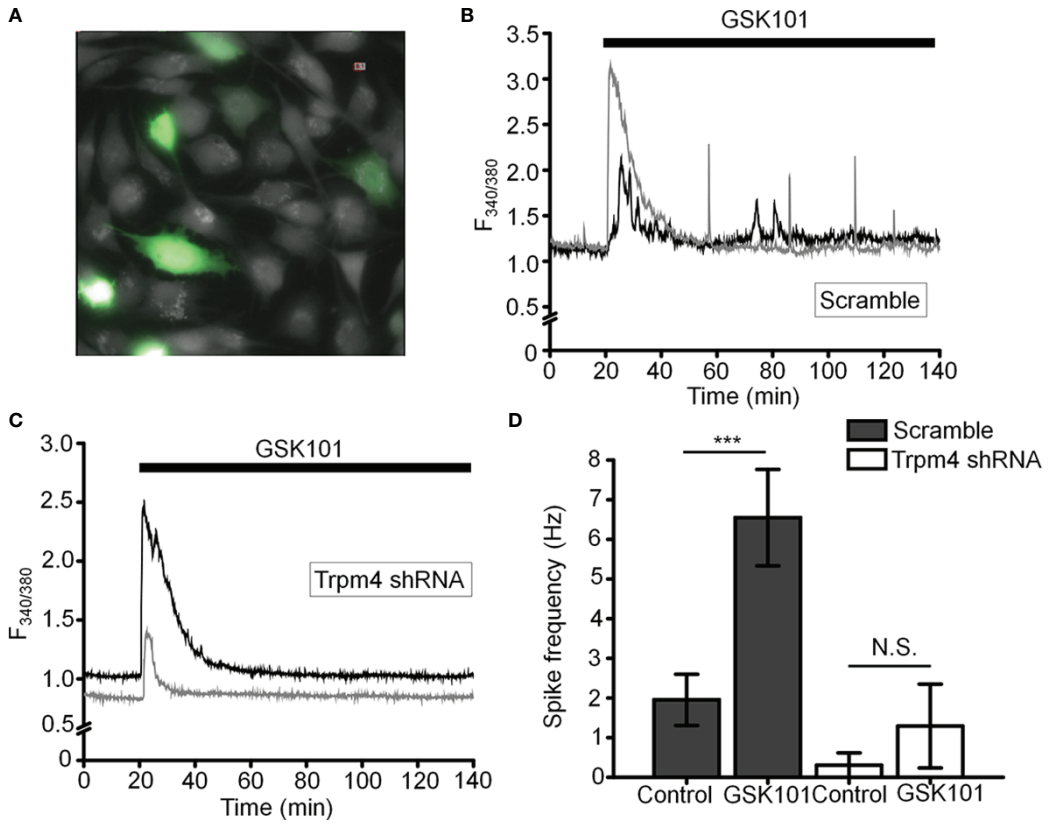

FIGURE 7 | TRPM4 knockdown disrupts GSK101-triggered $[Ca^{2+}]_i$ fluctuations. **(A)** TM cells treated with Sc-GFP, and TRPM4 shRNA-GFP constructs. **(B, D)** Sc-shRNA-transfected cells exhibit fluctuating $[Ca^{2+}]_i$ signals, which show **(C, D)** reduced frequency in TRPM4-shRNA-treated cells. Data shown as mean ± S.E.M. ***P < 0.001, $^{N.S.}$P > 0.05, paired t-test, n = 116 cells and n = 27 cells for Sc- and TRPM4 shRNAs, respectively.

signals resembles mechanosensory clusters enriched in TRPV4, paxillin and pFAK described in TM cells and embryonic fibroblasts (14, 55). Consistent with biochemical analyses, TM cells showed current-voltage relationship and pharmacological profiles characteristic of nonselective calcium-activated monovalent current mediated by TRPM4 (i.e., inhibition by Ruthenium Red, 9-PA and shRNA). Its quasi-linearity points at the membrane presence of PIP2 (56) whereas inhibition by BAPTA indicates that the channel is activated within membrane microdomains within which TRPV4 and TRPM4 functionally interact. Ca^{2+} fluctuations and calcium-activated monovalent current were observed in ~50% of recorded cells, possibly because the cells were derived from multiple TM populations or existed in different stages of the cell cycle. An immortalized atrial cardiomyocyte cell line similarly showed TRPM4-dependent Ca^{2+} oscillations in ~30% cells (28).

The advantage of the synthetic agonist GSK101 was that it allowed us to track signaling mechanisms associated with TRPV4 in the absence of concurrent activation of Piezo1 and TREK-1 stretch-activated channels (e.g (10, 11). In contrast to previous studies in myocytes, smooth muscle cells, neurons and immune cells (27–29, 57) which linked TRPM4-dependent $[Ca^{2+}]_i$ oscillations to obligatory voltage-gated Ca^{2+} influx, TM cells did not show functional voltage-operated calcium channels expression under our experimental conditions. Thus, depolarization had no discernible effect on $[Ca^{2+}]_i$ and the transmembrane current, and Ba^{2+} concentrations that reliably trigger voltage-operated calcium channels-mediated spiking and suppress store release in retinal neurons (15, 41) had no discernable effects on TM signaling. The absence of coupling between the membrane potential, $[Na^+]_i$ and Ca^{2+} oscillations indicates that Ca^{2+} fluctuations reflect intracellular and/or voltage-independent mechanisms. Previous investigation of TRPM4-TRPC3 interactions in HEK293 cells showed that cell depolarization caused by Na^+ influx transiently suppresses TRP-mediated Ca^{2+} influx by reducing the inward electrochemical driving force for Ca^{2+} (48). TRPM4 signaling and oscillations in cardiomyocytes were attributed to redistribution of mitochondrial Ca^{2+} stores into the cytosol (28) but it remains to be determined whether Ca^{2+} transients that underlie the oscillatory response involve ψ_m and mitochondrial transporters (Na^+/Ca^{2+}-Li^+ exchangers, Ca^{2+}/H^+ exchange, and/or MCU uniporters). A simple model delineating the potential players associated with TRPV4-dependent calcium oscillations is shown in **Figure 9**. Another potential source could include reciprocal interactions between Ca^{2+} influx and the IP3R store (55, 55) mediated through contacts between the C-terminus CaM-binding site of TRPV4 and

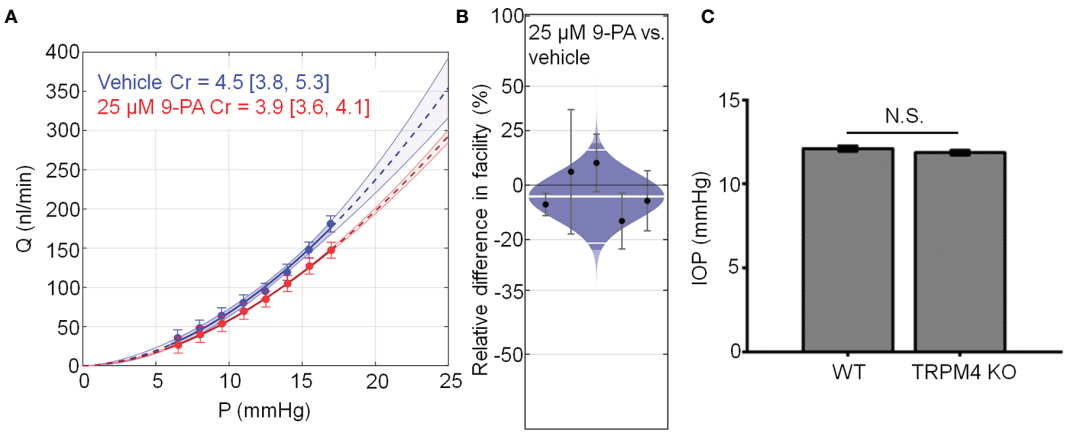

FIGURE 8 | TRPM4 does not regulate trabecular outflow and steady-state intraocular pressure. **(A)** Representative flow-pressure (*Q* – *P*) plot for contralateral eyes perfused with 25 µM 9-PA versus vehicle. Curves show the optimal fit from Equation 1, with 95% confidence bounds and error bars show 95% confidence intervals. **(B)** Relative difference in outflow facility between contralateral eyes perfused with 25 µM 9-PA versus vehicle. The relative difference in facility is defined as the ratio of C_r in the experimental eye perfused with 9-PA relative to vehicle-perfused contralateral eye minus unity, expressed as a percentage. Each data point represents the relative difference in facility for an individual mouse. Error bars are 95% confidence intervals. Shaded regions represent the best estimate of the sample distributions, with the central white line representing the geometric mean. Dark central bands represent the 95% CI on the mean, and the outer white lines represent the limits encompassing 95% of the population. **(C)** Averaged results for intraocular pressure in wild-type (WT, n = 14 eyes) and TRPM4 KO (n = 36 eyes) mice. $^{N.S.}$ = P > 0.05.

the IP3R receptor (58) and depolarization-dependent reduction of the driving force for Ca^{2+} influx through CRAC/Orai channels (27).

TRPM4 was suggested to be directly activated by membrane stretch (59) but this conclusion has been controversial (58, 60, 61). A compelling aspect of our findings is that its role in mechanosignaling might instead reflect activation downstream from stretch-activated channels. Chemical activation of TRPV4 reproduced time-dependent behavior of pressure-induced Ca^{2+}

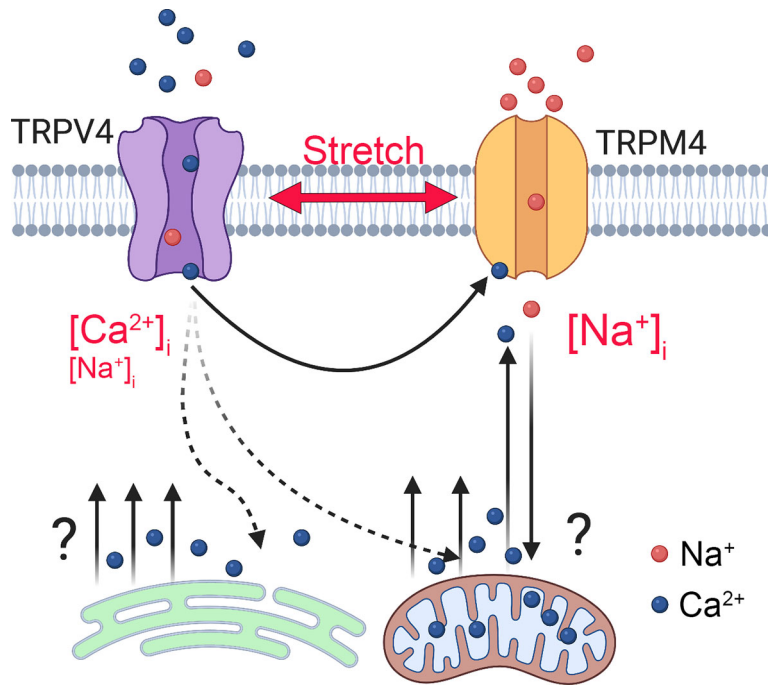

FIGURE 9 | Model of TRPM4-dependent calcium oscillations downstream from TRPV4. Mechanical stretch triggers cation influx through TRPV4 to elevate $[Ca^{2+}]_i$ and activate TRPM4, a Ca^{2+}-dependent Na^+ channel to depolarize the TM cells and increase $[Na^+]_i$. TRPM4 activation is required for voltage-independent oscillatory release of Ca^{2+} from a yet-unknown intracellular compartment.

events in human TM cells (62) and oscillatory phenotypes in TRPV4-expressing macrophages/monocytes, fibroblasts, keratinocytes, endothelial cells, chondrocytes, and glia (50, 55) that have been linked to cellular microcontractions, ECM remodeling and transfer of mechanical force across load-bearing focal adhesions (49, 50, 63). In macrophages, TRPM4 regulates cellular calcium oscillations and contractility *via* FAK and Rac GTPases (27, 53, 55), processes that may be downstream from TRPV4 (14; **Figure 4**). Together, these data implicate TRPV4-TRPM4 interactions in endogenous, cell-generated control of stretch-sensitive tyrosine phosphorylations, RhoA signaling and contractility. Another intriguing possibility is that TRPV4-dependent Ca^{2+} oscillations operate at the threshold of contractile, RhoA-dependent (14) vs. relaxing, nitric oxide-dependent (64) states associated with myogenic-like contractility (62, 65, 66). TRPM4 shares the regulatory sulphonylurea receptor (SUR1/2) with inward rectifying K^+ (Kir6.1 and Kir6.2) subunits that form K_{ATP} channels sensitive to $[Ca^{2+}]_i$ and intracellular ATP (67, 68) and regulate NFATc1 signaling in immune cells (39). The effect of K_{ATP} channel openers on intraocular pressure (69) could include parallel modulation of the SUR1-TRPM4 complex, Ca^{2+} and Na^+ homeostasis. The small, non-significant decrease in outflow facility in the presence of 9-PA and ocular normotension in mice with ablated TRPM4 gene suggest that TRPM4 is not required for steady-state IOP maintenance but it remains to be seen whether the contribution of TRPM4 channels can be unmasked under conditions associated with maximal TRPV4 activation.

In conclusion, our findings bring mechanistic evidence for novel interactions between mechanotransducers, TRPM4 channels and Ca^{2+} stores that may, in the presence of increased membrane strain, alter the cells' membrane potential together with intracellular $[Ca^{2+}]_i$ and $[Na^+]_i$. Analogy with other load-bearing and immune-like cells, suggests that a persistent pacemaking loop between Ca^{2+} influx, release and Ca^{2+}-activated channels downstream from TRPV4 could suggests that a time-dependently coordinate transcription factors, actomyosin-driven tension, mechanical load transfer across focal contacts, and secretion of matrix metalloproteinases. While investigations of TM biology typically focus on smooth muscle cell- and endothelial-like properties of resident cells, it is worth underscoring their role in IOP-dependent innate immune regulation in the anterior eye. Aqueous humor inhibits immune effector cells (70) and thus key phagocytic, scavenger and immune functions in the outflow pathway are relegated to TM cells (70–72), which express immune-like markers such as complement C1QB, the tyrosine kinase binding protein (TYROBP), major histocompatibility complex proteins and TLR4 (7, 64, 73, 74). We found that, similar to macrophages/monocytes and mast cells, TM cells utilize TRPM4 for oscillatory activity, which is triggered downstream from the TRPV4 channel that integrates mechanical, temperature and chemical inputs (15–17). This suggests that TRPM4-dependent calcium oscillations and their role in TLR4-dependent phagocytosis, cytokine production and survival (31, 32) might be informed by the biomechanical milieu. TLR4 signaling regulates TM TGFβ production (7) and has been linked to both TRPV4 and TRPM4 activation (19, 31, 39). Owing to their role in translayer Ca^{2+}, Na^+ and water transport dynamics, myofibroblast transformation and immune regulation, TRPV4-TRPM4 interactions could therefore be targeted by translational interventions aimed at fine-tuning the homeostatic functions of the conventional outflow pathway and regulation of intraocular pressure.

DATA AVAILABILITY STATEMENT

The original contributions presented in the study are included in the article/**Supplementary Material**. Further inquiries can be directed to the corresponding author.

ETHICS STATEMENT

The animal study was reviewed and approved by Institutional Animal Care and Use Committee - University of Utah.

AUTHOR CONTRIBUTIONS

OY, TP, FV, JB, Jv, SR, ML, CR and JB carried out the experiments. OY, JB, SR and Jv performed the statistical analyses. EH and MF provided reagents/animal models. OY and DK drafted the manuscript. OY, DO and DK conceived and coordinated the study. The authors read and approved the final manuscript.

FUNDING

Supported by, National Institutes of Health (R01EY027920, R01EY031817, P30EY014800, T32EY024234), Stauss-Rankin Foundation, USAMRAA (VR200079) and unrestricted support from Research to Prevent Blindness to the Moran Eye Institute at the University of Utah.

SUPPLEMENTARY MATERIAL

The Supplementary Material for this article can be found online at: https://www.frontiersin.org/articles/10.3389/fimmu.2022.805076/full#supplementary-material

Supplementary Figure 1 | Validation of TRPM4 shRNA constructs. **(A)** Typical WB results representing knockdown effects of the TRPM4 shRNA constructs in the HEK-293 overexpression system. **(B)** Quantification of results shown in (A). The results are representative of three independent experiments.

Supplementary Figure 2 | HEK293 cells. TRPV4 and TRPM4 coexpression is sufficient to sustain calcium oscillations in the presence of GSK101. Representative traces of ratiometric signals in **(A)** TRPV4 + TRPM4 DNA-transfected cells and **(B)** Cells transfected with TRPV4 alone. **(C)** Averaged frequency of $[Ca^{2+}]_i$ transients in TRPV4+TRPM4 expressing cells before and after GSK101 exposure.

REFERENCES

1. Coulombre AJ, Steinberg SN, Coulombre JL. The Role of Intraocular Pressure in the Development of the Chick Eye. V. Pigmented Epithelium. *Invest Ophthalmol* (1963) 2:83–9.
2. Acott TS, Kelley MJ, Keller KE, Vranka JA, Abu-Hassan DW, Li X, et al. Intraocular Pressure Homeostasis: Maintaining Balance in a High-Pressure Environment. *J Ocul Pharmacol Ther* (2014) 30:94–101. doi: 10.1089/jop.2013.0185
3. Bradley JM, Kelley MJ, Zhu X, Anderssohn AM, Alexander JP, Acott TS. Effects of Mechanical Stretching on Trabecular Matrix Metalloproteinases. *Invest Ophthalmol Vis Sci* (2001) 42:1505–13.
4. Rohen JW, Lütjen-Drecoll E, Flügel C, Meyer M, Grierson I. Ultrastructure of the Trabecular Meshwork in Untreated Cases of Primary Open-Angle Glaucoma (POAG). *Exp Eye Res* (1993) 56:683–92. doi: 10.1006/exer.1993.1085
5. Last JA, Pan T, Ding Y, Reilly CM, Keller K, Acott TS, et al. Elastic Modulus Determination of Normal and Glaucomatous Human Trabecular Meshwork. *Invest Ophthalmol Vis Sci* (2011) 52:2147–52. doi: 10.1167/iovs.10-6342
6. Patel G, Fury W, Yang H, Gomez-Caraballo M, Bai Y, Yang T, et al. Molecular Taxonomy of Human Ocular Outflow Tissues Defined by Single-Cell Transcriptomics. *Proc Natl Acad Sci USA* (2020) 117:12856–67. doi: 10.1073/pnas.2001896117
7. Hernandez H, Medina-Ortiz WE, Luan T, Clark AF, McDowell CM. Crosstalk Between Transforming Growth Factor Beta-2 and Toll-Like Receptor 4 in the Trabecular Meshwork. *Invest Ophthalmol Vis Sci* (2017) 58:1811–23. doi: 10.1167/iovs.16-21331
8. Poyomtip T. Roles of Toll-Like Receptor 4 for Cellular Pathogenesis in Primary Open-Angle Glaucoma: A Potential Therapeutic Strategy. *J Microbiol Immunol Infect* (2019) 52(2):201–6. doi: 10.1016/j.jmii.2018.12.006
9. Filla MS, Faralli JA, Peotter JL, Peters DM. The Role of Integrins in Glaucoma. *Exp Eye Res* (2017) 158:124–36. doi: 10.1016/j.exer.2016.05.011
10. Yarishkin O, Phuong TTT, Bretz CA, Olsen KW, Baumann JM, Lakk M, et al. TREK-1 Channels Regulate Pressure Sensitivity and Calcium Signaling in Trabecular Meshwork Cells. *J Gen Physiol* (2018) 150:1660–75. doi: 10.1085/jgp.201812179
11. Yarishkin O, Phuong TTT, Baumann JM, De Ieso ML, Vazquez-Chona F, Rudzitis CN, et al. Piezo1 Channels Mediate Trabecular Meshwork Mechanotransduction and Promote Aqueous Fluid Outflow. *J Physiol* (2021) 599:571–92. doi: 10.1113/JP281011
12. Luo N, Conwell MD, Chen X, Kettenhofen CI, Westlake CJ, Cantor LB, et al. Primary Cilia Signaling Mediates Intraocular Pressure Sensation. *Proc Natl Acad Sci U.S.A.* (2014) 111:12871–6. doi: 10.1073/pnas.1323292111
13. Ryskamp DA, Frye AM, Phuong TTT, Yarishkin O, Jo AO, Xu Y, et al. TRPV4 Regulates Calcium Homeostasis, Cytoskeletal Remodeling, Conventional Outflow and Intraocular Pressure in the Mammalian Eye. *Sci Rep* (2016) 6:30585. doi: 10.1038/srep30583
14. Lakk M, Križajs D. TRPV4-Rho Signaling Drives Cytoskeletal and Focal Adhesion Remodeling in Trabecular Meshwork Cells. *Am J Physiol - Cell Physiol* (2021) 320:C1013–30. doi: 10.1152/ajpcell.00599.2020
15. Križaj D. *What is Glaucoma? Webvision Organ Retin Vis Syst*. Salt Lake City: University of Utah Health Sciences Center (2019).
16. White JPM, Cibelli M, Urban L, Nilius B, McGeown JG, Nagy I. TRPV4: Molecular Conductor of a Diverse Orchestra. *Physiol Rev* (2016) 96:911–73. doi: 10.1152/physrev.00016.2015
17. Berna-Erro A, Izquierdo-Serra M, Sepúlveda RV, Rubio-Moscardo F, Doñate-Macián P, Serra SA, et al. Structural Determinants of 5',6'-Epoxyeicosatrienoic Acid Binding to and Activation of TRPV4 Channel. *Sci Rep* (2017) 7:10522. doi: 10.1038/s41598-017-11274-1
18. Thibodeau ML, Peters CH, Townsend KN, Shen Y, Hendson G, Adam S, et al. Compound Heterozygous TRPV4 Mutations in Two Siblings With a Complex Phenotype Including Severe Intellectual Disability and Neuropathy. *Am J Med Genet A* (2017) 173:3087–92. doi: 10.1002/ajmg.a.38400
19. Rahaman SO, Grove LM, Paruchuri S, Southern BD, Abraham S, Niese KA, et al. TRPV4 Mediates Myofibroblast Differentiation and Pulmonary Fibrosis in Mice. *J Clin Invest* (2014) 124:5225–38. doi: 10.1172/JCI75331
20. Sharma S, Goswami R, Rahaman SO. The TRPV4-TAZ Mechanotransduction Signaling Axis in Matrix Stiffness- and Tgfβ1-Induced Epithelial-Mesenchymal Transition. *Cell Mol Bioeng* (2019) 12:139-52. doi: 10.1007/s12195-018-00565-w
21. Lorenzo IM, Liedtke W, Sanderson MJ, Valverde MA. TRPV4 Channel Participates in Receptor-Operated Calcium Entry and Ciliary Beat Frequency Regulation in Mouse Airway Epithelial Cells. *Proc Natl Acad Sci USA* (2008) 105:12611–6. doi: 10.1073/pnas.0803970105
22. Goswami C, Kuhn J, Heppenstall PA, Hucho T. Importance of non-Selective Cation Channel TRPV4 Interaction With Cytoskeleton and Their Reciprocal Regulations in Cultured Cells. *PloS One* (2010) 5:e11654. doi: 10.1371/journal.pone.0011654
23. Jo AO, Ryskamp DA, Phuong TTT, Verkman AS, Yarishkin O, Macaulay N. Križaj D. TRPV4 and AQP4 Channels Synergistically Regulate Cell Volume and Calcium Homeostasis in Retinal Müller Glia. *J Neurosci* (2015) 35:13525–73. doi: 10.1523/JNEUROSCI.1987-15.2015
24. Li P, Bian X, Liu C, Wang S, Guo M, Tao Y, et al. STIM1 and TRPV4 Regulate Fluid Flow-Induced Calcium Oscillation at Early and Late Stages of Osteoclast Differentiation. *Cell Calcium* (2018) 71:45–52. doi: 10.1016/j.ceca.2017.12.001
25. Voets T, Prenen J, Vriens J, Watanabe H, Janssens A, Wissenbach U, et al. Molecular Determinants of Permeation Through the Cation Channel TRPV4. *J Biol Chem* (2002) 277:33704–10. doi: 10.1074/jbc.M204828200
26. Guinamard R, Demion M, Magaud C, Potreau D, Bois P. Functional Expression of the TRPM4 Cationic Current in Ventricular Cardiomyocytes From Spontaneously Hypertensive Rats. *Hypertension* (2006) 48:587–94. doi: 10.1161/01.HYP.0000237864.65019.a5
27. Launay P, Cheng H, Srivatsan S, Penner R, Fleig A, Kinet JP. TRPM4 Regulates Calcium Oscillations After T Cell Activation. *Science* (2004) 306:1374–77. doi: 10.1126/science.1098845
28. Burt R, Graves BM, Gao M, Li C, Williams DL, Fregoso SP, et al. 9-Phenanthrol and Flufenamic Acid Inhibit Calcium Oscillations in HL-1 Mouse Cardiomyocytes. *Cell Calcium* (2013) 54:193–201. doi: 10.1016/j.ceca.2013.06.003
29. Simard C, Sallé L, Rouet R, Guinamard R. Transient Receptor Potential Melastatin 4 Inhibitor 9-Phenanthrol Abolishes Arrhythmias Induced by Hypoxia and Re-Oxygenation in Mouse Ventricle. *Br J Pharmacol* (2012) 165:2354–64. doi: 10.1111/j.1476-5381.2011.01715.x
30. Jo AO, Lakk M, Frye AM, Phuong TT, Redmon SN, Roberts R, et al. Differential Volume Regulation and Calcium Signaling in Two Ciliary Body Cell Types is Subserved by TRPV4 Channels. *Proc Natl Acad Sci U.S.A.* (2016) 113:3885–90. doi: 10.1073/pnas.1515895113
31. Serafini N, Dahdah A, Barbet G, Demion M, Attout T, Gautier G, et al. The TRPM4 Channel Controls Monocyte and Macrophage, But Not Neutrophil, Function for Survival in Sepsis. *J Immunol* (2012) 189:3689–99. doi: 10.4049/jimmunol.1102969
32. Scheraga RG, Abraham S, Niese KA, Southern BD, Grove LM, Hite RD, et al. TRPV4 Mechanosensitive Ion Channel Regulates Lipopolysaccharide-Stimulated Macrophage Phagocytosis. *J Immunol* (2016) 196:428–36. doi: 10.4049/jimmunol.1501688
33. Lakk M, Yarishkin O, Baumann JM, Iuso A, Križaj D. Cholesterol Regulates Polymodal Sensory Transduction in Müller Glia. *Glia* (2017) 65:2038–50. doi: 10.1002/glia.23213
34. Redmon SN, Yarishkin O, Lakk M, Jo A, Mustafić E, Tvrdik P, et al. TRPV4 Channels Mediate the Mechanoresponse in Retinal Microglia. *Glia* (2021) 69:1563–82. doi: 10.1002/glia.23979
35. Molnár T, Yarishkin O, Iuso A, Barabas P, Jones B, Marc RE, et al. Store-Operated Calcium Entry in Müller Glia is Controlled by Synergistic Activation of TRPC and Orai Channels. *J Neurosci* (2016) 36:3184–98. doi: 10.1523/JNEUROSCI.4069-15.2016
36. Yarishkin O, Phuong TTT, Križaj D. Trabecular Meshwork TREK-1 Channels Function as Polymodal Integrators of Pressure and pH. *Investig Ophthalmol Vis Sci* (2019) 60:2294–303. doi: 10.1167/iovs.19-26851
37. Sherwood JM, Reina-Torres E, Bertrand JA, Rowe B, Overby DR. Measurement of Outflow Facility Using Iperfusion. *PloS One* (2016) 11:e0150694. doi: 10.1371/journal.pone.0150694
38. Sherwood JM, Boazak EM, Feola AJ, Parker K, Ethier CR, Overby DR. Measurement of Ocular Compliance Using Iperfusion. *Front Bioeng Biotechnol* (2019) 7:276. doi: 10.3389/fbioe.2019.00276
39. Kurland DB, Gerzanich V, Karimy JK, Woo SK, Vennekens R, Freichel M, et al. The Sur1-Trpm4 Channel Regulates NOS2 Transcription in TLR4-Activated Microglia. *J Neuroinflamm* (2016) 13(1):130. doi: 10.1186/s12974-016-0599-2

40. Earley S, Waldron BJ, Brayden JE. Critical Role for Transient Receptor Potential Channel TRPM4 in Myogenic Constriction of Cerebral Arteries. *Circ Res* (2004) 95:922–9. doi: 10.1161/01.RES.0000147311.54833.03
41. Akopian A, Križaj D, Witkovsky P. Both High- and Low Voltage-Activated Calcium Currents Contribute to the Light-Evoked Responses of Luminosity Horizontal Cells in the Xenopus Retina. *Brain Res* (1997) 762:121–30. doi: 10.1016/S0006-8993(97)00374-0
42. Yarishkin OV, Hwang EM, Kim D, Yoo JC, Kang SS, Kim DR, et al. Diclofenac, a Non-Steroidal Anti-Inflammatory Drug, Inhibits L-Type Ca Channels in Neonatal Rat Ventricular Cardiomyocytes. *Korean J Physiol Pharmacol* (2009) 13:437–42. doi: 10.4196/kjpp.2009.13.6.437
43. Križaj D, Bao JX, Schmitz Y, Witkovsky P, Copenhagen DR. Caffeine-Sensitive Calcium Stores Regulate Synaptic Transmission From Retinal Rod Photoreceptors. *J Neurosci* (1999) 19:7249–61. doi: 10.1523/jneurosci.19-17-07249.1999
44. Grand T, Demion M, Norez C, Mettey Y, Launay P, Becq F, et al. 9-Phenanthrol Inhibits Human TRPM4 But Not TRPM5 Cationic Channels. *Br J Pharmacol* (2008) 153:1697–705. doi: 10.1038/bjp.2008.38
45. Guinamard R, Hof T, Del Negro CA. The TRPM4 Channel Inhibitor 9-Phenanthrol. *Br J Pharmacol* (2014) 171:1600–13. doi: 10.1111/bph.12582
46. Demion M, Bois P, Launay P, Guinamard R. TRPM4, a Ca2+-Activated Nonselective Cation Channel in Mouse Sino-Atrial Node Cells. *Cardiovasc Res* (2007) 73:531–8. doi: 10.1016/j.cardiores.2006.11.023
47. Yarishkin OV, Hwang EM, Park JY, Kang D, Han J, Hong SG. Endogenous TRPM4-Like Channel in Chinese Hamster Ovary (CHO) Cells. *Biochem Biophys Res Commun* (2008) 369:712–7. doi: 10.1016/j.bbrc.2008.02.081
48. Park JY, Hwang EM, Yarishkin O, Seo JH, Kim E, Yoo J, et al. TRPM4b Channel Suppresses Store-Operated Ca2+ Entry by a Novel Protein-Protein Interaction With the TRPC3 Channel. *Biochem Biophys Res Commun* (2008) 368:677–83. doi: 10.1016/j.bbrc.2008.01.153
49. Holmes DF, Yeung C-YC, Garva R, Zindy E, Taylor SH, Lu Y, et al. Synchronized Mechanical Oscillations at the Cell-Matrix Interface in the Formation of Tensile Tissue. *Proc Natl Acad Sci USA* (2018) 115:E9288–97. doi: 10.1073/pnas.1801759115
50. Gilchrist CL, Leddy HA, Kaye L, Case ND, Rothenberg KE, Little D, et al. TRPV4-Mediated Calcium Signaling in Mesenchymal Stem Cells Regulates Aligned Collagen Matrix Formation and Vinculin Tension. *Proc Natl Acad Sci USA* (2019) 116:1992–7. doi: 10.1073/pnas.1811095116
51. Piao H, Takahashi K, Yamaguchi Y, Wang C, Liu K, Naruse K. Transient Receptor Potential Melastatin-4 is Involved in Hypoxia-Reoxygenation Injury in the Cardiomyocytes. *PloS One* (2015) 10:e0121703. doi: 10.1371/journal.pone.0121703
52. Stokum JA, Kwon MS, Woo SK, Tsymbalyuk O, Vennekens R, Gerzanich V, et al. SUR1-TRPM4 and AQP4 Form a Heteromultimeric Complex That Amplifies Ion/Water Osmotic Coupling and Drives Astrocyte Swelling. *Glia* (2018) 66:108–25. doi: 10.1002/glia.23231
53. Launay P, Fleig A, Perraud AL, Scharenberg AM, Penner R, Kinet JP. TRPM4 is a Ca2+-Activated Nonselective Cation Channel Mediating Cell Membrane Depolarization. *Cell* (2002) 109:531–8. doi: 10.1016/S0092-8674(02)00719-5
54. Vennekens R, Nilius B. Insights Into TRPM4 Function, Regulation and Physiological Role. *Handb Exp Pharmacol* (2007) 179:269–85. doi: 10.1007/978-3-540-34891-7_16
55. Cáceres M, Ortiz L, Recabarren T, Romero A, Colombo A, Leiva-Salcedo E, et al. TRPM4 Is a Novel Component of the Adhesome Required for Focal Adhesion Disassembly, Migration and Contractility. *PloS One* (2015) 10:e0130540. doi: 10.1371/journal.pone.0130540
56. Gerzanich V, Kwon MS, Woo SK, Ivanov A, Simard JM. SUR1-TRPM4 Channel Activation and Phasic Secretion of MMP-9 Induced by tPA in Brain Endothelial Cells. *PloS One* (2018) 13:e0195526. doi: 10.1371/journal.pone.0195526
57. O'Malley JJ, Seibt F, Chin J, Beierlein M. TRPM4 Conductances in Thalamic Reticular Nucleus Neurons Generate Persistent Firing During Slow Oscillations. *J Neurosci* (2020) 40:4813–23. doi: 10.1523/JNEUROSCI.0324-20.2020
58. Garcia-Elias A, Lorenzo IM, Vicente R, Valverde MA. IP3 Receptor Binds to and Sensitizes TRPV4 Channel to Osmotic Stimuli *via* a Calmodulin-Binding Site. *J Biol Chem* (2008) 283:31284–8. doi: 10.1074/jbc.C800184200
59. Morita H, Honda A, Inoue R, Ito Y, Abe K, Nelson MT, et al. Membrane Stretch-Induced Activation of a TRPM4-Like Nonselective Cation Channel in Cerebral Artery Myocytes. *J Pharmacol Sci* (2007) 103:417–26. doi: 10.1254/jphs.fp0061332
60. Gonzales AL, Yang Y, Sullivan MN, Sanders L, Dabertrand F, Hill-Eubanks DC, et al. A Plcγ1-Dependent, Force-Sensitive Signaling Network in the Myogenic Constriction of Cerebral Arteries. *Sci Signal* (2014) 7:ra49. doi: 10.1126/scisignal.2004732
61. Constantine M, Liew CK, Lo V, Macmillan A, Cranfield CG, Sunde M, et al. Heterologously-Expressed and Liposome-Reconstituted Human Transient Receptor Potential Melastatin 4 Channel (TRPM4) is a Functional Tetramer. *Sci Rep* (2016) 6:19352. doi: 10.1038/srep19352
62. Matsuo T, Matsuo N. Intracellular Calcium Response to Hydraulic Pressure in Human Trabecular Cells. *Br J Ophthalmol* (1996) 80:561–6. doi: 10.1136/bjo.80.6.561
63. Castella LF, Buscemi L, Godbout C, Meister J-J, Hinz B. A New Lock-Step Mechanism of Matrix Remodelling Based on Subcellular Contractile Events. *J Cell Sci* (2010) 123:1751–60. doi: 10.1242/jcs.066795
64. Patel PD, Chen Y-L, Kasetti RB, Maddineni P, Mayhew W, Millar JC, et al. Impaired TRPV4-eNOS Signaling in Trabecular Meshwork Elevates Intraocular Pressure in Glaucoma. *Proc Natl Acad Sci USA* (2021) 118:e2022461118. doi: 10.1073/pnas.2022461118
65. Wiederholt M, Thieme H, Stumpff F. The Regulation of Trabecular Meshwork and Ciliary Muscle Contractility. *Prog Retin Eye Res* (2000) 19:271–95. doi: 10.1016/s1350-9462(99)00015-4
66. Guinamard R, Demion M, Chatelier A, Bois P. Calcium-Activated Nonselective Cation Channels in Mammalian Cardiomyocytes. *Trends Cardiovasc Med* (2006) 16:245–50. doi: 10.1016/j.tcm.2006.04.007
67. Guinamard R, Demion M, Launay P. Physiological Roles of the TRPM4 Channel Extracted From Background Currents. *Physiol (Bethesda)* (2010) 25:155–64. doi: 10.1152/physiol.00004.2010
68. Woo SK, Tsymbalyuk N, Tsymbalyuk O, Ivanova S, Gerzanich V, Simard JM. SUR1-TRPM4 Channels, Not KATP, Mediate Brain Swelling Following Cerebral Ischemia. *Neurosci Lett* (2020) 718:108–25. doi: 10.1016/j.neulet.2019.134729
69. Chowdhury UR, Holman BH, Fautsch MP. ATP-Sensitive Potassium (K(ATP)) Channel Openers Diazoxide and Nicorandil Lower Intraocular Pressure. *vivo Invest Ophthalmol Vis Sci* (2013) 54:4892–9. doi: 10.1167/iovs.13-11872
70. Streilein JW. Ocular Immune Privilege: Therapeutic Opportunities From an Experiment of Nature. *Nat Rev Immunol* (2003) 3:879–88. doi: 10.1038/nri1224
71. Biros D. Anterior Chamber-Associated Immune Deviation. *Vet Clin North Am - Small Anim Pract* (2008) 38:309–21. doi: 10.1016/j.cvsm.2007.12.006
72. Latina M. Immunohistochemical Staining of the Human Anterior Segment. *Arch Ophthalmol* (1988) 106:95–9. doi: 10.1001/archopht.1988.01060130101037
73. Tripathi BJ, Tripathi RC, Wong P, Raja S. Expression of HLA by the Human Trabecular Meshwork and Corneal Endothelium. *Exp Eye Res* (1990) 51:269–76. doi: 10.1016/0014-4835(90)90023-N
74. Grybauskas A, Koga T, Kuprys PV, Nolan M, McCarty R, Walker L, et al. ABCB1 Transporter and Toll-Like Receptor 4 in Trabecular Meshwork Cells. *Mol Vis* (2015) 21:201–12.

Conflict of Interest: The authors declare that the research was conducted in the absence of any commercial or financial relationships that could be construed as a potential conflict of interest

Publisher's Note: All claims expressed in this article are solely those of the authors and do not necessarily represent those of their affiliated organizations, or those of the publisher, the editors and the reviewers. Any product that may be evaluated in this article, or claim that may be made by its manufacturer, is not guaranteed or endorsed by the publisher.

Advantages of publishing in Frontiers

OPEN ACCESS
Articles are free to read for greatest visibility and readership

FAST PUBLICATION
Around 90 days from submission to decision

HIGH QUALITY PEER-REVIEW
Rigorous, collaborative, and constructive peer-review

TRANSPARENT PEER-REVIEW
Editors and reviewers acknowledged by name on published articles

Frontiers
Avenue du Tribunal-Fédéral 34
1005 Lausanne | Switzerland

Visit us: www.frontiersin.org
Contact us: frontiersin.org/about/contact

REPRODUCIBILITY OF RESEARCH
Support open data and methods to enhance research reproducibility

DIGITAL PUBLISHING
Articles designed for optimal readership across devices

FOLLOW US
@frontiersin

IMPACT METRICS
Advanced article metrics track visibility across digital media

EXTENSIVE PROMOTION
Marketing and promotion of impactful research

LOOP RESEARCH NETWORK
Our network increases your article's readership